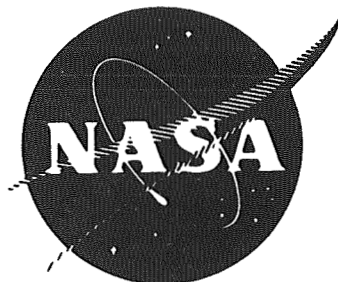N70-19729

NASA CR-72617

INTERIM REPORT

CRYOGENIC ALLOY SCREENING

By F. R. Schwartzberg, R. D. Keys,
and T. F. Kiefer

CASE FILE
COPY

Prepared under Contract No. NAS3-11203 by
MARTIN MARIETTA CORPORATION
Denver, Colorado
for
NATIONAL AERONAUTICS AND SPACE ADMINISTRATION

Requests for copies of this report should be referred to:

National Aeronautics and Space Administration
Office of Scientific and Technical Information

Attention: AFSS-A
Washington, D. C. 20546

NASA CR-72617

INTERIM REPORT
CRYOGENIC ALLOY SCREENING

By F. R. Schwartzberg, R. D. Keys, and T. F. Kiefer

FEB 1970

Technical Management
NASA Lewis Research Center
Cleveland, Ohio
Liquid Rocket Technology Branch
J. R. Faddoul

FOREWORD

This interim report was prepared by Martin Marietta Corporation
under contract Number NAS3-11203, "Cryogenic Alloy Screening," for
the Lewis Research Center of the National Aeronautics and Space Ad-
ministration. The work was administered under the technical direc-
tion of the Liquid Rocket Technology Branch, with Mr. James Faddoul
acting as Project Manager.

Mr. F. R. Schwartzberg served as Martin Marietta Program Mana-
ger and Mr. R. D. Keys as Technical Director. Mr. T. F. Kiefer was
responsible for the testing effort. The authors gratefully acknowl-
edge the assistance of the following colleagues: L. M. Hanzlick,
J. LeBeau, S. H. Osgood, and H. J. Brown. We particularly wish to
acknowledge the work performed by Dr. D. Eash of Los Alamos Scien-
tific Laboratories to provide us with data on dynamic modulus and
thermal expansion behavior.

CRYOGENIC ALLOY SCREENING

by

F. R. Schwartzberg, R. D. Keys and T. F. Kiefer

ABSTRACT

Three materials, 2021-T81 and X7007-T6 aluminum alloys and
cryogenically stretched 301 stainless steel, were evaluated in
order to determine their mechanical properties, static fracture
toughness, cyclic flaw-growth behavior and sustained load thresh-
old stress intensity. Testing was performed for both parent metal
and welded material at 70, -320, and -423°F. Surface flaw and
compact tension specimens were used for the fracture mechanics
portion of the evaluation.

The results showed that the two aluminum alloys were quite
tough. The 2021-T61 alloy is not greatly superior to 2014-T6
from a strength standpoint, but may be desirable from a weld-
ability standpoint. X7007-T6 exhibits excellent static and cy-
clic strength properties but appears to have a low threshold.
The cryogenically stretched stainless steel exhibits an excel-
lent combination of properties.

Additional work to further characterize the aluminum alloys
was defined and is currently being performed in the continuing
effort.

CONTENTS

SUMMARY

The objective of this program was to characterize the routine
mechanical properties, static fracture toughness, cyclic flaw-
growth behavior, and sustained load threshold stress intensity of
two newly developed aluminum alloys, 2021-T81 and X7007-T6 and a
cryogenically stretched type 301 stainless steel. The three
alloys were evaluated in both the parent metal and welded condi-
tions at 70, -320, and -423°F.

The mechanical property data showed the two aluminum alloys
to be slightly stronger than the currently used compositions. The
stainless steel exhibits excellent strength properties, compared
with titanium compositions on a strength/density basis we find it
comparable to 6Aℓ-4V titanium at 70°F but inferior in the cryogenic
range.

The static fracture toughness behavior of the two aluminum
alloys is comparable to currently used compositions. The stain-
less steel exhibits excellent toughness at 70°F, over 100 ksi $\sqrt{in.}$,
but despite a marked decrease with decreasing temperature, its
toughness at -423°F is remarkably high, considering that its
strength is about 350 ksi.

Cyclic growth behavior of the three alloys is similar to the
aluminum and titanium compositions used to compare mechanical
property and static toughness behavior.

Sustained load behavior was conducted using a limited number
of specimens and as a result was only approximate. However, our
data indicate that the parent metal X7007-T6 and welded 2021-T81
exhibit low threshold levels at 70°F. Under other conditions, the
threshold levels appeared normal. The 301 stainless steel exhi-
bits threshold levels clearly lower than reported for titanium
alloys.

As a result of the findings reported in this document addi-
tional work dealing with welded aluminum alloys was identified
and is being performed in the continuing effort.

I. INTRODUCTION

The objective of the work described in this interim report
was to evaluate the cryogenic mechanical properties, fracture
toughness, and flaw-growth characteristics of Aℓ 2021-T81, Aℓ
X7007-T6, and Type 301 stainless steel in the parent metal and
welded conditions. To do so, conventional mechanical properties
were determined for each alloy and condition and used to establish
baseline data at 70, -320, and 423°F. The static fracture tough-
ness, cyclic crack-growth behavior, and sustained-load crack-
growth behavior for each alloy were determined in the same way.
These data are presented in Appendix A and are summarized in the
body of the report.

The entire program consists of eight tasks. Brief descriptions
of each task are as follows:

Task I - Literature Survey

The literature survey is to be conducted to obtain infor-
mation on fabrication techniques, mechanical properties,
and methods of acceptance testing of the three alloys to
determine their suitability for structural applications.

Task II - Parent Metal Properties

Characterization of mechanical properties, static fracture
toughness, cyclic crack-growth behavior, and sustained-
load crack growth behavior of the three subject alloys
in the parent metal condition.

Task III - Weld Metal Properties

Same as Task II except for welded joints.

Task IV - Influence of Welding Procedure on Fracture
          Toughness of Aluminum Alloys

Determination of the effect of welding procedure and de-
fect location on the static fracture toughness of 2021-
T81 and X7007-T6 aluminum alloy. Alloy 2014-T6 included
for comparison purposes.

Task V - Static Fracture Toughness Characterization of
        Aluminum Welds

Determination of behavior of optimized welds and effect
of weld repair of same alloys evaluated in Task IV.

Task VI - Environmental Threshold Stress Intensity Evalua-
        tion

Determination of effect of defect location and a deleterious
environment on sustained load threshold of the alloys
evaluated in Tasks IV and V.

Task VII - Response of Materials to a Corrosion Environ-
        ment

Determination of general and stress corrosion resistance
of the three aluminum alloys described above plus several
additional compositions for control purposes.

Task VIII - Data Evaluation

Analysis of test data from all tasks data and comparison
of behavior with compositions currently being utilized
for structural service.

In this interim report, the complete results of Tasks II and
III are presented. In addition, the stainless steel literature
survey portion of Task I is presented. Data analysis (Task VIII)
is presented for Task II and III.

Cryogenic metallic materials available on the market have
invariably been compositions whose properties represent a com-
promise. There have been few attempts to develop alloys speci-
fically for low-temperature applications. The two new aluminum
alloys recently developed by Alcoa* (2021-T81 and X7007-T6) that
are intended to provide high strength, toughness, and weldability
represent the first attempt to meet the needs of those designing
and building structures that must withstand low temperatures.
Cryogenically stretched type 301 stainless steel, chemically
modified to provide improved toughness compared with cryogenically-
stretched, normal-grade type 301, is another new material made
specifically for cryogenic service.

Industry's requirements for flightweight structures has led to the use of high-strength materials, particularly in solid-propellant rocket motor cases. Materials selected for liquid-propellant tanks and pressurization spheres that operate at cryogenic temperatures normally exhibit moderate strength at room temperature; however, because their strength increases with decreases in temperature, these materials can also join the high-strength category at cryogenic service temperatures.

At high-strength levels, many materials become brittle and fracture, often because of small defects or flaws that are produced during the manufacturing process. Such defects can cause materials to fracture even though the stress is below the level at which yielding and plastic deformation occurs.

For many years, researchers have studied brittle fracture in metallic materials. Although interest has increased through the years, catastrophes often spark additional concern. Such was the case when welded ship structures frequently failed in World War II, and more recently, when failures were noted in high-strength missile tanks. Two active committees have been created to study the subject: ASTM's Committee on the Fracture Testing of High-Strength Sheet Materials, and ASME's Research Committee on the Prevention of Fracture in Metals.

For many years, the structural design approach has often been of the handbook type, based on conservative industry code requirements. In some cases where high efficiency was required, the build-it-and-test-it approach has been used to identify the weak links for subsequent "beefing up." Although the latter approach has some merit, it is not the best engineering approach; for certain spacecraft applications, service testing has been difficult to simulate. Not even the more conservative approach of using large safety factors has proved completely trustworthy, because brittle fractures and other types of failures have still occurred -- often at stresses well below the design yield strength.

Subsequent failure analyses often showed that designers had not always considered every pertinent factor when establishing their design, and that, in many cases, the simulated service tests to support the designer were not always valid. In the past, our ability to simulate these tests has been poor. This ability, however, has improved significantly as a result of greater knowledge of the effect of defects on strength and the introduction of linear elastic fracture mechanics as a tool to relate the permissable stress to the allowable defect size.

II. BACKGROUND AND ANALYTICAL TECHNIQUES

A. STRESS INTENSITY FOR SURFACE-FLAWED SPECIMENS

Irwin (Ref 1) has estimated the effect of shape on stress intensity in a semielliptical surface flaw subject to a normal load by using the following equation:

$$K_I = \frac{M_1 \sqrt{\pi a}\ \sigma \left(\sin^2 \varphi + \dfrac{a^2}{c^2} \cos^2 \varphi\right)^{\frac{1}{4}}}{\left[\Phi^2 - 0.212 \left(\dfrac{\sigma}{\sigma_{ys}}\right)^2\right]^{\frac{1}{2}}}$$

where:

M_1 is a free-surface correction factor originally reported as 1.2, but now generally taken as 1.1;

σ is the applied tensile stress;

a is the length of the semiminor axis;

φ is the angle between the major axis and any point on the flaw front;

c is the length of the semimajor axis;

Φ is the complete elliptical integral of the second kind and may be expressed by:

$$\Phi = \int_0^{\pi/2} \sqrt{1 - \frac{c^2 - a^2}{c^2} \sin^2 \varphi}\ d\varphi.$$

The term $\left[\Phi^2 - 0.212 \left(\dfrac{\sigma}{\sigma_{ys}}\right)^2\right]$ is commonly called Q. By letting $\varphi = 90°$ the limiting equation for stress intensity can be expressed as:

$$K_I = 1.1 \sqrt{\pi}\ \sigma \left(\frac{a}{Q}\right)^{\frac{1}{2}}.$$

Several modifications have been made to the above approximate solutions in order to account for the effect of the proximity of the back face. These have been reported by Kobayashi (Ref 2) and Smith (Ref 3). Recent experiments performed by Larson (Ref 4) and Smith (Ref 5) using cast epoxy specimens indicate that the back-surface correction factors are approximately 20 to 25% lower than those predicted by Smith (Ref 3).

In this work, attempts were made to avoid making cracks deep enough to require back-surface correction of the stress-intensity factor. Back-surface correction factors were not used because there is still some uncertainty as to the magnitude of the elastic magnification factors, and in addition, the effects of plasticity have still not been assessed.

B.   STRESS INTENSITY FOR COMPACT-TENSION SPECIMENS

Optimization studies of the Westinghouse WOL (wedge opening loading) specimen have resulted in a modification of the T design to accommodate dual pin loading. The resulting design has been designated the compact-tension (CT) specimen. Increasing the crack length-to-width ratio (a/W) to a nominal value of 0.5 has effected a reduction in the size and load requirements. The principal advantage of the CT specimen is that it has a higher toughness measurement capacity than the WOL specimen. For example, the 1X-WOL specimen has a tentative capacity (defined by the ratio K_{Ic}/σ_{ys}) of 0.45; the 1T-CT specimen is estimated to have a capacity of 0.63. For the rather tough aluminum materials tested in this program, a high measurement capacity was essential.

Wessel (Ref 6) shows that the stress intensity equation for the CT specimen is of the form:

$$K_I = Y \frac{P \sqrt{a}}{BW},$$

where:

$$Y = 23.12 - 67.67\left(\frac{a}{W}\right) + 97.31\left(\frac{a}{W}\right)^2 \text{ for } \frac{a}{W} = 0.4 \text{ to } 0.6$$

$$\text{and } \frac{H}{W} = 0.60;$$

H = half beam height;

P = load;

a = crack length;

B = thickness;

W = beam width.

Experience with the use of compact-tension specimens has shown that the crack front does not grow uniformly. Normally, the crack front grows in a concave manner -- that is, deeper in the center. Therefore, it is necessary to adjust the crack-length measurements to provide a weighted average. In this work, a weighted average of four times the mid-thickness plus the depth at each surface has been used to represent the average crack depth.

C. CYCLIC FLAW GROWTH

During cyclic loading, a small amount of growth is considered to have occurred during each load cycle. If the increment of crack extension that occurs during a specific number of cycles can be determined, it is possible to prepare a crack extension curve of crack length (a) vs number of cycles (N). The slope of the curve at any point is the crack growth rate (da/dN). From an experimental standpoint, this technique is relatively simple to apply for through-cracked specimens. However, for semielliptical surface flawed specimens this is not readily accomplished because the critical crack parameter, the crack depth, is not visually measurable from the surface. Because the shape of the crack usually changes as the crack grows in depth, determining the crack width, which is readily discernible on the surface, does not provide quantitative information.

Boeing (Ref 7 and 8) has evaluated flaw-growth behavior in surface-flawed specimens using the "end point analysis" method. In this method, the initial stress intensity $\left(K_{Ii}\right)$ is plotted against the number of cycles to failure, and these data are converted to an initial crack size (a/Q) vs N curve at a given stress. From this curve, the slope or crack growth rate [d(a/Q)/dN] can be obtained for a specific a/Q. The latter can be converted to a value of K_I at a given stress, and as a result, a stress

intensity vs growth rate curve can be obtained.

This method is dependent on several factors:

1) The specimen must be taken to fracture;

2) The critical crack depth must be sufficiently less
    than the thickness to avoid plasticity effects;

3) The critical crack size must be distinguishable
    from the rapid fracture;

4) A semielliptical shape must be maintained.

Satisfying these criteria gives a simple method for determining
crack growth.

Another method, used in this program, can be called the
"linear interpolation" technique. This approach is to minimize
the amount of flaw growth, thereby making the initial and final
stress intensities similar enough so that a rate based on the
initial and final crack sizes is a valid linear interpolation of
the slope of the crack size vs number of cycles curve. It is
important to make a small linear interpolation because the error
that can result in a power function relationship, in this case
one theorized to be a fourth power relationship, can be quite
significant. As described elsewhere in this report, using the
linear interpolation method, multiple data can be obtained from
a single surface-flawed specimen by flexural fatiguing between
increments of axial cyclic growth.

III. EXPERIMENTAL PLAN

The object of this investigation was to characterize the mechanical properties and behavior of the three subject alloys and compare them to those of currently-used structural alloys.

The program consisted of the following tasks:

Task I   - Literature Survey;

Task II   - Parent-Metal Evaluation;

Task III   - Weld Metal Evaluation;

Task IV   - Influence of Welding Procedure on Fracture Toughness of Aluminum Alloys;

Task V   - Static Fracture Toughness Characterization of Aluminum Welds;

Task VI   - Environmental Threshold Stress Intensity Evaluation;

Task VII   - Response of Materials to a Corrosive Environment;

Task VIII   - Data Evaluation.

The following sections discuss the nature of the work required under each task.

A. TASK I -- LITERATURE SURVEY

Two literature surveys were to be conducted, one for the aluminum alloys and one for the stainless steel, to collect data on the mechanical properties, fabrication techniques, and acceptance tests associated with each material.

The aluminum survey is being conducted by Martin Marietta Corporation and will be included in the final report. The stainless steel survey was subcontracted to Arde, Inc; as the developers of the cryogenic stretch-forming process, they were the obvious choice for the performance of this subtask. The stainless steel survey is presented in Appendix B.

B.   TASK II -- PARENT-METAL EVALUATION

The following nominal thicknesses were planned for use in this evaluation:

Cryoformed Stainless Steel = 0.125 in.;

Aℓ 2021-T81   = 1.00 in.;

Aℓ X7007-T6   = 1.00 in.

Tests were conducted at three temperatures:

70°F (ambient air);

-320°F (liquid nitrogen);

-423°F (liquid hydrogen).

During the experimental program, the configuration and orientation of some specimens had to be changed in order to obtain the required information. These changes are discussed later in the report.

1.   Mechanical Property Tests

The uniaxial tensile data gathered for each alloy included:

1)   Ultimate strength;   6)   Strain-hardening exponent;

2)   Yield strength;   7)   Poisson's ratio;

3)   Elongation;   8)   Conventional stress-strain behavior;

4)   Reduction in area;

5)   Elastic modulus;   9)   True stress-strain behavior.

The testing was conducted in both the longitudinal and transverse directions. Six replicate tests were performed for each condition and temperature.

2.   Static Fracture-Toughness Tests

Static fracture-toughness tests were conducted for each alloy in the longitudinal and transverse directions. Triplicate tests were performed for each condition and temperature.

3. Cyclic-Load Flaw-Enlargement Tests

Cyclic-load flaw-enlargement tests were conducted for each alloy and temperature in one grain direction. Triplicate specimens were tested for each condition and temperature.

4. Sustained-Load Flaw-Enlargement Tests

Sustained-load flaw-enlargement tests were conducted for each alloy and temperature in one grain direction. Triplicate specimens were tested for each condition and temperature.

C. TASK III -- WELDED METAL EVALUATION

The testing conducted in this task was essentially identical to that described in the preceding section, except that only one grain direction was evaluated. The aluminum alloys were tested in the as-welded condition; the stainless steel was tested in the aged condition.

D. TASK IV -- INFLUENCE OF WELDING PROCEDURE ON FRACTURE TOUGHNESS OF ALUMINUM ALLOYS

In this task the effect of overheating will be compared to the normal procedure used in Task III. The effect of defect location (heat affected zone, fusion line, and weld centerline) will also be evaluated. For comparison purposes, alloy 2014-T6 will also be studied. A second heat of 2021-T81 and X7007-T6 will be obtained for this work.

E. TASK V -- STATIC FRACTURE TOUGHNESS CHARACTERIZATION OF ALUMINUM WELDS

Using an optimized weld procedure from Task IV, toughness will be determined for the three alloys (2021-T81, X7007-T6, and 2014-T6). The effect of weld repairing will also be determined.

F.   TASK VI -- ENVIRONMENTAL THRESHOLD STRESS INTENSITY
     EVALUATION

     The effect of defect location and environment (air and a de-
leterious environment) on the sustained load threshold stress
intensity of the three alloys (2021-T81, X7007-T6, and 2014-T6)
will be determined.

G.   TASK VII -- RESPONSE OF MATERIALS TO A CORROSIVE
     ENVIRONMENT

     In this task, the general and stress corrosion resistance
(in a simulated laboratory and actual seacoast environment) of
the three above alloys plus several additional compositions for
control purposes will be evaluated.

H.   TASK VIII -- DATA EVALUATION

     The data obtained from the alloy tests described in the pre-
ceding sections will be compared to the data for currently-used
alloys in order to determine whether the new alloys were supe-
rior to present materials.

IV. MATERIAL PROCUREMENT AND PROCESSING

A. ALUMINUM ALLOYS

The aluminum alloy plate purchased from Alcoa was 84 in. long,
36 in. wide, one in. thick, and was fully heat-treated. All sam-
ples of each alloy were obtained from a single batch of material.
Alcoa's certification report listed these properties at room tem-
perature:

Aluminum Alloy*	Lot No.	Tensile Strength (ksi)	Yield Strength (ksi)	Elongation (%)
X2021-T8E31	105-267	72.0	63.0	3.8
X7007-T6E136	105-266	72.2	66.7	14.0

*The designations for the alloys are those used at
the time the plates were purchased. The experi-
mental or X designation for the 2021 alloy has since
been removed. In this report, the two alloys will be
designated as 2021-T81 and X7007-T6.

Because the elongation level of the Aℓ 2021 appeared abnormally
low, standard 0.505-in.-diameter round bars were machined and
tested in both the longitudinal and transverse grain directions.
The test data shown below confirmed that the transverse elonga-
tion was low.

Grain Direction	Tensile Strength (ksi)	Elongation (%)
Longitudinal	72.2 71.6	8.0 8.5
Transverse	70.8 70.6	4.5 4.5

Alcoa was contacted in order to determine whether this material
was representative of the subject alloy. Photomicrographs of
the structure and a small quantity of material were forwarded to
Alcoa for their review and analysis. Alcoa reviewed the complete
processing records for this material and found no basis for recom-
mending that the material be rejected, although they did confirm
that the ductility was at the low end of the specification limit.

At the request of the NASA project engineer, the Al 2021 was
further evaluated to determine whether the cryogenic ductility
was adversely affected. The test results showed that there was
no further loss of ductility with reductions in temperature, rather
only the normal increase in elongation observed for aluminum alloys
(see Table IV-1).

Table IV-1   Strength and Ductility of Parent Metal Specimens[*]
             (2021-T81 Aluminum Alloy)

Temperature (°F)	Ultimate Strength (ksi)		Elongation (%)	
	Longitudinal Direction	Transverse Direction	Longitudinal Direction	Transverse Direction
70	70.9 72.0 71.4	71.0 71.7 71.4	9.0 8.5 8.8	4.0 5.0 4.5
-320	86.7 87.5 87.1	88.4 87.7 88.0	11.5 11.2 11.4	6.5 7.9 7.2
-423	99.9 99.8 99.8	101.7 99.7 100.7	13.4 14.4 13.9	11.0 11.0 11.0

[*] 0.250-in.-diameter round bar specimens.

Panels of both alloys were prepared for welding in the follow-
ing manner. First the alloys were degreased in trichlorethylene
vapor, soaked in an alkaline solution for 15 minutes, and deox-
idized for 10 minutes. Then the edges were filed, and after the
corners were broken slightly, a one-in.-wide surface next to the
edge was cleaned with a wire brush. The specimens were welded
transverse to the grain direction using a direct-current, straight-
polarity, 800-amp Sciaky Zero Error supply and an Airline Welding
fixture. One pass was made on each side without using filler wire.
This was followed by making a second pass on each side using filler
wire (the Al 2021 was welded with Al 2319 filler; the Al X7007 was
welded with Al 5356 filler). The specimens were air-cooled to
room temperature after each pass.

Welding Parameters	Aluminum Alloy	
	2021	X7007
Current (amp)		
1st Pass	575	580
2nd Pass	350	375
Voltage (v)		
1st Pass	12	11.5
2nd Pass	13	13
Torch Speed (in./minute)		
1st Pass	6	6
2nd Pass	6.5	6.5
Wire Feed (in./minute)		
2nd Pass	15	10
Helium Gas Coverage (cfh) All Passes	110	110

Subsequent radiographic inspection showed no evidence of defects or porosity and the welds were declared acceptable. No post-weld aging was used.

A metallographic examination of each alloy showed structures typical for 2000- and 7000-series alloys. Figure IV-1 shows a longitudinal section of 2021-T81 parent metal. This alloy exhibits slightly more second-phase precipitate than lower-strength 2000-series compositions. A macro section of a 2021 welded joint is shown in Fig. IV-2. The heat-affected zone (see Fig. IV-3) shows depletion, presumably of copper, along the grain boundary and around the intermetallic particles. This depletion might cause reductions in strength and in stress-corrosion resistance.

An examination of the X7007-T6 alloy showed the highly-oriented structure typical for high-strength 7000-series compositions. The amount of second-phase precipitate in the X7007 (see Fig. IV-4) was slightly less than that observed in 7075 alloy (see Fig. IV-5). Figure IV-6 shows a macrosection of a X7007 welded joint; the rather significant mushrooming effect noted near the surface in the heat-affected zone probably results from deformation at the welding temperature, due to the rather low yield strength of aluminum-zinc alloys at high temperatures. An examination of the heat-affected zone showed grain-boundary coarsening rather than the recrystallization that commonly is found in other aluminum alloys.

Fig. IV-1 Microstructure of Parent-Metal
           2021-T81; Longitudinal Direction
           (Enlarged 100X)
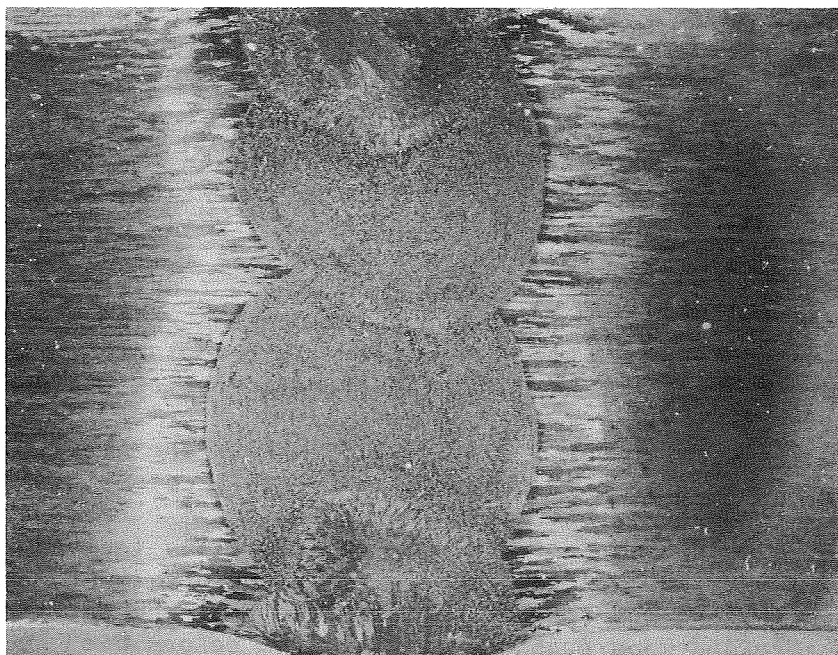
Fig. IV-2 Macrosection of a 2021-T81
           Welded Joint (Enlarged 3X)

Fig. IV-3 Microstructure of 2021-T81
           Heat-Affected Zone Showing
           Depleted Zones (White Areas)
           (Enlarged 400X)

Fig. IV-4 Microstructure of Parent-
           Metal X7007-T6; Longitudinal
           Direction (Enlarged 100X)

Fig. IV-5 Microstructure of Parent-
           Metal 7075-T6; Longitudinal
           Direction (Enlarged 100X)

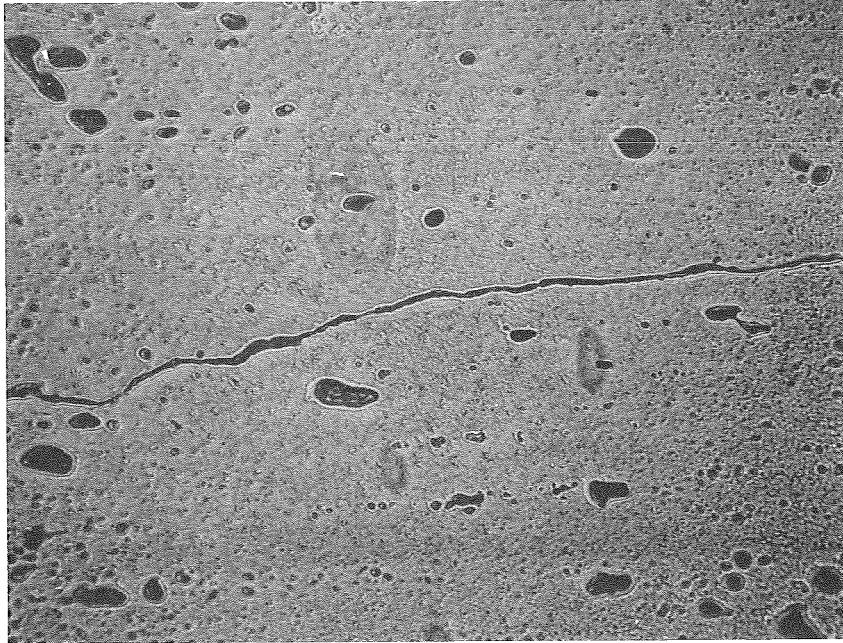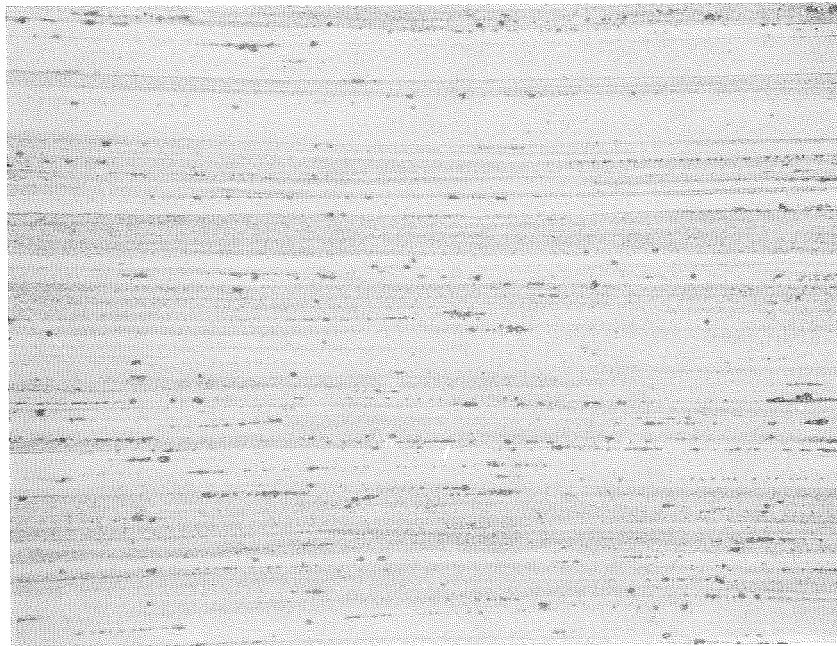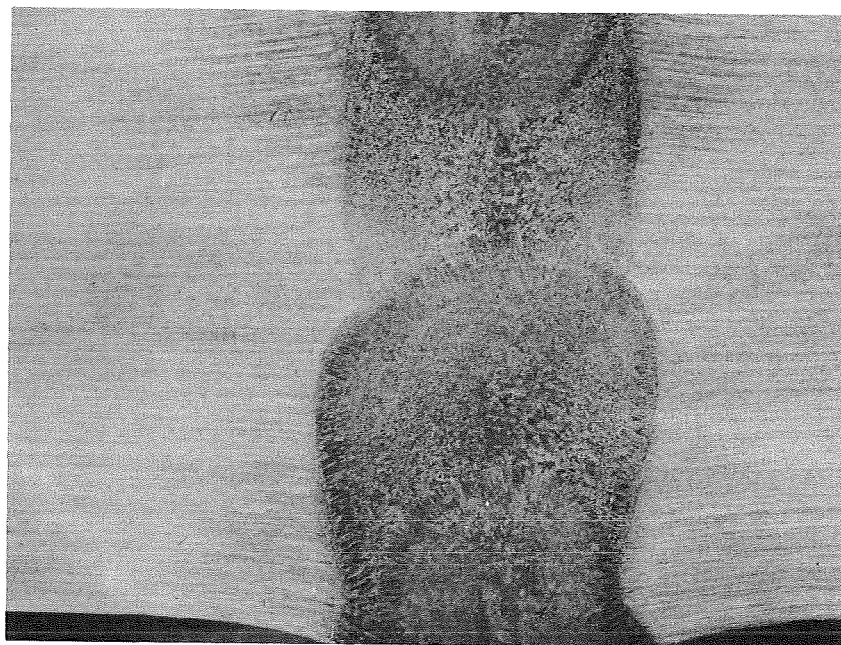Fig. IV-6 Macrosection of an X7007-T6
           Welded Joint (Enlarged 3X)

B. STAINLESS STEEL ALLOY

Arde, Inc supplied three 120-in.-long by 36-in.-wide by 0.140-in.-thick sheets of modified, Type 301, low-silicon (less than 0.1%) stainless steel (Latrobe Heat No. 50793) to Martin Marietta.

Martin Marietta cut the material into panels for subsequent cryogenic stretching in liquid nitrogen (-320°F). These panels had a gage width of 13 in. and a reduced section length of 48 in.

Next, the panels were sent back to Arde, Inc, where they were welded, re-annealed, pickled, and passivated. Then the panels were shipped back to Denver, where they were stretched and ma- chined into test coupons. Finally, the coupons were returned to Arde for aging, cleaning, and passivating.

The panels were stretched in our 500,000-lb testing machine. The machine was placed horizontally and a large pan, approximately 10 ft long x 3 feet wide x $1\frac{1}{2}$ ft deep, was placed in the throat of the machine to provide the environmental control for stretch- ing. A typical stretched panel is shown in Fig. IV-7.

Of the first nine panels stretched, six were satisfactory. In the other three, there were premature failures in the joint between the grip and the test section. This weld was to have been made automatically, but was found to be a manual weld that exhib- ited very poor weld penetration. Three additional panels were fabricated using automatic welding equipment. A fourth panel, which showed indications of cracks, was returned to Arde for auto- matic rewelding, but was only repaired. Back at Denver, the three automatically-welded panels were stretched satisfactorily, but the repaired panel failed during stretching.
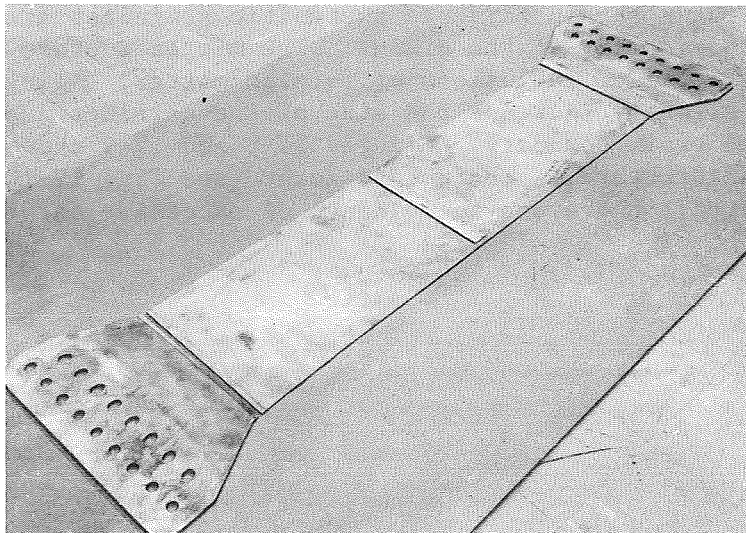
Fig. IV-7   Typical Cryogenically-Stretched Stainless Steel Panel

Single tension specimens were machined from each of the first nine stretched panels. No tensile specimens were taken from the four additional panels. These specimens were aged at 790°F for 2 hr, air-cooled, and then tensile-tested at 70°F. Except for Panel 4, which obviously did not receive enough prestress to achieve the desired strength level, there was good agreement between the tensile properties of each panel. Panels 6 and 7, which failed prematurely, were as strong as the panels that were given the full prestress, and were deemed satisfactory for use.

Table IV-2   Tensile Properties of Cryogenically-
Stretched Parent Metal Specimens*

Panel Number	Cryogenic Prestress (kips)	Ultimate Strength (ksi)	Yield Strength (ksi)	Elongation (%)
1	400	235.2	232.9	7.3
2	400	234.4	228.7	8.0
3	410	236.1	231.6	6.8
4	325†	217.0	208.2	8.0
5	400	237.6	236.9	7.5
6	364†	237.3	233.5	8.0
7	380†	236.6	235.1	7.8
8	405	244.3	241.3	6.8
9	403	241.8	236.5	7.3

*Single tensile specimen removed from each panel.

†Failed during stretching.

A metallographic examination of the cryogenically-stretched stainless steel showed that the material structure was typical of that for a strain-hardened austenitic stainless steel. Twins were noted in many of the grains. The microstructure showed a very low level of inclusions or foreign matter. Aging appeared to only slightly increase the size of the carbides deposited along the grain boundary. Figures IV-8 and IV-9 show the unaged and aged structures. The welded joint (see Fig. IV-10 appeared quite normal; there was no evidence of excessive carbide precipitation.

Fig. IV-8 Microstructure of Unaged,
  Cryogenically-Stretched Type 301
  Stainless Steel; Parent Metal;
  Longitudinal Direction
 (Enlarged 250X)

Fig. IV-9 Microstructure of Aged
  Cryogenically-Stretched Type 301
  Stainless Steel; Parent Metal;
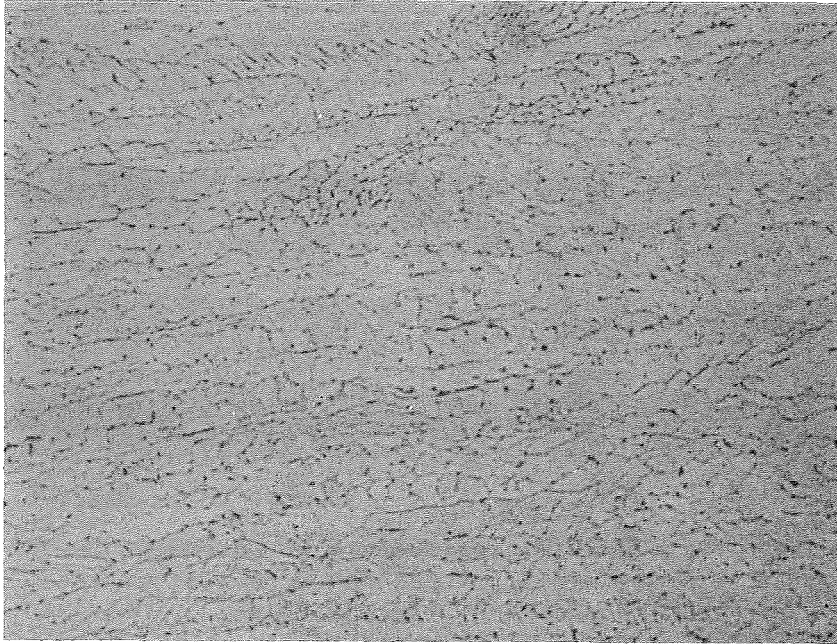 Longitudinal Direction
  (Enlarged 250X)

Fig. IV-10 Microstructure of Aged,
Cryogenically-Stretched Type 301
Stainless Steel; Welded Metal;
Longitudinal Direction
(Enlarged 250X)

V. EXPERIMENTAL PROCEDURE AND TECHNIQUES

A. MECHANICAL PROPERTY TESTING

The mechanical property testing techniques used in this program were relatively routine. Emphasis was placed on obtaining multiple strain data, and as a result, many resistance strain gages were used.

1. Specimen Design

Two types of tensile specimens were used in the aluminum investigation. One series of tests was performed using full-thickness specimens, and though this approach necessitated using loads that were higher than those on the round bar specimens, it was considered superior because it allowed us to evaluate the entire cross-section without disturbing metallurgical inhomogeneities that may exist near the surface of the rolled plate. The room-temperature specimens were friction-gripped; the cryogenic specimens were pin-loaded (Fig. V-1).

A second series of aluminum specimens was machined to the standard diameter of 0.505 in. so that their elongation, which depends on shape and gage length, could be compared with that of other alloys.

The stainless steel specimens were machined according to our standard design for sheet gage materials and were pin-loaded at all temperatures. Figure V-2 gives the specifications for these specimens.

On both the aluminum and the stainless-steel specimens, the weld beads were machined flush with the surface.

2. Instrumentation

Bonded resistance strain gages and strain beam extensometers were used to determine the strains. Bonded foil gages were used to obtain elastic-modulus and deformation data into the yield-strength range. We used series-connected gages, mounted on opposite surfaces, to compensate for small misalignments and bending. Our approach in using strain gages is to establish a full bridge circuit of strain gages and to compensate for temperature

Note: All dimensions in inches.

Figure V-1   Specifications for Cryogenic Aluminum Tensile Specimen

Figure V-2   Specifications for Tensile Specimens (Type 301 Stainless Steel)

effects in the bridge by bonding the strain gages to dummy boards
made of the same type of material being evaluated. For cryogenic
testing, the entire bridge is submerged in the liquid. Using this
technique, no external resistors or balancing systems are required.
120-ohm constantan gages (Micromeasurements No. EA-13-500-BH-120L)
were used for 70°F testing. For cryogenic testing, a special lot
of 350-ohm nichrome gages (Micromeasurements EK-13-500-BH-350LE)
was obtained.

Strain beam extensometers were used to obtain plastic defor-
mation data for stress-strain curves. Separate independent strain
records were made: one of the output of the bonded gage that was
used to measure strain in the elastic and the initial plastic
range, and the other of the output of the extensometer. This was
achieved using dual Baldwin-Lima-Hamilton (B-L-H) SRA-7 strain
recorders mounted in tandem on the testing machine or by using a
single SRA-7 recorder and an X-Y plotter (see Fig. V-3 and V-4).

Poisson's ratio was determined using bonded resistance strain
gages mounted on test specimens in the longitudinal and transverse
directions. The specimens were loaded below the elastic limit and
the data were autographically recorded.

3. Testing Procedure

Tensile specimens were tested at -320°F using a liquid nitro-
gen bath in an open-mouthed, foam-insulated cryostat. The tests
at -423°F were performed using liquid hydrogen in sealed, double-
walled, vacuum-jacketed cryostats. The stainless steel specimens
were tested in our 50,000-lb cryostat (see Fig. V-5), and the
aluminum alloy specimens were tested in the 400,000-lb-capacity
cryostat system shown in Fig. V-6.

B. STATIC FRACTURE TOUGHNESS TESTING

1. Specimen Design

The original plans called for all static fracture toughness
tests to be performed using surface-flawed specimens. During the
course of the experimental program, however, we found it necessary
to also test aluminum 1T compact-tension specimens in order to
provide baseline data for the cyclic and sustained-load tests.
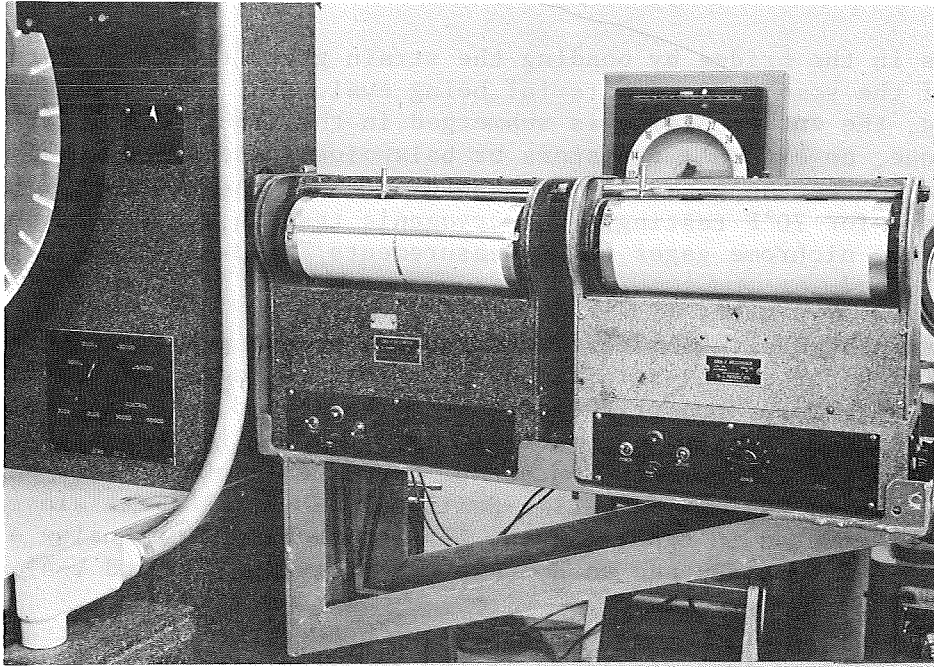
Fig. V-3   Dual SRA-7 Autographic Strain Recorders Mounted
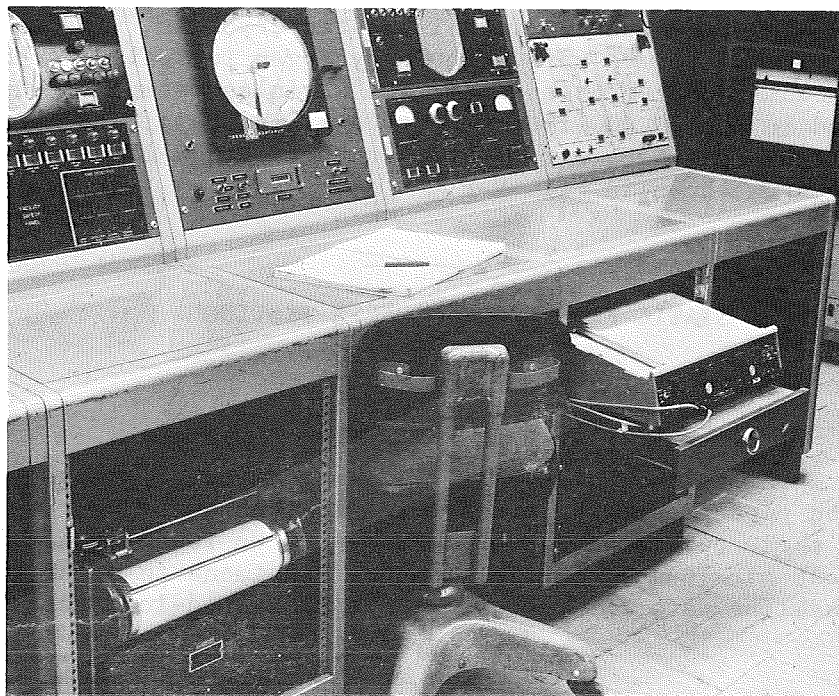   on Universal Testing Machine

Fig. V-4   SRA-7 Recorder and X-Y Plotter Used with
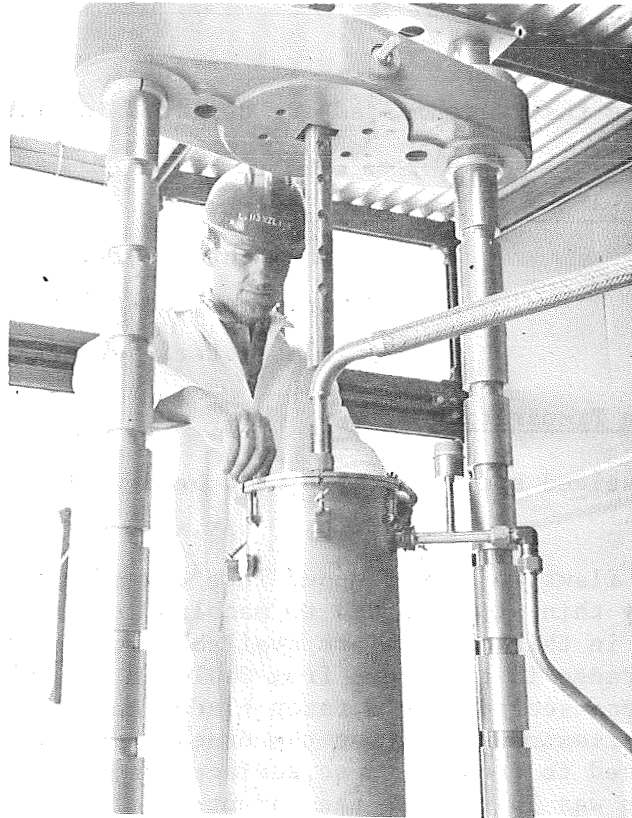   400,000-lb Testing Machine

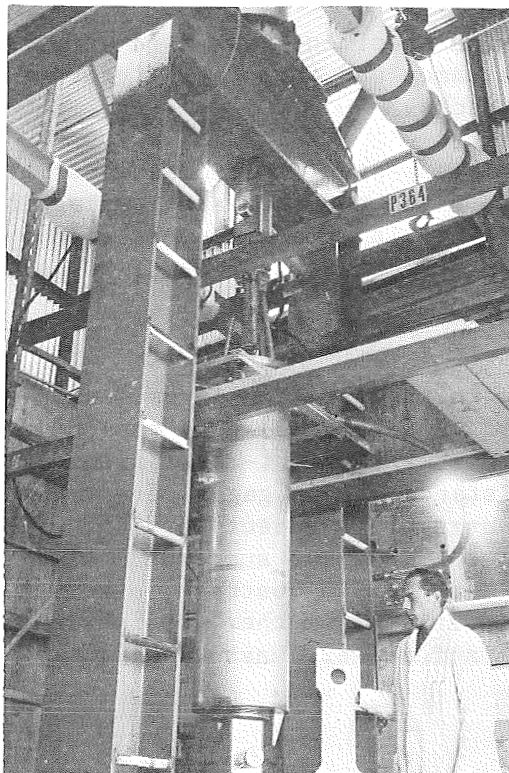Fig. V-5   50,000-1b Liquid-Hydrogen Testing System

Fig. V-6   400,000-1b Liquid-Hydrogen Testing System

The specimens that were tested are depicted in the following figures:

Figure No.	Description
V-7	Aluminum surface-flawed specimen;
V-8	Aluminum compact-tension specimen;
V-9	Stainless-steel surface-flawed specimen.

2. Specimen Preparation

In all welded specimens, the weld bead was machined flush with the surface.

Surface flaws were introduced into the aluminum specimens by using a very thin slitting saw to machine precracks. The saw blades used in this machine are available in diameters from one in. up and range in thickness from 0.010 to 0.015 in. Next, the precracks were scored with a razor blade, and the specimens were fatigued in flexure to sharpen the cracks. Figure V-10 shows the apparatus used to produce these surface cracks. The maximum outer fiber stress was 30 ksi for the parent-metal specimens and 15 ksi for the welded-joint specimens. In a few cases, high $\frac{a}{2c}$ ratios were desired and electro-discharge machining was used.

Compact-tension specimen flaws were prepared by notching the specimens with a razor and then fatiguing them in axial tension to sharpen the cracks.

Flaws in stainless-steel specimens were introduced by grinding a shallow starter notch and then arc-burning this notch to create local embrittlement. The crack was extended by bending the specimens at a maximum outer fiber stress of 90 ksi.

3. Instrumentation

Normally, no instrumentation is used when testing surface-flawed specimens. However, because "pop-in" behavior was encountered during some of the parent-metal aluminum tests, small (1/32- to 1/4-in.) resistance strain gages were located near the ends of the crack in an attempt to detect the load at which "pop-in" occurred. This technique was successful when the "pop-in" zone was sufficiently large. In contrast, attempts to calculate critical stress intensities from the "pop-in" load and the direction of the initial fracture were unsuccessful.
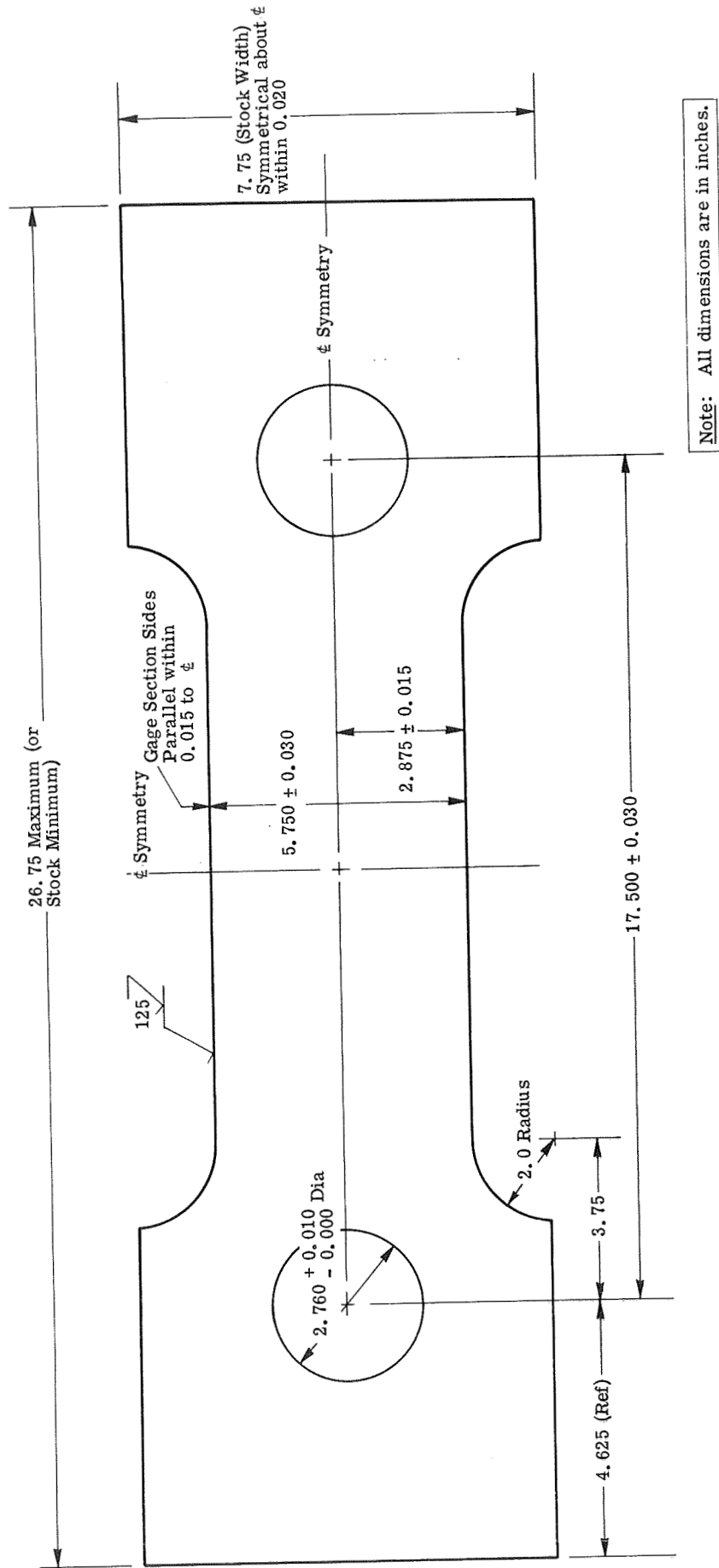
Fig. V-7 Specifications for Surface-Flawed Fracture Toughness Specimens (Aluminum Alloy)
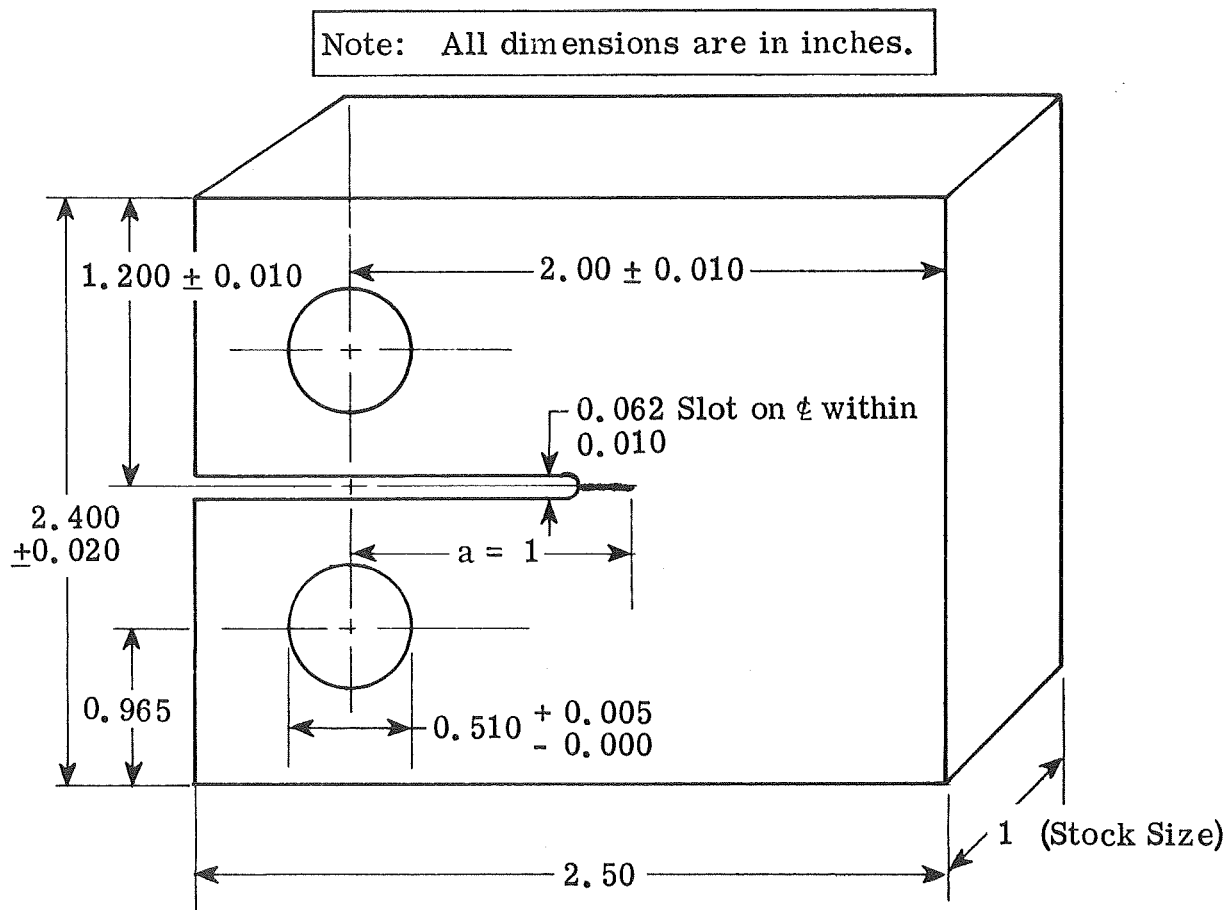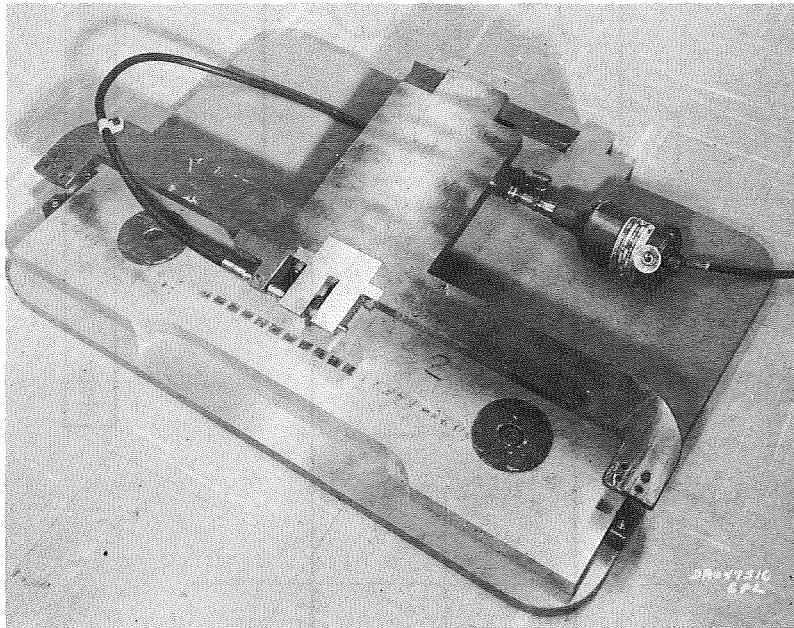
Note: All dimensions are in inches.

Fig. V-8   Specifications for Compact Tension Specimens

MCR-69-386

Note: All dimensions are in inches.

Fig. V-9   Specifications for Surface-Flawed Fracture Toughness Specimens (Type 301 Stainless Steel)

(a)   Overall View
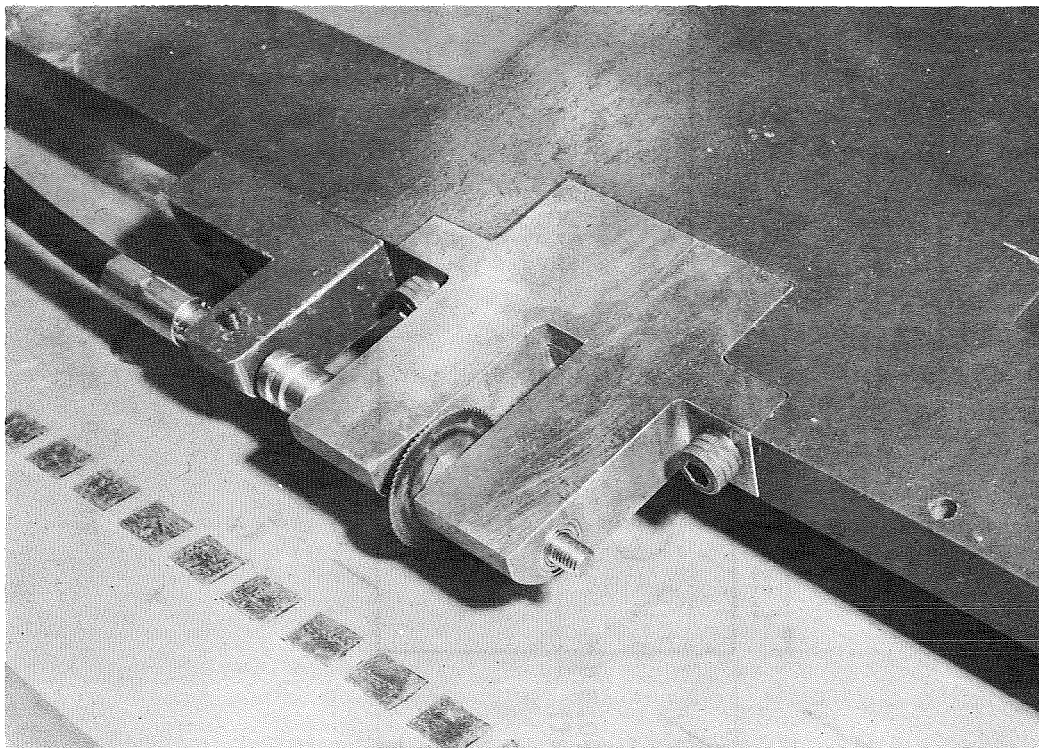
(b)   Close-up View

Fig. V-10   Apparatus for Machining Precrack in Aluminum
Fracture-Toughness Specimens

"Pop-in" in compact-tension specimens was measured with a simple beam extensometer that was clipped into standoffs attached to the edge of the specimen with self-tapping screws (see Fig. V-11). This technique is simpler, just as accurate, and less expensive than machining mounting slits across the defect.

4. Testing Procedure

Aluminum surface-flawed specimens were tested to failure or to a high percentage of the yield strength in our 500,000-lb-capacity testing machine. This testing was performed at a rate in excess of 40,000 psi per minute.

Compact-tension specimens were tested in a variety of conventional machines whose capacities ranged from 10,000 to 50,000 lb.

Stainless-steel surface-flawed specimens were tested at 70 and -320°F in a 150,000-lb-capacity system and were tested at -423°F in our 50,000-lb-capacity system.
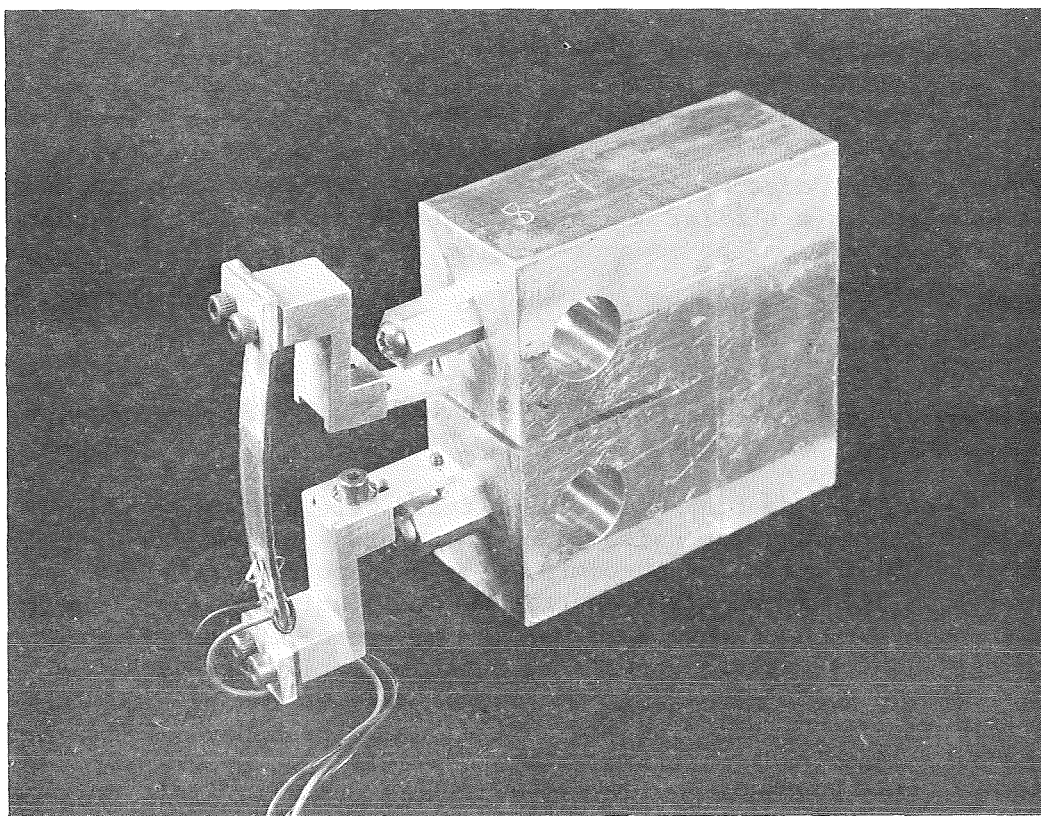

Fig. V-11   Compact-Tension Specimen with Strain Beam Extensometer

C. CYCLIC-LOAD FLAW-ENLARGEMENT TESTS

Cyclic-load flaw-enlargement tests were performed on both surface-flawed and compact-tension specimens, using the same machines that had been used for the static fracture-toughness tests.

Parent metal tests were performed using only compact-tension specimens because of the unusual behavior noted during the static fracture-toughness tests. All cyclic-test specimens were identical to those used in the static tests (ref Fig. V-7 thru V-9) and were prepared according to the procedures described in the preceding section.

No instrumentation was used for cyclic testing. Instead, we attempted to obtain multiple data for each welded-aluminum, sur-face-flawed specimen. For example, we applied axial loads to each specimen to extend the crack, tried to mark the extent of the crack by flexurally fatiguing the specimen, and repeated this process several times. Although this technique worked reasonably well, in several cases it was virtually impossible to distinguish each cyclic growth band.

We attempted to produce a minimum amount of crack growth in the compact-tension specimens so that the initial and final stress intensities would be similar. In this way, the linear interpola-tion of the slope of the crack-growth-rate vs stress-intensity curve would be reasonably accurate. The stainless-steel specimens were cycled in a similar manner. No attempts were made to obtain multiple data from the compact-tension or stainless-steel, surface-flawed specimens.

D. SUSTAINED-LOAD FLAW-ENLARGEMENT TESTS

Sustained-load flaw-enlargement tests were performed to de-termine the stress intensity below which crack growth does not occur. Compact-tension specimens were used to determine the be-havior of the parent metal and the welded aluminum alloys, and surface-flawed specimens were used to determine the behavior of the Type 301 stainless steel. No instrumentation was used for testing the stainless steel specimens. Many of the aluminum spe-cimens were compliance-checked before and after being exposed to the sustained load to determine where significant growth had oc-curred. All specimens were fatigue-marked after being exposed to the load in order to clearly show the presence or absence of slow crack extension.

The aluminum specimens were tested in 20,000-lb (dead weight) creep frames. For the -423°F tests, a creep rack was moved to our liquid hydrogen laboratory and equipped with a large cryostat (see Fig. V-12). The cryostat had a high thermal efficiency and could be operated for periods of seven or eight hr before it had to be filled with liquid hydrogen. As a result, continuous testing was achieved without the need for constant monitoring.

Because the sustained load on the stainless-steel specimens had to be greater than 20,000 lb, these specimens were tested in tensile machines which incorporated a load-holding feature. The cryostat used to test these specimens at -423°F also had a high thermal efficiency, and required a minimum of refilling.

All the tests at -320°F were performed using cryostats which had automatic fill controllers to maintain the level of the liquid nitrogen.
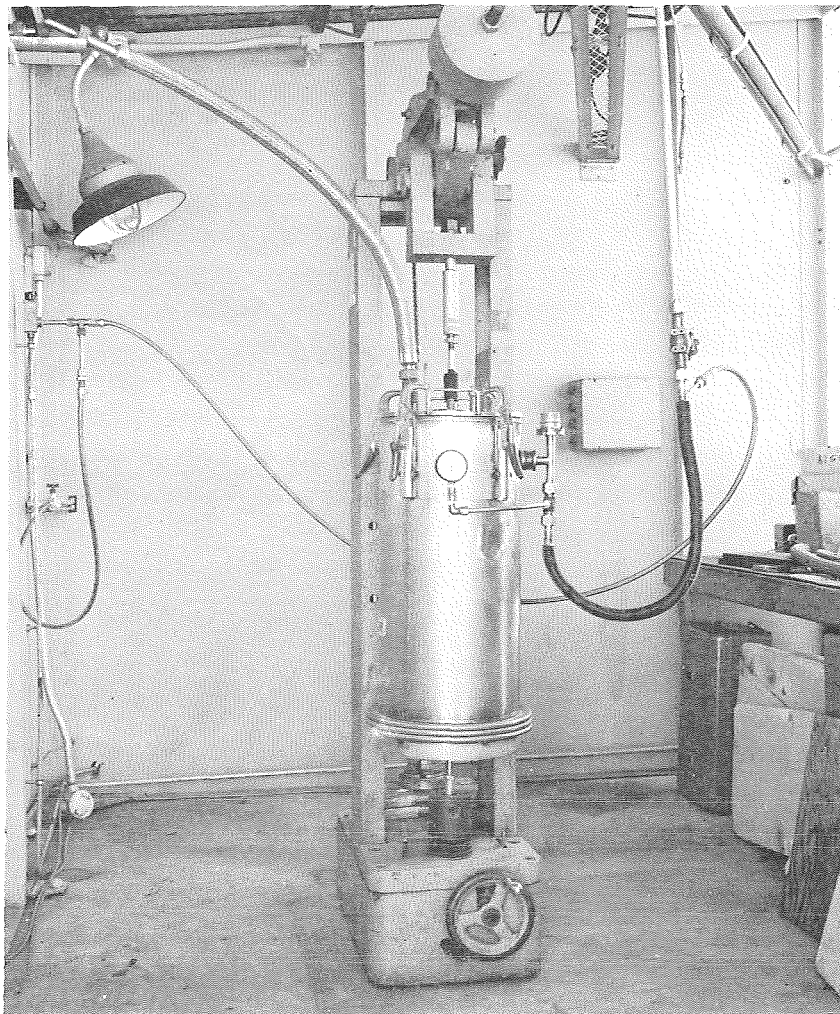
Fig. V-12   Creep Rack with Liquid-Hydrogen Cryostat

VI. EXPERIMENTAL DATA AND DISCUSSION OF RESULTS

This chapter summarizes test data in graphical and tabular form and discusses the test results. A guide to aid the reader in locating the data tabulated in Appendix A is given at the beginning of each section.

A. MECHANICAL PROPERTY TESTS

APPENDIX GUIDE - TENSILE PROPERTY TESTS		
Alloy	Description of Table	Appendix Table No.
Aℓ 2021-T81	Parent-Metal Plate Specimens	A-1
Aℓ 2021-T81	Parent-Metal Round Bar Specimens	A-2
Aℓ 2021-T81	Welded Specimens	A-3
Aℓ X7007-T6	Parent-Metal Plate Specimens	A-4
Aℓ X7007-T6	Parent-Metal Round Bar Specimens	A-5
Aℓ X7007-T6	Welded Specimens	A-6
Type 301 Stainless Steel	Parent-Metal Specimens	A-7
Type 301 Stainless Steel	Welded Specimens	A-8

1. Aluminum Alloys

a. Strength and Ductility

The tensile properties of unnotched, parent-metal Aℓ 2021-T81 are given in Table VI-1 and Fig. VI-1. Note the characteristic increase in strength that is typical of 2000-Series aluminum alloys. The ultimate strength is slightly more temperature dependent than that of the yield strength; and the elongation and the reduction in area increase with decreases in temperature. The ultimate strength, yield strength, and strain-hardening exponent exhibit little directionality, but the elongation and reduction in area do depend on the grain direction. In the transverse direction, the elongation and reduction in area are quite low.

Table VI-1   Tensile Properties of 2021-T81 Aluminum Alloy

Temperature (°F)	Grain Direction	Ultimate Strength (ksi)		Yield Strength (ksi)		Elongation (%)		Reduction in Area (%)	
		Plate Specimens	Round-Bar Specimens	Plate Specimens	Round-Bar Specimens	Plate Specimens	Round-Bar Specimens	Plate Specimens	Round-Bar Specimens
		Parent-Metal Specimens							
70	Longitudinal	72.6	71.4	63.2	62.7	7.3	8.0	7.7	10.5
-320	Longitudinal	87.8	87.4	72.9	74.9	10.5	12.0	10.3	11.9
-423	Longitudinal	99.2	99.5	80.8	79.8	9.8	12.0	11.8	18.8
70	Transverse	71.9	70.2	61.4	62.3	4.3	3.2	4.8	5.1
-320	Transverse	86.4	87.7	71.7	73.7	6.2	6.3	8.7	7.7
-423	Transverse	101.9	101.3	80.0	79.6	8.4	10.0	8.1	9.0
		Welded Specimens							
70	Longitudinal	42.3		19.2		5.8		9.8	
-320	Longitudinal	57.4		23.8		7.6		17.3	
-423	Longitudinal	68.1		28.8		9.7		9.9	
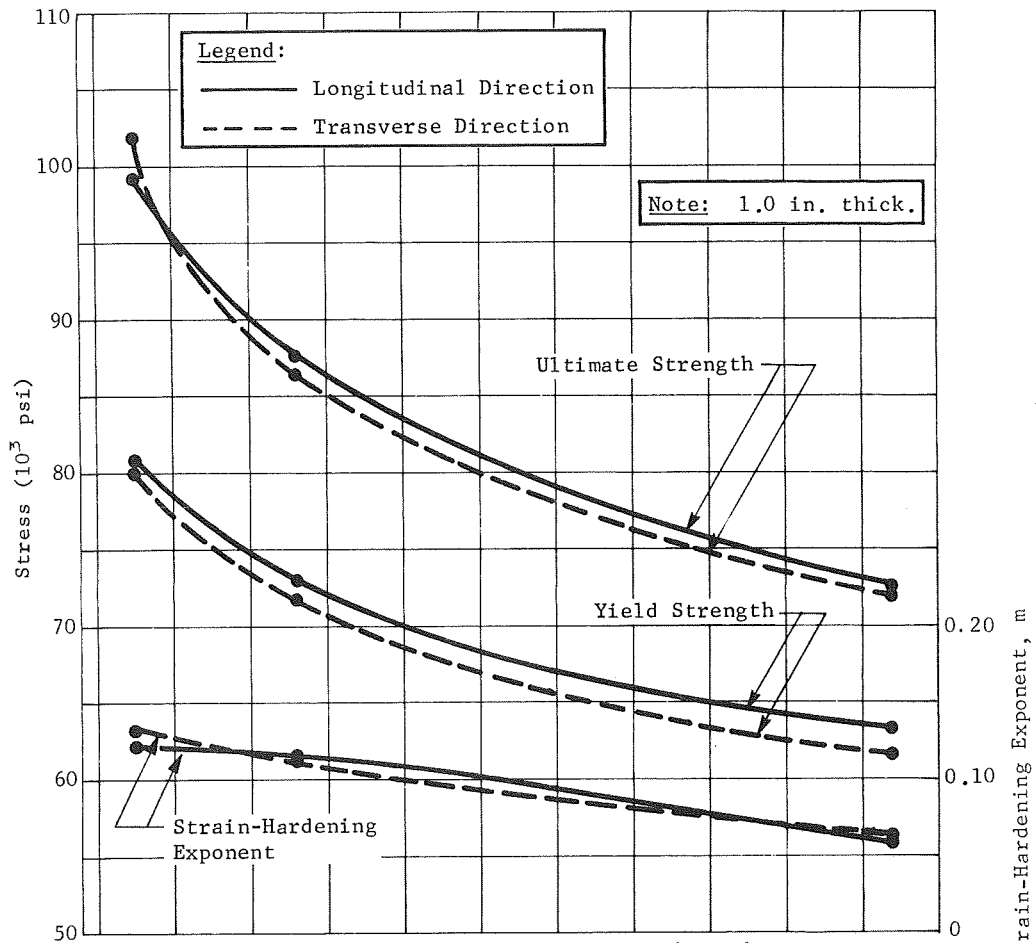
(a) Ultimate Strength, Yield Strength, and
     Strain-Hardening Exponent
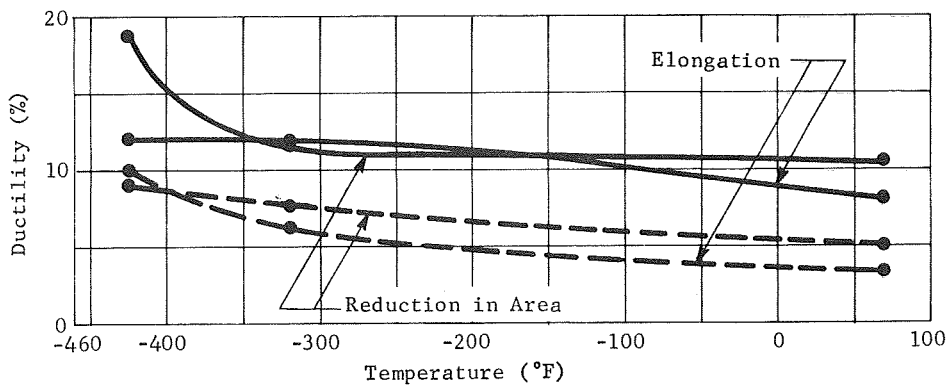
(b) Elongation and Reduction in Area

Fig. VI-1 Tensile Properties of Parent Metal
           (2021-T81 Aluminum Alloy)

The ultimate strengths and yield strengths that were de-
termined for the full-thickness plate specimens agree with the
values determined using standard 0.505-in.-diameter round bars.
Figure VI-1 was constructed using the strength data recorded for
the plates and the ductility data recorded for the round bars.

The tensile properties of unnotched Al X7007-T6 are given
in Table VI-2 and Fig. VI-2. At room temperature, the yield
strength and strain-hardening exponent for Al X7007-T6 are similar
to those for Al 2021-T81, but the elongation and reduction in area
are significantly higher. The ultimate strength of Al X7007-T6,
however, is more temperature-dependent than that of Al 2021-T81.
The ultimate strength, yield strength, and strain-hardening ex-
ponent of Al X7007-T6 are somewhat lower in the transverse direc-
tion. As is typical for 7000-series alloys, the ductility de-
creases as the temperature drops.

The most significant observation made during the Al
X7007-T6 tension tests was that a different kind of fracture
appeared at cryogenic temperatures. When the material was loaded
in the longitudinal direction, it sheared for long distances in
an interlaminar fashion, as shown vividly in Fig. VI-3.* (How-
ever, it should be emphasized that the fracture strain was quite
high.) At room temperature, the material failed in a character-
istic slant manner, but a tendency toward laminar fracture was
noted (see Fig. VI-4). When the loads were applied in the trans-
verse direction, indications of laminar fractures were found, but
were much less pronounced.

The ultimate strengths and yield strengths recorded for
the welded Al 2021-T81 specimens were typical of those for 2000-
series alloys. The yield strength (measured directly on the weld)
was rather low, and the ductility (measured over a one-in. gage
length) was quite high. These properties are summarized in
Table VI-1 and Fig. VI-5.

As shown in Fig. VI-6, the welded Al X7007-T6 specimens
exhibited excellent strength at 70°F (51 ksi) and -320°F (69 ksi),
but did not strengthen with further decreases in temperature. The
yield strength of the Al X7007-T6 at 70°F was remarkably high for
a welded specimen; the ductility was quite satisfactory, but did
decrease as the temperature was reduced (see Table VI-2 and Fig.
VI-6).

---

*From the available evidence, it appears that no delamination
occurred before the materials fractured; rather, the interlaminar
fracture was merely the mode of failure.

Table VI-2 Tensile Properties of X7007-T6 Aluminum Alloy

Temperature (°F)	Grain Direction	Ultimate Strength (ksi)		Yield Strength (ksi)		Elongation (%)		Reduction in Area (%)	
		Plate Specimens	Round-Bar Specimens	Plate Specimens	Round-Bar Specimens	Plate Specimens	Round-Bar Specimens	Plate Specimens	Round-Bar Specimens
Parent-Metal Specimens									
70	Longitudinal	72.1	73.3	68.7	69.0	17.3	13.8	30.4	36.0
-320	Longitudinal	94.8	98.1	82.0	85.5	12.1	12.7	*	8.6
-423	Longitudinal	107.5	114.0	91.6	91.7	8.2	13.0	12.1	*
70	Transverse	70.4	70.4	66.2	64.5	17.1	14.3	29.4	35.0
-320	Transverse	85.4	92.0	72.0	80.0	8.2	11.7	8.7	15.2
-423	Transverse	102.4	105.3	85.7	84.8	5.7	11.5	5.5	14.1
Welded Specimens									
70	Longitudinal	50.7		36.5		6.3		28.5	
-320	Longitudinal	68.6		42.2		10.7		10.3	
-423	Longitudinal	69.1		47.3		6.7		6.5	

*No reduction in area could be measured because of excessive delamination.
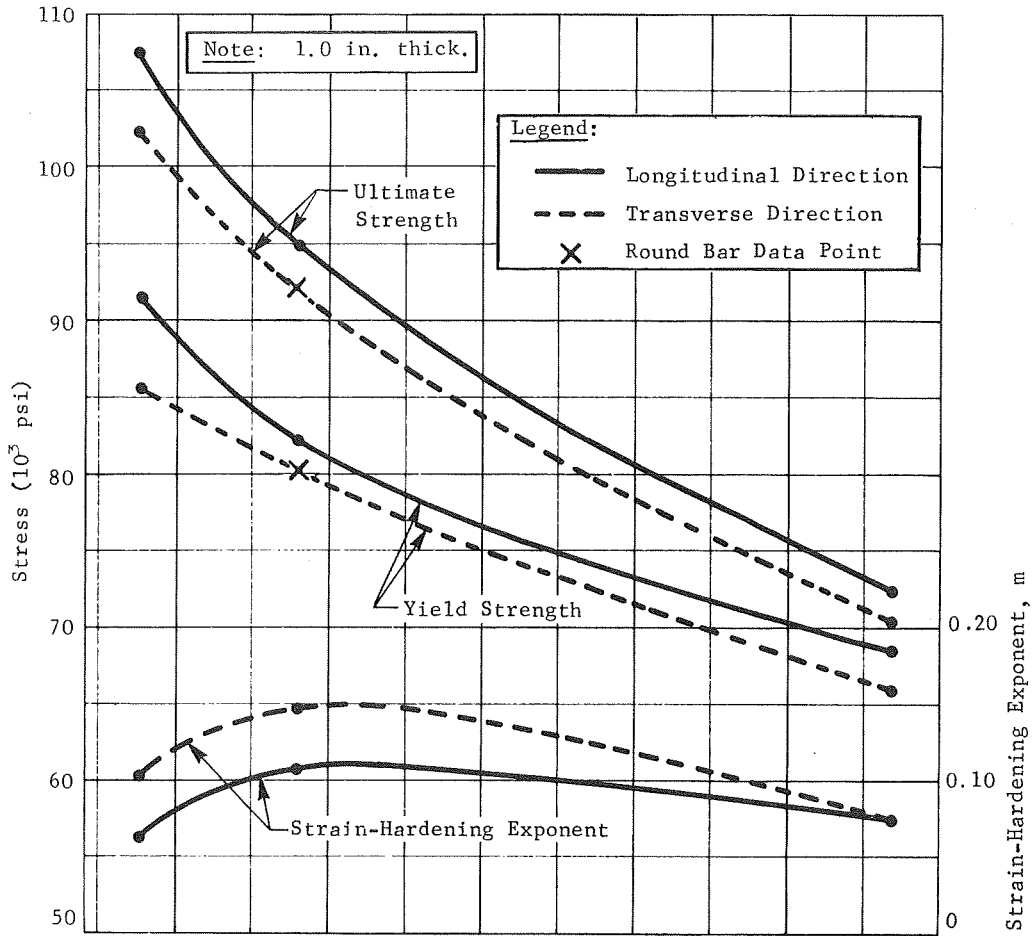
(a)   Ultimate Strength and Yield Strength
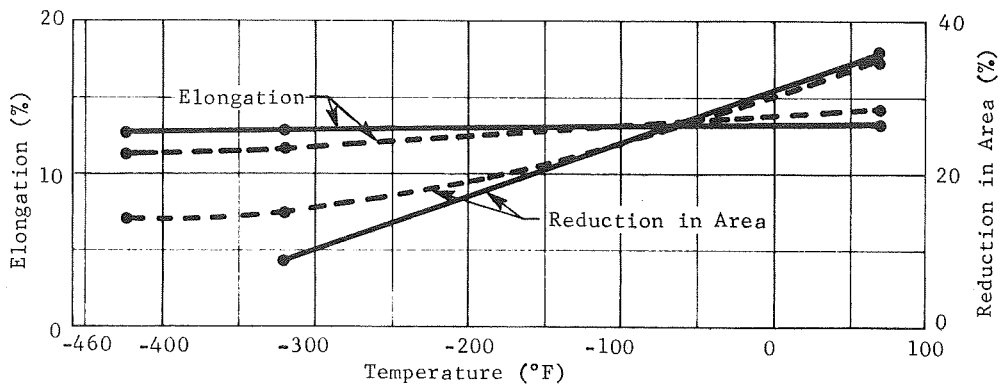
(b)   Elongation and Reduction in Area

Fig. VI-2   Tensile Properties of Parent Metal (X7007-T6 Aluminum Alloy)

Fig. VI-3 Fractured Aℓ X7007-T6
  Tension Specimen, Load Applied
  in Longitudinal Direction,
  Temperature = -320°F
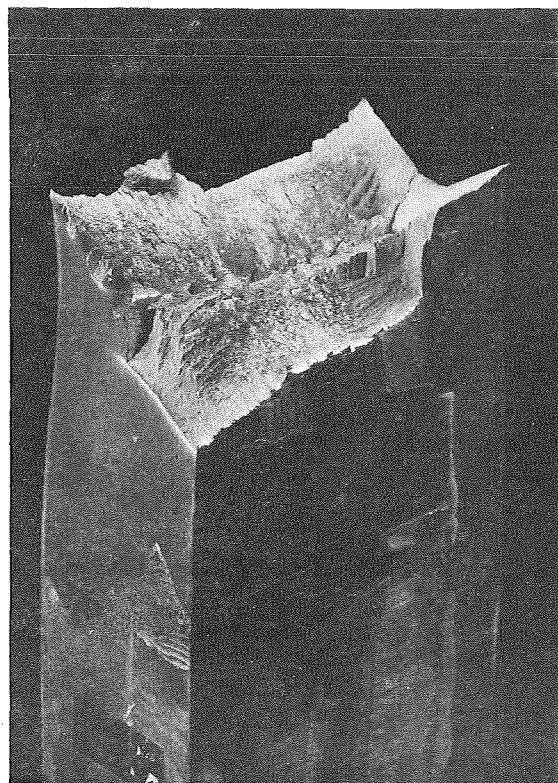
Fig. VI-4 Fractured Aℓ X7007-T6
  Tension Specimen, Load Applied
  in Longitudinal Direction,
  Temperature = 70°F

(a) Ultimate Strength and Yield Strength

(b) Elongation and Reduction in Area

Fig. VI-5 Tensile Properties of Welded 2021-T81 Aluminum Alloy

(a)   Ultimate Strength and Yield Strength
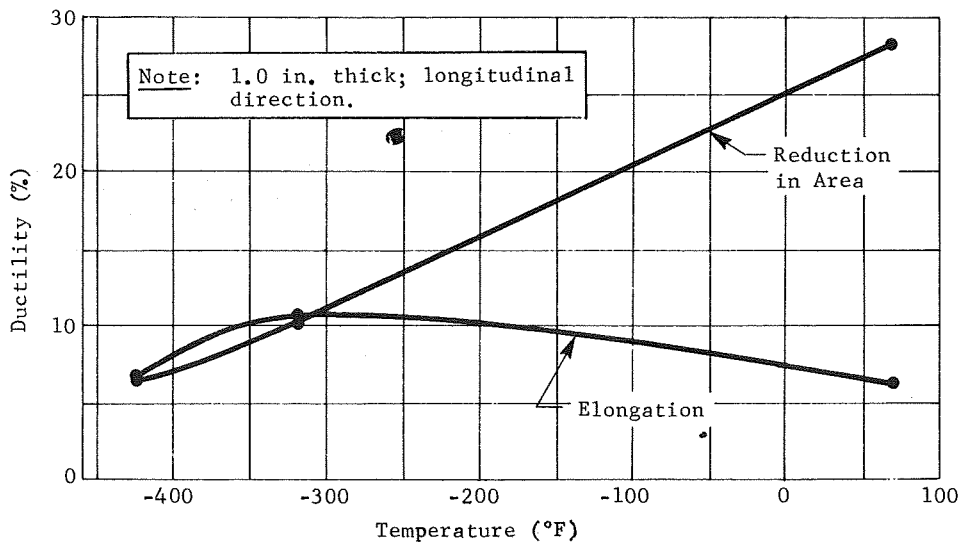
(b)   Elongation and Reduction in Area

Fig. VI-6   Tensile Properties of Welded X7007-T6 Aluminum Alloy
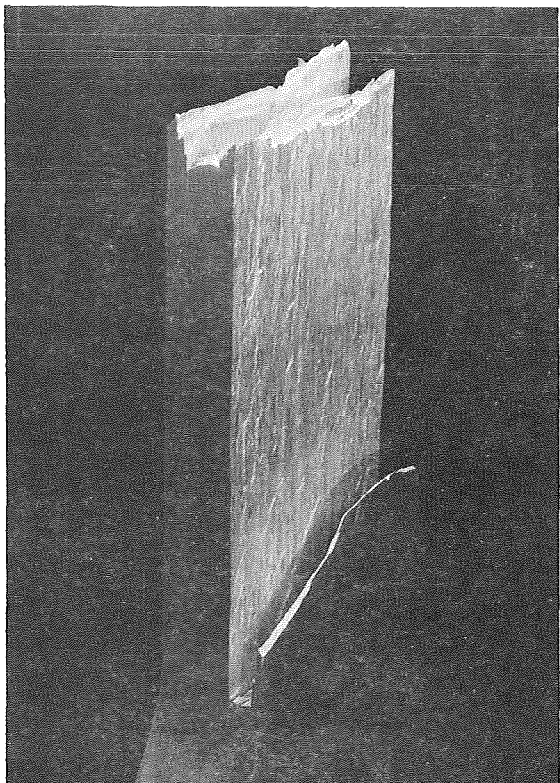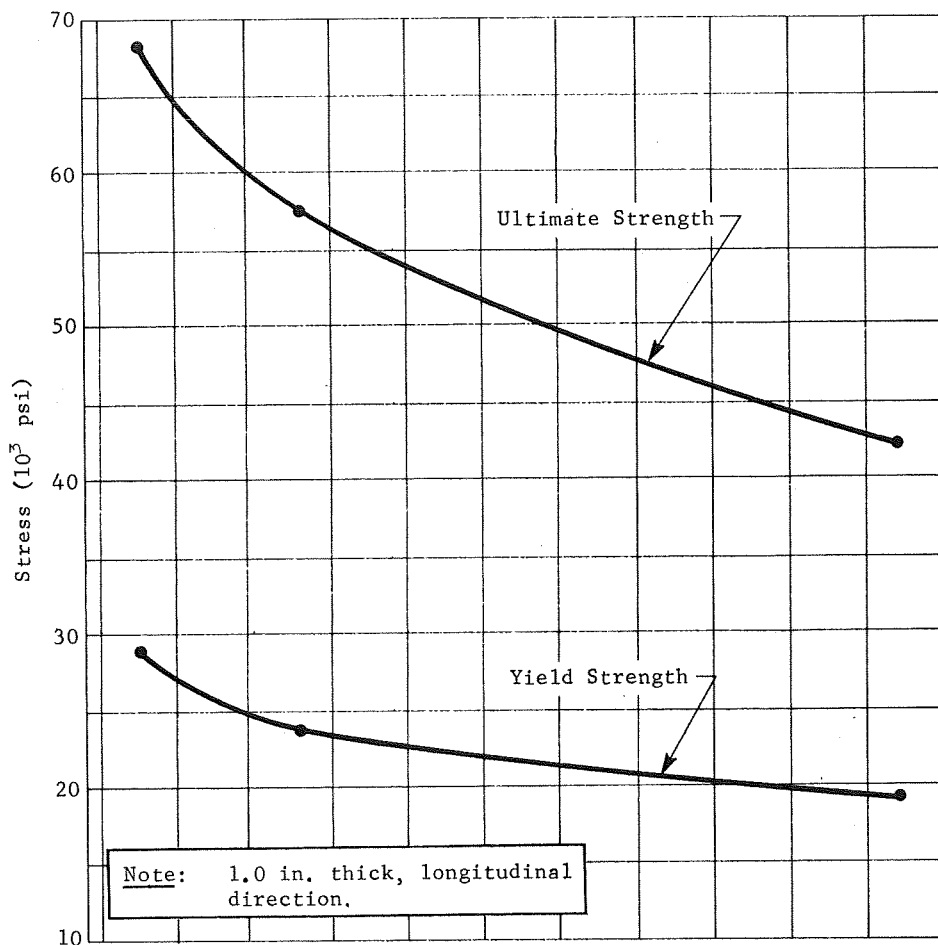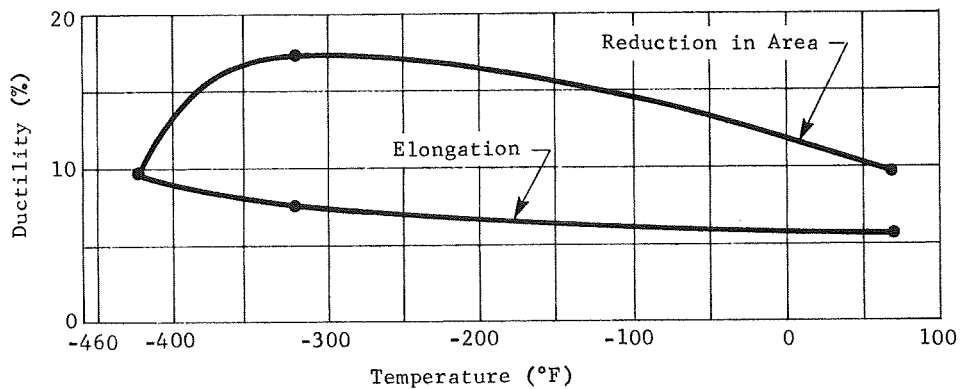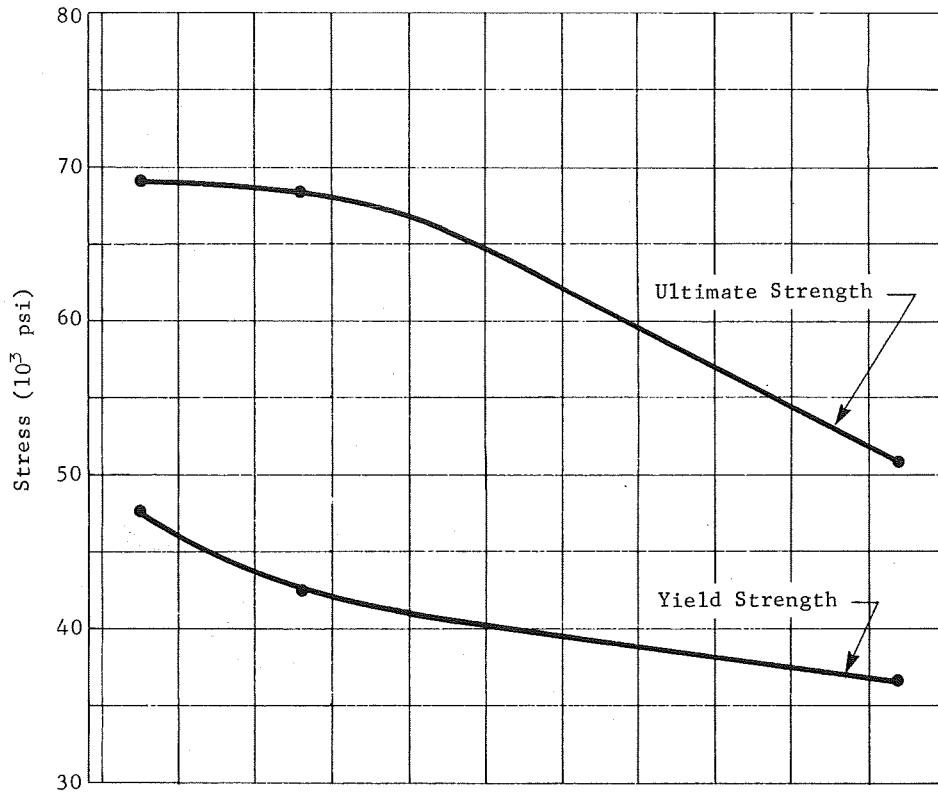
The locations at which the fractures occurred and the appearances of the welded tension specimens after failure were quite interesting. The Aℓ X7007-T6 specimen that failed at 70°F exhibited necking in the heat-affected zone, approximately ½ in. from the centerline of the weld and, to a lesser degree, in the center of the weld bead; at -320°F failures occurred at the centerline of the weld, and although necking occurred in the heat-affected zone, it was less pronounced than at 70°F. The Aℓ 2021-T81 exhibited a fracture at 70°F that completely followed the fusion line (see Fig. VI-7); at -320°F, however, the failure occurred through the center of the weld bead.

Fig. VI-7   Macrosection through the Center of an
            Aℓ 2021-T81 Welded Tension Specimen

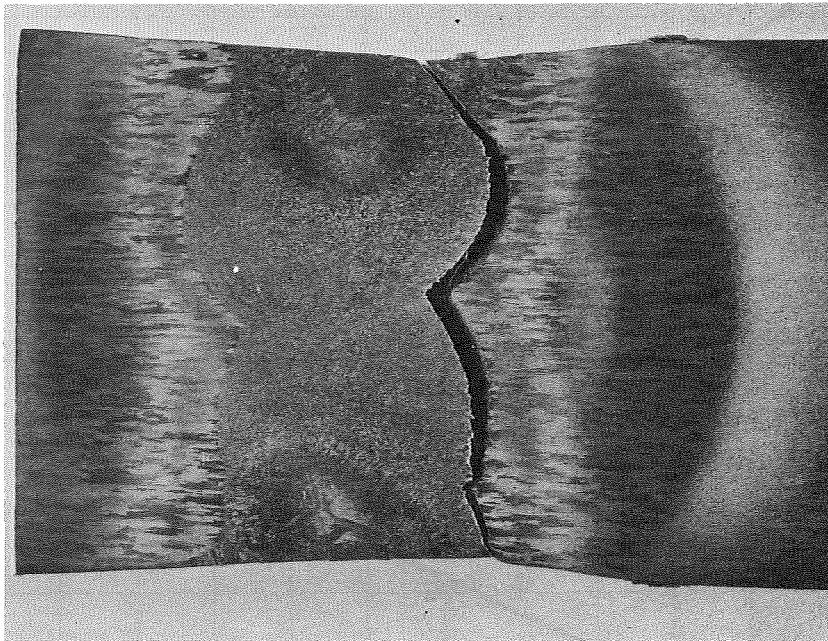b. Elastic Properties

     The modulus of elasticity for each alloy was determined
by using the static-loading and the dynamic-excitation methods.
The latter work was performed by Dr. D. Eash of the Los Alamos
Scientific Laboratory, who used specimens from the two subject
heats of material so that the data obtained using each method
could be compared. The detailed data obtained using the dynamic
method are presented in Appendix C.

     Figure VI-8 shows that there is general agreement be-
tween the data obtained using the different methods. These data
are given in Table VI-3. The data also agree with the 70°F data
obtained from Alcoa. For Aℓ X7007-T6, the modulus of elasticity
obtained from the dynamic tests was significantly higher than that
from the static tests. The 70°F Alcoa data are in good agreement
with the static data.

     Values of Poisson's ratio are plotted in Fig. VI-9 and
are tabulated in Table VI-4. These data were obtained in both
the long and short transverse directions and were similar for
both alloys. The sharp increase in Poisson's ratio that was
noted between -320 and -423°F was confirmed in additional tests.

c. Plastic Properties

     Conventional stress-strain curves for both alloys are
given in the following figures:

Aluminum Alloy	Grain Direction	Specimen	Figure
2021-T81	Longitudinal	Parent Metal	VI-10
2021-T81	Transverse	Parent Metal	VI-11
2021-T81	Longitudinal	Welded	VI-12
X7007-T6	Longitudinal	Parent Metal	VI-13
X7007-T6	Transverse	Parent Metal	VI-14
X7007-T6	Longitudinal	Welded	VI-15
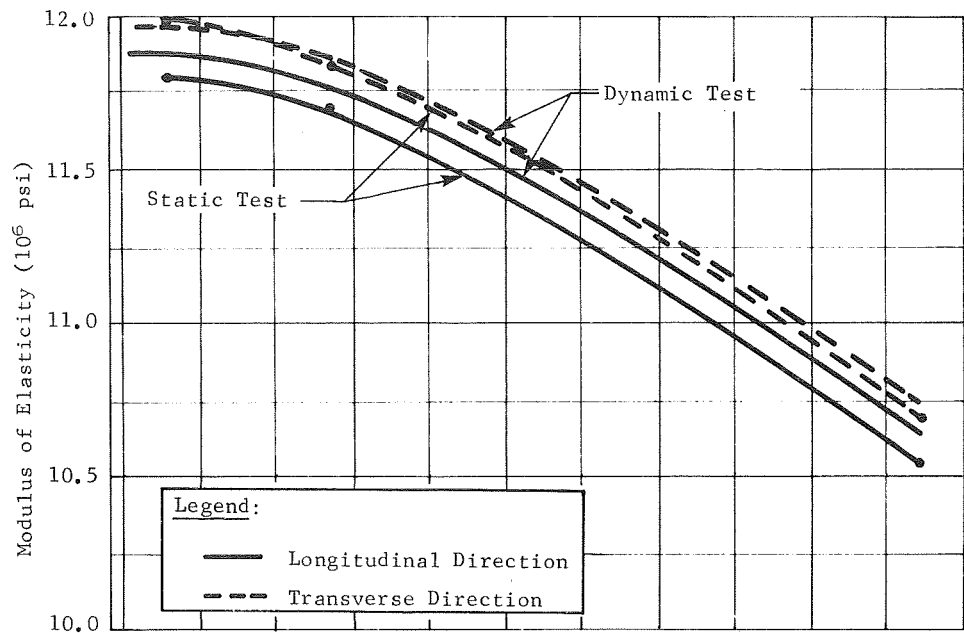
(a)   2021-T81 Aluminum Alloy
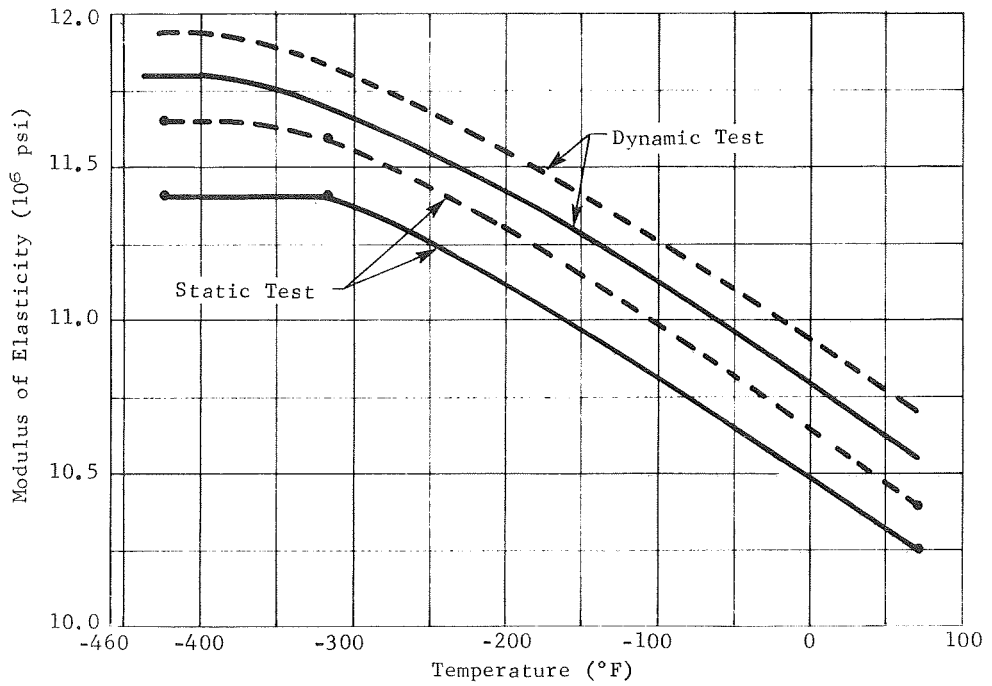
(b)   X7007-T6 Aluminum Alloy

Fig. VI-8   Modulus of Elasticity for Two Aluminum Alloys

Table VI-3 Modulus of Elasticity for Two Aluminum Alloys

Aluminum Alloy	Temperature (°F)	Grain Direction	Determined by Martin Marietta Using the Strain-Gage Method	Determined by Los Alamos Scientific Laboratory Using the Dynamic-Loading Method	Determined by Alcoa Using ASTM E-III
2021-T81	70	Longitudinal	10.6	10.7	10.6
2021-T81	70	Transverse	10.7	10.7	10.6
2021-T81	-320	Longitudinal	11.7	11.8	
2021-T81	-320	Transverse	11.8	11.9	
2021-T81	-423	Longitudinal	11.8	11.9	
2021-T81	-423	Transverse	12.0	12.0	
X7007-T6	70	Longitudinal	10.3	10.6	10.4
X7007-T6	70	Transverse	10.4	10.7	10.4
X7007-T6	-320	Longitudinal	11.4	11.7	
X7007-T6	-320	Transverse	11.6	11.8	
X7007-T6	-423	Longitudinal	11.4	11.8	
X7007-T6	-423	Transverse	11.6	11.9	

(a)   2021-T81 Aluminum Alloy
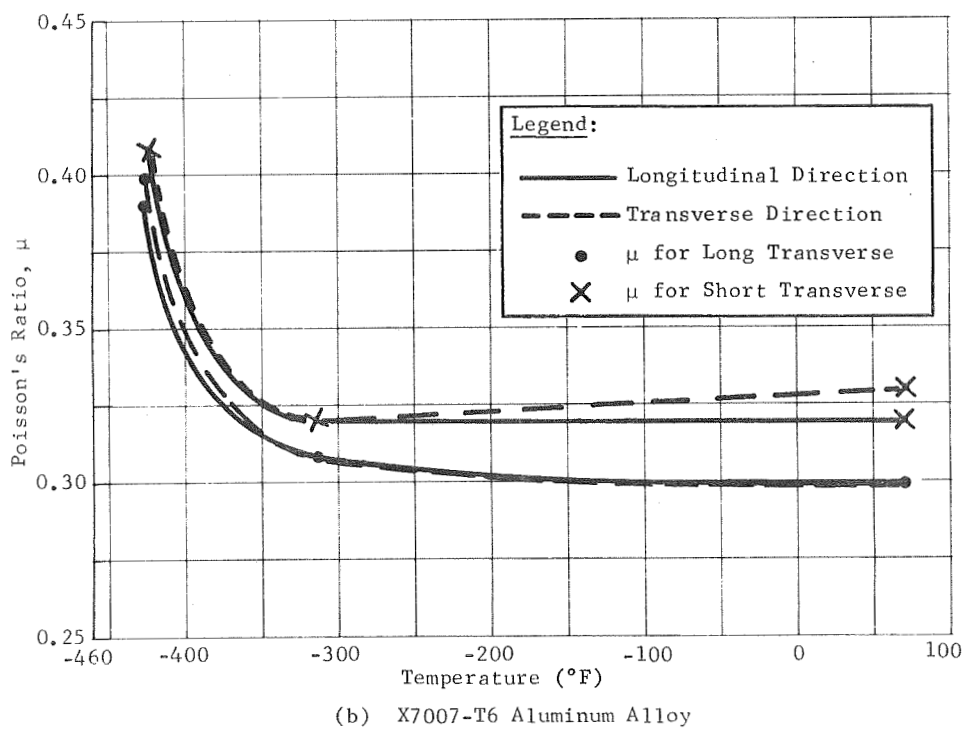
(b)   X7007-T6 Aluminum Alloy
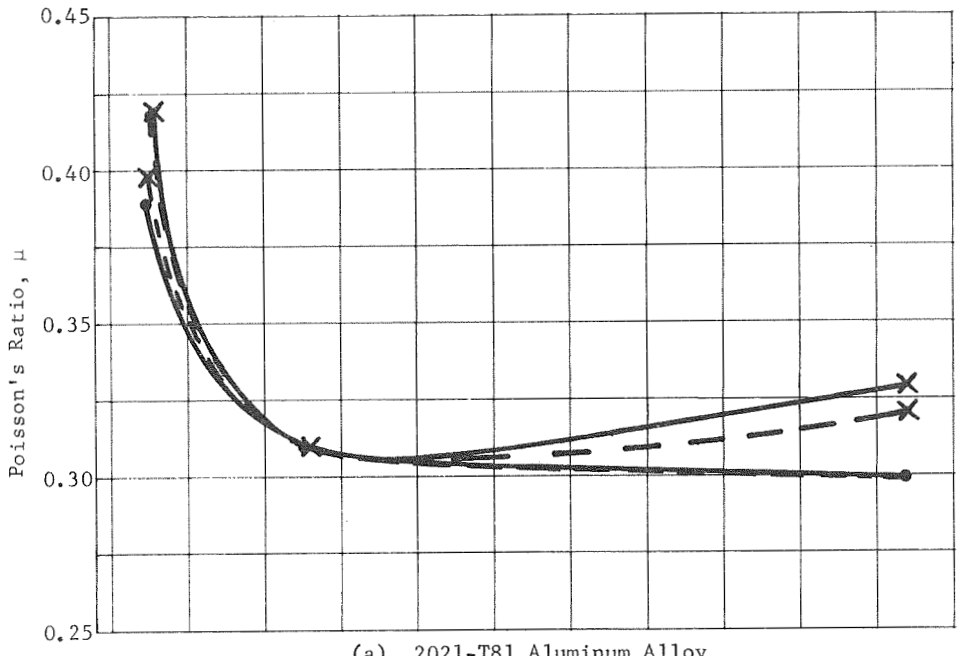
Fig. VI-9   Poisson's Ratio for Two Aluminum Alloys

Table VI-4 Poisson's Ratio for Two Aluminum Alloys

Aluminum Alloy	Temperature (°F)	Grain Direction	Poisson's Ratio	
			Long Transverse Direction	Short Transverse Direction
2021-T81	70	Longitudinal	0.30	0.33
2021-T81	70	Transverse	0.30	0.32
2021-T81	-320	Longitudinal	0.31	0.31
2021-T81	-320	Transverse	0.31	0.31
2021-T81	-423	Longitudinal	0.39	0.42
2021-T81	-423	Transverse	0.42	0.40
X7007-T6	70	Longitudinal	0.30	0.32
X7007-T6	70	Transverse	0.30	0.33
X7007-T6	-320	Longitudinal	0.31	0.32
X7007-T6	-320	Transverse	0.31	0.31
X7007-T6	-423	Longitudinal	0.39	0.41
X7007-T6	-423	Transverse	0.40	0.41

Fig. VI-10 Conventional Stress vs Strain Curve for Parent Metal Specimens
(2021-T81 Aluminum Alloy; Longitudinal Direction)

Fig. VI-11 Conventional Stress vs Strain Curve for Parent Metal Specimens
(2021-T81 Aluminum Alloy; Transverse Direction)

Fig. VI-12 Conventional Stress vs Strain Curve for Parent Metal Specimens
(X7007-T6 Aluminum Alloy; Longitudinal Direction)

Fig. VI-13 Conventional Stress vs Strain Curve for Parent Metal Specimens
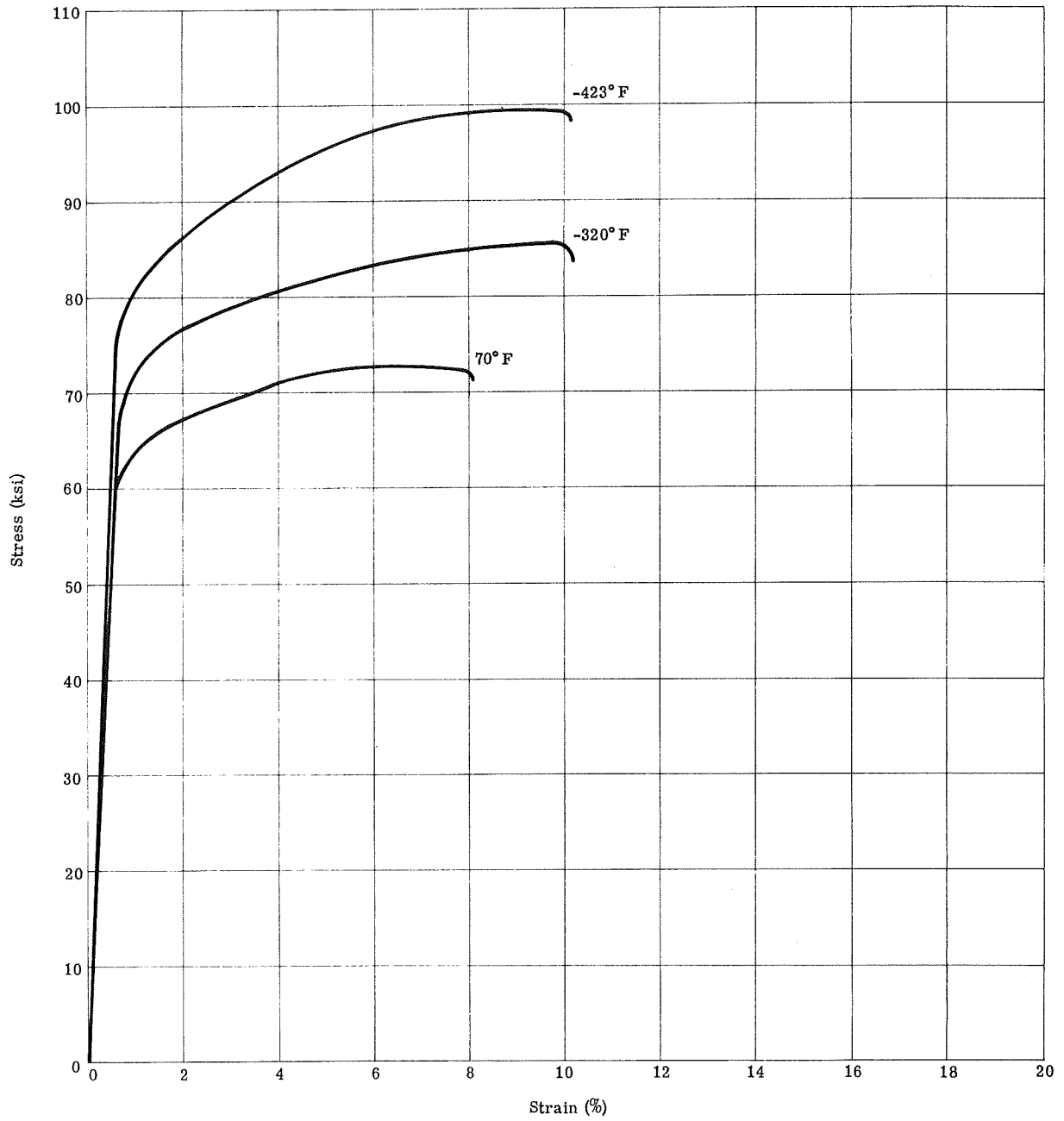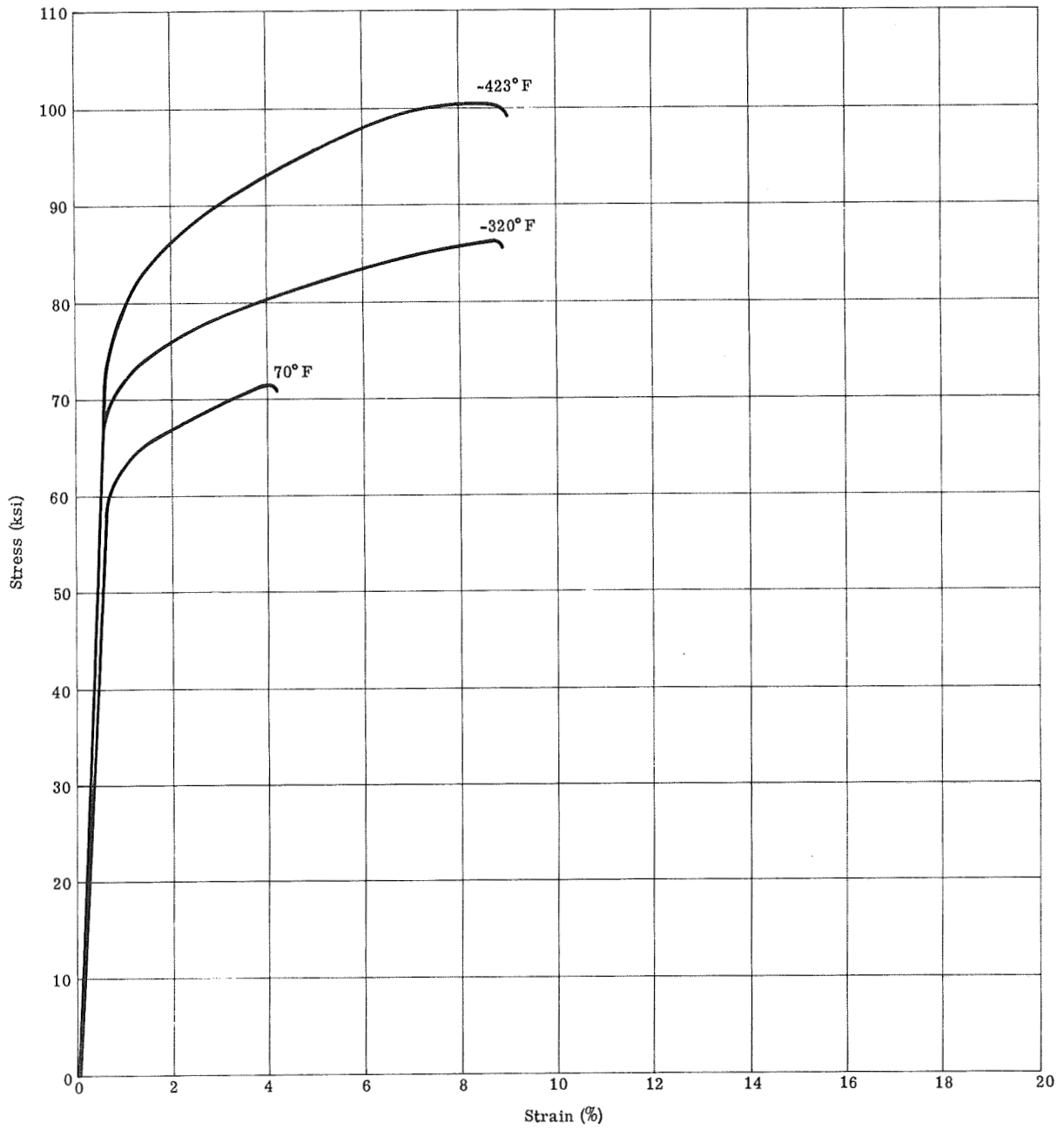(X7007-T6 Aluminum Alloy; Transverse Direction)

Fig. VI-14 Conventional Stress vs Strain Curve for Welded Specimens
(2021-T81 Aluminum Alloy; Longitudinal Direction)

Fig. VI-15 Conventional Stress vs Strain Curve for Welded Specimens
(X7007-T6 Aluminum Alloy; Longitudinal Direction)

True stress vs true strain curves were prepared only for parent-metal specimens. These curves, which are typical of those for heat-treated aluminum alloys, are given in the following figures:

Aluminum Alloy	Grain Direction	Figure
2021-T81	Longitudinal	VI-16
2021-T81	Transverse	VI-17
X7007-T6	Longitudinal	VI-18
X7007-T6	Transverse	VI-19

From these curves, the strain-hardening exponent, m, was determined. The strain-hardening data, which are presented in Fig. VI-1 and VI-2, show that the exponent for Aℓ 2021-T81 increases almost linearly, and that the exponent for Aℓ X7007-T6 increases as the temperature goes from 70 to -320°F, but then decreases as the temperature drops below -320°F.

The necking strain also shows a similar trend. Theoretically, necking occurs when the true plastic strain equals the strain-hardening exponent.* These values are compared in Table VI-5.

---

*If the true stress/true strain curve is a straight line on log-log paper, it can be represented by the formula

$$\sigma = B \epsilon^m,$$

where σ is the true stress, m is the strain-hardening exponent, and ϵ is the logarithmic plastic strain.

The strain-hardening exponent can then be analytically determined from ϵ and σ.

$$m = \frac{d \log \sigma}{d \log \epsilon} = \frac{\epsilon}{\sigma} \frac{d\sigma}{d\epsilon}. \qquad [1]$$

At instability,

$$ds = \frac{\sigma \, d\epsilon}{(1 + \epsilon)} = \sigma \, de$$

and

$$\frac{d\sigma}{d\epsilon} = \sigma. \qquad [2]$$

Substituting Eq [2] into Eq [1], we obtain:

$$m = \frac{\epsilon}{\sigma} \frac{d\sigma}{d\epsilon} = \frac{\epsilon}{\sigma} \sigma = \epsilon = \epsilon_{neck}.$$

Fig. VI-16 True Stress vs True Strain Curve for Parent Metal Specimens
(2021-T81 Aluminum Alloy; Longitudinal Direction)

Fig. VI-17 True Stress vs True Strain Curve for Parent Metal Specimens
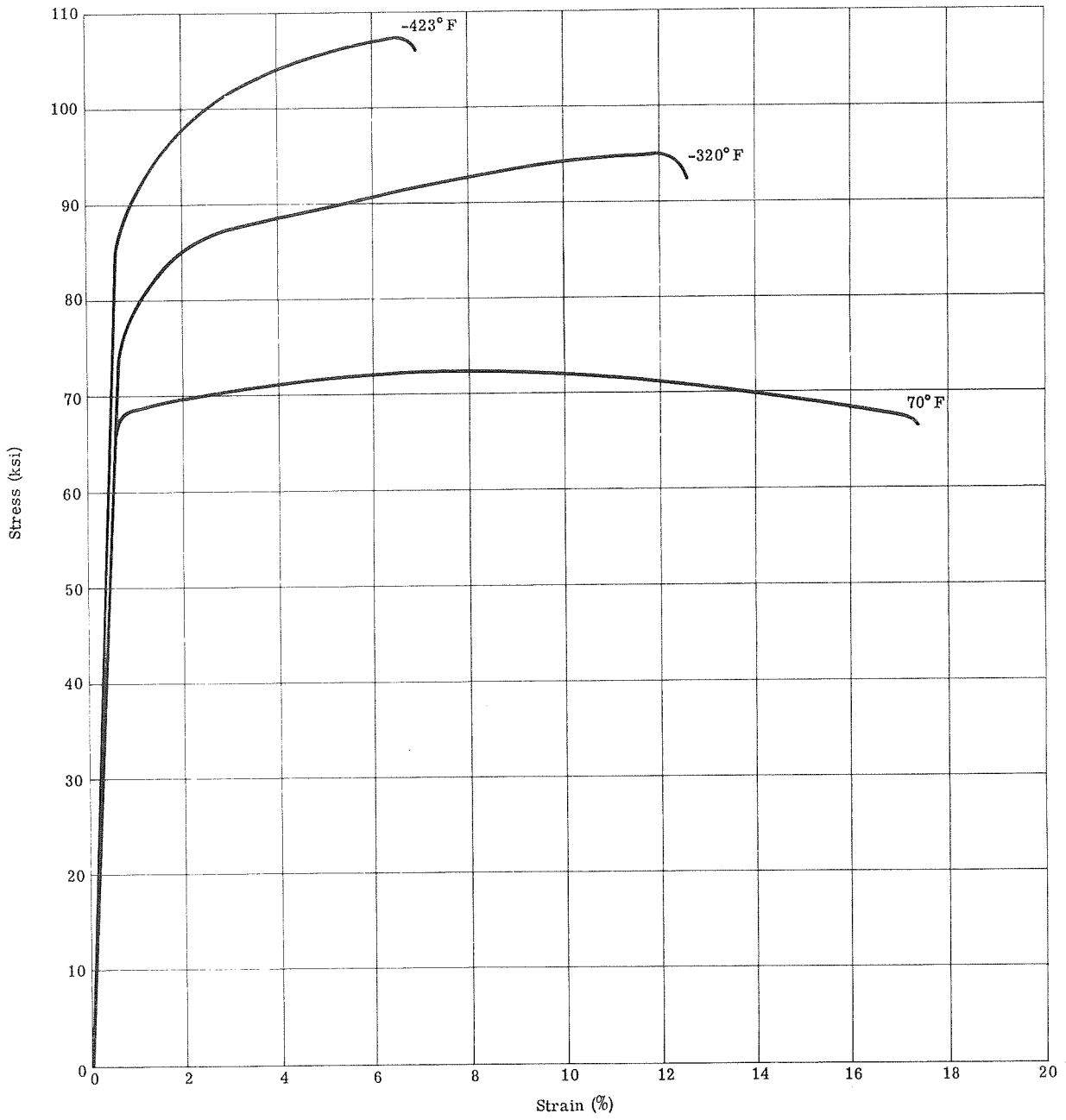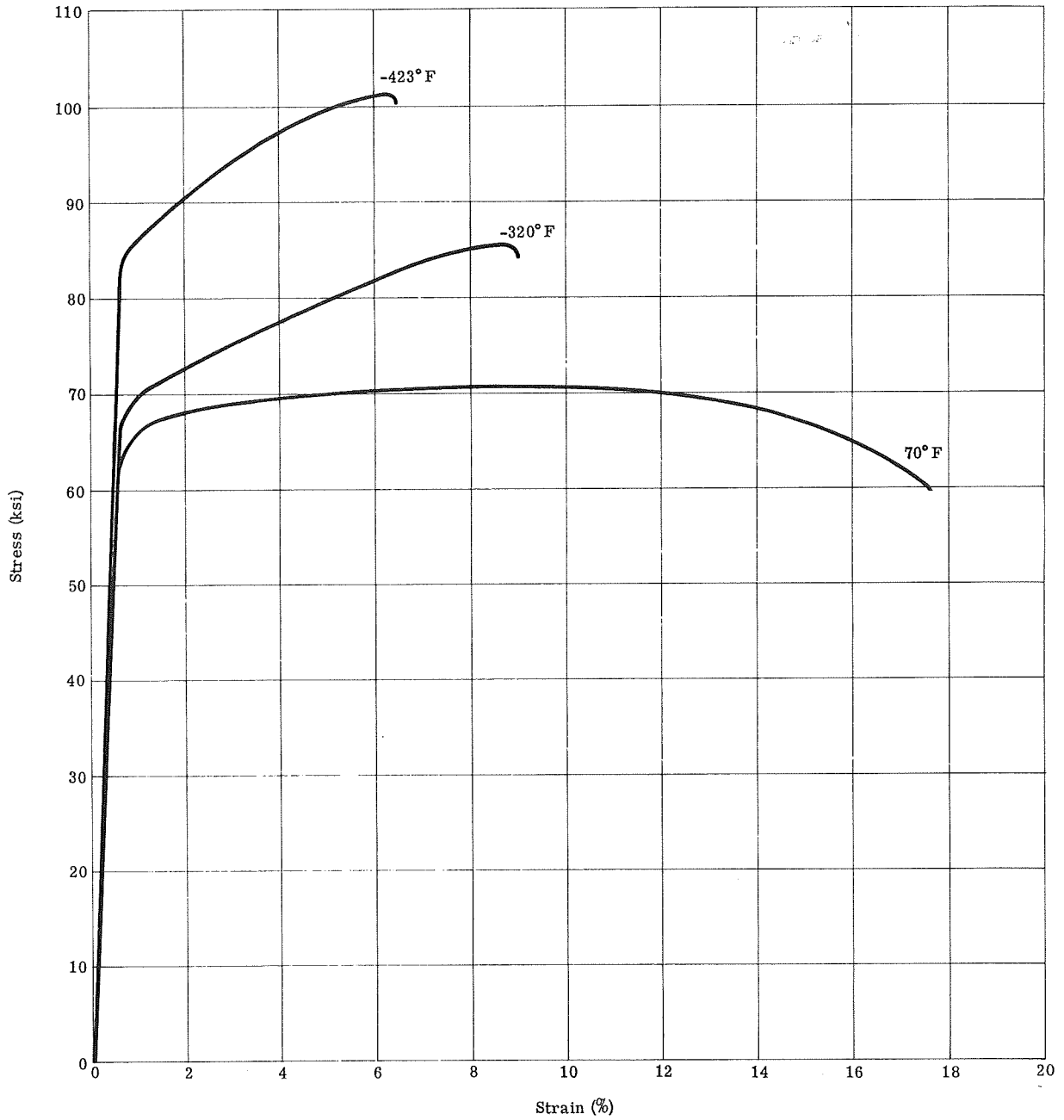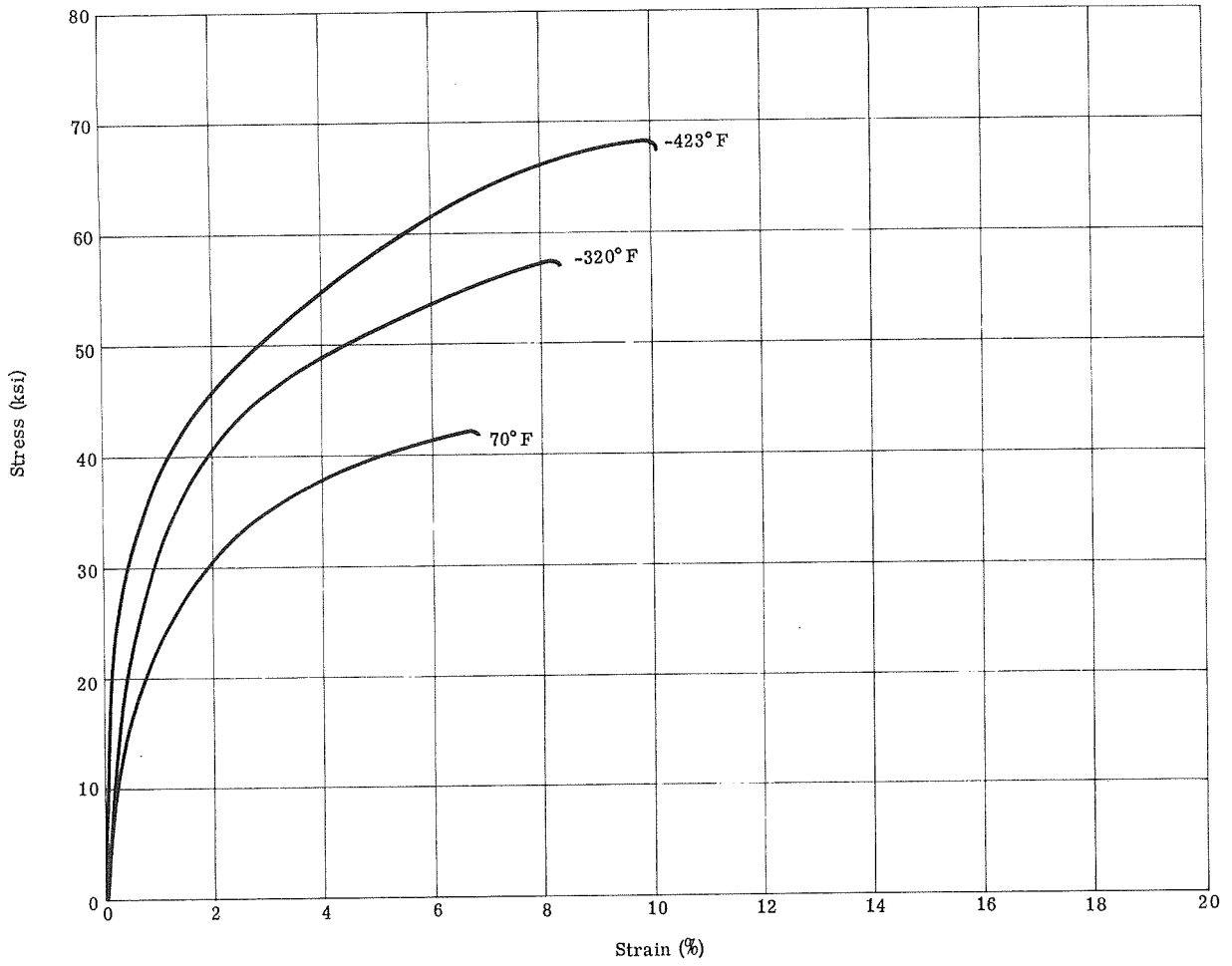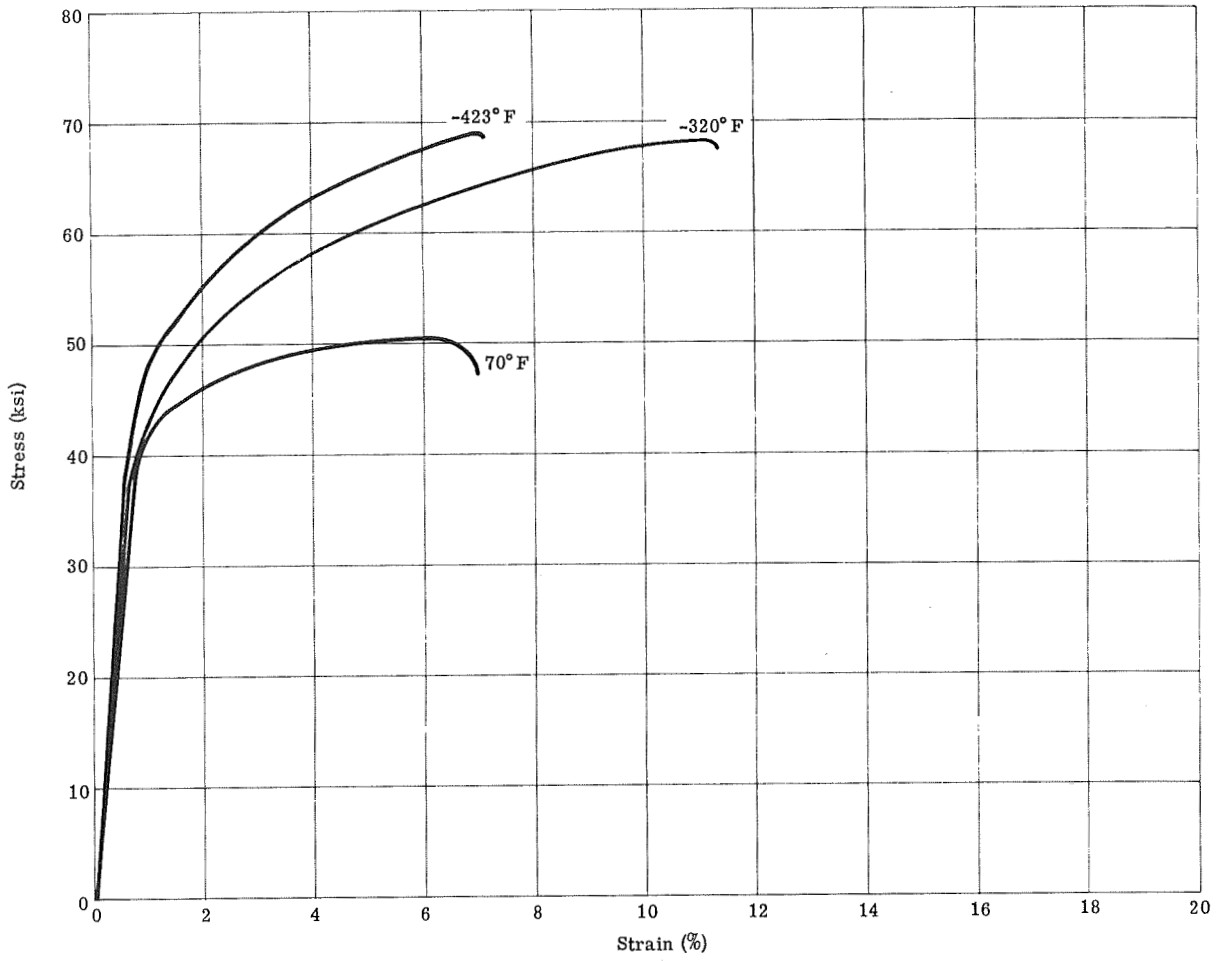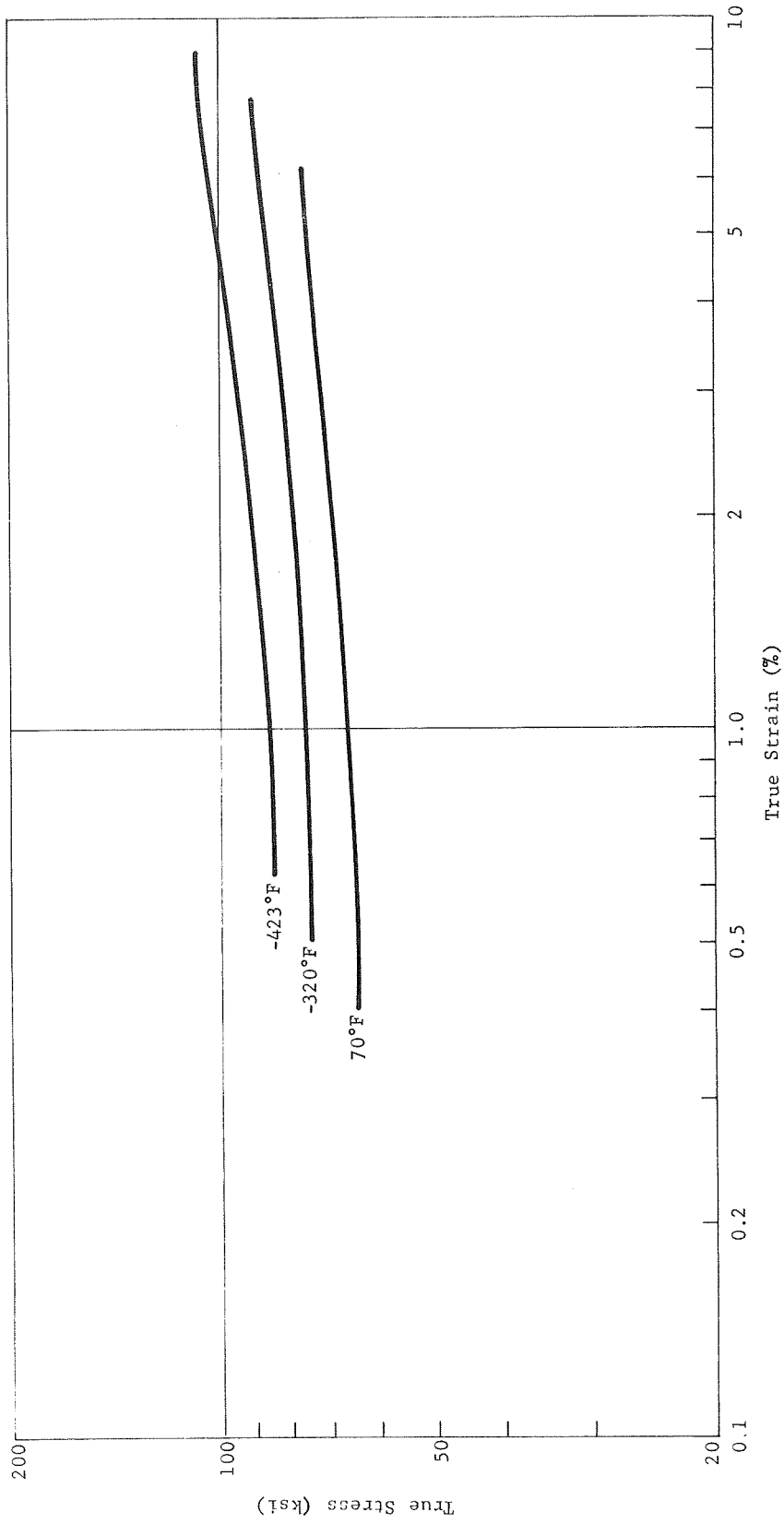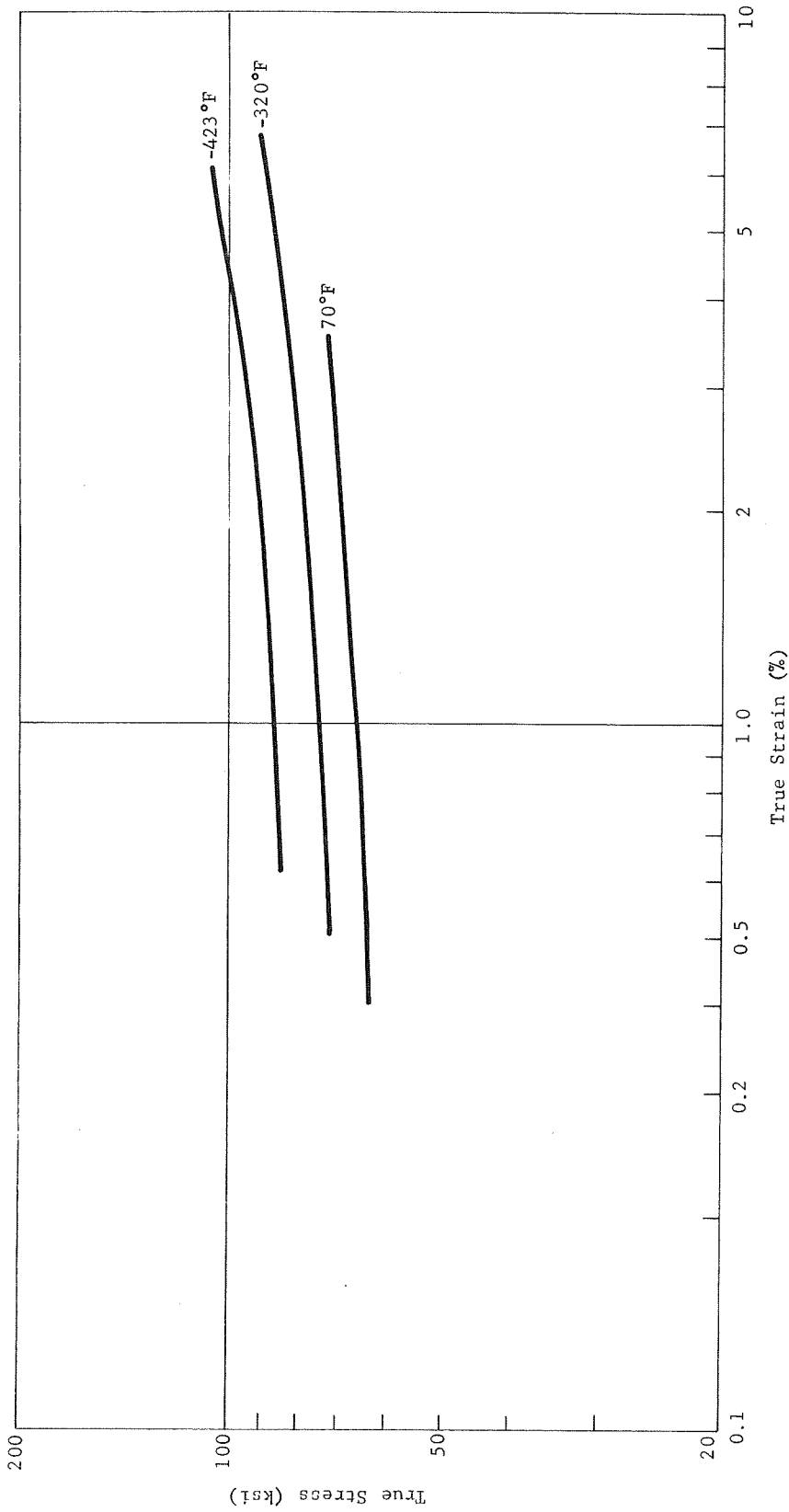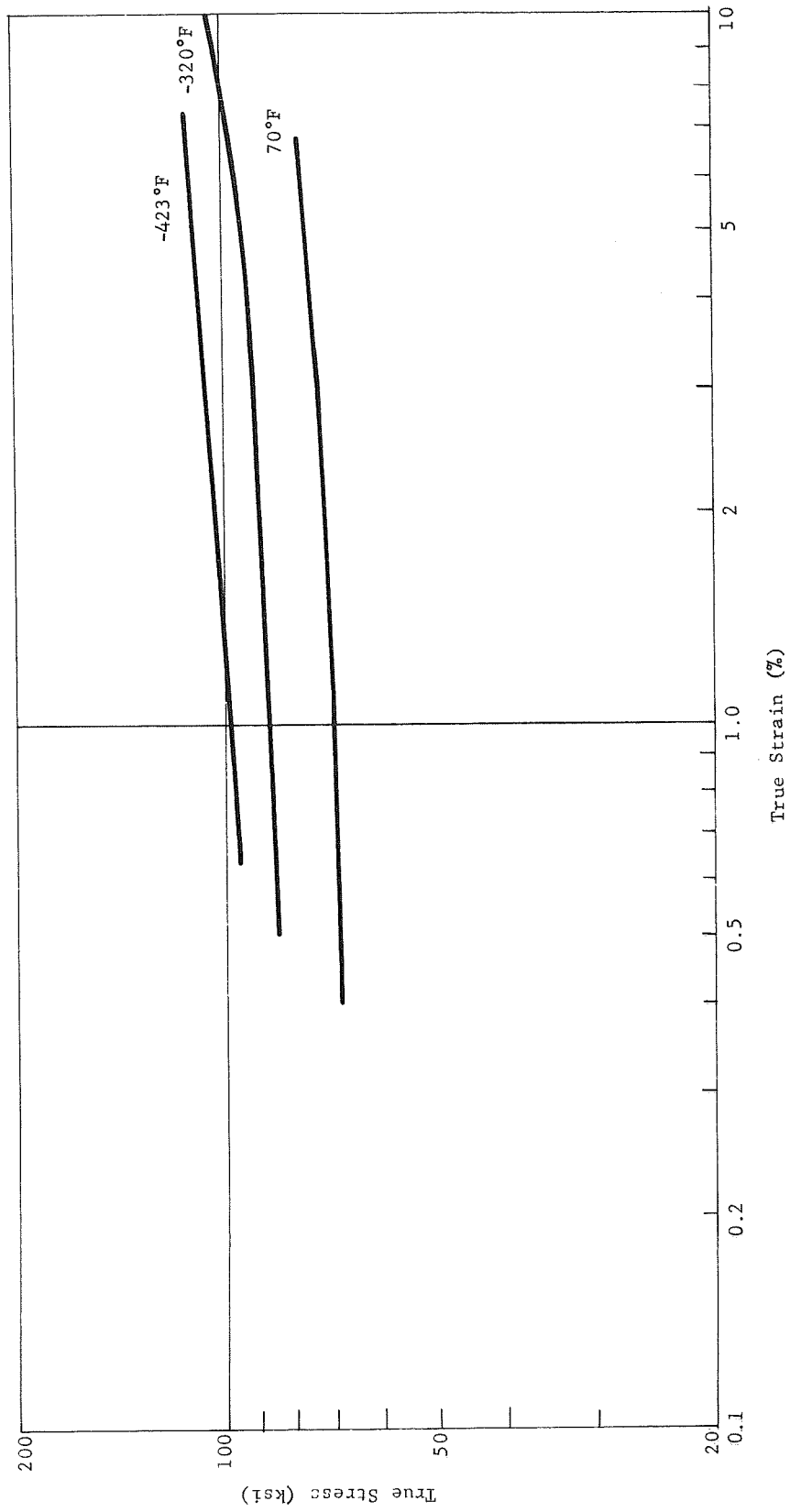(2021-T81 Aluminum Alloy; Transverse Direction)

Fig. VI-18 True Stress vs True Strain Curve for Parent Metal Specimens
(X7007-T6 Aluminum Alloy; Longitudinal Direction)
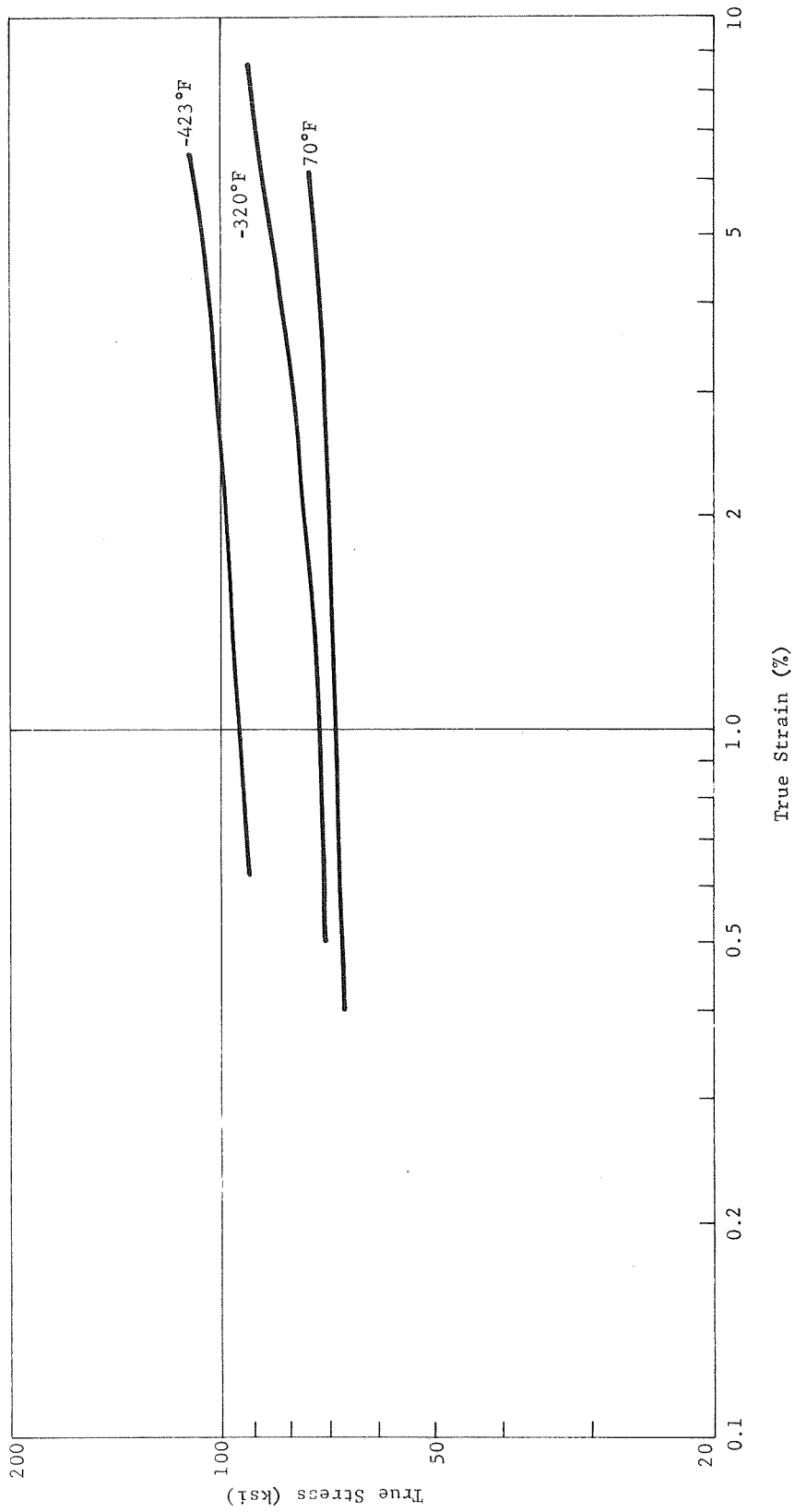
Fig. VI-19 True Stress vs True Strain Curve for Parent Metal Specimens
            (X7007-T6 Aluminum Alloy; Transverse Direction)

Table VI-5   Strain-Hardening Exponent and Necking Strain for
Two Aluminum Alloys

Aluminum Alloy	Temperature (°F)	Grain Direction	Strain Hardening Exponent, m	Necking Strain*
2021-T81	70	Longitudinal	0.063	†
2021-T81	70	Transverse	0.058	0.062
2021-T81	-320	Longitudinal	0.118	0.082
2021-T81	-320	Transverse	0.117	0.077
2021-T81	-423	Longitudinal	0.120	0.092
2021-T81	-423	Transverse	0.132	0.061
X7007-T6	70	Longitudinal	0.076	0.086
X7007-T6	70	Transverse	0.076	0.054
X7007-T6	-320	Longitudinal	0.110	0.113
X7007-T6	-320	Transverse	0.150	0.086
X7007-T6	-423	Longitudinal	0.105	0.065
X7007-T6	-423	Transverse	0.066	0.072

*True strain.

†Failed without necking.

2.   Cryogenically-Stretched Type 301 Stainless Steel

a.   Strength and Ductility

The tensile properties of unnotched, parent-metal, cryo-genically-stretched Type 301 stainless steel are given in Fig. VI-20 and Table VI-6. As the temperature decreases from 70 to -423°F, the ultimate strength and the yield strength increase more than 100 ksi. The ductility increases as the temperature goes from 70 to -320°F, but then decreases as the temperature drops below -320°F. The elongation at -423°F (3.5%) is quite satisfactory, considering that the ultimate strength is over 350 ksi.
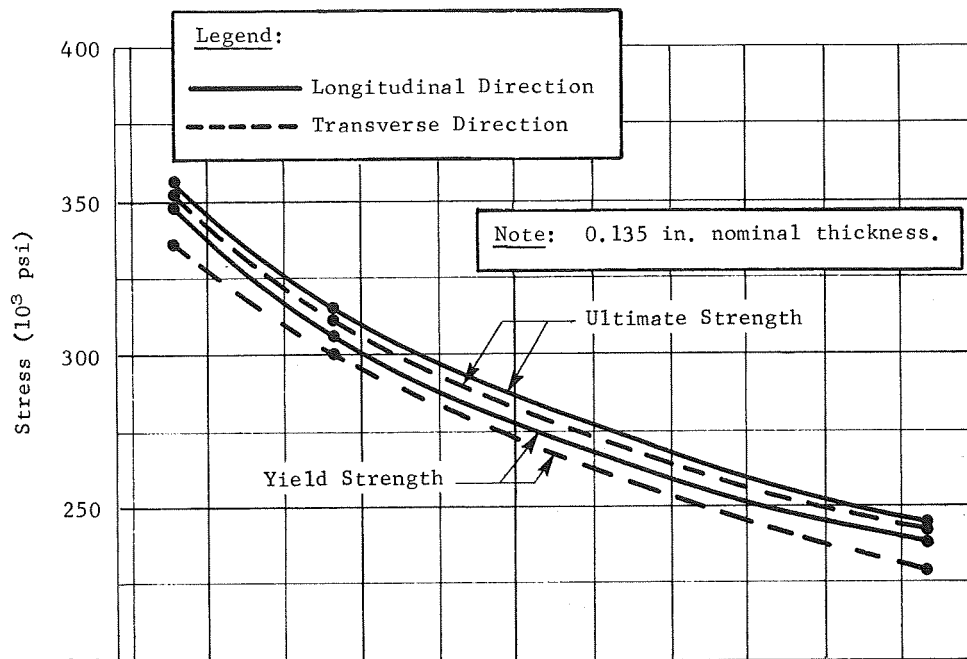
(a)   Ultimate Strength and Yield Strength
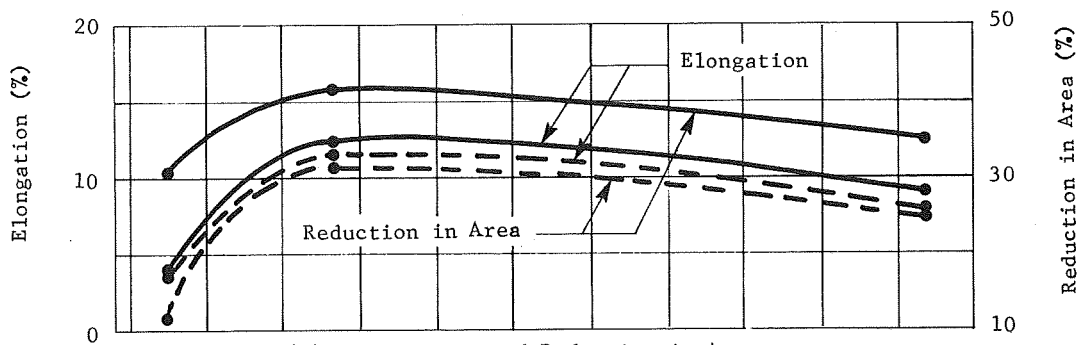
(b)   Elongation and Reduction in Area
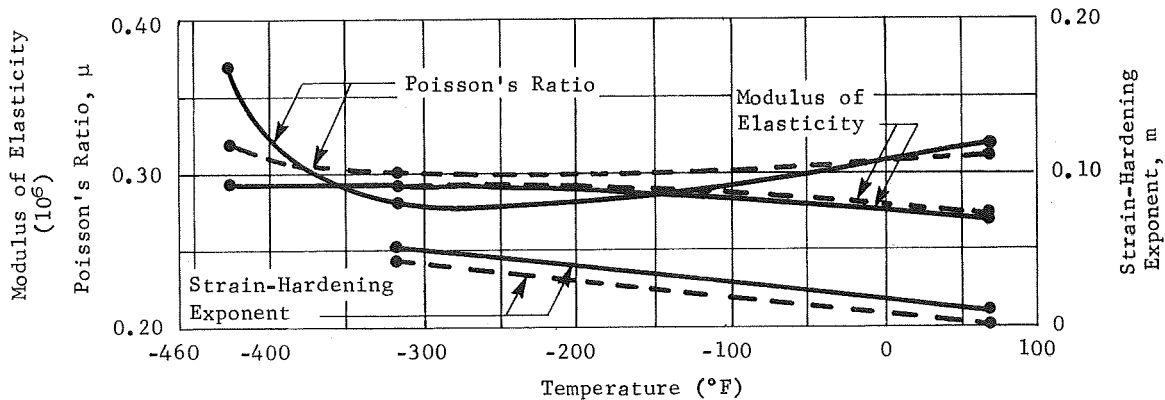
(c)   Poisson's Ratio, Modulus of Elasticity, and Strain-Hardening Exponent

Fig. VI-20 Tensile Properties of Cryogenically-Stretched Parent Metal (Type 301 Stainless Steel)

Table VI-6   Tensile Properties of Cryogenically-Stretched
Type 301 Stainless Steel*

Temperature (°F)	Grain Direction	Ultimate Strength (ksi)	Yield Strength, 0.2% Offset (ksi)	Elongation (%)	Reduction in Area (%)
Parent Metal Specimens					
70	Longitudinal	244.5	239.1	7.8	34.8
-320	Longitudinal	310.1	306.4	12.3	41.1
-423	Longitudinal	355.8	350.7	3.5	30.0
70	Transverse	241.1	229.0	7.1	28.1
-320	Transverse	315.3	301.2	11.6	31.1
-423	Transverse	353.2	337.7	3.3	11.0
Welded Specimens					
70	Longitudinal	227.8	207.7	5.3	27.7
-320	Longitudinal	301.2	292.8	9.2	33.1
-423	Longitudinal	339.6	336.3	3.8	17.3
*Nominal thickness = 0.135 in.					

Figure VI-21 and Table VI-6 show that welded, cryogen-
ically-stretched specimens exhibited excellent strength properties,
and the efficiency of the welded joint averaged approximately 95%.
The ductility was similar to that observed for the parent metal.

b. Elastic Properties

The modulus of elasticity of parent metal (see Table VI-7
and Fig. VI-20) increased almost 10% when the specimen was cooled
from 70 to 320°F, but did not increase as the temperature was re-
duced further. This modulus was independent of the grain orienta-
tion.

In the longitudinal direction, Poisson's ratio exhibited
the same low-temperature behavior that was observed for the alu-
minum alloys; in the transverse direction, however, Poisson's
ratio was almost independent of temperature. These data are given
in Table VI-7 and Fig. VI-20.

(a) Ultimate Strength and Yield Strength
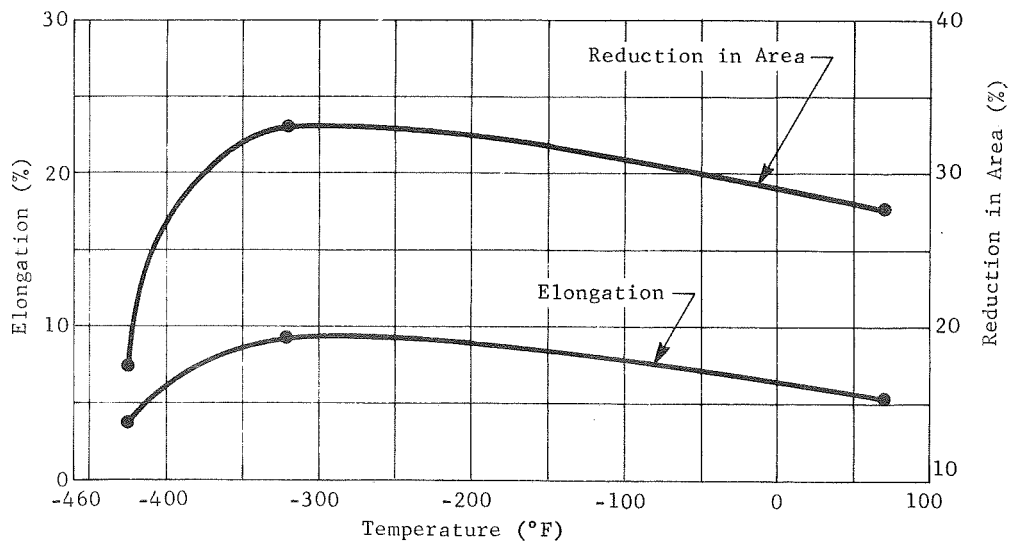
(b) Elongation and Reduction in Area

Fig. VI-21 Tensile Properties of Welded, Cryogenically-Stretched Type 301 Stainless Steel

Table VI-7   Elastic Properties of Cryogenically-
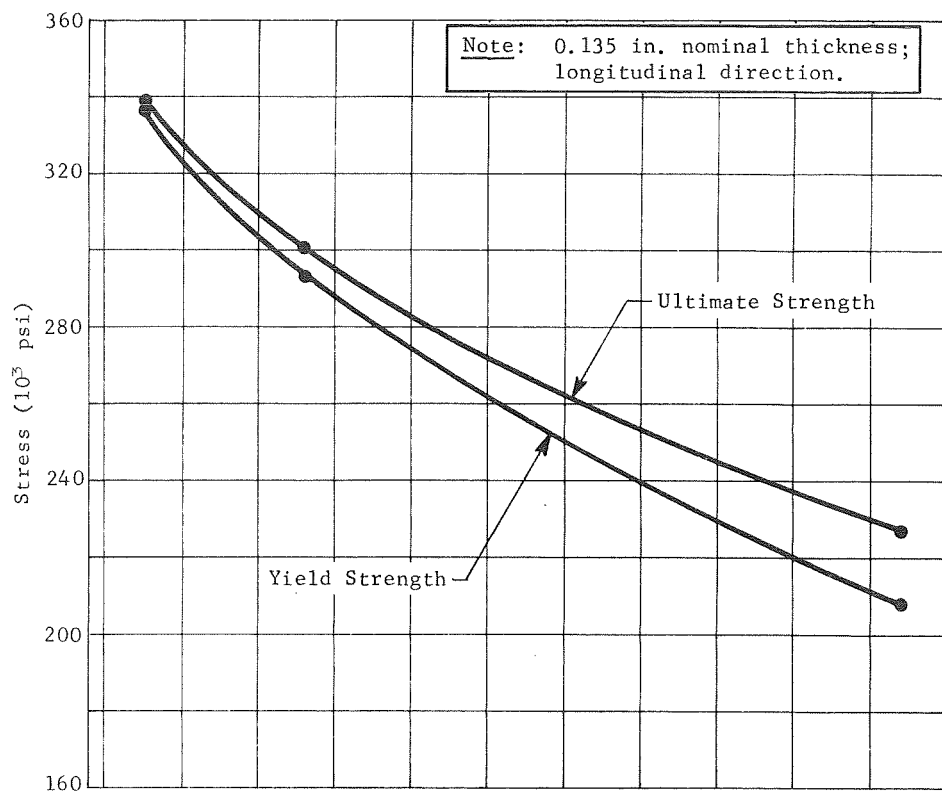Stretched Type 301 Stainless Steel

Temperature (°F)	Grain Direction	Modulus of Elasticity (x 10^6 psi)	Poisson's Ratio, μ
70	Longitudinal	27.2	0.32
70	Transverse	27.6	0.31
-320	Longitudinal	29.6	0.28
-320	Transverse	29.6	0.30
-423	Longitudinal	29.6	0.37
-423	Transverse	29.7	0.32

c. Plastic Properties

Conventional stress-strain curves for each grain direc-
tion and type of specimen are given in the following figures:

Grain Direction	Specimen	Figure
Longitudinal	Parent Metal	VI-22
Transverse	Parent Metal	VI-23
Longitudinal	Welded	VI-24

Interestingly, the uniform elongation or necking strain
was very low: at 70 and -320°F, for example, the maximum stress
was attained at a total strain of approximately 1%. Although the
uniform elongation occurred at a low strain level, the subsequent
decrease in stress was very gradual. In contrast to this low value
of uniform strain, the total elongation was markedly higher. At
-423°F, it appeared that the specimen fractured before necking,
but the fracture strain (approximately 3.5%) was rather low.

True stress vs true strain curves for parent-metal speci-
mens in the longitudinal and transverse directions are given in
Fig. VI-25 and VI-26, respectively. The strain-hardening expo-
nent and the necking strain are given below.

Temperature (°F)	Grain Direction	Strain-Hardening Exponent, m	Necking Strain*
70	Longitudinal		0.010
70	Transverse	0.012	0.005
-320	Longitudinal	0.052	0.010
-320	Transverse	0.042	0.068
-423	Longitudinal		
-423	Transverse		

*True strain.
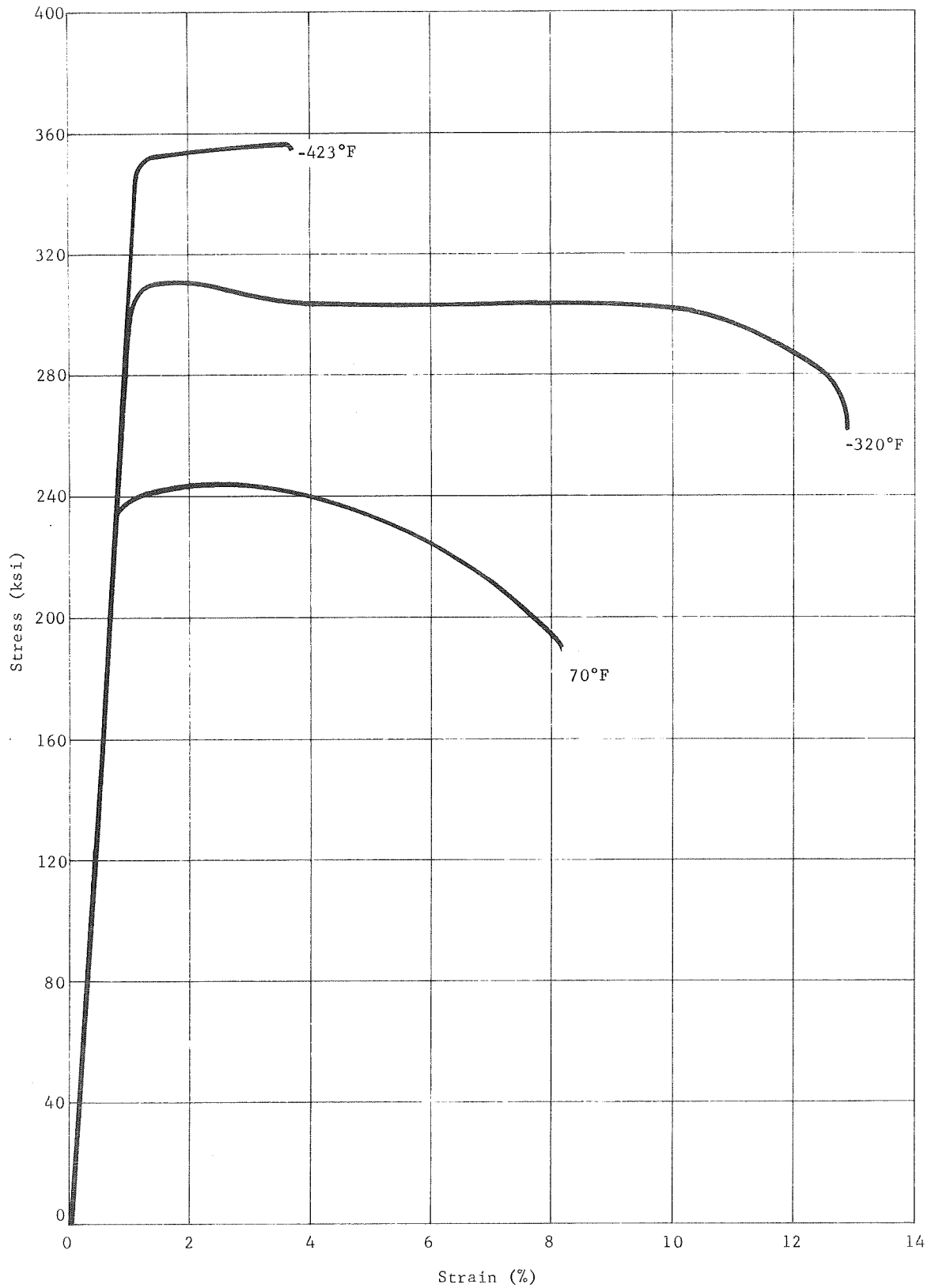
Fig. VI-22 Conventional Stress vs Strain Curve for Cryogenically-Stretched
            Parent Metal Specimens (Type 301 Stainless Steel; Longitudinal
            Direction)
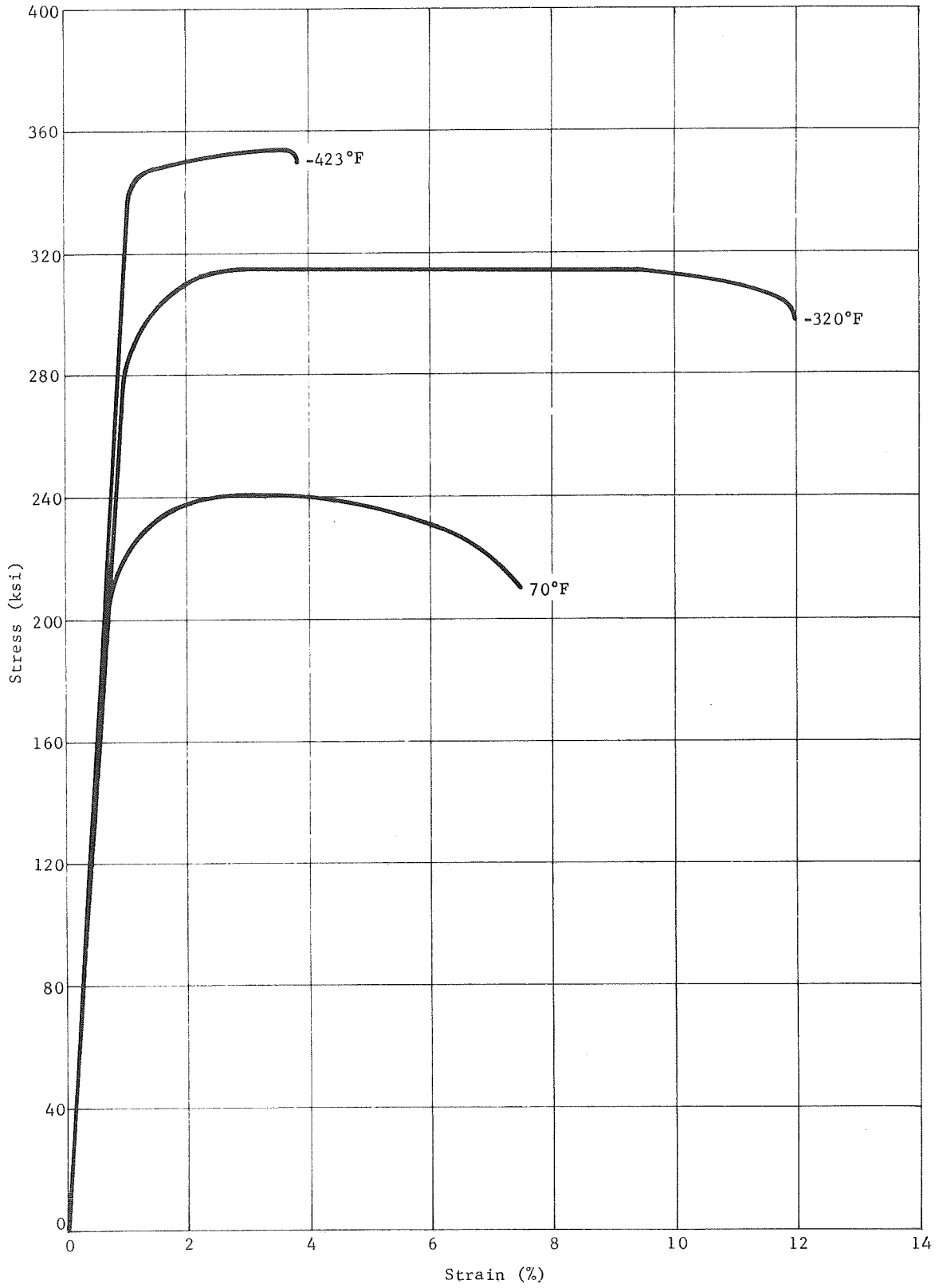
Fig. VI-23 Conventional Stress vs Strain Curve for Cryogenically-Stretched
Parent Metal Specimens (Type 301 Stainless Steel; Transverse
Direction)
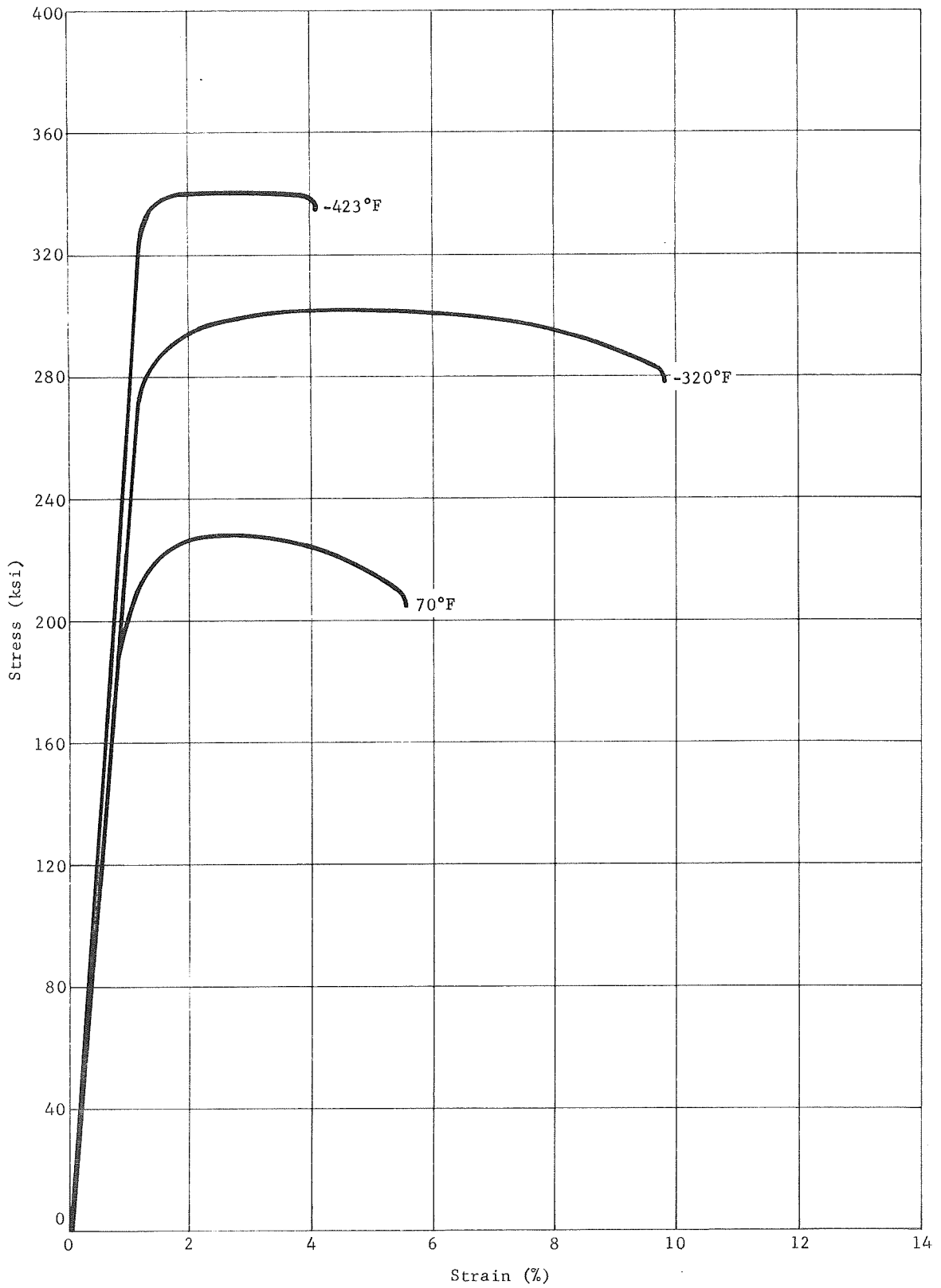
Fig. VI-24 Conventional Stress vs Strain Curve for Welded Cryogenically-
Stretched Specimens (Type 301 Stainless Steel; Longitudinal
Direction)
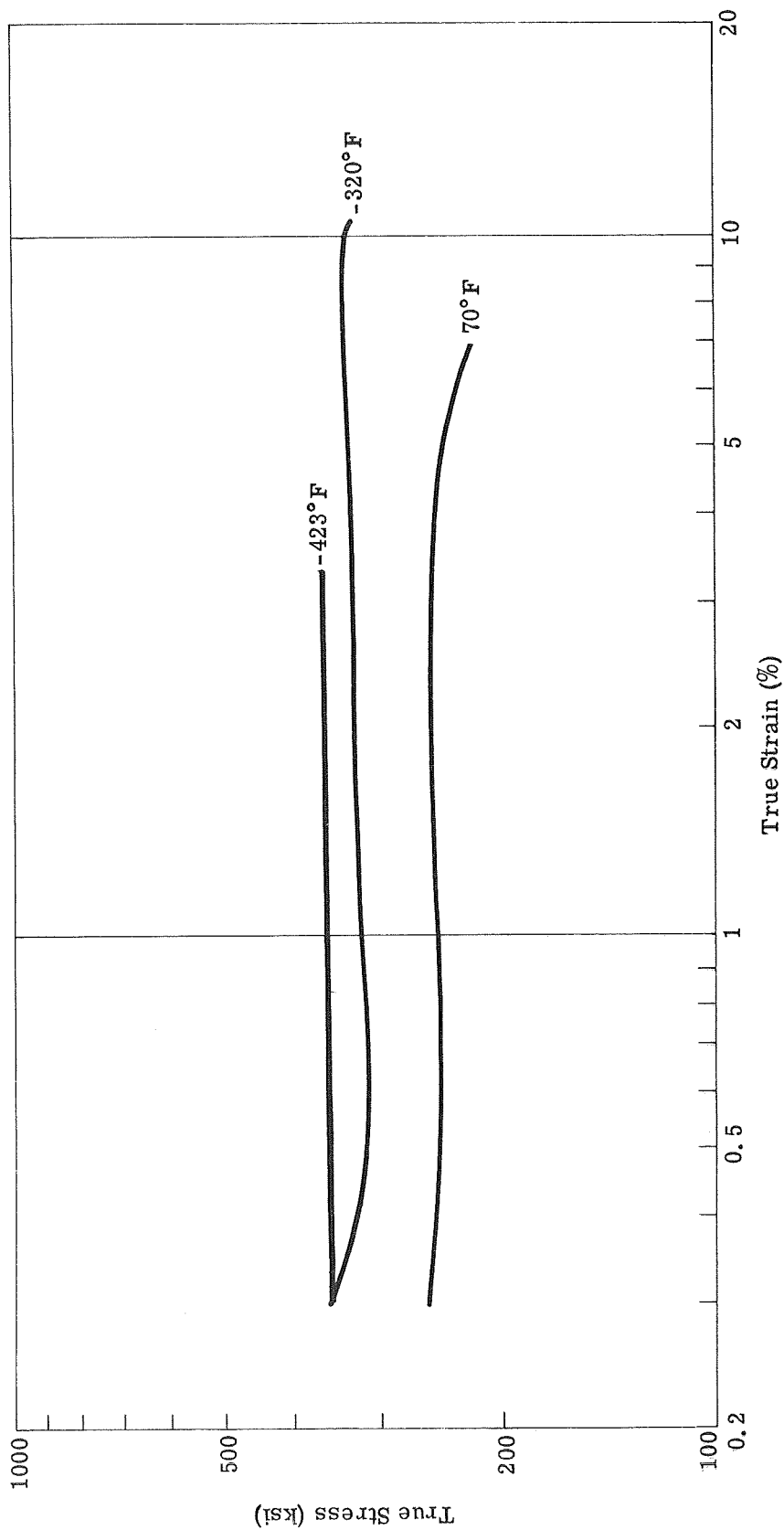
Fig. VI-25   True Stress vs True Strain Curve for Cryogenically-Stretched Parent
Metal Specimens (Type 301 Stainless Steel; Transverse Direction)
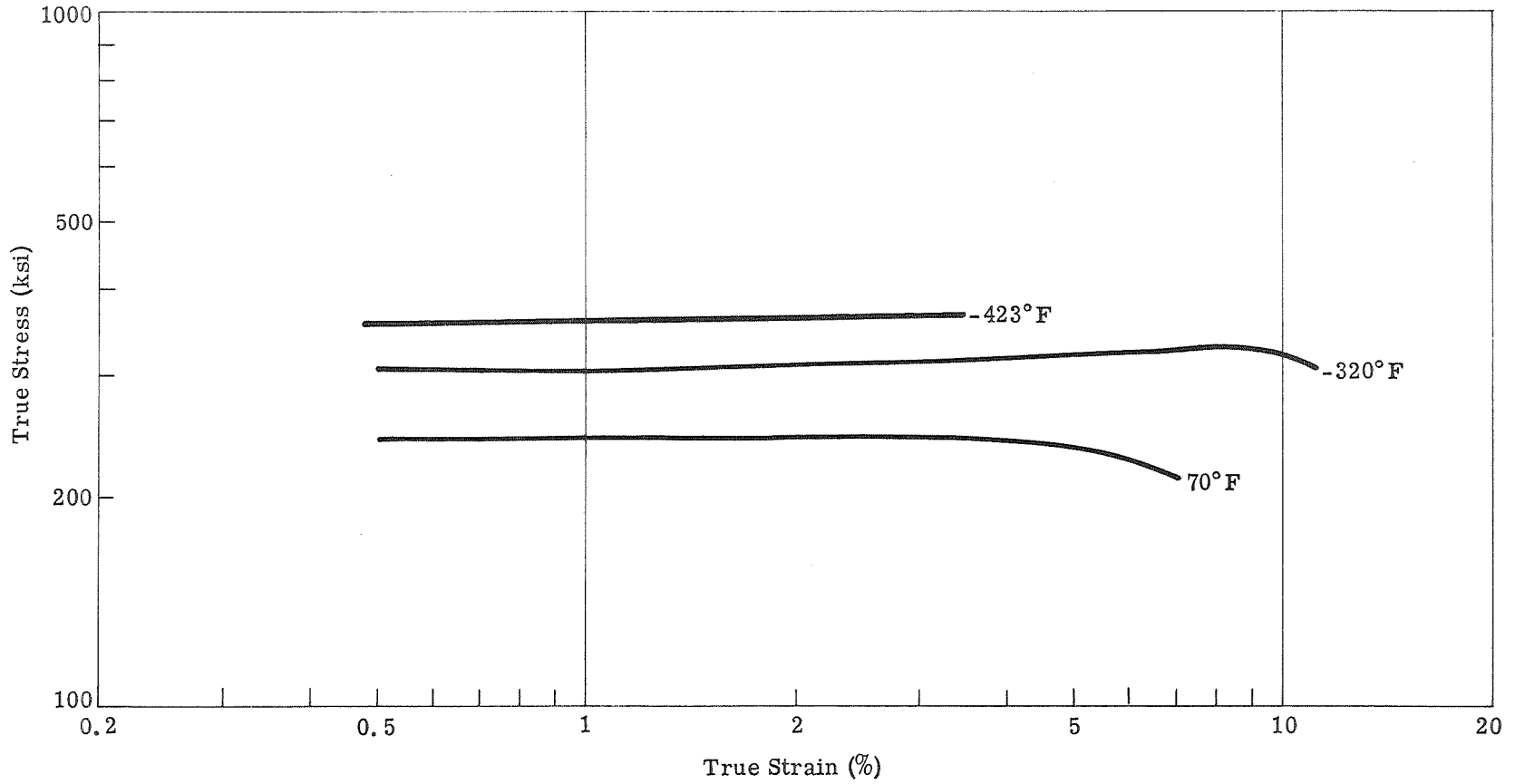
Fig. VI-26   True Stress vs True Strain Curve for Cryogenically-Stretched Parent Metal
Specimens (Type 301 Stainless Steel; Longitudinal Direction)

B. STATIC FRACTURE-TOUGHNESS TESTS

APPENDIX GUIDE - STATIC FRACTURE TOUGHNESS TESTS		
Alloy	Description of Table	Appendix Table No.
Aℓ 2021-T81	Surface-Flawed Parent Metal Specimens	A-9
Aℓ 2021-T81	Compact-Tension Parent Metal Specimens	A-10
Aℓ 2021-T81	Surface-Flawed Welded Specimens	A-11
Aℓ 2021-T81	Compact-Tension Welded Specimens	A-12
Aℓ X7007-T6	Surface-Flawed Parent Metal Specimens	A-14
Aℓ X7007-T6	Surface-Flawed Welded Specimens	A-15
Aℓ X7007-T6	Compact-Tension Welded Specimens	A-16
Type 301 Stainless Steel	Surface-Flawed Parent Metal Specimens	A-17
Type 301 Stainless Steel	Surface-Flawed Welded Specimens	A-18

1. Aluminum Alloys

    a. Parent-Metal Tests

        Surface-cracked specimens of Aℓ 2021-T81 were tested for
fracture toughness in the transverse orientation. At 70°F, their
fracture strength was approximately 50% of the yield strength and
their plane-strain fracture toughness averaged 34 ksi $\sqrt{in}$. We
noted that the fatigued precrack did not have the smooth appear-
ance that is typical of aluminum alloys; instead, it appeared
very coarse; and the rapid-fracture area, although relatively
flat, had laminar cracks in the region ahead of the semiminor
axis, but not in the regions away from this area. In tests at
-320°F, cracks of a size equivalent to those tested at 70°F
caused failure at stresses approaching 80% of the yield stress.
The average plane-strain fracture toughness was 54 ksi $\sqrt{in}$. At
-423°F, the fracture faces appeared much smoother than those ob-
served in the 70°F tests, there was virtually no evidence of
laminar cracking, and the plane-strain fracture toughness in-
creased to 59 ksi $\sqrt{in}$.

        The toughness of transverse compact-tension specimens in-
creased as the temperature decreased. The toughness values for
these specimens did not agree with those for the surface-flawed
specimens, but this is not surprising since the cracks grow in

different directions. In edge-notched, compact-tension specimens, cracks grow into the width direction, but in surface-cracked specimens they grow into the thickness direction. Plane-strain fracture toughness levels for the two types of specimens are compared below.

| Temperature (°F) | Critical Stress Intensity (ksi $\sqrt{in.}$) | |
	Surface-Cracked Specimens	Compact-Tension Specimens
70	34	26
-320	54	36
-423	59	40

Test data for parent-metal and welded specimens of Aℓ 2021-T81 are presented in Fig. VI-27. Note that in the longitudinal direction, surface-cracked specimens could not be fractured at stresses below the yield strength. After opening the first few specimens, we noted that a small area of "pop-in" existed near the front face, so we placed small (1/32 to 1/4 in.) resistance strain gages at the ends of the crack in an attempt to determine the "pop-in" load. The data we obtained were generally inconclusive, because the "pop-in" area was very small.

The fracture-toughness tests on the surface-cracked, parent-metal Aℓ X7007-T6 specimens produced some equally surprising results. In the longitudinal direction, the "pop-in" behavior was similar to that noted in the Aℓ 2021-T81 specimens, but was of much greater magnitude.

Delamination around the crack front prevented the Aℓ X7007-T6 specimens from fracturing below their yield strength. Figure VI-28 shows a typical specimen that was opened after being loaded to a high percentage of its yield strength at -320°F. From the appearance of this specimen we concluded that it failed when delamination occurred at the high-stress-intensity area at the front of the crack. Note that where this delamination occurred, the crack front is generally oriented in the width direction.
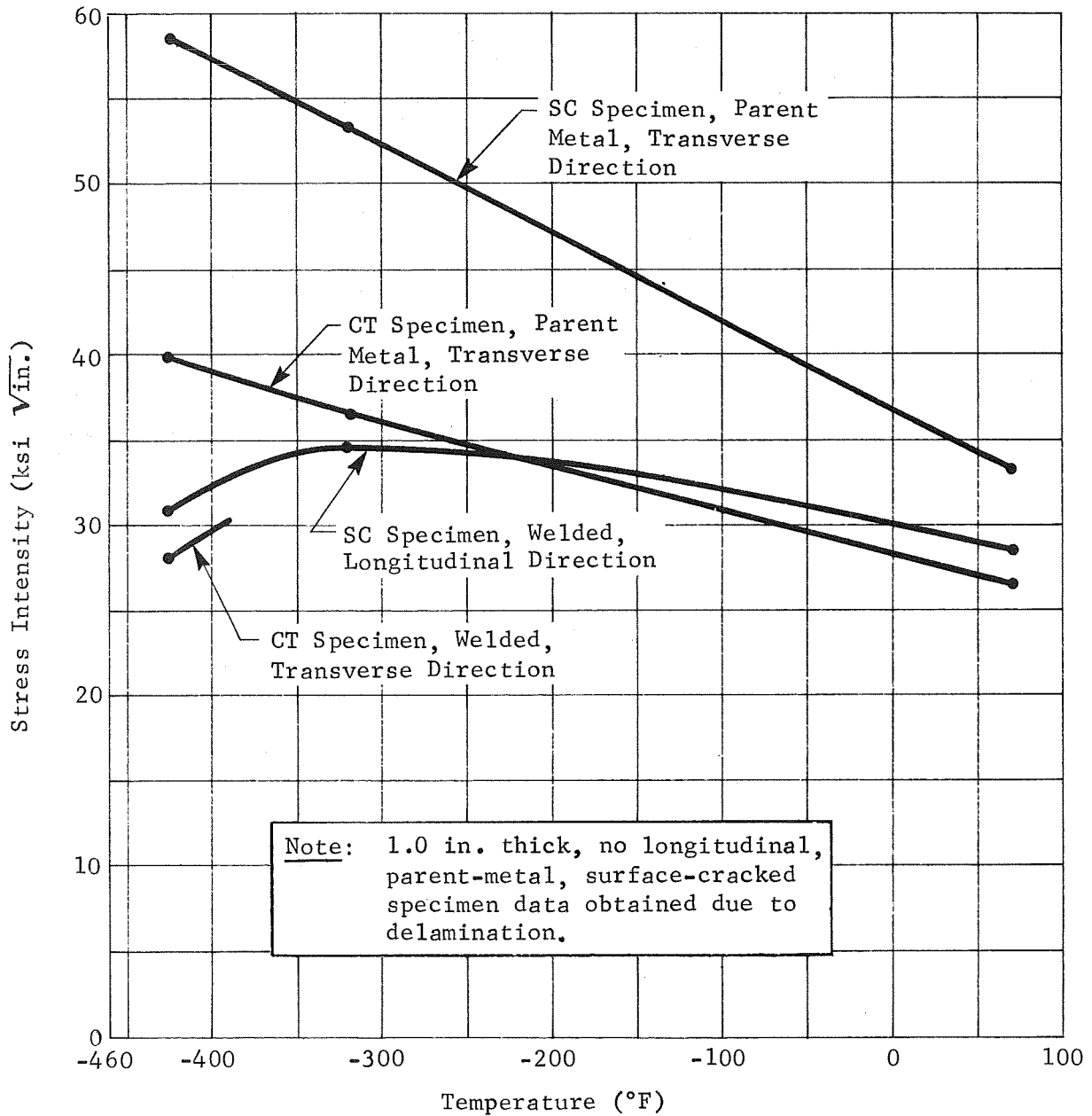
Fig. VI-27 Static Fracture Toughness of 2021-T81 Aluminum Alloy
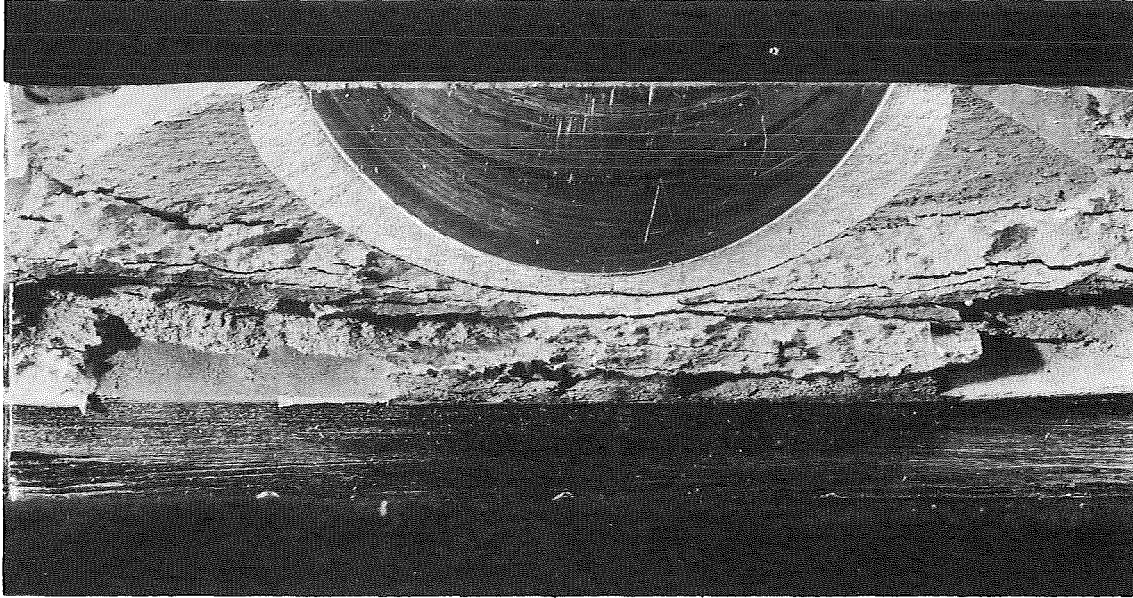
Fig. VI-28   Fracture Face of Aℓ X7007-T6 Surface-Flawed
             Specimen, Load Applied in the Longitudinal
             Direction, Temperature = -320°F

It appears that, when the specimen is loaded to a level
that should be the critical stress intensity at the nose of the
crack (the end of the semiminor axis), fracturing cannot occur
because the crack front becomes blunted; and because the stress
intensity decreases from a maximum at the nose of the crack to a
minimum at the free face, fracturing cannot occur elsewhere along
the crack front. Then, as the applied load is increased, the
stress intensity increases until it reaches a critical value at
some point on the crack front that is not blunted, and the frac-
ture begins. However, as the crack begins to spread, laminar crack-
ing occurs in the width direction and arrests the growth of the
crack, and a region of higher fracture toughness near the surface
prevents the crack from extending. When this occurs, a small
fracture region appears near the face of the crack.

This type of "pop-in" behavior has been confirmed by
staining the test specimens before opening them and by strain
gage data (see Fig. VI-29) obtained during the tests. Figure
VI-29 shows that there is local yielding at the end of the crack,
although the nominal strain away from the crack is still elastic.
At the "pop-in" load, the slope of the curve decreases abruptly.

Our attempts to calculate the critical stress intensities
from the "pop-in" load and the direction in which the fractures
began did not produce satisfactory data.
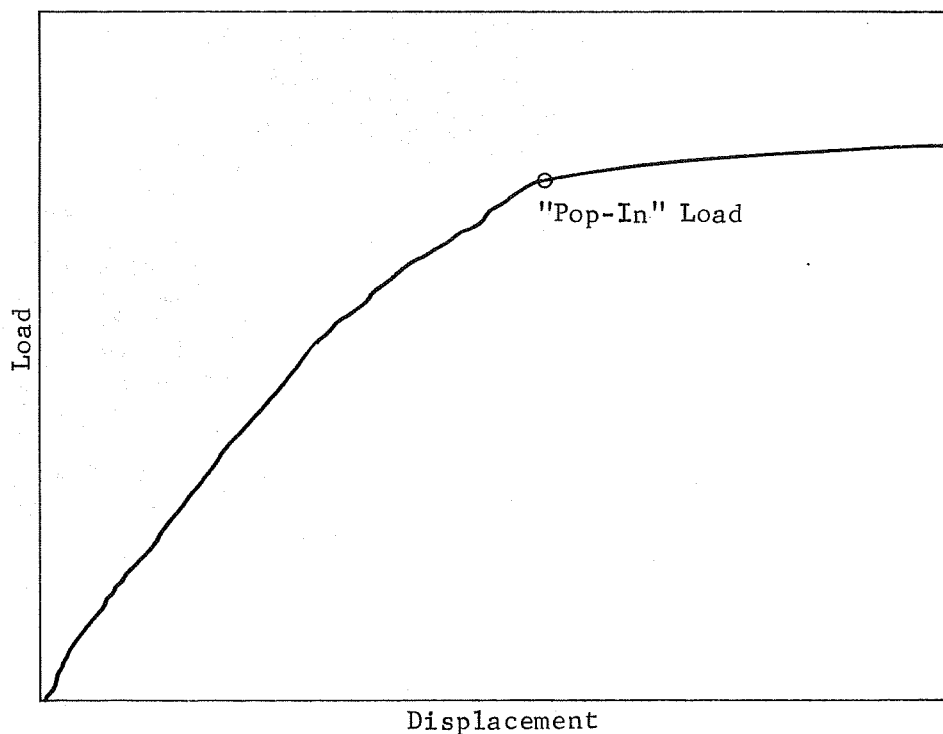
Fig. VI-29 Load vs Displacement for the Specimen Shown in
Fig. VI-28

Toughness tests conducted at -423°F produced complete
fractures that were not arrested. An examination of the fracture
face (see Fig. VI-30) revealed the same type of crack blunting
at the end of the semiminor axis and indicated that the fractures
began near the front face. However, unlike the fractures produced
at 70 and -320°F, the cracks proceeded for a significant distance
on each side of the defect. The resulting fractures apparently
progressed via shearing in the thickness direction.

In the transverse direction, the Aℓ X7007-T6 surface-
cracked parent metal specimens fractured at stresses below the
yield strength. In these cases, the fractures did not appear to
begin at the nose of the precrack. Examinations disclosed that
these fractures also began near the surface, like those that oc-
curred in longitudinally-loaded specimens of the parent metal
(see Fig. VI-31). In these cases, however, the laminar cracking
was not extensive enough to arrest the growth of the crack. Al-
though complete fractures occurred, toughness data calculated for
this series of tests are not reliable, and have not been included
in this report.
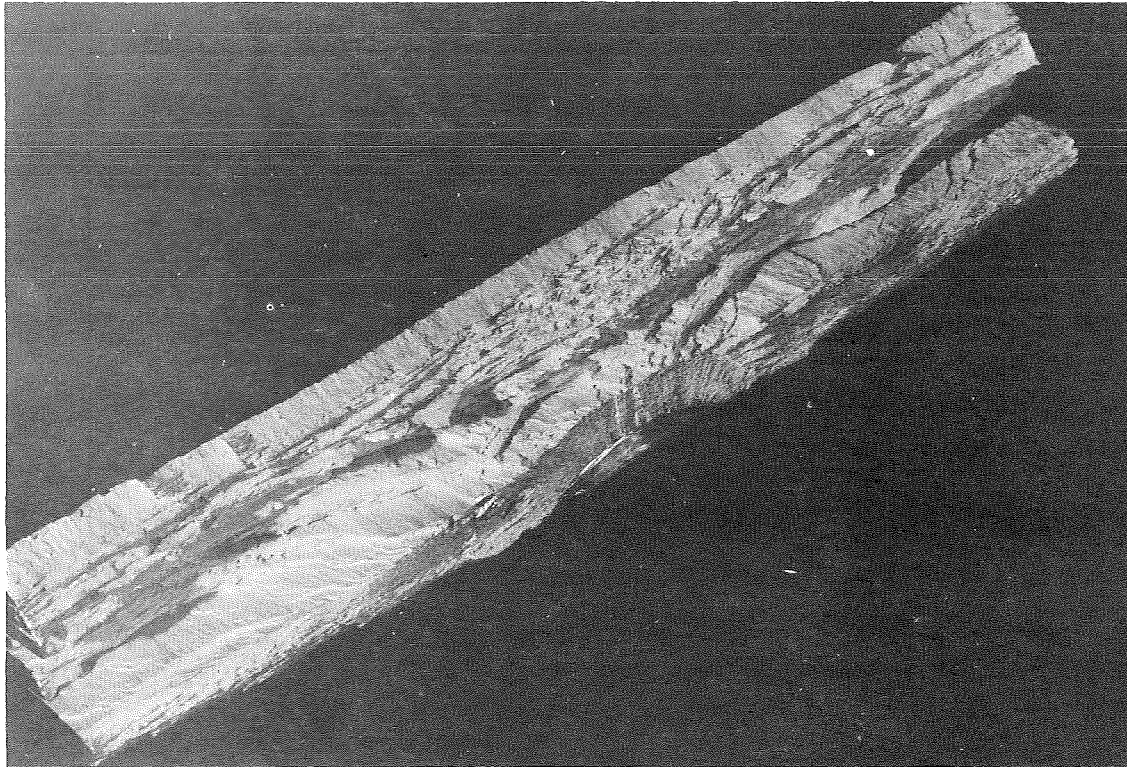
Fig. VI-30   Fracture Face of an Aℓ X7007-T6 Surface-Flawed Specimen, Load Applied in the Longitudinal Direction, Temperature = -423°F
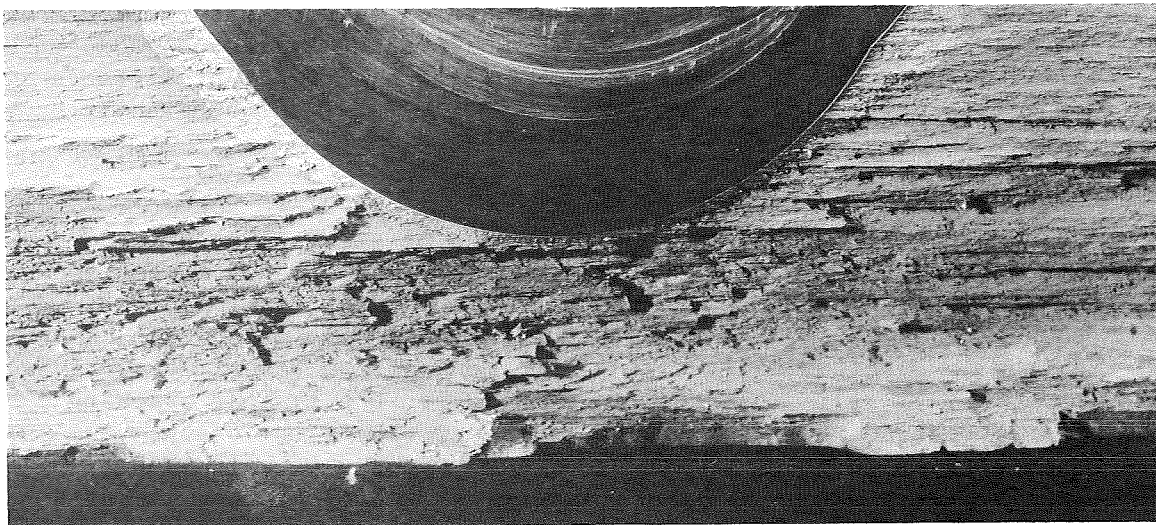
Fig. VI-31   Fracture Face of an Aℓ X7007-T6 Surface-Flawed Specimen, Load Applied in the Transverse Direction, Temperature = 70°F

Fracture-toughness values were calculated for compact-tension specimens that had been tested in the transverse direction. These values are shown below.

Temperature (°F)	Critical Stress Intensity (ksi $\sqrt{in.}$)
70	32
-320	23
-423	28

In these cases, the direction in which the cracks extended was normal to the direction of the laminations, and blunting did not appear to occur. Figure VI-32 shows the fracture face of a typical compact-tension specimen.

Fracture-toughness test data for parent-metal and welded specimens of Aℓ X7007-T6 are shown in Fig. VI-33.

b. Welded-Metal Tests

Fracture-toughness tests (in the longitudinal direction only) were performed on welded surface-cracked and compact-tension specimens of the two alloys.

As shown below, the toughness of the Aℓ 2021-T81 surface-flawed specimens increased as the temperature decreased. The one-in. thickness of the welded plates proved inadequate for obtaining fracture data for the through-cracked compact tension specimen, except at -423°F.

Temperature (°F)	Critical Stress Intensity (ksi $\sqrt{in.}$)	
	Surface-Cracked Specimens	Compact-Tension Specimens
70	29	
-320	35	
-423	31	28

The data for -423°F show relatively good agreement. (Although this type of comparison could not be made for wrought material, the directionality effects in a cast structure are limited enough so that the data for the two types of specimens can be compared.)

Fig. VI-32   Fracture Face of Parent-Metal X7007-T6
             Compact-Tension Specimen

Fig. VI-33 Static Fracture Toughness of X7007-T6 Aluminum Alloy

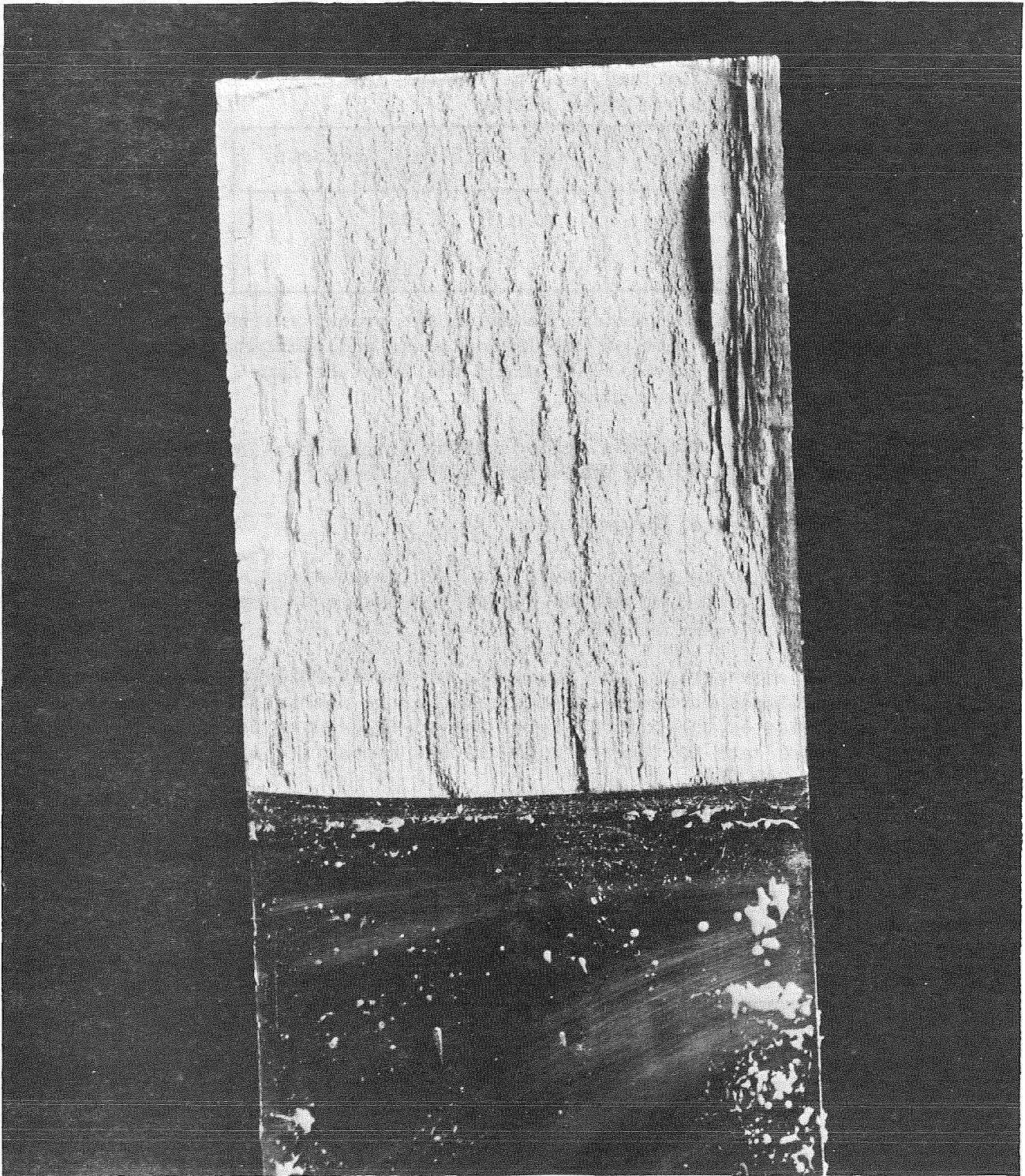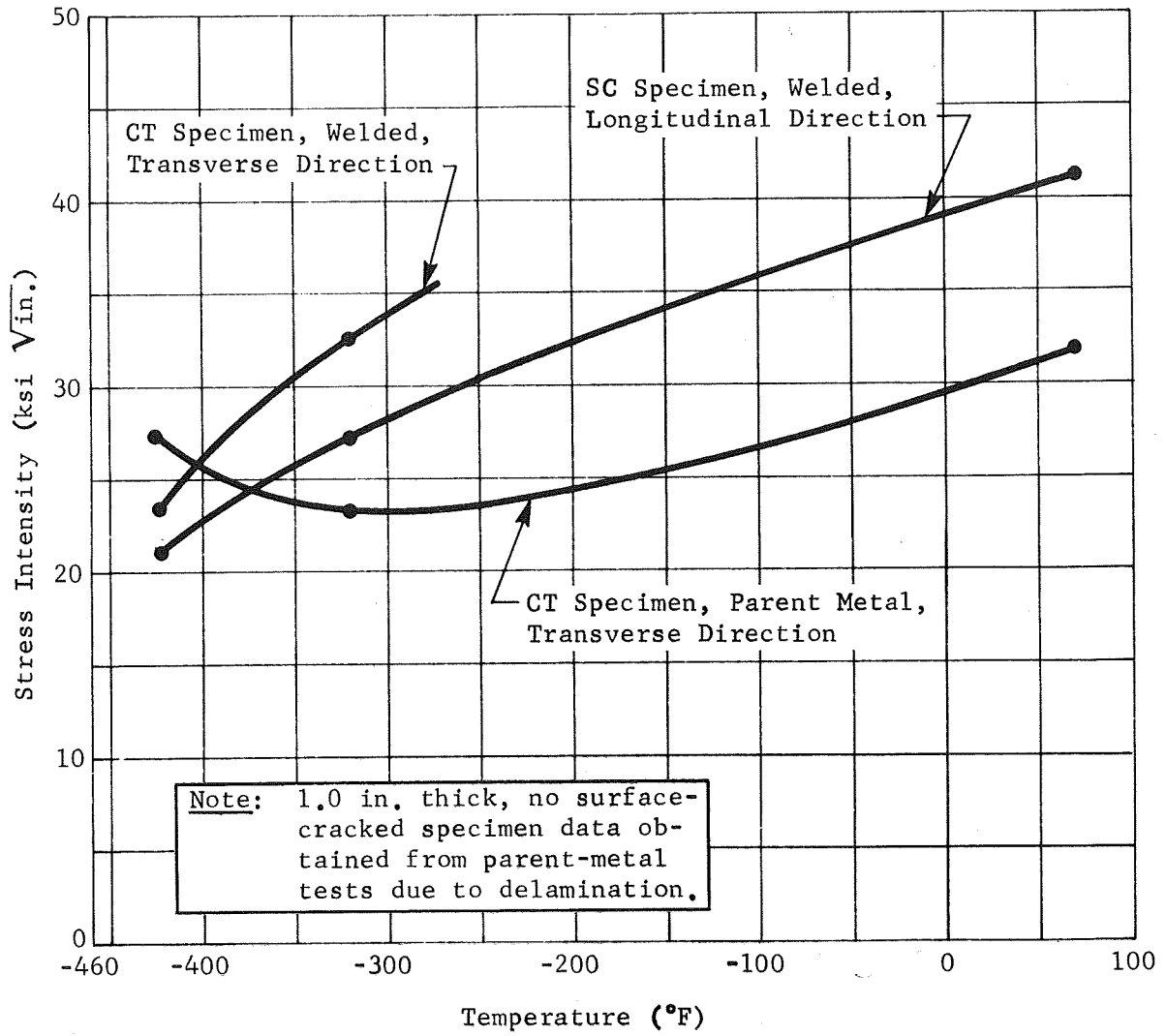The fracture stress/yield stress ratio was well above 1.0 for all surface-cracked specimens, and was typically between 1.2 and 1.4. Normally, such a high fracture stress/yield stress ratio would tend to invalidate the test results. However, in this case the welded material had not been stress-relieved, and the behavior can be readily explained.

When making a multipass weld on wide plates (our plates were two ft wide), the residual stresses at right angles to the weld can become significant. Although these residual stresses exist as tension stresses at the surface of the material, equilibrium requirements tell us that there should be transverse compressive stresses in the central portion of the weld zone. Now, if there is a crack approximately halfway through the plate, there may be rather high residual compression forces on the nose of the crack. Because these must be overcome during loading, the nominal stress can be greater than the local stress in the center of the weld, and the fracture stress/yield stress ratio may suggest that yielding has occurred even though the center of the weld is still elastic.

Test data for the Aℓ 2021-T81 specimens are presented in Fig. VI-27.

Because of the location of the failures in the 70°F, unnotched Aℓ 2021-T81 welded tension specimens and of reports of possible low toughness in the heat-affected zone, several specimens that had defects as close as possible to the fusion line were prepared and tested. In two samples, the tip of the defect was actually in the heat-affected zone, very close to the fusion line. Cross-sectional examinations of the failed specimens showed that the path of the fracture was not in the plane of the defect, but jumped to the fusion line and followed it for some distance. The toughness values for two replicate specimens were 27 and 28 ksi $\sqrt{in}$. A third specimen failed at a slightly lower level (22 ksi $\sqrt{in}$.); subsequent examination showed that the defect was in the cast material very close to the fusion line and followed the fusion line during fracture.

The Aℓ X7007-T6 exhibited the decrease in toughness with reductions in temperature that is characteristic of 7000-Series alloys. However, at room temperature, the toughness (41 ksi $\sqrt{in}$.) was quite high. The stress-intensity data for the two types of specimens follow and are also shown in Fig. VI-33.

Temperature (°F)	Critical Stress Intensity (ksi $\sqrt{in}$.)	
	Surface-Cracked Specimens	Compact-Tension Specimens
70	41	
-320	28	33
-423	21	24

At 70°F, there was not enough "pop-in" in the compact-tension welded specimens for us to determine the fracture toughness, but the cryogenic toughness levels obtained from the two types of specimens were in reasonably good agreement.

The fracture faces of the welded A𝓁 X7007-T6 specimens had several interesting features. The fatigued precrack did not exhibit the smooth, fine-grained appearance that is characteristic of aluminum alloys; instead, the surface patterns (see Fig. VI-34) matched the distribution of second-phase particles found in the macro- and micro-sections that were taken through the weld. These same patterns were apparent in the area of rapid fracture.

2. Cryogenically-Stretched Type 301 Stainless Steel

a. Parent-Metal Tests

Room-temperature tests performed using surface-flawed specimens showed that the fracture toughness was slightly higher than 100 ksi $\sqrt{in}$. In the longitudinal direction, one specimen was loaded to 108 ksi $\sqrt{in}$. $\left(\sigma / \sigma_{ys} = 1.00\right)$ without failing. The remaining specimens were cracked to create deeper flaws and failed at 102 ksi $\sqrt{in}$. The transverse specimens failed at an average stress intensity of 103 ksi $\sqrt{in}$., showing no directionality effects.

At cryogenic temperatures, the fracture toughness decreased significantly and was lower in the transverse direction. The fracture-toughness data are shown below and in Fig. VI-35.

Temperature (°F)	Critical Stress Intensity (ksi $\sqrt{in}$.)	
	Longitudinal Direction	Transverse Direction
70	102	103
-320	66	52
-423	55	44

Even though the toughness of the stainless steel decreased about 50% as the temperature went from 70 to -423°F, this was still a high level of toughness, considering that the tensile strength was so high (350 ksi).
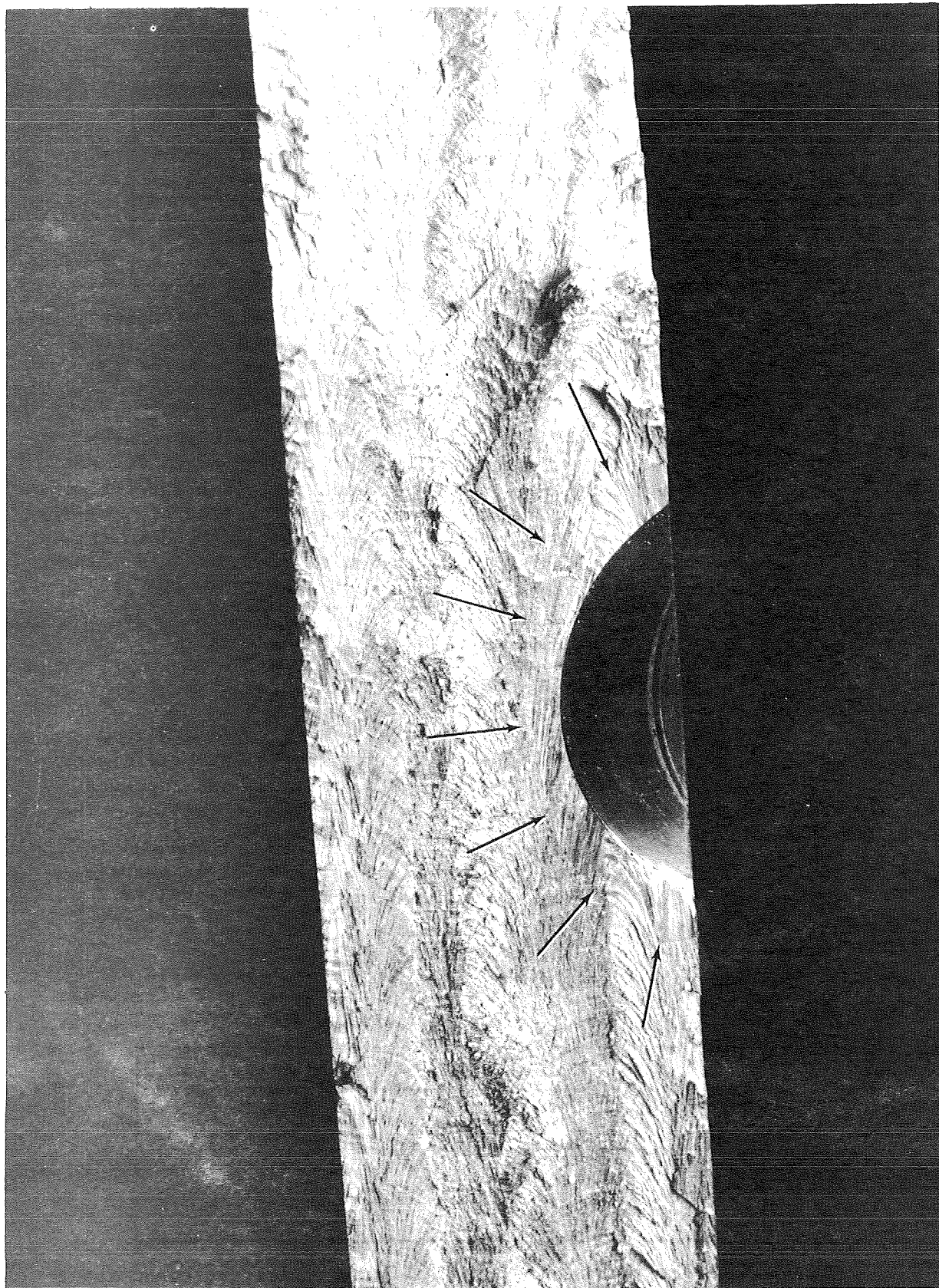
Fig. VI-34 Fracture Face of Welded X7007-T6 Surface-Flawed Specimen
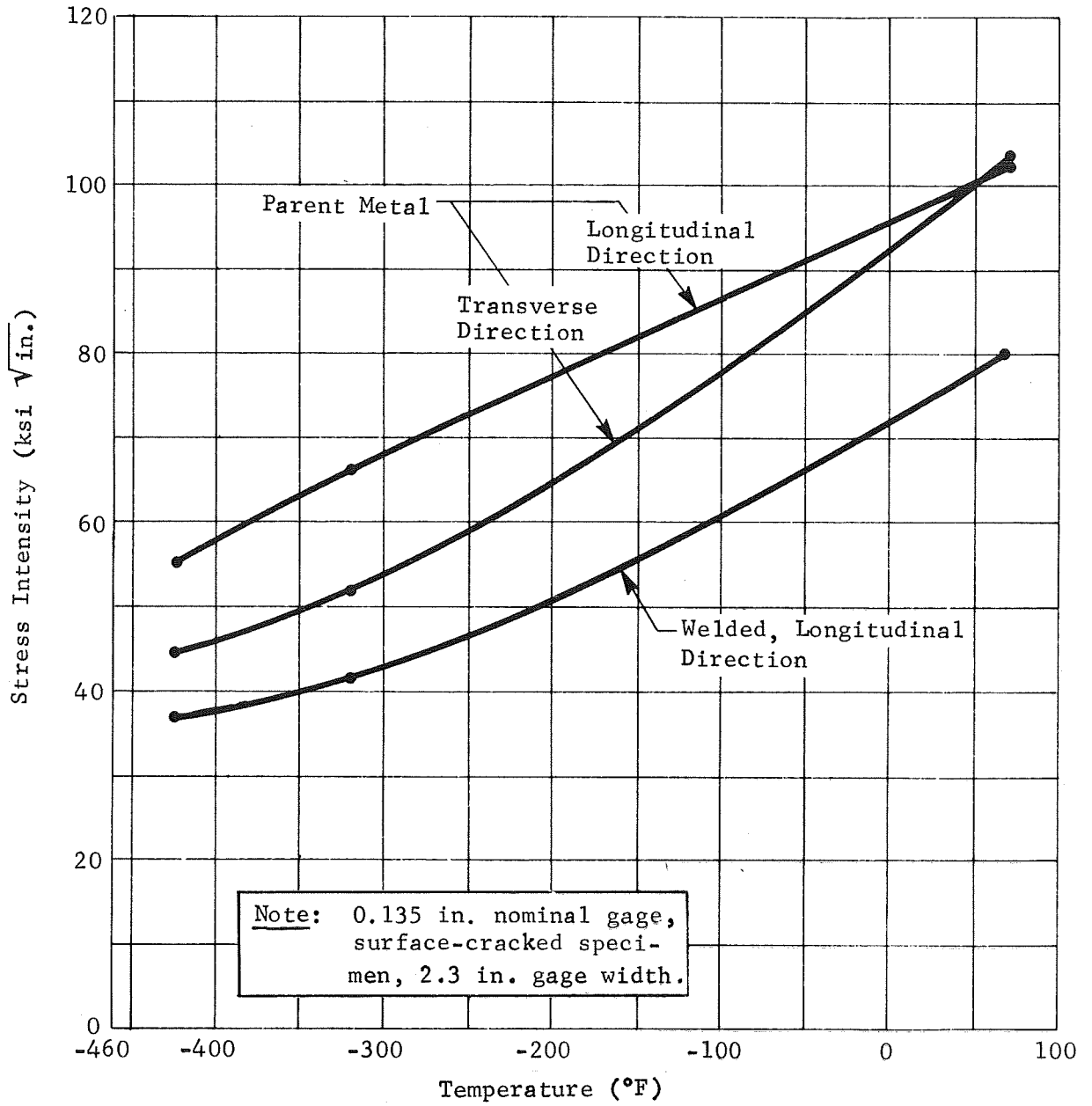
Fig. VI-35 Static Fracture Toughness of Cryogenically-Stretched
            Type 301 Stainless Steel

b. Welded-Metal Tests

At room temperature, the fracture toughness of surface-cracked welded specimens (80 ksi $\sqrt{in.}$) was approximately 78% of that for the parent metal. At cryogenic temperatures, the fracture toughness decreases further: at -320 and -423°F, the toughness was 42 and 37 ksi $\sqrt{in.}$, respectively, or only about 65% as tough as the parent metal. These test data are presented in Fig. VI-35.

C. CYCLIC-LOAD FLAW-ENLARGEMENT TESTS

APPENDIX GUIDE - CYCLIC LOAD TESTS

Alloy	Description of Table	Appendix Table Number
Aℓ 2021-T81	Compact-Tension Parent Metal Specimens	A-19
Aℓ 2021-T81	Surface-Flawed Welded Specimens	A-20
Aℓ X7007-T6	Compact-Tension Parent Metal Specimens	A-21
Aℓ X7007-T6	Surface-Flawed Welded Specimens	A-22
Type 301 Stainless Steel	Surface-Flawed Parent Metal Specimens	A-23
Type 301 Stainless Steel	Surface-Flawed Welded Specimens	A-24

In most cases, only three tests were performed to characterize crack-growth behavior. From this limited amount of testing, we can obtain only a crude idea of this process (the exponential crack-growth function, for example, cannot be calculated with such limited information). Therefore, the prime purpose for conducting these tests was to compare our results with available data.

In all cyclic tests, the stress ratio, R, was less than 0.05; in most cases, it was about 0.02. As a result, the data are treated as though R = 0. Instead of using $\Delta K = K_{max} - K_{min}$, we have presented the test data as K_{max}; but for convenience, we have called the stress intensity K rather than K_{max} in order to indicate that we are using the average maximum stress intensity, not the initial stress intensity.

In these tests, we tried to keep the difference between the initial stress intensity and the final stress intensity small. By doing so, we were able to obtain a more accurate linear interpolation of the crack-growth rate.

1. Aluminum Alloys

    a. Parent-Metal Tests

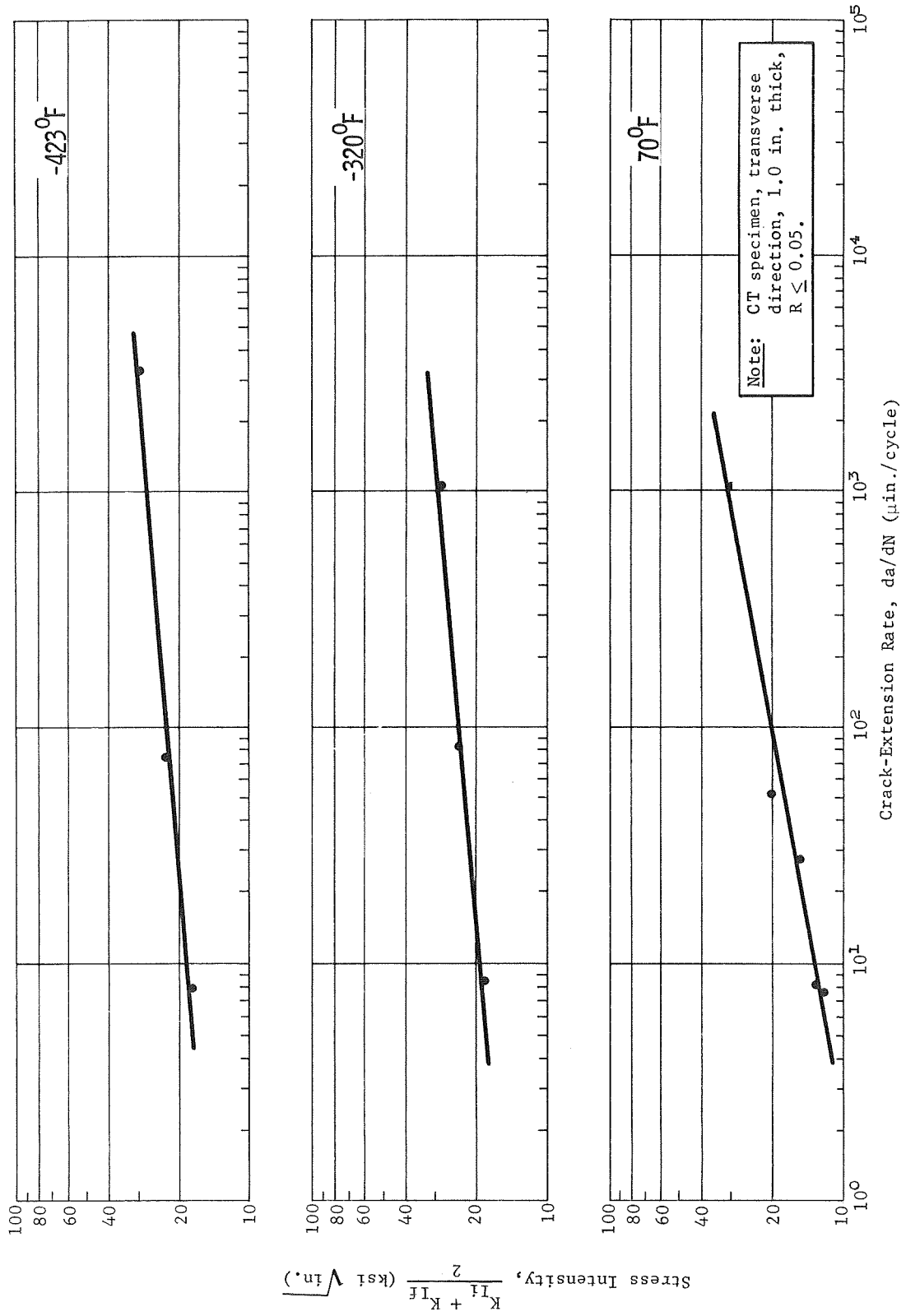   Test data for compact-tension specimens are presented in Fig. VI-36 and VI-37.

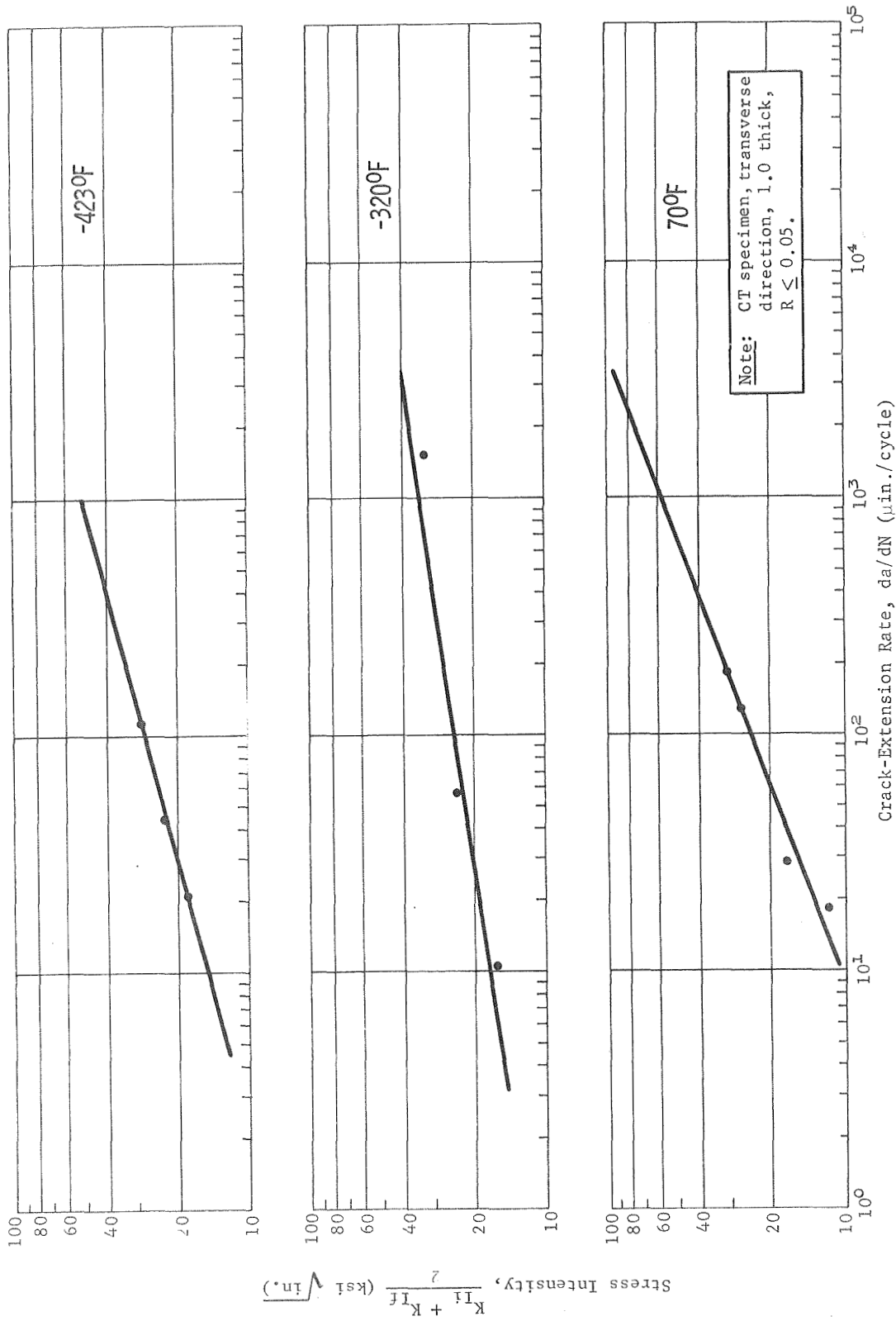Fig. VI-36 Cyclic Crack-Extension Rates for Parent Metal (2021-T81 Aluminum Alloy)

Fig. VI-37 Cyclic Crack-Extension Rates for Parent Metal (X7007-T6 Aluminum Alloy)

b.   Welded-Metal Tests

Surface-cracked specimens were used to obtain the data presented in Fig. VI-38 and VI-39. In some cases, multiple data were obtained by periodically fatigue-marking the specimens. Figure VI-40 shows the fracture face of a typical, fatigue-marked, Aℓ 2021-T81 welded specimen.

Surface-flawed specimens were not intentionally cycled to failure. Had we attempted to induce fractures at stresses below the yield strength, the end of the semiminor crack axis would have been so close to the back face that the stress intensity would be meaningless.

2.   Cyrogenically-Stretched Type 301 Stainless Steel

Surface-cracked specimens were tested to determine the crack-growth rates for parent-metal and welded specimens. The data from these tests (see Fig. VI-41) show that, at 70 and -320°F, cracks grew faster (at a specific stress intensity) in the welded material, and that, at -423°F, both types of specimens had identical crack-growth rates.
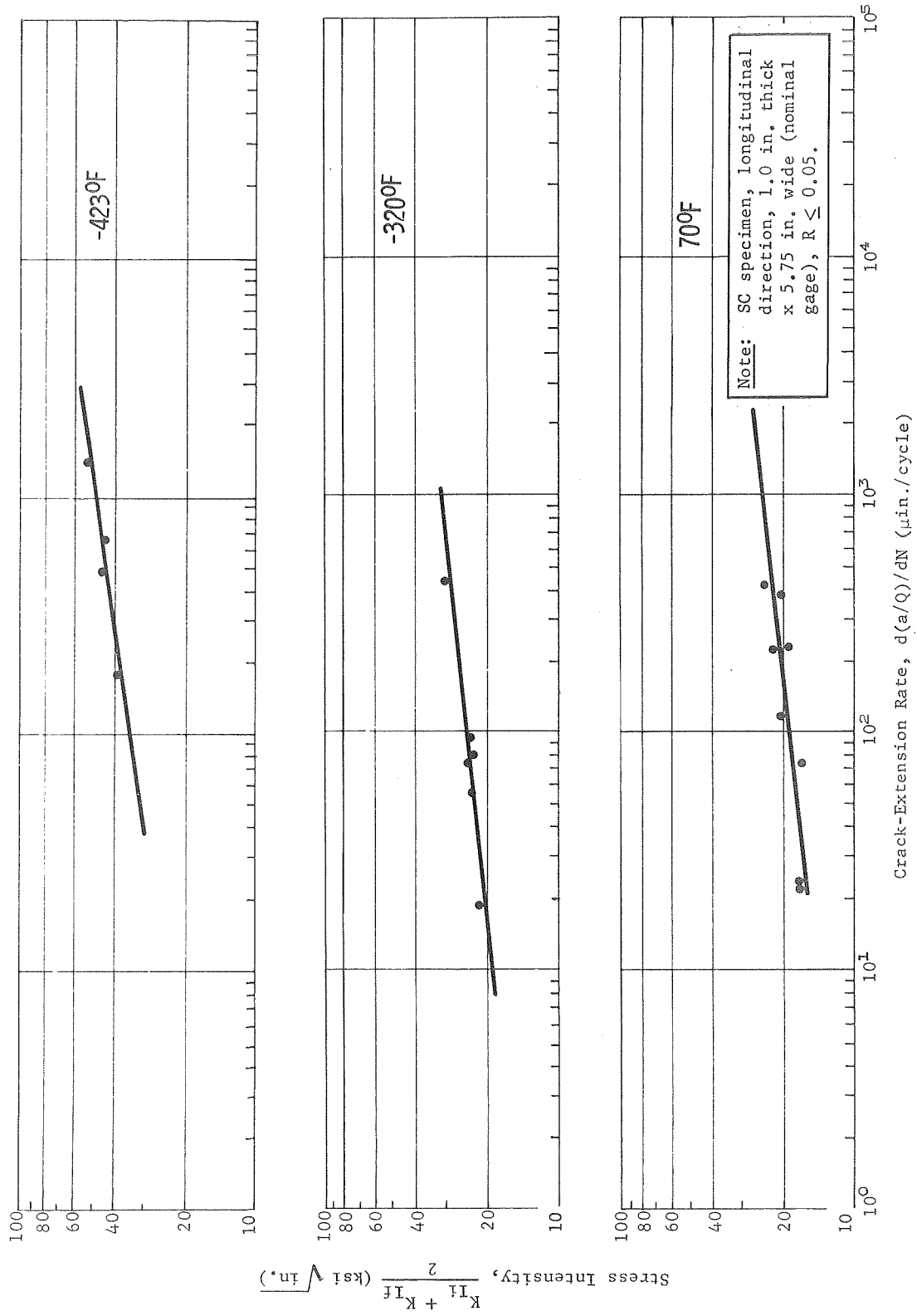
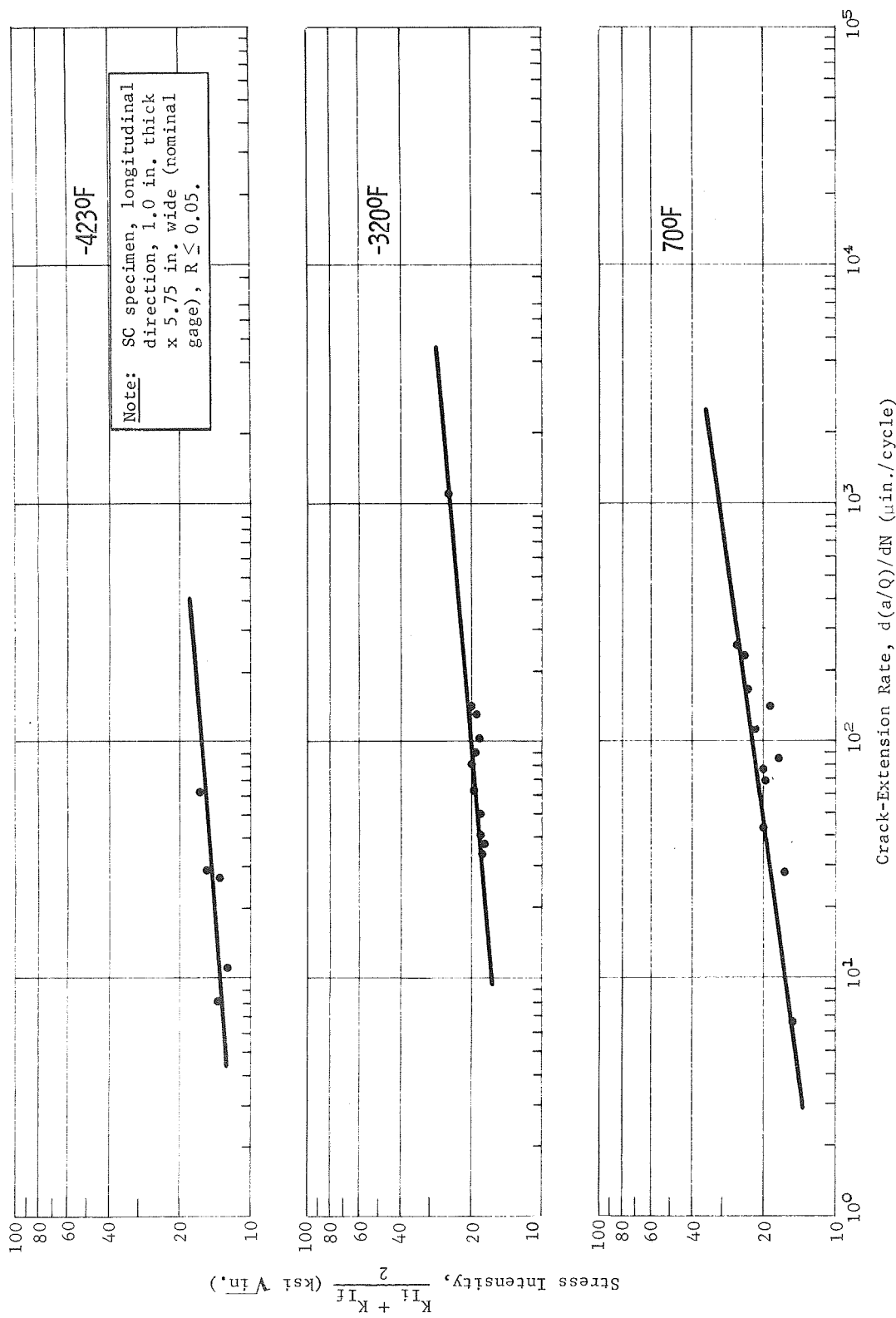Fig. VI-38 Cyclic Crack-Extension Rates for Welded 2021-T81 Aluminum Alloy

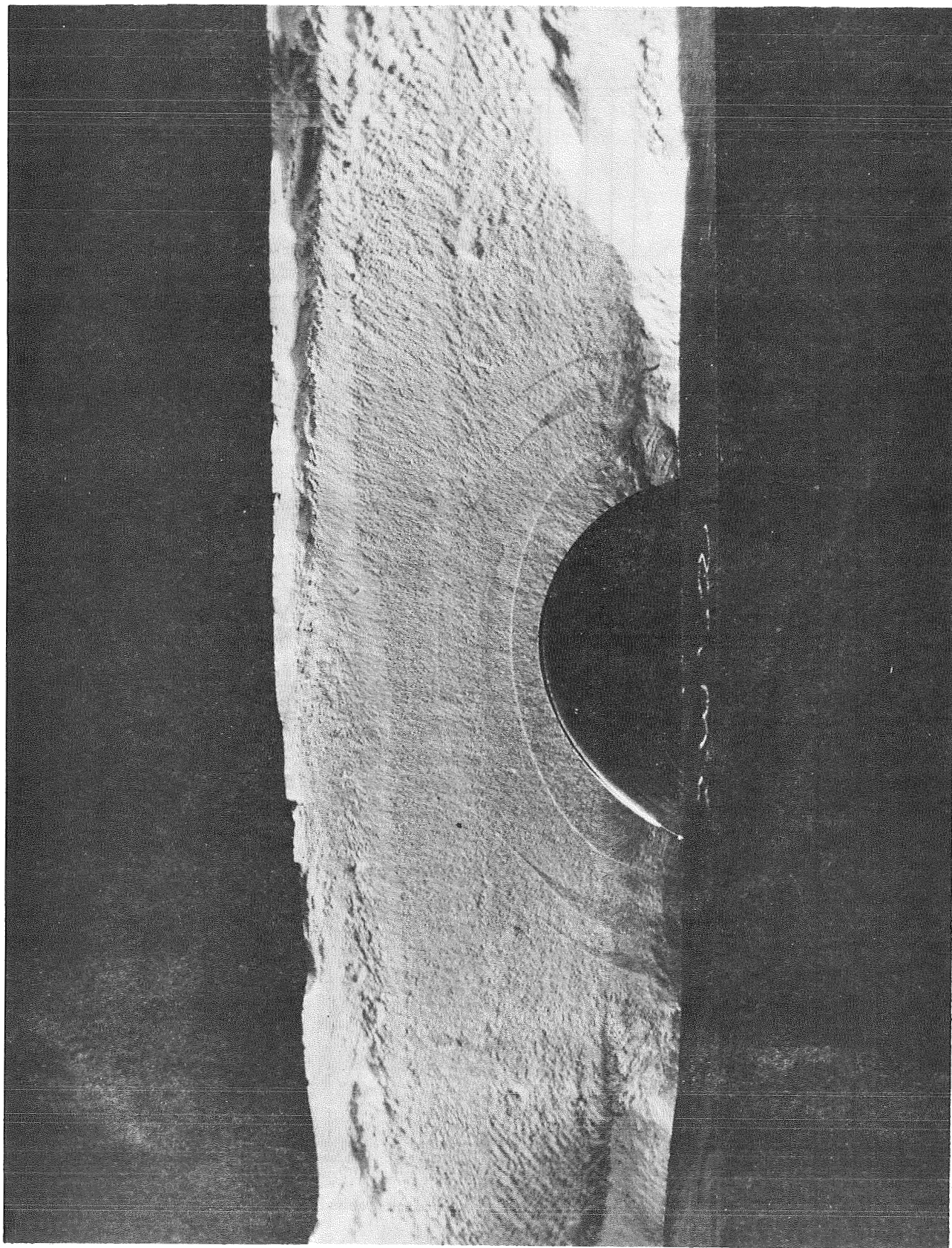Fig. VI-39   Cyclic Crack-Extension Rates for Welded X7007-T6 Aluminum Alloy

Fig. VI-40   Fracture Face of Fatigue-Marked 2021-T81
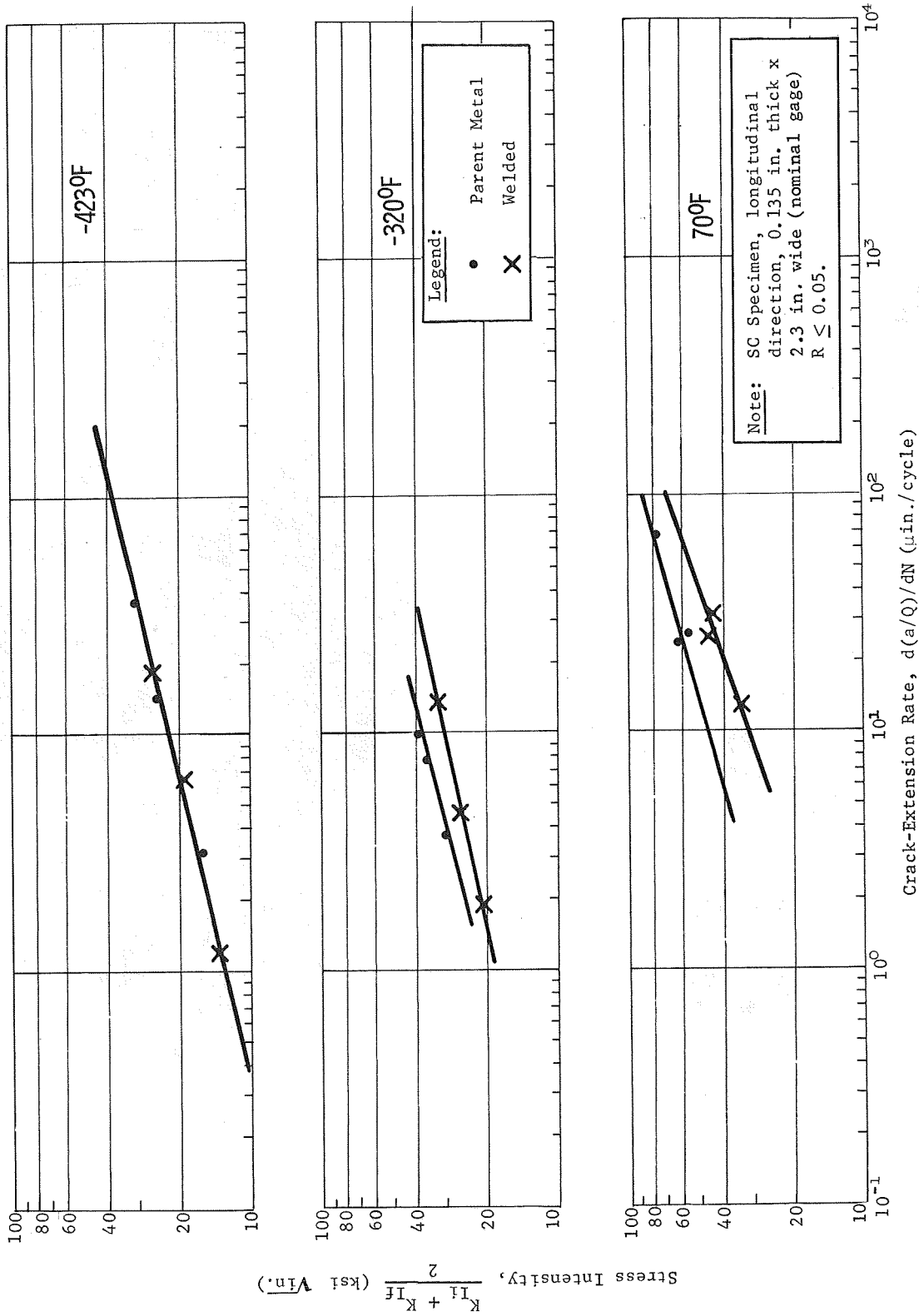Cyclic Fracture-Toughness Specimen

Fig. VI-41 Cyclic Crack-Extension Rates for Parent Metal and Welded Cryogenically-Stretched 301 Stainless Steel

D.   SUSTAINED-LOAD FLAW-ENLARGEMENT TESTS

APPENDIX GUIDE - SUSTAINED LOAD TESTS		
Alloy	Description of Table	Appendix Table No.
Aℓ 2021-T81	Compact-Tension Parent Metal Specimens	A-25
Aℓ 2021-T81	Compact-Tension Welded Specimens	A-26
Aℓ X7007-T6	Compact-Tension Parent Metal Specimens	A-27
Aℓ X7007-T6	Compact-Tension Welded Specimens	A-28
Type 301 Stainless Steel	Surface-Flawed Parent Metal Specimens	A-29
Type 301 Stainless Steel	Surface-Flawed Welded Specimens	A-30

These tests were performed to determine the minimum stress in-
tensity that would produce subcritical flaw growth in the various
alloy specimens at each test temperature. In general, three spe-
cimens were used to bracket the threshold level, but in some cases,
it was necessary to use extra specimens. Because time and funds
did not permit us to confirm the exact levels, these data are only
approximate.

1. Aluminum Alloys

    a.   Parent-Metal Tests

    The threshold data for Aℓ 2021-T81 and Aℓ X7007-T6 are
summarized in the following table.

Aluminum Alloy	Temperature (°F)	Stress-Intensity Ratio, K_{Ii}/K_{Ic}	Crack Growth
2021-T81	70	0.77	No
2021-T81	70	0.77	No
2021-T81	70	0.82	Yes
2021-T81	70	0.83	Yes
2021-T81	-320	0.73	No
2021-T81	-320	0.82	No
2021-T81	-320	0.82	Yes
2021-T81	-320	0.88	Yes
2021-T81	-423	0.76	Yes*
2021-T81	-423	0.79	Yes
2021-T81	-423	0.90	Yes
2021-T81	-423	0.91	Yes
X7007-T6	70	0.36	No
X7007-T6	70	0.48	Yes[†]
X7007-T6	70	0.53	Yes[†]
X7007-T6	70	0.64	Yes
X7007-T6	70	0.71	Yes
X7007-T6	-320	0.73	No
X7007-T6	-320	0.82	Yes
X7007-T6	-320	0.96	Yes
X7007-T6	-320	1.04	Yes
X7007-T6	-320	1.07	Yes
X7007-T6	-423	0.71	No
X7007-T6	-423	0.80	Yes

*Very slight.

†Slight.

On the basis of these results, the following threshold levels have been tentatively selected for the parent metals.

Aluminum Alloy	Threshold Level, K_{TH}/K_{Ic}		
	70°F	-320°F	-423°F
2021-T81	$0.77 < K_{TH}/K_{Ic} < 0.82$	$K_{TH}/K_{Ic} = 0.82$	$K_{TH}/K_{Ic} < 0.76$
X7007-T6	$0.38 < K_{TH}/K_{Ic} < 0.48$	$0.73 < K_{TH}/K_{Ic} < 0.82$	$0.71 < K_{TH}/K_{Ic} < 0.80$

The data for Aℓ 2021-T81 are typical of aluminum alloys in an inert environment. X7007-T6 has a very low threshold at room temperature, but at cryogenic temperatures, the threshold level is more typical.

b. Welded Metal Tests

The threshold data for welded specimens of both aluminum alloys are summarized below.

Aluminum Alloy	Temperature (°F)	Stress-Intensity Ratio, K_{Ii}/K_{Ic}	Crack Growth
2021-T81	70	0.50	No
2021-T81	70	0.58	Yes*
2021-T81	70	0.61	No
2021-T81	70	0.63	Yes
2021-T81	70	0.65	Yes
2021-T81	-320	0.62	No
2021-T81	-320	0.69	Yes
2021-T81	-320	0.73	Yes
2021-T81	-423	0.69	No
2021-T81	-423	0.72	Yes
2021-T81	-423	0.79	Yes
X7007-T6	70	0.81	No
X7007-T6	70	0.85	No
X7007-T6	70	0.90	Yes
X7007-T6	70	0.90	Yes
X7007-T6	70	0.91	Yes
X7007-T6	70	1.01	Yes
X7007-T6	-320	0.59	No
X7007-T6	-320	0.74	Yes
X7007-T6	-320	0.79	Yes
X7007-T6	-423	0.50	No
X7007-T6	-423	0.62	Yes*

*Very slight.

On the basis of the above data, the following threshold levels have been determined for welded joints.

Aluminum Alloy	Threshold Level, K_{TH}/K_{Ic}		
	70 °F	-320 °F	-423 °F
2021-T81	$0.58 < K_{TH}/K_{Ic} < 0.61$	$0.62 < K_{TH}/K_{Ic} < 0.69$	$0.69 < K_{TH}/K_{Ic} < 0.72$
X7007-T6	$0.85 < K_{TH}/K_{Ic} < 0.90$	$0.59 < K_{TH}/K_{Ic} < 0.74$	$0.50 < K_{TH}/K_{Ic} < 0.62$

The data suggest that welded Aℓ 2021-T81 has a rather low threshold at room temperature with a slight increase at cryogenic temperatures. The testing to be performed in the forthcoming work under this contract should provide enough additional data to determine whether the threshold really is this low at room temperature.

The data for welded Aℓ X7007-T6 specimens are more difficult to interpret. Examinations of the surfaces showed that the fatigue precrack was not smooth and that the surface was faceted with numerous cracks (see Fig. VI-42). In addition, the crack front was usually quite irregular, which made it extremely difficult to tell whether crack growth had occurred. As a result, we feel that the stress intensity could not be calculated accurately. In future tests, we will control the amount of fatigue growth from the razor-sharpened precrack in order to minimize the type of fracturing described above and to improve the validity of the data.

2. Type 301 Stainless Steel

a. Parent Metal Tests

The threshold data for cryogenically-stretched Type 301 stainless steel specimens are summarized in the following table.

Temperature (°F)	Stress-Intensity Ratio, K_{Ii}/K_c	Crack Growth
70	0.67	No
70	0.79	Yes*
70	0.80	Yes*
70	0.88	Yes
-320	0.42	No
-320	0.46	No
-320	0.58	No
-320	0.68	Yes*
-423	0.55	No
-423	0.65	Yes
-423	0.76	Yes
*Slight.		

On the basis of these results, the following threshold levels have been tentatively selected for the parent metal stainless steel.
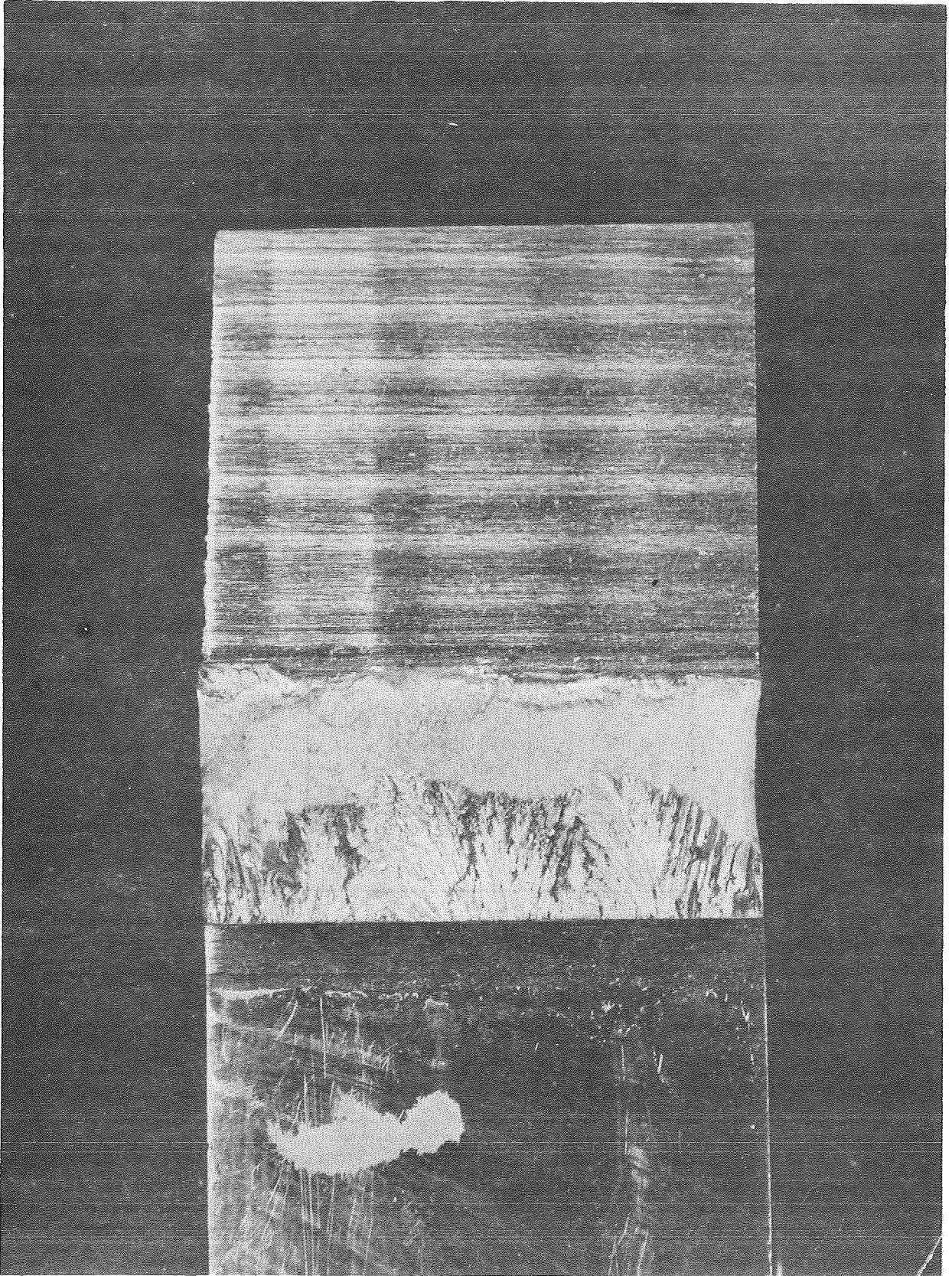
Fig. VI-42   Fracture Surface of Sustained-Load, Welded X7007-T6 Specimen

Threshold Level, K_{TH}/K_{Ic}		
70°F	-320°F	-423°F
$0.67 < K_{TH}/K_{Ic} < 0.79$	$0.58 < K_{TH}/K_{Ic} < 0.68$	$0.55 < K_{TH}/K_{Ic} < 0.65$

The threshold level at 70°F is probably close to the upper-limit value since the amount of crack growth at values of 0.79 and 0.80 was slight. The cryogenic threshold levels are approximately 60% of the critical stress intensity.

b. Welded Metal Tests

The threshold data for welded Type 301 stainless steel specimens are summarized below.

Temperature (°F)	Stress-Intensity Ratio, K_{Ii}/K_{Ic}	Crack Growth
70	0.58	No
70	0.64	Yes
70	0.77	Yes
-320	0.72	No
-320	0.88	No
-320	0.90	Yes
-423	0.65	No
-423	0.72	Yes*
-423	0.79	Yes
-423	0.91	Yes†
*Slight.		
†Failed.		

The following threshold levels have been tentatively selected for the welded material.

Threshold Level, K_{TH}/K_{Ic}		
70°F	-320°F	-423°F
$0.58 < K_{TH}/K_{Ic} < 0.64$	$0.88 < K_{TH}/K_{Ic} < 0.90$	$0.65 < K_{TH}/I_{Ic} < 0.72$

At room temperature, the threshold level for the welded specimens appears to be slightly lower than that for the parent metal, which is not surprising. The cryogenic behavior is somewhat confusing as a result of the rather high level indicated at -320°F.

VII. DATA COMPARISON, CONCLUSIONS, AND RECOMMENDATIONS FOR
      FUTURE WORK

This chapter compares the experimental data for Aℓ X7007-T6,
Aℓ 2021-T81, and Type 301 stainless steel obtained during this
program with data for materials currently used in liquid propel-
lant systems, discusses the overall suitability of these new
compositions for potential applications, and presents recommenda-
tions for additional work, based on the present state of behav-
ioral knowledge.

A. MECHANICAL PROPERTIES

The Aℓ 2021-T81 and Aℓ X7007-T6 alloys were developed as
high-strength, weldable, cryogenic alloys. A comparison of the
parent-metal strength properties of these two alloys with those
of the currently-used high-strength compositions (see Fig. VII-1)
illustrates that Aℓ 2021-T81 and Aℓ X7007-T6 are slightly stronger.
The data for the high-strength compositions now in use are taken
from the Cryogenic Materials Data Handbook (Ref 9) and represent
typical properties for a variety of gages, and therefore may not
clearly show the superiority of the two new alloys, since the in-
clusion of sheet-gage property data in the typical properties
presumably raises the average value.

Another point to be considered is the report by Alcoa to
Martin Marietta that the heats of material obtained for this
work have properties at the lower end of the strength band. New
heats of material of each composition have been procured from
Alcoa and studied. The new sample of Aℓ X7007-T6 has signifi-
cantly higher strength at room temperature, whereas the strength
of the new sample of Aℓ 2021-T81 is similar to that shown by the
original sample.

The weld strengths of Aℓ 2021-T81 and Aℓ X7007-T6 appear to
be at least as high as those of the currently-used high-strength
alloys.
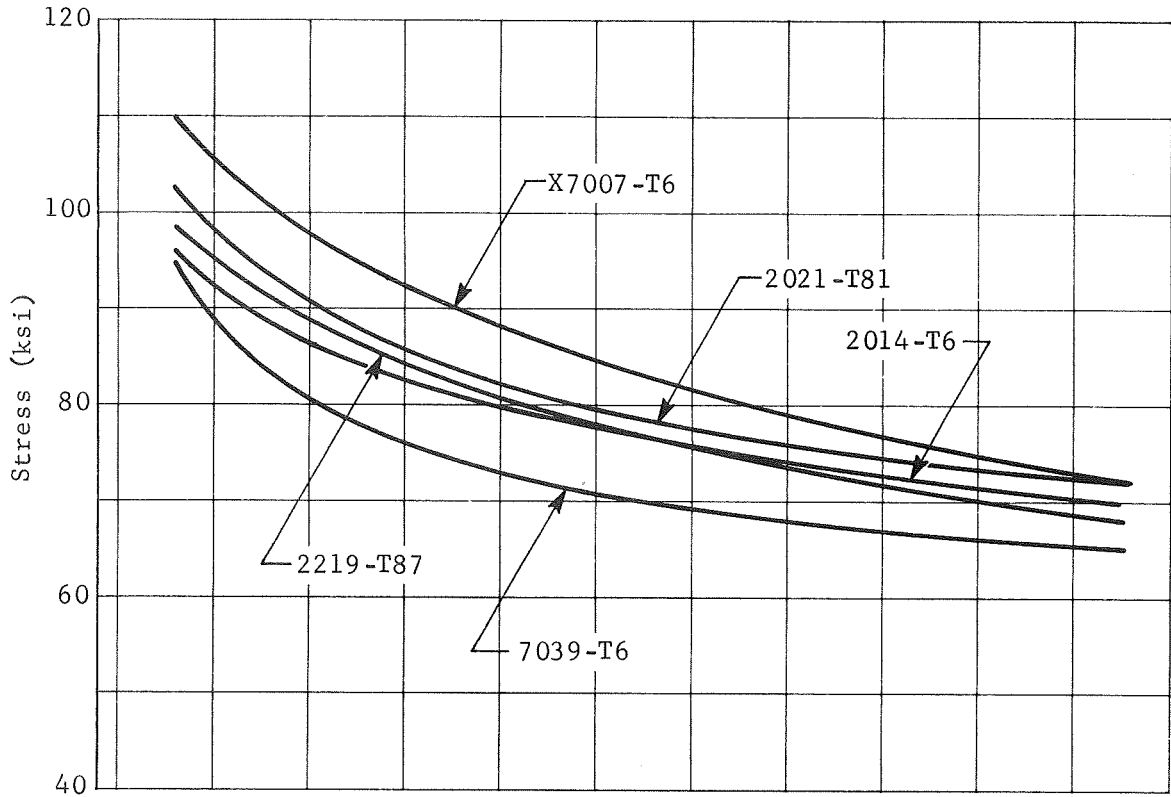
(a)   Ultimate Strength
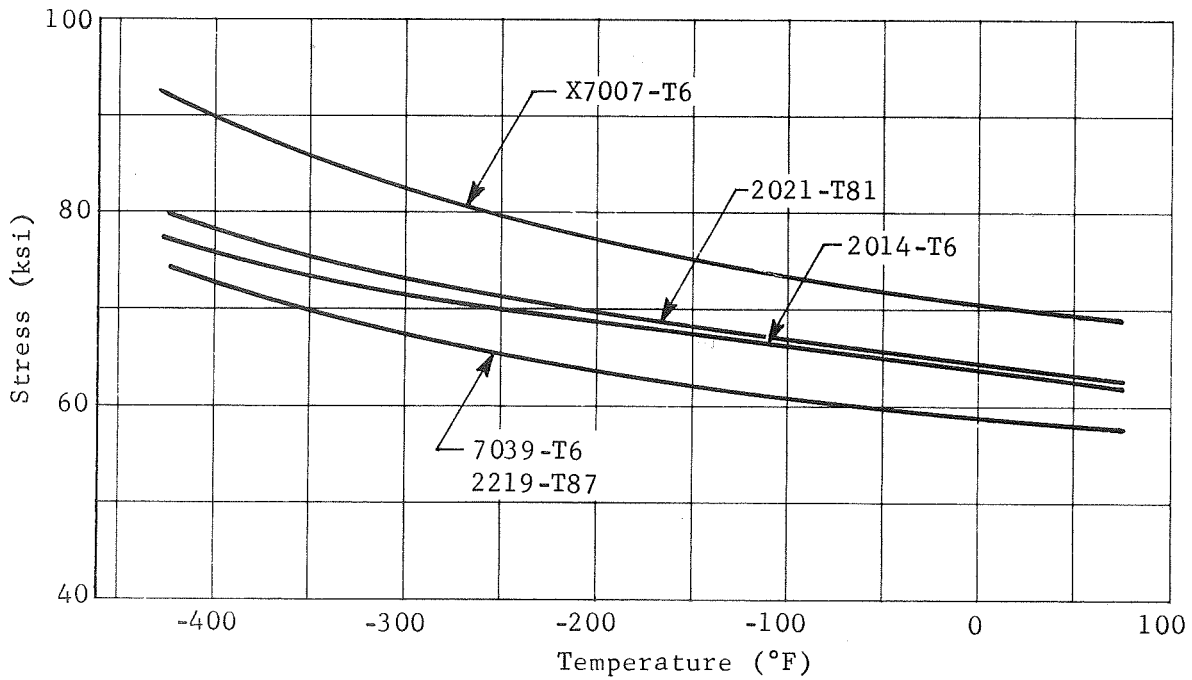
(b) Yield Strength

Fig. VII-1 Ultimate Strength and Yield Strength of Various Aluminum Alloys

As a candidate for high-strength applications, cryogenically-stretched Type 301 stainless steel can best be compared to titanium alloys. For cryogenic service, the only titanium alloys that can be considered are 5Aℓ-2.5Sn (ELI) and 6Aℓ-4V (ELI, annealed) titanium. As shown in Fig. VII-2, the stainless steel is significantly stronger than the titanium alloys. However, on a strength-density basis, the stainless steel is comparable only with the 6Aℓ-4V titanium and only at 70°F; below room temperature, the titanium is clearly superior. The strength-density value for the stainless steel in the cryogenic range is slightly lower than that of the 5Aℓ-2.5Sn composition.

The weld-joint efficiency for the stainless steel, 95%, is approximately that obtained using titanium alloys. Therefore, the strength of the various welded specimens will exhibt the same relationship as that shown for the various parent-metal specimens.

The rather peculiar behavior of Poisson's ratio of aluminum and stainless steel as a function of temperature (i.e., the sharp increase between -320 and -423°F) was also noted by Boeing during an investigation of deep flaws in thin-walled 2219-T87 aluminum alloy and 5Aℓ-2.5Sn titanium tanks (Ref 10). Although no logical explanation for this behavior is apparent, two independent investigations have shown similar behavioral trends.

B.   STATIC FRACTURE TOUGHNESS

The comparison of the static fracture-toughness of the two candidate aluminum alloys with that of those alloys now in use must be a qualitative one because the bulk of our parent-metal tests and those reported in the literature were made using different types of specimens.

The static fracture-toughness of parent-metal 2021-T81 is similar to that of other 2000-series compositions, such as 2014-T6 and 2219-T87. The significant increase in toughness with decreasing temperature found for the 2021-T81 alloy is similar to that noted by Hall (Ref 8) for 2014-T6, and somewhat greater than observed for 2219-T87 (Ref 7 and 11). In the as-welded condition, we noted a toughness level greater than that reported by Lockheed (Ref 12) for welded and aged material. A comparison of the average room-temperature toughness welded of 2021-T81 with preliminary data for 1-in.-thick 2014-T6 welded at Martin Marietta using essentially the same techniques and procedures indicates that the 2021-T81 is significantly tougher.
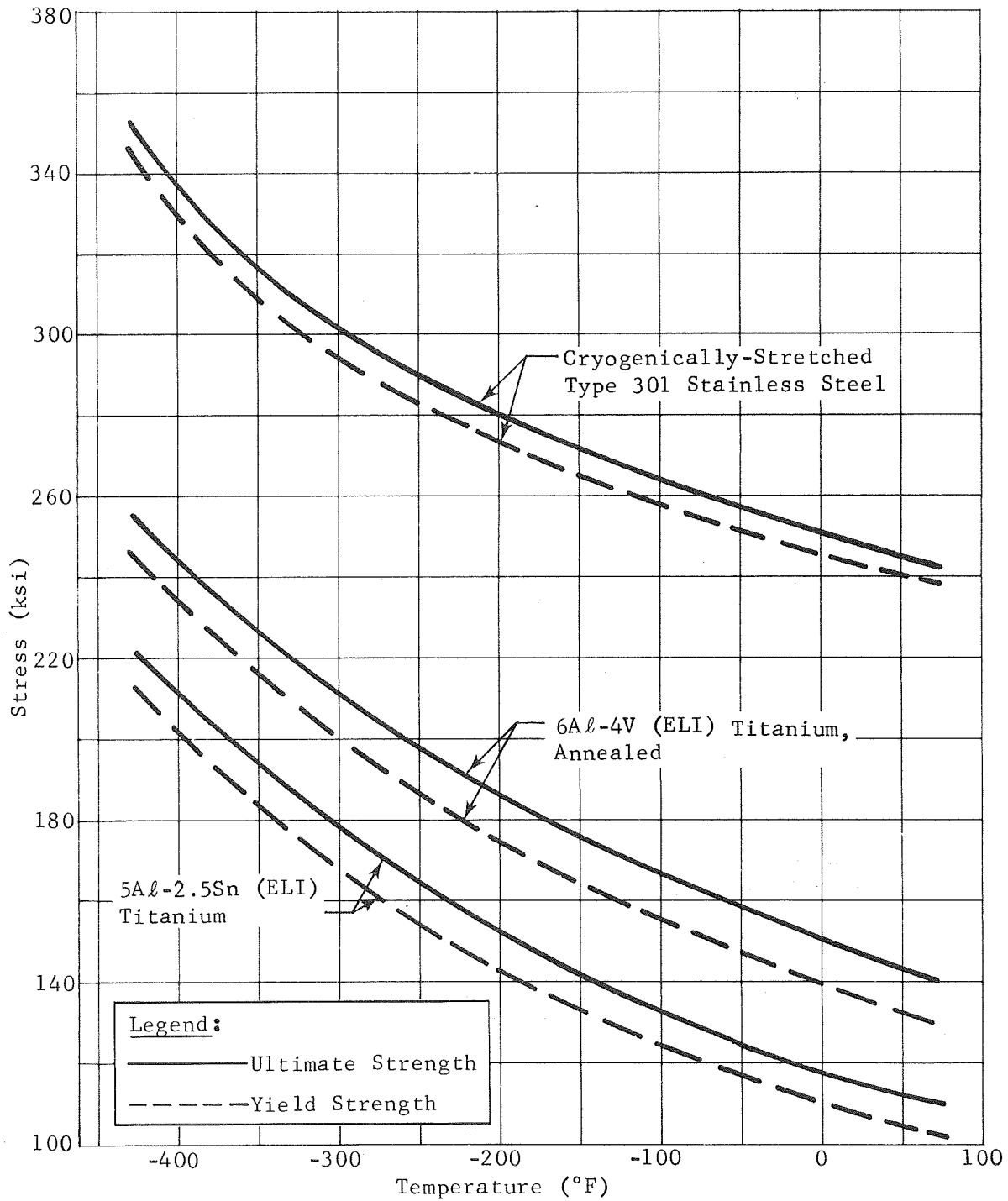
Fig. VII-2   Ultimate Strength and Yield Strength of Various Titanium
             Alloys and Cryogenically-Stretched Type 301 Stainless Steel

However, Boeing data (Ref 8) indicate that thinner gages of 2014-T6 (1/2- and 5/8-in. thicknesses) have a fracture toughness comparable to the value we measured for 2021-T81. Available data on 2219 alloy (Ref 7 and 11) indicate that it may be slightly tougher than 2021-T81 at 70°F.

It is difficult to compare the static fracture toughness of parent-metal specimens of X7007-T6 with that of other aluminum alloys because only compact-tension-specimen data were obtained. However, it appears that the room-temperature toughness is at least comparable with that of the 2000-series alloys. Unlike the 2000-series alloys, however, the toughness of the X7007-T6 composition decreases with decreasing temperature. The static fracture-toughness of the welded X7007-T6 is extremely high (more that 40 ksi $\sqrt{in.}$) at 70°F, but decreases sharply as the temperature decreases. However, even at -423°F, the X7007 is still tough enough to be considered a candidate composition.

The parent-metal stainless steel exhibits tough behavior at 70°F. According to the ASTM recommendations for the thickness required to obtain valid plane-strain fracture-toughness data, our room-temperature specimens were not sufficiently thick. However, there is no doubt that the apparent toughness, more than 100 ksi $\sqrt{in.}$, is outstanding for such high-strength material. By comparison with titanium, we found that the toughness of the parent-metal 301 stainless steel is below that of 5Aℓ-2.5Sn (ELI) titanium, but above that of 6Aℓ-4V (ELI) titanium. As noted earlier, although the toughness of 301 stainless steel decreases markedly with temperature reductions, its toughness at -423°F is remarkably high, considering that its strength is about 350 ksi. This toughness at -423°F is comparable to that of 6Aℓ-4V (solution-treated and aged) titanium at ambient temperature. The welded specimens of 301 stainless showed less fracture toughness than we had expected. Although as-welded 6Aℓ-4V (ELI) titanium exhibits a lower fracture toughness efficiency (ratio of parent-metal/welded fracture toughness) than the 301 stainless steel (Ref 8), the titanium can be stress-relieved to increase the efficiency to a level higher than that of the stainless steel. The limited data available on the fracture toughness of welded 5Aℓ-2.5Sn (ELI) titanium (Ref 7) indicate that its efficiency ratio exceeds unity even down to cryogenic temperatures.

C.   CYCLIC-LOAD FLAW ENLARGEMENT

    In any analysis of cyclic crack-growth data, one of the first
considerations to be made is whether the data truly follow a
power-function relationship. For the plane-stress condition,
using through-cracked specimens, Paris (Ref 13) has shown that
the behavior can be characterized by the equation

$$\frac{da}{dN} = C \,\Delta K^n,$$

where:

$\frac{da}{dN}$ = the cyclic crack-growth rate;

   C = a coefficient that takes into effect material and con-
       dition, stress ratio, loading conditions, etc;

   ΔK = the difference between the maximum and minimum stress
       intensities $\left(K_{max} - K_{min}\right)$ that occur during a loading
       cycle.

    The exponent n was found to be approximately equal to four
for a variety of materials. However, recent work seems to ques-
tion the validity of the functional relationship, and particu-
larly the value commonly accepted.

    An evaluation of our limited data showed a wide variation of
the exponent n. Our values varied from approximately three to
10. Other data for surface-flawed specimens, such as those re-
ported by Hall (Ref 8) showed a similar variation in the value
of n. However, his predictions of cyclic-load flaw enlargement
behavior were based on the assumption that n $\simeq$ 4 did typify the
experimental data.

    Since the amount of data generated in this program and that
available from previous work were too limited to confidently es-
tablish the power-function relationship, we decided to compare
the cyclic-load flaw-enlargement behavior of the three materials
studied in this program with that of other materials on a graphical
basis. The behavior of 2021-T81 and X7007-T6 was compared with
that of 2219 and 2014, and the behavior of high-strength, cryo-
stretched 301 stainless steel was compared with that of 6Aℓ-4V
and 5Aℓ-2.5Sn titanium alloys.

A comparision of the data available for parent-metal aluminum
with our data was made difficult by the fact that surface-flawed
·specimens were used by other researchers, whereas our tests were
performed using compact-tension specimens. Figure VII-3 shows
that there is a similar crack-growth tendency for surface-flawed
specimens, but a significantly lower tendency toward crack growth
for compact-tension specimens, as evidenced by the greater slope.
However, since the direction of crack growth is different for the
two types of specimens we feel that there is no real basis for
comparision.

On the other hand, a comparison can be made for the welded
material. In this case, all the data were obtained using similar
surface-flawed specimens. The data, plotted in Fig. VII-4, show
surprisingly similar behavior. The 70°F data are interesting to
note: the six sets of data that are plotted fall into a rather
narrow band. At -320°F, similar behavior is noted.

The data for 301 stainless steel are compared with available
data for titanium in Fig. VII-5. At 70°F, the parent-metal 301
exhibits the greatest resistance to crack growth, i.e., shows the
lowest crack-growth rate for a given stress intensity. The be-
havior of welded stainless steel is similar to that for 6Aℓ-4V
ELI (parent-metal and welded) titanium at the higher stress in-
tensities. The 5Aℓ-2.5Sn (ELI) parent metal exhibited the least
resistance to crack growth. The data compared at -320°F were not
for overlapping stress intensities and are not exactly comparable.
The titanium curves appear flatter than those for 301 stainless
steel. The -423°F data are limited but suggest that there is
slightly less crack growth for the 6Aℓ-4V titanium than for the
301 stainless steel.

It appears from the available data that the cyclic growth be-
havior of the 2021-T81 and X7007-T6 is similar to that observed
for currently-used aluminum alloys. The amount of cyclic growth
observed in the cryogenically-stretched stainless steel is similar
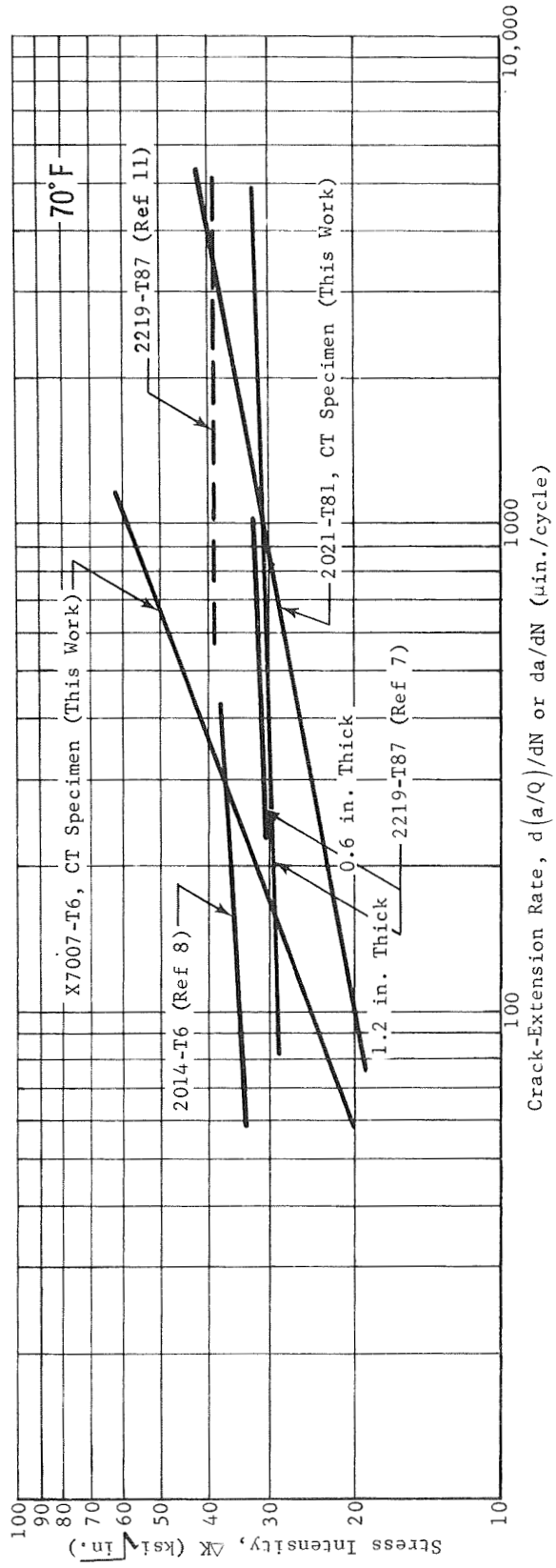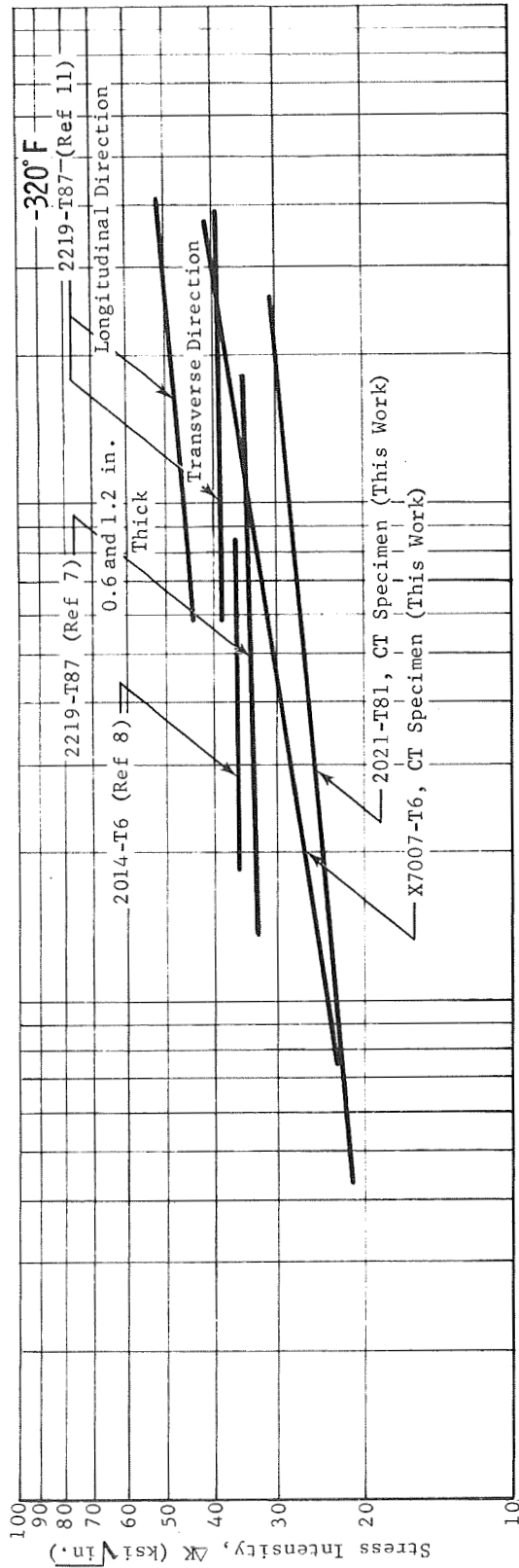in magnitude to that reported for titanium alloys.

Fig. VII-3   Cyclic Crack-Extension Rates for Various Parent-Metal Specimens (Aluminum Alloys)
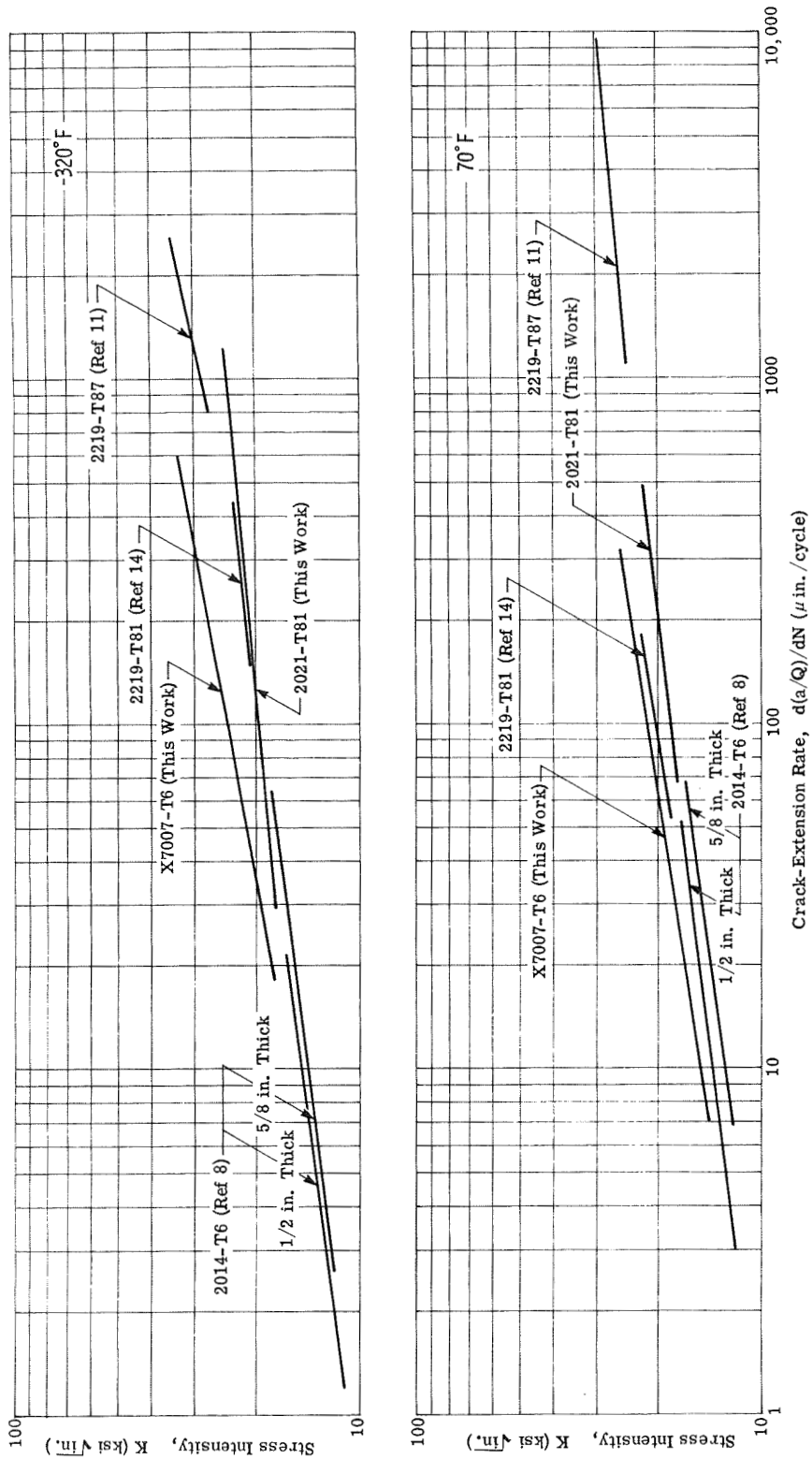
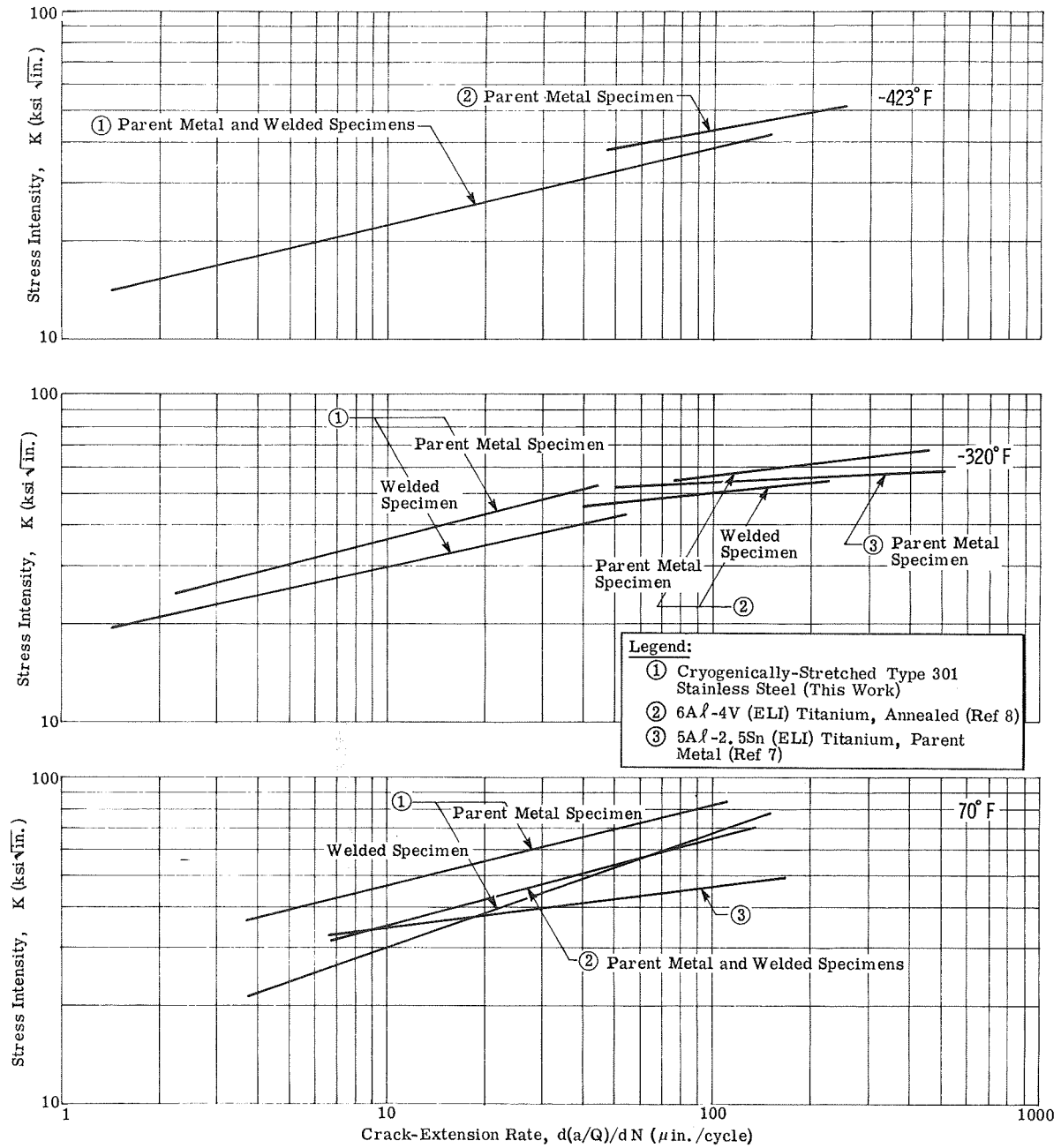Fig. VII-4 Cyclic Crack-Extension Rates for Various Welded Specimens (Aluminum Alloys)

Fig. VII-5 Cyclic Crack-Extension Rates for Various Titanium Alloys and
Cryogenically- Stretched Type 301 Stainless Steel

D. SUSTAINED-LOAD FLAW ENLARGEMENT

The sustained-load flaw growth behavior of the two aluminum alloys screened in this program must be compared with that of 2219-T81, the only aluminum alloy for which adequate data have been generated. Tiffany (Ref 15) has reported that two distinct threshold values can be established for surface-flawed aluminum alloys: a no-growth threshold, and a growth-no failure threshold. The following table summarizes his results for 2219-T81 parent metal.

Temperature (°F)	Threshold Level, K_{TH}/K_{Ic}*	
	No Growth	Growth-No Failure
70	0.63	0.90
-320	0.73	0.82
-423	0.75	0.87
*Time – approximately 10 hours.		

Previous data obtained by Tiffany (Ref 11) reported a parent-metal no-failure threshold at 70°F of approximately 95%. The threshold at -320°F decreased to less than 90%. These no-failure data are in substantial agreement with the later work in which the two thresholds were reported. The no-failure thresholds for welded material at 70 and -320°F appear to be slightly over 80% in 24 hr. No data for the no-growth threshold are available.

In our tests using compact-tension specimens, only a no-growth threshold was established. Therefore, we can only compare the parent metal on the no-growth criterion. Our comparisons of the welded metal must be more qualitative. However, since the entire comparison is being made using different types of specimens, it should be obvious that all of the remarks with respect to threshold are, at best, qualitative.

The parent-metal 2021-T81 appears to exhibit threshold data similar to those of the 2219-T81 at all temperatures. The X7007-T6 alloy exhibits a significantly, and quite disturbing, low level for the room-temperature threshold. However, at cryogenic temperatures, the level is restored to that of 2021 and 2219. Since the same low threshold in air at room temperature does not occur at cryogenic temperatures, it is quite possible that a stress-corrosion mechanism in air may be operative.

Welded material showed generally lower threshold values than the parent material. With 2219 aluminum, welding is performed using parent-metal composition filler, 2319, and hence the observance of a slightly-decreased threshold is attributable primarily to material structure and condition. However, with the 2021 and X7007, welding is performed using dissimilar filler material, and therefore threshold behavior is also a function of composition.

The welded 2021-T81 exhibited a rather low threshold at 70°F. Considering reports of the low stress-corrosion resistance of welded joints and the recommendations for aging welds to improve stress-corrosion behavior, it is quite possible that again a stress corrosion effect in air may be operative. At the cryogenic temperatures, the threshold level is slightly higher. In contrast to its poor parent-metal behavior, X7007-T6 exhibits an excellent weld threshold level at 70°F. This may be attributable to the filler alloy, 5356, which should improve the stress-corrosion resistance. The level for the onset of crack growth decreases at -320 and -423°F. Although the higher-strength 5000-series alloys have a tendency toward reduced toughness in the cryogenic region, it is difficult to ascribe the reduced threshold completely to this effect.

The 301 stainless steel exhibits a threshold level that is clearly lower than that reported for titanium alloys.

E.   GENERAL CONCLUSIONS

Considering all of the available data, it appears that all three compositions are worthy of further consideration as candidates for structural service. The following paragraphs present a summary of the behavior for each alloy.

1.   Aℓ 2021-T81

This composition exhibits good strength. Although somewhat superior to 2014-T6, the parent-metal tensile and yield strengths for the two heats evaluated in this study are not sufficiently greater to justify selection of this alloy on the basis of strength alone. However, its strength is superior to that of 2219-T87. The strength of the welded specimens are typical of those for 2000-series alloys. The static fracture toughness of

the parent metal is comparable to that of other 2000-series alloys. The tendency toward delamination in this alloy does not have to be considered a detriment, but in fact may be valuable in reducing the tendency toward premature fracture. The fracture toughness in the as-welded condition is between that of 2014-T6 and 2219-T87, and since both of these alloys are deemed adequate for structural service, 2021-T81 should also be satisfactory. In the welded-plus-aged condition, 2021-T81 is reported to exhibit lower toughness than in the as-welded condition. If it is necessary to use this alloy in the welded-plus-aged condition, the low weld toughness must be considered a detriment.

Under cyclic-loading conditions, the behavior of 2021 is typical of aluminum alloys. However under sustained loading, the threshold for the onset of subcritical crack growth is sufficiently low in the welded condition at 70°F to result in a low operating stress in structures designed on the basis of threshold-proof test approach. Postweld aging may improve the threshold ratio, but since the static toughness apparently decreases, this approach may not materially increase the operational stress.*

One of the key reasons for the possible application of this composition revolves around the question of its weldability. Our experience has shown that 2014-T6 is moderately difficult to weld, and that 2219-T87 is easier to weld because it has a reduced tendency toward hot shortness cracking. Although the amount of welding performed in this program was insufficient to evaluate the weldability rating of 2021-T81, there is general agreement that it is readily weldable. Therefore, the reason for the candidacy of 2021-T81 is that it is easier to weld than 2014-T6 and much stronger than 2219-T87. Postweld aging has been recommended in order to improve its stress-corrosion resistance, but the effect of this factor with respect to operating stress is being studied in current work. However, postweld aging increases the difficulty of fabrication, particularly for large structures.

---

*Operational stress based on following formula:

$$\sigma_o = \frac{K_{TH}}{K_{Ic}} \cdot \frac{\sigma_{proof}}{Safety\ Factor}$$

2. Aℓ X7007-T6

The tensile strength of X7007-T6 is clearly so superior to that of other weldable aluminum alloys that it must be considered a candidate for structural service. The high yield strength of welded joints is particularly significant. The static fracture toughness of both parent-metal and welded material is excellent at 70°F; and despite the normal decrease in toughness with decreasing temperature, the level at -423°F is deemed adequate for structural consideration. The severe delamination problem should not be troublesome in most applications; however, care should be taken to avoid stresses in the short transverse direction since we have not yet characterized the properties in that direction.

Cyclic crack-growth rates appear to be similar to those found for other aluminum alloys. The most significant handicap for X7007 is its very low parent-metal room-temperature threshold under sustained loading. This single factor is sufficient to cause a design analyst to predict a lower operating stress at room temperature than for most high-strength weldable aluminum alloys.

3. Cryogenically-Stretched Type 301 Stainless Steel

This material appears to be an excellent high strength candidate for cryogenic service. The ease of fabrication and the resultant integrity of the finished product makes this alloy very attractive for aerospace applications. This composition can be considered competitive with titanium alloys on the basis of strength. Since its tensile strength can be varied over a significant range as a result of cryogenic prestress, some versatility in design can be achieved with the cryogenically stretched steel. The static fracture toughness of this alloy is quite outstanding at all temperatures, both for the parent metal and for welded speciments.

Its subcritical crack-growth behavior under cyclic loading is similar to that observed for titanium alloys. Under sustained-load conditions, crack growth begins at a lower threshold ratio than that in titanium. Since its static toughness is between that of the two titanium candidate alloys, an operational stress based on the threshold-proof test approach could be higher or lower than that obtained using titanium.

The principal question with respect to application of the 301 stainless steel is that of adequate characterization of its threshold behavior in a variety of environments. Titanium was considered to be an outstanding material until premature failures occurred in many environments deemed to be non-deleterious. As a result, titanium alloys are now being thoroughly characterized for new environments as new applications arise. Although we expect austenitic stainless steel to exhibit excellent sustained-load behavior in many environments, the transformation processing takes this material out of the austenitic category. It is therefore necessary to scrutinize this composition as we do for martensitic, high-strength, precipitation-hardened stainless steels and to carefully evaluate environmental effects.

F.   CURRENT WORK

Tasks IV through VII were added to the program in an attempt to answer questions arising out of the information generated in Tasks II and III. The following paragraphs present our rationale in guiding the course of the current work.

The principal problem associated with the application of 2021 aluminum alloy to structural service is a lack of sufficient information dealing with the behavior of the weld area with respect to corrosion resistance, fracture toughness, and resistance to sustained-load flaw growth in the as-welded vs aged-after-welding condition and despite the tendency to exhibit delamination at the crack tip, both 2021 and X7007 alloys exhibit rather good mechanical properties. To determine the suitability of the X7007 alloy for service application, additional work is being to show the effect of deleterious environments on mechanical behavior and to further confirm the behavior of the parent metal in air.

Experience with welding 2014-T6 has shown that general corrosion is slightly more prevalent in the heat-affected zone than in the parent material. Aging after welding, decreases toughness and general corrosion resistance in the HAZ. Unlike the 2014, the 2021, alloy is reported by Alcoa to show the opposite effect, i.e., more corrosion in the as-welded condition. This report is somewhat confusing because the similarity of the chemical compositions between the two alloys does not suggest that such a difference should exist.

Our experience with general corrosion in weld zones has shown it to be relatively minor. In addition, protective coatings can eliminate general corrosion.

Since it is relatively simple to assess the effects of exposure to corrosive environments, we are performing general corrosion tests of the two subject alloys, as well as of several common alloys in order to provide data for baseline comparison.

The stress-corrosion resistance of the 2021 alloy is reported to be rather low, but little information is available for the X7007 composition. We are therefore characterizing this facet of behavior.

Much of the previous fracture-mechanics work associated with weldments has ignored full consideration of varibles such as defect location and weldment condition. It has been common to locate the defect in the center of the weld zone and ignore the heat-affected zone and fusion area. Weldments have usually been evaluated in the as-welded condition; the effects of aging, weld repairing, weld repairing plug aging, overheating, etc, have not been studied. Studies of the effects of these variables have been ignored for static-fracture work as well as sustained-load flaw-extension behavior. To characterize weldments of these two alloys, it is essential to obtain the results of the additional work we are currently preforming.

VIII. REFERENCES

1. G. R. Irwin: "Crack-Extension Force for a Part-Through Crack
    in a Plate." Journal of Applied Mechanics, Vol 84E, No. 4,
    December 1962, pp 651 thru 654.

2. A. S. Kobayashi: On the Magnification Factors of Deep Surface
    Flaws. Structural Development Research Memorandum No. 16.
    The Boeing Company, December 1965.

3. F. W. Smith: Stress-Intensity Factors for a Semielliptical
    Flaw. Structural Development Research Memorandum No. 17.
    The Boeing Company, August 1966.

4. L. J. Larson: Depth Effect for Semielliptical Surface Flaws.
    R-69-14. Martin Marietta Corporation, Denver, Colorado,
    October 1969.

5. F. W. Smith: Stress-Intensity Factors for Surface-Flawed
    Fracture Specimens. R-69-15. Martin Marietta Corporation,
    Denver, Colorado, October 1969.

6. E. T. Wessel: "State-of-the-Art of the WOL Specimen for K_{Ic}
    Fracture-Toughness Testing." Engineering Fracture Mechanics,
    Vol I, No. 1, June 1968, p 77.

7. C. F. Tiffany, P. M. Lorenz, and L. R. Hall: Investigation
    of Plane-Strain Flaw Growth in Thick-Walled Tanks. NASA CR-
    54837. The Boeing Company, February 1966.

8. L. R. Hall: Plane-Strain Cyclic Flaw Growth in 2014-T62
    Aluminum and 6Aℓ-4V (ELI) Titanium. NASA CR-72396. The Boeing
    Company, November 1968.

9. F. R. Schwartzberg, S. H. Osgood, and R. G. Herzog: Cryogenic
    Materials Data Handbook. AFML-TDR-64-280 and Supplements.
    Martin Marietta Corporation, Denver, Colorado, August 1968.

10. J. N. Masters, W. P. Haese, and R. W. Finger: Investigation
     of Deep Flaws in Thin Wall Tanks. NASA CR 72606. The Boeing
     Company, December, 1969.

11. C. F. Tiffany and P. M. Lorenz: Fracture-Toughness and Sub-
     critical-Flaw-Growth Characteristics of Saturn SI-C Tankage
     Materials. D2-22802 (Contract NAS8-5608). The Boeing Com-
     pany, April 1964.

12. Personal Communications with E. Willner of Lockheed Missile and Space Company, 1968 and 1969.

13. P. C. Paris, M. P. Gomez, and W. E. Anderson: "A Rational Analytic Theory of Fatigue." Trends in Engineering (University of Washington), Vol 13, No. 1, 1961.

14. W. E. Witzell and C. J. Kropp: Weldment Flaw-Growth Characteristics of 2219-T81 Aluminum Alloy. NASA CR-72288. General Dynamics/Convair, San Diego, California, September 1967.

15. C. F. Tiffany, P. M. Lorenz, and R. C. Shah: Extended Loading of Cryogenic Tanks. NASA CR 72252. The Boeing Company, July 1967.

APPENDIX A

TABULATED EXPERIMENTAL DATA

CONTENTS

Table A-1   Tensile Properties of Parent-Metal Plate Specimens* (2021-T81 Aluminum Alloy)

Specimen Number	Temperature (°F)	Grain Direction	Ultimate Strength (ksi)	Yield Strength (ksi)		Elongation (% in 4.0 in.)	Reduction in Area (%)
				0.02% Offset	0.2% Offset		
T2PLR1	70	Longitudinal	72.9	55.7	63.6	7.2	6.7
T2PLR2	70	Longitudinal	72.6	54.9	63.1	8.0	7.7
T2PLR3	70	Longitudinal	72.3	55.8	62.8	6.8	8.6
			72.6	55.5	63.2	7.3	7.7
T2PTR1	70	Transverse	71.7	52.6	61.9	4.2	4.4
T2PTR2	70	Transverse	72.2	54.7	61.4	4.2	4.5
T2PTR3	70	Transverse	71.7	51.9	61.0	4.5	5.5
			71.9	53.1	61.4	4.3	4.8
T2PLN1	-320	Longitudinal	86.4	62.8	72.1	11.5	13.5
T2PLN2	-320	Longitudinal	87.1	66.9	74.5	9.5	10.0
T2PLN3	-320	Longitudinal	85.8	66.0	72.1	9.5	7.5
			87.8	65.2	72.9	10.2	10.3
T2PTN1	-320	Transverse	87.8	65.2	73.2	6.5	9.0
T2PTN2	-320	Transverse	†	64.4	72.6	†	†
T2PTN3	-320	Transverse	85.1	57.6	69.3	6.0	8.4
			86.4	62.4	71.7	6.2	8.7
T2PLH1	-423	Longitudinal	97.0	68.9	81.4	8.0	12.0
T2PLH2	-423	Longitudinal	‡	69.2	77.9	‡	‡
T2PLH3	-423	Longitudinal	101.3	71.6	83.0	11.5	11.7
			99.2	69.9	80.8	9.8	11.8
T2PTH1	-423	Transverse	103.8	67.6	77.3	8.5	8.5
T2PTH2	-423	Transverse	100.4	75.7	82.3	8.0	8.3
T2PTH3	-423	Transverse	101.6	68.3	80.4	8.8	7.6
			101.9	70.5	80.0	8.4	8.1

*1.0 in. thick x 1.8 in. wide (nominal gage) cross section.

†Failed through pin hole.

‡Failed outside gage length; premature failure.

Table A-2   Tensile Properties of Parent-Metal Round Bar Specimens* (2021-T81 Aluminum Alloy)

Specimen Number	Temperature (°F)	Grain Direction	Ultimate Strength (ksi)	Yield Strength 0.2% Offset (ksi)	Elongation (% in 2.0 in.)	Reduction in Area (%)
T2PLR4	70	Longitudinal	71.4	63.3	8.0	10.2
T2PLR5	70	Longitudinal	71.1	62.4	7.5	9.1
T2PLR7	70	Longitudinal	71.8	62.4	8.5	12.2
			71.4	62.7	8.0	10.5
T2PTR4	70	Transverse	70.4	62.2	3.0	4.1
T2PTR5	70	Transverse	70.4	62.2	3.5	6.6
T2PTR6	70	Transverse	69.8	62.4	3.0	4.6
			70.2	62.3	3.2	5.1
T2PLN4	-320	Longitudinal	87.1	74.6	12.0	12.2
T2PLN5	-320	Longitudinal	87.6	74.6	13.0	12.2
T2PLN6	-320	Longitudinal	87.6	75.6	11.0	11.2
			87.4	74.9	12.0	11.9
T2PTN4	-320	Transverse	87.6	72.6	6.5	7.6
T2PTN5	-320	Transverse	87.8	74.9	6.0	8.1
T2PTN6	-320	Transverse	87.6	73.6	6.5	7.4
			87.7	73.7	6.3	7.7
T2PLH4	-423	Longitudinal	99.5	80.2	12.0	18.8
T2PLH6	-423	Longitudinal	99.5	80.0	13.5	20.3
T2PLH7	-423	Longitudinal	99.5	79.1	10.5	17.3
			99.5	79.8	12.0	18.8
T2PTH4	-423	Transverse	101.0	79.7	8.5	8.1
T2PTH5	-423	Transverse	101.5	79.5	9.0	13.8
T2PTH6	-423	Transverse	101.3	79.7	11.5	5.1
			101.3	79.6	10.0	9.0

*Standard 0.505-in.-diameter round bars.

Table A-3 Tensile Properties of Welded Specimens* (2021-T81 Aluminum Alloy; Longitudinal Direction)

Specimen Number	Temperature (°F)	Ultimate Strength (ksi)	Yield Strength (ksi)		Elongation (% in 2.0 in.)	Reduction in Area (%)
			0.02% Offset	0.2% Offset		
T2WLR1	70	41.2	9.2	18.8	6.2	9.2
T2WLR2	70	42.5	9.4	18.3	5.3	9.2
T2WLR3	70	43.1	9.6	20.5	5.9	10.9
		42.3	9.4	19.2	5.8	9.8
T2WLN1	-320	57.0	14.9	25.1	7.3	16.9
T2WLN2	-320	57.6	12.3	23.4	8.3	18.1
T2WLN3	-320	57.5	12.3	22.9	7.3	16.9
		57.4	13.2	23.8	7.6	17.3
T2WLH1	-423	65.9	15.6	26.6	9.0	9.1
T2WLH2	-423	68.3	16.6	31.7	10.0	10.7
T2WLH3	-423	70.3	17.2	28.2	10.0	10.0
		68.1	16.4	28.8	9.7	9.9

*1.0 in. thick x 1.8 in. wide (nominal gage) cross-section.

Table A-4 Tensile Properties of Parent-Metal Plate Specimen* (X7007-T6 Aluminum Alloy)

Specimen Number	Temperature (°F)	Grain Direction	Ultimate Strength (ksi)	Yield Strength (ksi)		Elongation (% in 4.0 in.)	Reduction in Area (%)
				0.02% Offset	0.2% Offset		
T7PLR1	70	Longitudinal	72.2	61.2	68.8	17.1	31.9
T7PLR2	70	Longitudinal	72.0	†	†	17.5	28.6
T7PLR3	70	Longitudinal	72.0	62.4	68.6	17.2	30.8
			72.1	61.8	68.7	17.3	30.4
T7PTR1	70	Transverse	70.5	59.6	66.3	16.5	29.2
T7PTR2	70	Transverse	70.2	59.5	66.2	17.2	29.8
T7PTR3	70	Transverse	70.4	61.2	66.0	17.5	29.1
			70.4	60.1	66.2	17.1	29.4
T7PLN1	-320	Longitudinal	94.7	74.4	82.1	10.5	‡
T7PLN2	-320	Longitudinal	94.5	72.4	81.3	13.8	‡
T7PLN3	-320	Longitudinal	95.3	70.1	82.7	12.0	‡
			94.8	72.2	82.0	12.1	
T7PTN1	-320	Transverse	84.1	59.6	68.5	9.2	6.8
T7PTN2	-320	Transverse	84.2	58.9	69.9	8.8	8.8
T7PTN3	-320	Transverse	87.9	68.6	77.5	6.5	10.6
			85.4	62.4	72.0	8.2	8.7
T7PLH1	-423	Longitudinal	108.3	80.1	91.5	10.5	13.7
T7PLH2	-423	Longitudinal	107.7	80.5	91.6	8.0	10.7
T7PLH3	-423	Longitudinal	106.6	80.7	91.8	6.2	12.1
			107.5	81.4	91.6	8.2	12.1
T7PTH1	-423	Transverse	103.7	75.9	86.0	6.2	4.5
T7PTH2	-423	Transverse	102.5	74.4	86.6	6.0	6.5
T7PTH3	-423	Transverse	101.0	73.2	85.6	5.2	5.6
			102.4	74.5	85.7	5.7	5.5

*1.0 in. thick x 1.8 in. wide (nominal gage) cross-section.

†Load train slipped; no yield data available.

‡No reduction in area could be measured because of excessive delamination.

Table A-5   Tensile Properties of Parent-Metal Round Bar Specimens*
(X7007-T6 Aluminum Alloy)

Specimen Number	Temperature (°F)	Grain Direction	Ultimate Strength (ksi)	Yield Strength 0.2% Offset (ksi)	Elongation (% in 2.0 in.)	Reduction in Area (%)
T7PLR5	70	Longitudinal	73.3	68.5	13.0	35.0
T7PLR6	70	Longitudinal	73.3	69.0	15.0	37.5
T7PLR7	70	Longitudinal	73.3	69.5	13.5	35.5
			73.3	69.0	13.8	36.0
T7PTR4	70	Transverse	70.3	64.4	14.5	35.0
T7PTR6	70	Transverse	70.8	64.5	15.0	37.0
T7PTR7	70	Transverse	70.1	64.5	13.5	33.0
			70.4	64.5	14.3	35.0
T7PLN4	-320	Longitudinal	98.0	85.3	15.0	7.6
T7PLN5	-320	Longitudinal	98.2	85.9	12.5	8.1
T7PLN6	-320	Longitudinal	98.2	85.3	10.5	10.2
			98.1	85.5	12.7	8.6
T7PTN4	-320	Transverse	91.9	79.2	12.5	17.3
T7PTN5	-320	Transverse	92.1	80.7	10.5	13.2
T7PTN6	-320	Transverse	92.1	80.2	12.0	15.2
			92.0	80.0	11.7	15.2
T7PLH4	-423	Longitudinal	114.2	92.6	13.0	†
T7PLH5	-423	Longitudinal	114.2	92.1	13.0	†
T7PLH6	-423	Longitudinal	113.7	90.4	13.0	†
			114.0	91.7	13.0	
T7PTH4	-423	Transverse	104.0	86.3	11.5	12.2
T7PTH5	-423	Transverse	105.6	82.9	11.5	15.0
T7PTH6	-423	Transverse	106.3	85.3	11.5	15.0
			105.3	84.8	11.5	14.1

*Standard 0.505-in.-diameter round bars.

†No reduction in area could be measured because of excessive delamination.

Table A-6   Tensile Properties of Welded Specimens* (X7007-T6 Aluminum Alloy; Longitudinal Direction)

Specimen Number	Temperature (°F)	Ultimate Strength (ksi)	Yield Strength (ksi)		Elongation (% in 1.0 in.)	Reduction in Area (%)
			0.02% Offset	0.2% Offset		
T7WLR1	70	49.5	28.3	36.5	6.0	28.6
T7WLR2	70	51.5	28.2	36.0	9.0	27.5
T7WLR3	70	51.0	27.0	37.1	4.0	29.5
		50.7	27.8	36.5	6.3	28.5
T7WLN1	-320	68.7	32.2	42.8	11.0	7.0
T7WLN2	-320	68.4	32.8	41.8	11.0	12.9
T7WLN3	-320	68.6	30.8	42.1	10.0	11.1
		68.6	31.9	42.2	10.7	10.3
T7WLH1	-423	72.4	32.6	46.2	5.5	4.1
T7WLH2	-423	59.7	32.2	49.4	7.0	6.5
T7WLH3	-423	75.4	32.2	46.4	7.5	8.9
		69.1	32.3	47.3	6.7	6.5

*1.0 in. thick x 1.8 in. wide (nominal gage) cross-section.

Table A-7 Tensile Properties of Cryogenically-Stretched Parent Metal* (Type 301 Stainless Steel)

Specimen Number	Temperature (°F)	Grain Direction	Ultimate Strength (ksi)	Yield Strength (ksi)		Elongation (% in 2.0 in.)	Reduction in Area (%)
				0.02% Offset	0.2% Offset		
T3PLR1	70	Longitudinal	246.2	169.2	241.1	7.8	31.1
T3PLR2	70	Longitudinal	239.8	180.8	234.6	7.8	36.2
T3PLR3	70	Longitudinal	242.5	173.2	236.6	8.0	31.0
T3PLR4	70	Longitudinal	248.4	176.1	241.8	7.8	46.1
T3PLR5	70	Longitudinal	242.0	190.2	236.8	8.2	35.5
T3PLR6	70	Longitudinal	<u>247.9</u>	<u>226.0</u>	<u>243.8</u>	<u>7.0</u>	<u>28.9</u>
			244.5	185.9	239.1	7.8	34.8
T3PTR1	70	Transverse	243.7	171.3	229.7	8.5	31.6
T3PTR2	70	Transverse	243.7	178.5	230.4	8.0	29.9
T3PTR3	70	Transverse	242.3	185.7	229.2	6.5	29.2
T3PTR4	70	Transverse	239.6	184.0	227.0	5.8	22.8
T3PTR5	70	Transverse	241.5	165.9	228.1	7.0	28.3
T3PTR6	70	Transverse	<u>235.6</u>	<u>178.9</u>	<u>229.7</u>	<u>7.0</u>	<u>26.6</u>
			241.1	177.4	229.0	7.1	28.1
T3PLN1	-320	Longitudinal	307.9	222.1	305.4	12.5	45.5
T3PLN2	-320	Longitudinal	315.1	223.4	309.9	9.5	47.3
T3PLN3	-320	Longitudinal	308.4	179.6	302.4	15.8	36.2
T3PLN4	-320	Longitudinal	311.7	215.7	308.7	12.0	35.9
T3PLN5	-320	Longitudinal	309.6	215.1	312.2	9.0	45.6
T3PLN6	-320	Longitudinal	<u>308.3</u>	<u>187.2</u>	<u>303.1</u>	<u>15.5</u>	<u>36.3</u>
			310.1	213.1	306.4	12.3	41.1
T3PTN1	-320	Transverse	314.9	224.9	306.8	11.5	28.6
T3PTN2	-320	Transverse	316.6	246.3	302.5	11.5	28.4
T3PTN3	-320	Transverse	315.8	206.5	298.7	11.5	30.2
T3PTN4	-320	Transverse	318.0	226.6	302.9	13.5	35.8
T3PTN5	-320	Transverse	313.6	216.2	299.3	11.0	32.1
T3PTN6	-320	Transverse	<u>313.0</u>	<u>235.6</u>	<u>297.5</u>	<u>11.0</u>	<u>31.7</u>
			315.3	226.0	301.2	11.6	31.1
T3PLH1	-423	Longitudinal	346.9	260.4	341.8	3.8	35.3
T3PLH2	-423	Longitudinal	361.3	280.0	353.0	2.8	33.4
T3PLH3	-423	Longitudinal	346.9	276.7	341.7	3.5	25.4
T3PLH4	-423	Longitudinal	363.1	279.4	358.6	3.5	30.5
T3PLH5	-423	Longitudinal	357.8	258.5	352.0	4.0	28.3
T3PLH6	-423	Longitudinal	<u>358.7</u>	<u>267.9</u>	<u>357.2</u>	<u>3.5</u>	<u>27.4</u>
			355.8	270.5	350.7	3.5	30.0
T3PTH1	-423	Transverse	349.9	228.8	341.1	3.0	12.9
T3PTH2	-423	Transverse	349.3	264.7	341.2	4.0	17.8
T3PTH3	-423	Transverse	357.8	235.5	†	3.0	10.0
T3PTH4	-423	Transverse	‡	227.7	329.1	‡	‡
T3PTH5	-423	Transverse	353.6	231.7	336.4	2.8	7.5
T3PTH6	-423	Transverse	<u>355.5</u>	<u>247.4</u>	<u>340.7</u>	<u>3.5</u>	<u>6.7</u>
			353.2	239.3	337.7	3.3	11.0

*0.135 in. thick x 0.5 in. wide (nominal gage) cross-section.

†Strain gage failed.

‡Loading pin failed; specimen did not fracture.

Table A-8   Tensile Properties of Welded Cryogenically-Stretched Specimens*
(Type 301 Stainless Steel; Longitudinal Direction)

Specimen Number	Temperature (°F)	Ultimate Strength (ksi)	Yield Strength (ksi)		Elongation (% in 2.0 in.)	Reduction in Area (%)
			0.02% Offset	0.2% Offset		
T3WLR1	70	226.9	154.7	206.2	5.5	30.0
T3WLR2	70	236.5	168.4	220.4	5.5	26.0
T3WLR3	70	220.1	161.9	196.4	5.0	27.0
		227.8	161.7	207.7	5.3	27.7
T3WLN1	-320	299.5	275.2	291.4	7.5	31.5
T3WLN2	-320	302.0	262.8	293.1	10.0	32.1
T3WLN3	-320	302.0	265.8	293.9	10.0	35.8
		301.2	267.8	292.8	9.2	33.1
T3WLH1	-423	337.5	319.7	335.3	3.5	17.1
T3WLH2	-423	342.7	296.3	338.9	3.0	16.1
T3WLH3	-423	338.6	303.9	334.8	5.0	18.8
		339.6	306.6	336.3	3.8	17.3

*0.135 in. thick x 0.5 in. wide (nominal gage) cross-section.

Table A-9 Static Fracture-Toughness Properties of Surface-Flawed Parent Metal Specimens*
(2021-T81 Aluminum Alloy)

Specimen Number	Temperature (°F)	Grain Direction	Flaw Size			Fracture Stress (ksi)	Fracture Stress/Yield Stress Ratio	Critical Stress Intensity (ksi√in.)	Remarks
			Depth, a (in.)	Length, 2c (in.)	Shape, a/Q				
F2PLR1	70	Longitudinal	0.30	1.15	0.228	48.8†	0.77		Pop-in observed.
F2PLR2	70	Longitudinal	0.37	1.44	0.272	47.2†	0.75		Pop-in observed.
F2PLR3	70	Longitudinal	0.50	1.95	0.380	52.2†	0.82		No pop-in observed.
F2PTR1	70	Transverse	0.36	1.28	0.240	34.0	0.55	32.5	
F2PTR2	70	Transverse	0.40	1.48	0.272	33.5	0.55	34.1	
F2PTR3	70	Transverse	0.43	1.72	0.305	31.1	0.51	33.5	
								33.3	
F2PLN1	-320	Longitudinal	0.43	1.18	0.242	57.5†	0.78		Test discontinued.
F2PLN2	-320	Longitudinal	0.34	1.45	0.288	28.4†	0.35		Erroneous pop-in; test discontinued.
F2PLN3	-320	Longitudinal				59.6†	0.82		No pop-in observed.
F2PTN1	-320	Transverse	0.32	1.25	0.237	57.1	0.80	54.2	
F2PTN2	-320	Transverse	0.41	1.18	0.243	51.5	0.72	49.5	
F2PTN3	-320	Transverse	0.32	1.61	0.269	55.6	0.78	56.3	
								53.3	
F2PLH1	-423	Longitudinal	0.50	2.00	0.388	63.5	0.80		Delaminated.
F2PTH1	-423	Transverse	0.30	1.25	0.244	66.2	0.83	63.7	
F2PTH2	-423	Transverse	0.32	1.30	0.250	61.1	0.77	59.5	
F2PTH3	-423	Transverse	0.41	1.57	0.297	49.5	0.72	52.6	
								58.6	

*1.0 in. thick x 5.75 in. wide (nominal gage) cross-section.

†Maximum load; no failure.

Table A-10   Static Fracture-Toughness Properties of Compact-Tension Parent Metal Specimens*
(2021-T81 Aluminum Alloy; Transverse Direction)

| Specimen Number | Temperature (°F) | Flaw Size | | Stress-Intensity Parameter, Y | Pop-In Load (lb) | Critical Stress Intensity (ksi$\sqrt{\text{in.}}$) | Remarks |
		a_{avg} (in.)	a/W				
FC2PTR1	70	1.06	0.530	14.6	3360	25.4	
FC2PTR2	70	1.01	0.505	13.8	3795	26.4	
FC2PTR3	70	1.07	0.535	14.8	4150	31.6	
FC2PTR4	70	1.02	0.510	13.9	3160	22.2	
						26.4	
FC2PTN1	-320	1.05	0.525	14.4	5160	38.2	
FC2PTN2	-320	1.02	0.510	13.9			No pop-in.
FC2PTN3	-320	1.00	0.500	13.6	4820	33.3	
FC2PTN4	-320	1.00	0.500	13.6	5280	38.0	
						36.5	
FC2PTH1	-423	1.01	0.505	13.8	5630	39.6	
FC2PTH2	-423	1.01	0.505	13.8	5350	37.8	
FC2PTH3	-423	1.02	0.510	13.9	5930	42.2	
						39.9	

*1.0 in. thick.

Table A-11 Static Fracture-Toughness Properties of Welded Surface-Flawed Specimens (2021-T81 Aluminum Alloy; Longitudinal Direction)

Specimen Number	Temperature (°F)	Flaw Size			Fracture Stress (psi)	Fracture Stress/Yield Stress Ratio	Critical Stress Intensity (ksi $\sqrt{in.}$)
		Depth, a (in.)	Length, 2c (in.)	Shape, a/Q			
F2WLR1	70	0.35	1.21	0.254	26.8	1.40	26.3
F2WLR2	70	0.47	1.50	0.322	27.0	1.41	29.9
F2WLR3	70	0.46	1.52	0.322	26.8	1.40	29.6
							28.6
F2WLN1	-320	0.39	1.35	0.283	33.3	1.40	34.6
F2WLN2	-320	0.57	1.62	0.349	29.5	1.24	34.0
F2WLN3	-320	0.45	1.57	0.328	31.0	1.30	34.6
							34.4
F2WLH1	-423	0.41	1.33	0.277	31.4	1.09	32.2
F2WLH2	-423	0.39	1.24	0.241	31.4	1.09	30.0
F2WLH3	-423	0.44	1.54	0.286	29.1	1.01	30.3
							30.8

*1.0 in. thick x 5.75 in. wide (nominal gage) cross-section.

Table A-12　Static Fracture-Toughness Properties of Welded Compact-Tension Specimens*
(2021-T81 Aluminum Alloy; Longitudinal Direction)

Specimen Number	Temperature (°F)	Flaw Size		Stress-Intensity Parameter, Y	Pop-in Load	Critical Stress Intensity (ksi $\sqrt{in.}$)	Remarks
		a_{avg} (in.)	a/W				
FC2WLR1	70	1.04	0.520	14.2			No pop-in.
FC2WLR2	70	1.03	0.515	14.1			No pop-in.
FC2WLR3	70	1.05	0.525	14.4			
FC2WLN1	-320	1.01	0.505	13.8			No pop-in.
FC2WLN2	-320	1.11	0.555	15.5			No pop-in.
FC2WLN3	-320	1.08	0.540	15.0			No pop-in.
FC2WLH1	-423	1.06	0.530	14.6	3700	27.4	
FC2WLH2	-423	1.08	0.540	15.0	3600	28.0	
FC2WLH3	-423	1.06	0.530	14.6	3900	28.9	
						$\underline{28.1}$	

*1.0 in. thick.

Table A-13 Static Fracture-Toughness Properties of Surface-Flawed Parent Metal Specimens* (X7007-T6 Aluminum Alloy)

Specimen Number	Temperature (°F)	Grain Direction	Flaw Size			Fracture Stress (ksi)	Fracture Stress/Yield Stress Ratio	Critical Stress Intensity (ksi√in.)	Remarks
			Depth, a (in.)	Length, 2c (in.)	Shape, a/Q				
F7PLR1	70	Longitudinal	0.40	1.33	0.258	28.0†	0.41		Pop-in observed.
F7PLR2	70	Longitudinal	0.34	1.40	0.262	46.4†	0.68		Pop-in observed.
F7PLR3	70	Longitudinal	0.56	2.07	0.396	44.9†	0.68		Pop-in observed.
F7PLR4	70	Longitudinal	0.50	1.83	0.333	22.6†	0.34		Pop-in observed.
F7PTR1	70	Transverse	0.37	1.38	0.285	49.8	0.75		Pop-in plus complete fracture.
F7PTR2	70	Transverse	0.38	1.41	0.289	52.2†	0.79		Pop-in observed.
F7PTR3	70	Transverse	0.51	2.04	0.386	46.6	0.76		Pop-in plus complete fracture.
F7PLN1	-320	Longitudinal	0.50	1.70	0.329	31.6†	0.39		Pop-in observed.
F7PLN2	-320	Longitudinal	0.52	1.72	0.340	47.2	0.58		Pop-in plus complete fracture.
F7PLN3	-320	Longitudinal	0.47	1.73	0.250	19.8	0.24		Small pop-in observed.
F7PTN1	-320	Transverse	0.48	1.88	0.347	31.4†	0.44		Small pop-in observed.
F7PTN2	-320	Transverse	0.41	1.11	0.226	28.8†	0.35		Pop-in observed.
F7PTN3	-320	Transverse	0.51	1.76	0.340	31.0	0.43		Pop-in plus complete fracture.
F7PLH1	-423	Longitudinal	0.37	1.30	0.246	48.3	0.60		Delaminated; complete fracture.
F7PTH1	-423	Transverse	0.31	1.24	0.225	43.0	0.51		Pop-in plus complete fracture.
F7PTH2	-423	Transverse	0.51	1.98	0.362	37.0	0.40		Pop-in plus complete fracture.

*1.0 in. thick x 5.75 in. wide (nominal gage) cross-section.

†Maximum load, no failure.

Table A-14   Static Fracture-Toughness Properties of Compact-Tension Parent Metal
             Specimens* (X7007-T6 Aluminum Alloy; Transverse Direction)

| Specimen Number | Temperature (°F) | Flaw Size | | Stress-Intensity Parameter, Y | Pop-In Load (lb) | Critical Stress Intensity (ksi√in.) |
		a_{avg} (in.)	a/W			
FC7PTR1	70	0.97	0.485	13.2	4590	30.1
FC7PTR2	70	0.96	0.480	13.1	5260	34.2
FC7PTR3	70	0.98	0.490	13.3	4670	31.1
						31.8
FC7PTN1	-320	0.99	0.495	13.5	3365	22.8
FC7PTN2	-320	0.98	0.490	13.3	3535	23.6
FC7PTN3	-320	0.97	0.485	13.2	3505	23.0
						23.1
FC7PTH1	-423	1.00	0.500	13.6	4200	27.2
FC7PTH2	-423	0.97	0.485	13.2	4010	27.8
						27.5

*1.0 in. thick.

Table A-15 Static Fracture-Toughness Properties of Welded Surface-Flawed Specimens* (X7007-T6 Aluminum Alloy; Longitudinal Direction)

| Specimen Number | Temperature (°F) | Flaw Size | | | Fracture Stress (ksi) | Fracture Stress/ Yield Stress Ratio | Critical Stress Intensity (ksi $\sqrt{in.}$) |
		Depth, a (in.)	Length, 2c (in.)	Shape, a/Q			
F7WLR1	70	0.62	2.16	0.437	32.3	0.88	42.2
F7WLR2	70	0.50	1.36	0.295	39.8	0.94	42.1
F7WLR3	70	0.44	1.51	0.315	36.2	0.99	39.6
							41.3
F7WLN1	-320	0.36	1.34	0.253	27.7	0.66	27.2
F7WLN2	-320	0.38	1.29	0.250	27.6	0.65	26.9
F7WLN3	-320	0.42	1.66	0.301	26.6	0.63	28.5
							27.5
F7WLH1	-423	0.56	1.30	0.265	18.7	0.40	18.8
F7WLH2	-423	0.41	1.34	0.256	23.6	0.50	23.4
F7WLH3	-423	0.46	1.54	0.289	19.2	0.41	20.4
C7WLH	-423	0.50	1.27	0.256	21.7	0.46	21.4
							21.0

*1.0 in. thick x 5.75 in. wide (nominal gage) cross-section.

Table A-16   Static Fracture-Toughness Properties of Welded Compact-Tension Specimens * (X7007-T6 Aluminum Alloy; Longitudinal Direction)

Specimen Number	Temperature (°F)	Flaw Size		Stress-Intensity Parameter, Y	Pop-In Load (lb)	Critical Stress Intensity (ksi $\sqrt{in.}$)	Remarks
		a_{avg} (in.)	a/W				
FC7WLR1	70	1.01	0.505	13.8			No pop-in.
FC7WLR2	70	1.11	0.555	15.5			No pop-in.
FC7WLR3	70	1.00	0.500	13.6			No pop-in.
FC7WLN1	-320	0.99	0.495	13.5	4130	28.1	
FC7WLN2	-320	1.06	0.530	14.6	4630	34.9	
FC7WLN3	-320	1.02	0.510	13.9	5080	36.0	
FC7WLN4	-320	0.98	0.490	13.3	5080	33.4	
FC7WLN5	-320	0.99	0.495	13.5	4730	31.5 / 32.8	
FC7WLH1	-423	1.05	0.525	14.4	3550	25.9	
FC7WLH2	-423	1.03	0.515	14.1	3080	21.9	
FC7WLH3	-423	1.03	0.515	14.1	3200	22.8 / 23.5	

*1.0 in. thick.

Table A-17 Static Fracture-Toughness Properties of Cryogenically-Stretched, Surface-Flawed Parent Metal Specimens* (Type 301 Stainless Steel)

Specimen Number	Temperature (°F)	Grain Direction	Flaw Size			Fracture Stress (ksi)	Fracture Stress/Yield Stress Ratio	Critical Stress Intensity (ksi √in.)	Remarks
			Depth, a (in.)	Length, 2c (in.)	Shape, a/Q				
F3PLR1	70	Longitudinal	0.0850	0.410	0.0708	187.4	0.80	>97	No fracture.
F3PLR2	70	Longitudinal	0.1000	0.530	0.0862	182.1	0.77	>104	No fracture.
F3PLR3	70	Longitudinal	0.0700	0.317	0.5990	227.0	1.00	>104	No fracture.
F3PLR4	70	Longitudinal	0.0835	0.400	0.0714	196.3	0.86	102.3	
F3PLR5	70	Longitudinal	0.0785	0.379	0.0671	203.1	0.89	102.6	
								102.4†	
F3PTR1	70	Transverse	0.0800	0.376	0.0672	199.1	0.87	100.6	
F3PTR2	70	Transverse	0.0811	0.430	0.0718	201.3	0.88	105.2	
F3PTR3	70	Transverse	0.0831	0.395	0.0700	198.2	0.87	102.4	
								102.7	
F3PLN1	-320	Longitudinal	0.0741	0.313	0.0537	139.2	0.45	63.0	
F3PLN2	-320	Longitudinal	0.0722	0.239	0.0460	167.5	0.55	69.9	
F3PLN3	-320	Longitudinal	0.0685	0.270	0.0482	151.5	0.49	65.0	
								66.0	
F3PTN1	-320	Transverse	0.0710	0.301	0.0511	119.9	0.40	52.8	
F3PTN2	-320	Transverse	0.0748	0.320	0.0538	102.6	0.34	46.4	
F3PTN3	-320	Transverse	0.0650	0.256	0.0455	135.1	0.45	56.1	
								51.8	
F3PLH1	-423	Longitudinal	0.0620	0.233	0.0419	135.4	0.39	54.1	
F3PLH2	-423	Longitudinal	0.0720	0.305	0.0518	128.0	0.36	56.9	
F3PLH3	-423	Longitudinal	0.0701	0.296	0.0501	124.4	0.35	54.3	
								55.1	
F3PTH1	-423	Transverse	0.0734	0.314	0.0524	99.0	0.29	44.2	M_K correction required.
F3PTH2	-423	Transverse	0.0814	0.367	0.0598	93.3	0.28	44.6	
F3PTH3	-423	Transverse	0.0964	0.580	0.0784	72.2	0.21	39.4	
								44.4†	

*0.135 in. thick x 2.3 in. wide (nominal gage) cross-section.

†Average of two measurements.

Table A-18   Static Fracture-Toughness Properties of Welded, Cryogenically-Stretched Surface-Flawed Specimens* (Type 301 Stainless Steel; Longitudinal Direction)

Specimen Number	Temperature (°F)	Flaw Size			Fracture Stress (psi)	Fracture Stress/Yield Stress Ratio	Critical Stress Intensity (ksi $\sqrt{\text{in.}}$)
		Depth, a (in.)	Length, 2c (in.)	Shape, a/Q			
F3WLR1	70	0.0780	0.360	0.0619	148.9	0.72	72.3
F3WLR2	70	0.0760	0.380	0.0644	168.7	0.81	83.6
F3WLR3	70	0.0710	0.308	0.0568	179.2	0.86	83.2
C3WLR4	70	0.0772	0.299	0.0576	172.0	0.83	<u>80.5</u>
							79.9
F3WLN1	-320	0.0741	0.330	0.0541	88.9	0.30	40.4
F3WLN2	-320	0.0589	0.263	0.0433	113.2	0.39	45.9
F3WLN3	-320	0.0725	0.304	0.0514	89.0	0.30	39.4
C3WLN4	-320	0.0718	0.311	0.0514	92.2	0.31	<u>40.8</u>
							41.6
F3WLH1	-423	0.0683	0.302	0.0499	89.0	0.26	38.7
F3WLH2	-423	0.0770	0.366	0.0583	77.8	0.23	36.6
F3WLH3	-423	0.0624	0.268	0.0620	85.2	0.25	<u>34.7</u>
							36.7

*0.135 in. thick x 2.3 in. wide (nominal gage) cross-section.

Table A-19 Cyclic* Crack-Extension Properties of Compact-Tension Parent Metal Specimens†
(2021-T81 Aluminum Alloy; Transverse Direction)

Specimen Number	Temperature (°F)	Flow Size, a_{avg} (in.)		Stress-Intensity Parameter, Y		Load (lb)	Stress Intensity (ksi √in.)			Cycles, N	Crack Extension, da (in.)	Crack Extension Rate, da/dN (μin./cycle)
		Initial	Final	Initial	Final		Initial	Final	Average			
C2PTR1	70	1.025	1.043	14.0	14.2	1800	12.8	13.1	13.0	2,500	0.018	7.2
C2PTR1	70	1.043	1.210	14.2	17.8	1800	13.1	17.8	15.5	6,000	0.170	28.0
C2PTR2	70	1.030	1.150	14.1	16.4	1500	10.8	13.4	12.1	17,650	0.120	6.8
C2PTR3	70	1.015	1.090	13.8	15.1	2750	19.2	21.5	20.3	1,270	0.075	52.0
C2PTR4	70	1.020	1.130	13.8	15.7	3900	27.6	32.9	30.3	104	0.110	1060.0
C2PTN1	-320	1.000	1.030	13.6	14.1	4100	28.2	29.4	28.8	288	0.030	1040.0
C2PTN2	-320	1.065	1.140	14.7	14.8	2850	21.6	25.4	23.5	900	0.075	83.0
C2PTN3	-320	1.010	1.030	13.8	14.1	2530	16.5	17.2	16.8	2,325	0.020	8.6
C2PTH1	-423	1.000	1.030	13.6	14.1	3200	22.1	23.1	22.6	400	0.030	75.0
C2PTH2	-423	1.015	1.025	13.8	13.9	2500	17.7	17.9	17.8	1,250	0.010	8.0
C2PTH3	-423	0.980	1.080	13.3	15.0	4000	26.9	31.8	29.4	300	0.100	333.0

*R < 0.05.

†1.0 in. thick.

Table A-20   Cyclic* Crack-Extension Properties of Welded Surface-Flawed Specimens† (2021-T81 Aluminum Alloy; Longitudinal Direction)

Specimen Number	Temperature (°F)	Flaw Size Initial Depth, a (in.)	Initial Length, 2c (in.)	Initial Shape, a/Q	Final Depth, a (in.)	Final Length, 2c (in.)	Final Shape, a/Q	Stress (ksi)	Stress Intensity (ksi√in.) Initial	Final	Average	Cycles, N	Crack Extension, da/Q_avg (µin.)	Crack-Extension Rate, $d(a/Q_{avg})/dN$ (µin./cycle)
C2WLR1	70	0.390	1.26	0.263	0.540	1.48	0.323	15.7	15.7	17.4	16.6	1350	95,500	71
C2WLR1	70	0.540	1.52	0.329	0.840	2.00	0.442	15.7	17.6	20.3	19.0	758	169,500	224
C2WLR1	70	0.840	2.01	0.442	0.890	2.11	0.468	15.7	20.3	20.9	20.6	70	26,300	376
C2WLR2	70	0.410	1.33	0.289	0.470	1.42	0.313	19.1	20.0	20.8	20.4	351	41,100	117
C2WLR2	70	0.470	1.44	0.318	0.590	1.56	0.355	19.1	21.0	22.2	21.6	355	76,400	215
C2WLR2	70	0.590	1.75	0.388	0.660	1.86	0.415	19.1	23.2	24.0	23.6	110	44,900	408
C2WLN1	-320	0.460	1.57	0.329	0.500	1.57	0.340	20.5	23.0	23.3	23.2	300	27,900	93
C2WLN1	-320	0.500	1.58	0.350	0.710‡		0.472‡	23.9	27.6	34.8**	31.2	260	138,700	533
C2WLN2	-320	0.360	1.18	0.254	0.380	1.19	0.260	22.7	22.3	22.6	22.4	251	13,900	55
C2WLN2	-320	0.380	1.19	0.260	0.410	1.21	0.268	22.7	22.6	23.0	22.8	251	20,000	80
C2WLN2	-320	0.410	1.21	0.268	0.440	1.29	0.288	22.7	23.0	23.8	23.4	266	19,600	74
C2WLN3	-320	0.450	1.46	0.306	0.460	1.46	0.309	19.9	21.5	21.6	21.6	300	5,400	18
C2WLH1	-423	0.372	1.20	0.243	0.508	1.38	0.292	22.0	21.2	23.2	22.2	400	82,900	207
C2WLH1	-423	0.508	1.47	0.310	0.555	1.57	0.330	23.8	25.8	26.6	26.2	50	28,300	566
C2WLH2	-423	0.410	1.27	0.264	0.500	1.40	0.298	21.7	21.7	23.1	22.4	250	37,300	149
C2WLH2	-423	0.500	1.48	0.299	0.560	1.48	0.308	17.6	18.7	19.1	18.9	500	34,500	69

* R ≤ 0.05.

† 1.0 in. thick x 5.75 in. wide (nominal gage) cross-section.

‡ Final crack size calculated from static fracture data for Q = 1.5.

** Static-fracture-toughness, critical-stress-intensity value.

Table A-21   Cyclic* Crack-Extension Properties of Compact-Tension Parent Metal Specimens[†]
(X7007-T6 Aluminum Alloy; Transverse Direction)

Specimen Number	Temperature (°F)	Flaw Size, a avg (in.)		Stress-Intensity Parameter, Y		Load (lb)	Stress Intensity (ksi $\sqrt{\text{in.}}$)			Cycle, N	Crack Extension, da (in.)	Crack-Extension Rate, da/dN (μin./cycle)
		Initial	Final	Initial	Final		Initial	Final	Average			
C7PTR1	70	1.010	1.070	13.8	14.8	2500	16.8	18.5	17.7	1970	0.060	30.4
C7PTR2	70	1.000	1.130	13.6	16.0	1500	10.3	12.5	11.4	7000	0.130	18.6
C7PTR3	70	0.990	1.035	13.5	14.1	3900	26.4	27.4	26.9	344	0.045	131.0
C7PTR4	70	1.000	1.060	13.6	14.6	4400	30.3	32.5	31.4	306	0.060	196.0
C7PTN1	-320	0.980	1.070	13.3	14.8	4550	30.3	34.4	32.4	575	0.090	1560.0
C7PTN2	-320	1.010	1.090	13.6	15.1	3250	22.3	25.9	24.1	1394	0.080	57.4
C7PTN3	-320	0.970	1.000	15.8	16.5	2400	15.8	16.5	16.2	2865	0.030	10.5
C7PTH1	-423	0.990	1.025	13.5	13.8	4200	28.4	29.6	29.0	300	0.035	117.0
C7PTH2	-423	0.990	1.060	13.5	14.6	3200	21.6	24.3	23.0	1500	0.070	46.7
C7PTH3	-423	0.990	1.020	13.5	14.0	2600	17.6	18.6	18.1	1420	0.030	21.3

*R ≤ 0.05.

[†]1.0 in. thick.

Table A-22 Cyclic* Crack-Extension Properties of Welded Surface-Flawed Specimens† (X7007-T6 Aluminum Alloy; Longitudinal Direction)

Specimen Number	Temperature (°F)	Flaw Size						Stress (ksi)	Stress Intensity (ksi √in.)			Cycles, N	Crack Extension, da/Q_avg (μin.)	Crack Extension Rate $d(a/Q_{avg})/dN$ (μin./cycle)
		Initial			Final									
		Depth, a (in.)	Length, 2c (in.)	Shape, a/Q	Depth, a (in.)	Length, 2c (in.)	Shape, a/Q		Initial	Final	Average			
C7WLR1	70	0.415	1.21	0.244	0.465	1.41	0.282	15.2	14.5	15.8	15.2	4620	29,900	6.5
C7WLR1	70	0.465	1.41	0.282	0.540	1.63	0.327	15.2	15.8	17.0	16.4	1647	45,500	28.0
C7WLR1	70	0.540	1.64	0.327	0.640	1.83	0.372	15.2	17.0	18.1	17.6	700	59,300	85.0
C7WLR2	70	0.440	1.33	0.242	0.490	1.45	0.265	21.0	20.1	21.1	20.6	415	31,600	76.0
C7WLR2	70	0.490	1.45	0.265	0.550	1.54	0.318	21.0	21.1	23.1	22.1	335	37,000	111.0
C7WLR2	70	0.550	1.54	0.318	0.650	1.66	0.346	21.0	23.1	24.1	23.6	350	58,100	166.0
C7WLR2	70	0.650	1.66	0.346	0.770	1.85	0.393	21.0	24.1	25.7	24.9	280	64,900	232.0
C7WLR2	70	0.770	1.85	0.393	0.860	2.05	0.430	21.0	25.7	26.9	26.3	185	47,000	254.0
C7WLR3	70	0.575	1.63	0.325	0.600	1.72	0.347	16.8	18.7	19.2	19.0	102	14,300	140.0
C7WLR3	70	0.605	1.72	0.352	0.630	1.84	0.373	16.8	19.5	20.1	19.8	220	14,700	67.0
C7WLR3	70	0.635	1.84	0.374	0.650	1.95	0.389	16.8	20.1	20.5	20.3	205	8,900	43.0
C7WLN1	-320	0.460	1.32	0.270	0.765‡		0.425‡	22.0	22.2	27.9**	25.0	157	171,000	1090.0
C7WLN2	-320	0.440	1.31	0.263	0.470	1.32	0.268	18.4	18.4	18.6	18.5	170	17,500	103.0
C7WLN2	-320	0.475	1.40	0.282	0.520	1.41	0.289	18.4	19.1	19.3	19.2	201	25,900	129.0
C7WLN2	-320	0.525	1.42	0.292	0.590	1.43	0.303	18.4	19.4	19.8	19.6	401	34,800	87.0
C7WLN3	-320	0.410	1.54	0.294	0.475	1.55	0.297	18.4	19.4	19.5	19.4	50	3,100	62.0
C7WLN3	-320	0.480	1.64	0.310	0.490	1.65	0.312	18.4	19.9	20.0	20.0	80	6,400	80.0
C7WLN3	-320	0.495	1.70	0.319	0.580	1.79	0.341	18.4	20.2	20.9	20.6	400	56,000	140.0
C7WLN4	-320	0.440	1.20	0.244	0.450	1.21	0.250	18.5	17.8	18.0	17.9	150	5,600	37.0
C7WLN4	-320	0.455	1.23	0.253	0.460	1.25	0.256	18.5	18.1	18.2	18.2	170	5,600	33.0
C7WLN5	-320	0.390	1.34	0.252	0.395	1.35	0.255	18.6	18.2	18.3	18.2	65	3,200	49.0
C7WLN5	-320	0.400	1.40	0.265	0.420	1.40	0.268	18.6	18.6	18.7	18.6	325	13,000	40.0
C7WLH1	-423	0.395	1.18	0.228	0.398	1.19	0.229	15.0	14.0	14.0	14.0	200	1,600	8.0
C7WLH1	-423	0.420	1.21	0.236	0.424	1.22	0.238	16.0	15.2	15.2	15.2	75	2,100	28.0
C7WLH1	-423	0.445	1.25	0.242	0.452	1.26	0.248	17.0	16.5	16.5	16.5	50	3,700	61.0
C7WLH2	-423	0.350	1.06	0.204	0.351	1.08	0.206	14.0	12.3	12.4	12.4	200	2,200	11.0
C7WLH2	-423	0.370	1.11	0.215	0.380	1.12	0.217	15.0	13.6	13.6	13.6	110	2,900	26.0

*R ≤ 0.05.

†1.0 in. thick x 5.75 in. wide (nominal gage) cross-section.

‡Final crack size calculated from static fracture data for Q = 1.8.

**Static-fracture-toughness, critical-stress-intensity value.

Table A-23 Cyclic* Crack-Extension Properties of Cryogenically-Stretched, Surface-Flawed Parent Metal Specimens†
(Type 301 Stainless Steel; Longitudinal Direction)

Specimen Number	Temperature (°F)	Flaw Size						Stress (ksi)	Stress Intensity (ksi √in.)			Cycles, N	Crack Extension, da/Q_avg (μin.)	Crack-Extension Rate, $d(a/Q_{avg})/dN$ (μin./cycle)
		Initial			Final				Initial	Final	Average			
		Depth, a (in.)	Length, 2c (in.)	Shape, a/Q	Depth, a (in.)	Length, 2c (in.)	Shape, a/Q							
C3PLR1	70	0.087	0.3141	0.0584	0.115	0.3182	0.0640	131.8	62.2	64.8	63.5	730	17,100	23.0
C3PLR2	70	0.072	0.333	0.0567	0.120	0.380	0.0790	153.4	71.2	84.0	77.6	500	35,000	70.0
C3PLR3	70	0.0655	0.290	0.0496	0.0944	0.339	0.0629	120.5	52.4	59.0	55.7	785	20,500	26.0
C3PLN2	-320	0.0765	0.331	0.0550	0.0797	0.342	0.0569	63.5	29.1	29.6	29.4	600	2,300	3.8
C3PLN3	-320	0.0636	0.230	0.0416	0.0668	0.240	0.0436	93.8	37.3	38.2	37.8	210	2,100	10.0
C3PLN4	-320	0.0612	0.230	0.0411	0.0712	0.242	0.0448	90.7	35.9	37.5	36.7	842	6,500	7.7
C3PLH1	-423	0.0633	0.259	0.0440	0.0830	0.272	0.0506	70.9	29.0	31.1	30.0	350	12,800	37.0
C3PLH3	-423	0.0643	0.252	0.0437	0.0728	0.266	0.0473	58.4	23.8	24.7	24.2	400	5,700	14.0
C3PLH4	-423	0.0535	0.181	0.0332	0.0589	0.184	0.0348	46.9	16.6	17.0	16.8	1031	3,300	3.2

*R ≤ 0.05.
†0.135 in. thick x 2.30 in. wide (nominal gage) cross-section.

Table A-24 Cyclic* Crack-Extension Properties of Welded, Cryogenically-Stretched Surface-Flawed Specimens†
(Type 301 Stainless Steel; Longitudinal Direction)

Specimen Number	Temperature (°F)	Flaw Size						Stress (ksi)	Stress Intensity (ksi √in.)			Cycles, N	Crack Extension. da/Q_avg (μin.)	Crack-Extension Rate, $d(a/Q_{avg})/dN$ (μin./cycle)
		Initial			Final				Initial	Final	Average			
		Depth, a (in.)	Length, 2c (in.)	Shape, a/Q	Depth, a (in.)	Length, 2c (in.)	Shape, a/Q							
C3WLR2	70	0.0654	0.273	0.0471	0.0697	0.276	0.0487	101.1	42.8	43.6	43.2	100	3100	31.0
C3WLR3	70	0.0750	0.365	0.0563	0.0850	0.387	0.0630	69.6	32.2	34.1	33.2	576	7500	13.0
C3WLR4	70	0.0745	0.292	0.0510	0.0772	0.299	0.0525	103.2	45.5	46.1	45.8	75	1800	25.0
C3WLN1	-320	0.0657	0.304	0.0487	0.0676	0.305	0.0493	59.9	25.6	25.8	25.7	310	1400	4.5
C3WLN2	-320	0.0823	0.389	0.0610	0.0850	0.389	0.0620	65.4	31.5	31.7	31.6	150	2000	13.0
C3WLN3	-320	0.0691	0.265	0.0464	0.0719	0.265	0.0473	49.5	20.8	20.9	20.8	1009	1900	1.9
C3WLH1	-423	0.0646	0.246	0.0431	0.0744	0.257	0.0468	59.1	24.0	24.9	24.4	350	6400	18.0
C3WLH2	-423	0.0605	0.221	0.0392	0.0615	0.221	0.0392	49.4	19.1	19.1	19.1	100	600	6.0
C3WLH3	-423	0.0671	0.272	0.0463	0.0676	0.272	0.0463	33.2	13.9	13.9	13.9	300	300	1.0

*R ≤ 0.05.
†0.135 in. thick x 2.30 in. wide (nominal gage) cross-section.

Table A-25 Sustained-Load Crack-Growth Threshold Properties of Parent Metal Specimens*
(2021-T81 Aluminum Alloy)

Specimen Number	Temperature (°F)	Flaw Size, a_{avg} (in.)	Stress-Intensity Parameter, Y	Load (lb)	Initial Stress Intensity, K_{Ii} (ksi $\sqrt{in.}$)	Stress-Intensity Ratio, K_{Ii}/K_{Ic}	Time (hr)	Crack Growth	Remarks
S2PTR1	70	1.04	14.2	2800	20.4	0.77	69	No	
S2PTR1	70	1.04	14.2	3000	21.9	0.83	174	Yes	
S2PTR2	70	1.01	13.8	3080	21.7	0.82	146	Yes	
S2PTR3	70	1.03	14.1	2800	20.2	0.77	121	No	
S2PTN1	-320	0.97	13.2	4000	26.5	0.73	142	No	
S2PTN2	-320	1.02	13.9	4200	29.8	0.82	48	No	
S2PTN2	-320	1.02	13.9	4500	32.0	0.88	44	Yes	
S2PTN3	-320	1.00	13.6	4340	29.9	0.82	96	Yes	Slight.
S2PTH1	-423	1.03	14.1	5000	36.1	0.90	34	Yes	
S2PTH2	-423	1.01	13.8	5200	36.5	0.91	48	Yes	
S2PTH3	-423	0.97	13.2	4800	31.6	0.79	66	Yes	
S2PTH4	-423	1.01	13.8	4225	30.3	0.76	48	Yes	Very slight.

*Compact tension specimen; transverse direction; 1.0 in. thick.

Table A-26   Sustained-Load Crack-Growth Threshold Properties of Welded Specimens*
(2021-T81 Aluminum Alloy)

Specimen Number	Temperature (°F)	Flaw Size, a_{avg} (in.)	Stress-Intensity Parameter, Y	Load (lb)	Initial Stress Intensity, K_{Ii} (ksi $\sqrt{in.}$)	Stress-Intensity Ratio, K_{Ii}/K_{Ic}	Time (hr)	Crack Growth	Remarks
S2WLR1	70	1.07	14.8	2500	18.9	0.65[†]	119	Yes	
S2WLR2	70	1.08	15.0	2300	17.5	0.61[†]	68	No	
S2WLR2	70	1.08	15.0	2400	18.3	0.63[†]	90	Yes	
S2WLR3	70	1.05	14.4	2000	14.5	0.50[†]	68	No	
S2WLR3	70	1.05	14.4	2300	16.7	0.58[†]	90	Yes	Very slight.
S2WLN1	-320	1.10	15.3	3000	24.0	0.69[†]	72	Yes	
S2WLN6	-320	1.11	15.5	2621	21.7	0.62[†]	48	No	
S2WLN7	-320	1.08	15.0	3190	25.3	0.73[†]	50	Yes	
S2WLH1	-423	1.06	14.6	3000	22.2	0.79	48	Yes	
S2WLH2	-423	1.06	14.6	2700	20.0	0.72	48	Yes	
S2WLH3	-423	1.06	14.6	2500	19.4	0.69	48	No	

*Compact tension specimen; longitudinal direction; 1.0 in. thick.

[†]K_{Ic} from surface-flawed specimens used to obtain ratio.

MCR-69-386

Table A-27 Sustained-Load Crack-Growth Threshold Properties of Parent Metal Specimens*
(X7007-T6 Aluminum Alloy)

Specimen Number	Temperature (°F)	Flaw Size, a_{avg} (in.)	Stress-Intensity Parameter, Y	Load (lb)	Initial Stress Intensity, K_{Ti} (ksi $\sqrt{in.}$)	Stress-Intensity Ratio, K_{Ti}/K_{Ic}	Time (hr)	Crack Growth	Remarks
S7PTR1	70	0.97	13.2	2590	17.0	0.53	72	Yes	Slight.
S7PTR2	70	0.96	13.1	3500	22.7	0.71	95	Yes	
S7PTR3	70	1.00	13.6	2960	20.4	0.64	75	Yes	
S7PTR4	70	1.01	13.8	2220	15.3	0.48	72	Yes	Slight.
S7PTR5	70	1.00	13.6	1680	11.4	0.36	75	No	
S7PTN1	-320	0.96	13.1	3800	24.7	1.07	0	Yes	Fractured on loading.
S7PTN2	-320	1.01	13.8	3200	22.3	0.96	46	Yes	
S7PTN3	-320	1.00	13.6	3500	24.1	1.04	48	Yes	
S7PTN4	-320	0.99	13.5	2800	19.0	0.82	48	Yes	
S7PTN5	-320	1.01	13.8	2400	16.8	0.73	48	No	
S7PTH1	-423	0.88	12.2	3800	22.1	0.80	48	Yes	
S7PTH3	-423	1.03	14.4	2640	19.5	0.71	48	No	

*Compact tension specimen; longitudinal direction; 1.0 in. thick.

Table A-28   Sustained-Load Crack-Growth Threshold Properties of Welded Specimens*
(X7007-T6 Aluminum Alloy)

Specimen Number	Temperature (°F)	Flaw Size, a_{avg} (in.)	Stress-Intensity Parameter, Y	Load (lb)	Initial Stress Intensity, K_{Ii} (ksi $\sqrt{in.}$)	Stress-Intensity Ratio, K_{Ii}/K_{Ic}	Time (hr)	Crack Growth	Remarks
S7WLR1	70	1.03	14.1	5000	35.1	0.90	65	Yes	
S7WLR2	70	1.01	13.8	5200	35.0	0.90	65	Yes	
S7WLR3	70	1.06	14.6	5300	39.2	1.01	42	Yes	
S7WLR4	70	1.02	13.9	4500	31.7	0.81	100	No	
S7WLR4	70	1.02	13.9	4700	33.2	0.85	96	No	
S7WLR5	70	1.05	14.4	4850	35.5	0.91	71	Yes	
S7WLN1	-320	1.00	13.6	3800	25.5	0.79	80	Yes	
S7WLN2	-320	1.06	14.6	3400	24.4	0.74	45	Yes	
S7WLN3	-320	1.05	14.4	2600	19.3	0.59	45	No	
S7WLH1	-423	0.91	12.5	2500	14.7	0.62	46	Yes	Very slight.
S7WLH2	-423	0.92	12.6	1960	11.8	0.50	48	No	

*Compact tension specimen; longitudinal direction; 1.0 in. thick.

Table A-29 Sustained-Load Crack-Growth Threshold Properties of Cryogenically-Stretched Parent Metal Specimens* (Type 301 Stainless Steel)

Specimen Number	Temperature (°F)	Flaw Size			Stress (ksi)	Initial Stress Intensity, K_{Ti} (ksi $\sqrt{in.}$)	Stress-Intensity Ratio, K_{Ti}/K_{Ic}	Time (hr)	Crack Growth	Remarks
		Depth, a (in.)	Length, 2c (in.)	Shape, a/Q						
S3PLR1	70	0.071	0.300	0.0555	197.8	91.0	0.88	72	Yes	
S3PLR2	70	0.068	0.280	0.0515	185.2	82.0	0.80	72	Yes	Slight.
S3PLR3	70	0.076	0.331	0.0588	171.5	81.3	0.79	72	Yes	Slight.
S3PLR4	70	0.075	0.310	0.0551	143.2	68.7	0.67	67	No	
S3PLN2	-320	0.060	0.248	0.0420	62.8	27.5	0.42	48	No	
S3PLN3	-320	0.067	0.327	0.0504	67.0	30.5	0.46	48	No	
S3PLN4	-320	0.068	0.285	0.0479	90.0	38.4	0.58	48	No	
S3PLN5	-320	0.060	0.247	0.0423	112.7	45.2	0.68	48	Yes	Slight.
S3PLH1	-423	0.065	0.283	0.0471	100.1	42.4	0.76	48	Yes	
S3PLH2	-423	0.062	0.290	0.0459	85.9	35.9	0.65	44	Yes	
S3PLH3	-423	0.066	0.365	0.524	68.6	30.6	0.55	48	No	

*Surface-cracked specimen; longitudinal direction; 0.135 in. thick x 2.3 in. (nominal gage) cross-section.

Table A-30   Sustained-Load Crack-Growth Threshold Properties of Welded Cryogenically-Stretched Specimens* (Type 301 Stainless Steel)

Specimen Number	Temperature (°F)	Flaw Size			Stress (ksi)	Initial Stress Intensity, K_{Ii} (ksi $\sqrt{in.}$)	Stress-Intensity Ratio, K_{Ii}/K_{Ic}	Time (hr)	Crack Growth	Remarks
		Depth, a (in.)	Length, 2c (in.)	Shape, a/Q						
S3WLR1	70	0.068	0.295	0.0500	135.2	60.1	0.77	72	Yes	
S3WLR2	70	0.068	0.295	0.0500	104.5	45.6	0.58	68	No	
S3WLR3	70	0.077	0.339	0.0570	107.8	50.2	0.64	66	Yes	
S3WLN1	-320	0.069	0.340	0.0526	67.2	29.9	0.72	48	No	
S3WLN2	-320	0.065	0.270	0.0460	88.0	36.7	0.88	48	No	
S3WLN3	-320	0.078	0.293	0.0522	84.5	37.6	0.90	76	Yes	
S3WLH1	-423	0.084	0.432	0.0646	69.1	34.2	0.91	8.9	Yes	Failed.
S3WLH2	-423	0.068	0.325	0.0508	67.6	29.5	0.79	48	Yes	
S3WLH3	-423	0.065	0.269	0.0455	65.4	27.2	0.72	48	Yes	Slight.
S3WLH4	-423	0.060	0.320	0.0459	58.9	24.6	0.65	54	No	

*Surface-cracked specimen; longitudinal direction; 0.135 in. thick x 2.3 in. (nominal gage) cross-section.

APPENDIX B

SURVEY ON CRYOGENICALLY-STRETCHED STAINLESS STEEL

Prepared by

R. H. Alper
Arde, Inc.

CONTENTS

Table

SUMMARY

This appendix presents information on cryogenically-stretch-formed, low-silicon, chrome-nickel stainless steel. This information was gathered from the literature, from unpublished test data, and from investigations performed at Arde, and is of the following nature:

1. **Mechanical Property Data Available from Tests Made by Arde and from the Literature**

These data consist of both uniaxial and biaxial test data which indicate yield strengths, ultimate strengths, and properties in the presence of notches or cracks (as available). Data obtained at test temperatures from room temperature to -423°F are reported. Specifically, all mechanical property data obtained during Arde's standard heat evaluation procedure for the particular heat being supplied to Martin Marietta are reported in detail. These heat evaluation data consist of -320°F uniaxial stress/strain curves of the annealed material at -320°F, and room-temperature and -320°F tensile properties after cryostraining and aging. In addition, -320°F stretch and burst test data for 6-in.-diameter spheres and cylinders are reported.

2. **Fabrication Techniques**

The various cryogenic-stretch-forming approaches used in fabricating both simple and complex shapes with attachments is presented. Specific processing information, such as welding techniques, cryogenic-stretch-forming procedure, etc, is also provided. This appendix also contains data on reproducibility of dimensions of finished pressure vessels, and methods for controlling dimensional tolerances.

3. **Acceptance Procedure and Quality Assurance**

In-process quality control and process specifications for welding, forming, machining, heat-treating, etc, are described. In addition, acceptance criteria and nondestructive test methods are described in detail. Arde's raw material evaluation testing and acceptance procedures are also contained in this appendix.

Assurance of the burst strength of pressure vessels that are fabricated by the cryogenic-stretch-forming process is discussed, and actual burst test data, indicating reproducibility of results, are included.

I. INTRODUCTION

A vital requirement for lightweight structures operating at temperatures down to -423°F is a high-strength material that exhibits high fracture toughness. The toughness must be sufficiently high to sustain proof, operating, and cyclic stress conditions in the presence of defects too small to detect by nondestructive test methods. Although many alloys with high strength at cryogenic temperatures exist, the number of those with sufficiently high fracture toughness for cryogenic service is limited.

An additional consideration is that the strength and toughness of welds in a structure are often less than those of the parent material. Finally, in many applications, mission conditions call for operation over the entire range of temperatures from -423°F to room temperature. Some alloys exhibit good toughness over the entire temperature range, but unfortunately weaken at temperatures approaching room temperature. Therefore, in order to enjoy widest applicability in structures for cryogenic service, a material should have the following characteristics:

1) High strength and fracture toughness over the entire range of temperatures from -423°F to room temperature;

2) Result in welded fabricated structures whose welds show high efficiency and reliability.

Arde, Inc has provided Martin Marietta with a quantity of low-silicon, chrome-nickel, stainless-steel alloy. This alloy will be evaluated by Martin Marietta with respect to the aforementioned characteristics for use in cryogenic applications down to -423°F. This low-silicon stainless steel must be cryogenically deformed at -320°F and then aged for 20 hr at 790°F in order to attain its useful mechanical properties.

Inasmuch as welding such work-hardened material anneals and locally reduces its strength, this alloy is particularly useful in fabricating pressure vessels by a cryogenic-stretch-forming process. In this process, welded, undersized pressure vessels, made from annealed, austenitic stainless steel, are immersed in boiling liquid nitrogen and expanded to the required size by internal pressurization. The aging treatment -- holding the material at 790°F for up to 20 hr -- further increases the yield strength and the ultimate strength of the material, which has already been cold-worked by cryogenic stretch-forming.

This appendix reviews the existing mechanical property data for this alloy. Data from Arde's files and from the literature are presented. In addition, since the alloy requires processing by cryogenic stretch-forming, design of preforms and fabrication techniques will be discussed. Material and component acceptance procedures and quality control during processing will also be discussed.

II. LOW-SILICON STAINLESS STEEL

A. DEVELOPMENT OF ALLOY COMPOSITION

The cryogenically-stretched, low-silicon, stainless-steel alloy that is the subject of this evaluation by Martin Marietta was developed specifically for improved fracture toughness. Before its development, a good deal of data was available on the mechanical properties of room-temperature, cold-worked, austenitic stainless steel over the temperature range from -423°F to room temperature. An excellent compilation of this data is contained in Ref. 1.[*] The room-temperature properties of cryogenically-cold-worked, austenitic stainless steel are available from Ref. 2.

In addition, the properties of cryogenically-worked Type 301 stainless steel at -320°F and below are presented in Ref. 3. The -320°F properties of cryogenically-stretched Type 301, including the results of tests on actual stretch-formed pressure vessels, are presented in Ref 4. Most of these investigations were limited to commercially-available materials, such as Type 301 stainless steel.

In considering the results of these investigations, the following observations can be made:

1) As the austenitic stability increases, the strengthening due to deformation at any temperature decreases. For example, Type 301 stainless steel can be work-hardened to higher strength levels that can Type 304.

2) Deformation at cryogenic temperatures results in higher strength than the same degree of deformation at room temperature.

3) The usefulness of work-hardened sheet is limited by the loss of strength and toughness in welds made after the sheet is rolled.

By means of the cryogenic-stretch-forming process, in which the work-hardening is accomplished with welded structures, full utilization of the work-hardened properties can be obtained. AISI Type 301 stainless steel has the lowest austenitic stability of all the 300-series stainless steel, and may, therefore,

---

[*]References for this appendix are listed on pp B-61 and B-62.

be work-hardened to the highest strength levels. Although the
strength of commercially-available Type 301 was attractive in
both its room-temperature work-hardened condition and its cryo-
genically-work-hardened condition, the loss of toughness of the
material at lower temperatures limited its use to temperatures
above -320°F. Furthermore, it was noted (Ref. 4) that aging the
cryogenically-stretched, commercially-available Type 301 strength-
ened it still further, but drastically reduced its toughness at
temperatures of -320°F and lower.

In 1963 and 1964, the effects of alloy composition of austen-
itic stainless steel on properties which resulted from cryogenic
deformation were studied by several researchers (Ref. 5 thru 7).
Reference 5 showed that the level of silicon, and to some extent,
manganese, in these alloys affected the fracture toughness at all
operating temperatures.

According to these investigators, reducing the silicon led to
marked improvement in fracture toughness. However, work at Arde
(Ref. 7) had indicated that the high strength of such alloys was
very dependent upon high silicon levels.

An evaluation was made of the low-silicon, stainless-steel
alloy at -320°F and 70°F using tensile specimens fabricated from
sheet material provided by the International Nickel Company. Al-
though, as anticipated, the strength of the alloy was somewhat
lower than that obtainable with commercial Type 301, the decided
improvement in toughness more than offset the slight strength
loss. Most striking is a comparison of the effect of 800°F aging
upon the toughness of the low-silicon alloy and a commerical,
Type 301 stainless-steel alloy. Table B-1 compares the notch
strengths of aged and unaged low-silicon material with that of
commercial 301. Whereas aging does not affect the toughness of
the Type 301 alloy at room temperature, a drastic reduction in
toughness occurs at -320°F. On the other hand, aged, low-silicon
material does not drop in toughness at -320°F.

Some specimens were thereupon submitted to NASA-Lewis Re-
search Center for evaluation at -423°F. The results of a few
tests at -423°F (Ref 3) were sufficiently encouraging to proceed
further with the alloy.

Table B-1   Comparison of Notch Properties of Low-
and Standard Silicon Content 301 Stain-
less Steel at -320°F

FRACTURE TOUGHNESS TYPE SPECIMEN[*]			
Standard Material		Low-Silicon Material	
Heat	Tensile Strength (ksi)	Heat	Tensile Strength (ksi)
75519	74	40226	317
73413	140	95013	301
		95178	277
		95124	300
		95136	308

TENSION TYPE SPECIMEN[†]			
Condition	Stress Concentration $\left(K_t\right)$	Tensile Strength (ksi)	
		Standard Material (Heat 72550)	Low-Silicon Material (Heat 40226)
Aged	1.0	367	310
Unaged	1.0	312	300
Aged	19.0	195	270
Unaged	19.0	260	265

[*]Part-though cracked specimen; 0.060 in. thick; 1 inch wide; crack
lengths = 0.10-0.15-in.; prestrained and aged condition.

[†]0.060-in. thick.

A cryogenically-stretched cylinder was fabricated from 0.060-in.-thick, low-silicon alloy for evaluation by NASA-Lewis Research Center. The results of these tests were very good and are reported in Ref. 8. Several important results are listed below:

1) The efficiency of welds made in an actual pressure vessel was found to be essentially 100% over the entire range of temperatures from room temperature to -423°F.

2) In addition, the -423°F toughness of the material was found to be satisfactory, and the alloy exhibited high strength even at room temperature.

Data from Ref. 8 are excerpted and presented in Chapter III of this appendix.

B. COMPOSITION SPECIFICATION

Arde, Inc has since procured a total of eight additional heats of the alloy in accordance with the compositional specification indicated in Table B-2. The low-silicon-alloy composition is compared with a commercial, Type 301 stainless steel in Table B-2.

Table B-2   Arde Specification Compositions

STANDARD TYPE 301 STAINLESS STEEL	
Carbon (%)	0.055 to 0.075
Manganese (%)	1.00 to 1.70
Silicon (%)	0.30 to 0.70
Chromium (%)	17.00 to 17.70
Nickel (%)	7.30 to 7.70
Molybdenum (%)	0.15 to 0.35
Nitrogen (%)	0.02 to 0.04
Phosphorous and Sulphur (Total %)	0.03*
Oxygen (ppm)	90*
Hydrogen (ppm)	3*
LOW-SILICON STAINLESS STEEL	
Carbon (%)	0.025 to 0.045
Manganese (%)	0.10*
Silicon (%)	0.10*
Chromium (%)	18.30 to 18.70
Nickel (%)	7.10 to 7.50
Molybdenum (%)	0.15 to 0.35
Nitrogen (%)	0.02 to 0.04
Phosphorous and Sulphur (Total %)	0.015*
Oxygen (ppm)	60*
Hydrogen (ppm)	2*
*Maximum	

On the basis of the results shown in Ref. 5, the silicon level is maintained at less than 0.1%, as is the manganese. Of importance in the alloy chemistry are the low oxygen and hydrogen levels specified. It has been determined that low oxygen levels tend to

reduce or eliminate weld cracking and improve the fracture toughness of the austenitic stainless steels. The hydrogen levels are maintained low for similar reasons. The carbon level is also maintained below 0.05% in this alloy. Although carbon presents no welding problems unless present at concentrations higher than 0.08% in this alloy, the toughness does appear to suffer at higher carbon levels. Therefore, the carbon level has been maintained at the level of the original heat tests at Arde.

Because of the requirement for low silicon in the alloy, a vacuum-melting technique is required to prepare the alloy with satisfactory low levels of oxygen composition. Composition tolerances were set at levels that are achievable at several steel mills, and yet, not so wide that large differences in mechanical properties would occur. To date, three different mills have successfully poured full-scale heats of the low-silicon alloy. These are Eastern Stainless Steel, Latrobe Steel, and Cameron Iron. The latter two mills have poured double-vacuum-melted ingots; the first mill poured induction-vacuum-melted ingots.

C. EFFECT OF COMPOSITION ON MATERIAL PROPERTIES

Although mill processing of the material is important in determining some characteristics of the finished product, evaluation has indicated that heat composition alone is of primary importance in determining the mechanical properties of the material. For example, in Ref. 7, excellent correlation was obtained between heat composition and tensile properties of 34 commerical, Type 301 stainless-steel heats. Figure B-1 shows a plot of the actual strength vs the strength predicted by a multiple linear regression analysis of the data. Since Ref. 7 was published, the mechanical properties of numerous additional heats have been shown to be closely predictable by means of the regression equations developed at that time. An insufficient number of heats of low-silicon, stainless-steel alloy have been poured to perform an analysis that will produce a regression equation of satisfactory certainty. Nevertheless, the heats which have been procured to the specification indicated previously have all demonstrated similar mechanical properties. For the low-silicon heats, therefore, this same strong dependence on heat composition, rather than on other factors such as mill processing, holds. In the mechanical properties chapter of this appendix, the mechanical properties at several heats are compared. The close range should be noted.
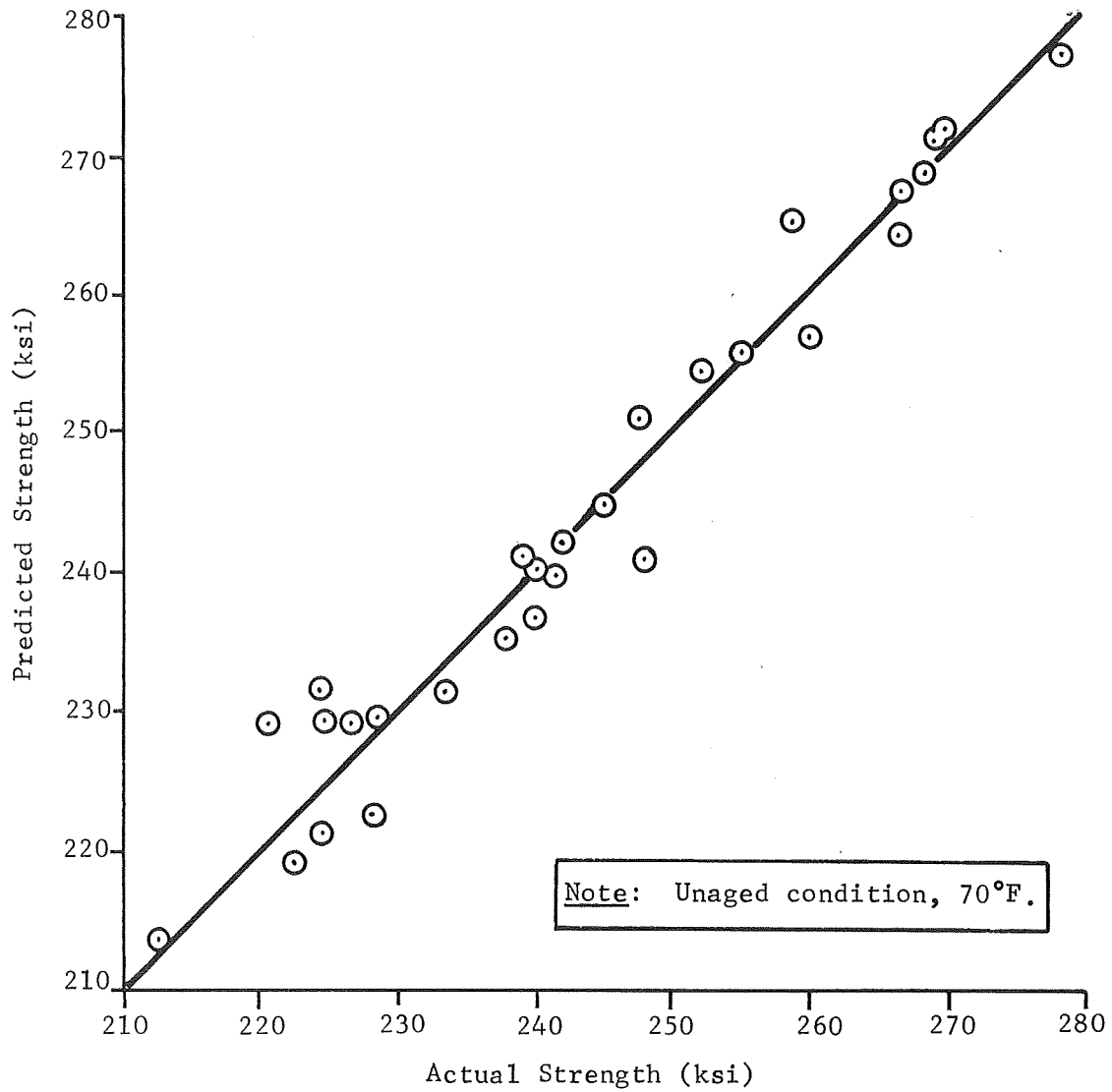
Fig. B-1   Predicted vs Actual Strength of Various Heats of
            301 Stainless Steel after Cryogenic Stretch-Forming

III. MECHANICAL PROPERTIES

Mechanical property data on the low-silicon, stainless-steel alloy were obtained from Arde's files and from Ref. 8 and 9. Data for Heat 50793, the material supplied to Martin Marietta for evaluation, are presented in this chapter. In addition, data accumulated on other heats of the low-silicon material are supplied. Most of the data was obtained at room temperature, -320°F, and -423°F with prestrained tensile specimens. Some data taken with tensile specimens cut from actual pressure vessels are excerpted from Ref 8 and presented in this chapter.

A. EXPERIMENTAL DATA

Inasmuch as the material achieves its strength through deformation at -320°F, specimens must first be prestrained at this temperature. The usual procedure is to first obtain a true stress/strain curve at -320°F for the material in the annealed condition. This establishes the maximum amount of cold work that can be applied to the specimen in uniaxial tension. Such a curve, marked σ_T, is shown for Heat 50793 in Fig. B-2. The nominal stress vs engineering strain curve for this same heat at -320°F is plotted in Fig. B-3. The material may be prestrained any amount up to the maximum shown in Fig. B-3; the tensile properties that result will, of course, depend on the prestrain. The effects of cryogenic prestresses (at -320°F) on the tensile strengths at 70, -320, and -423°F are summarized in Fig. B-4.

The increase in strength due to aging at 800°F for 20 hr may be seen by comparing the data for aged material shown in Fig. B-4 with similar curves for unaged specimens shown in Fig. B-5.

Additional properties of other heats of low-silicon stainless steel are shown in Fig. B-6 (yield strength) and Fig. B-7 (tensile strength).
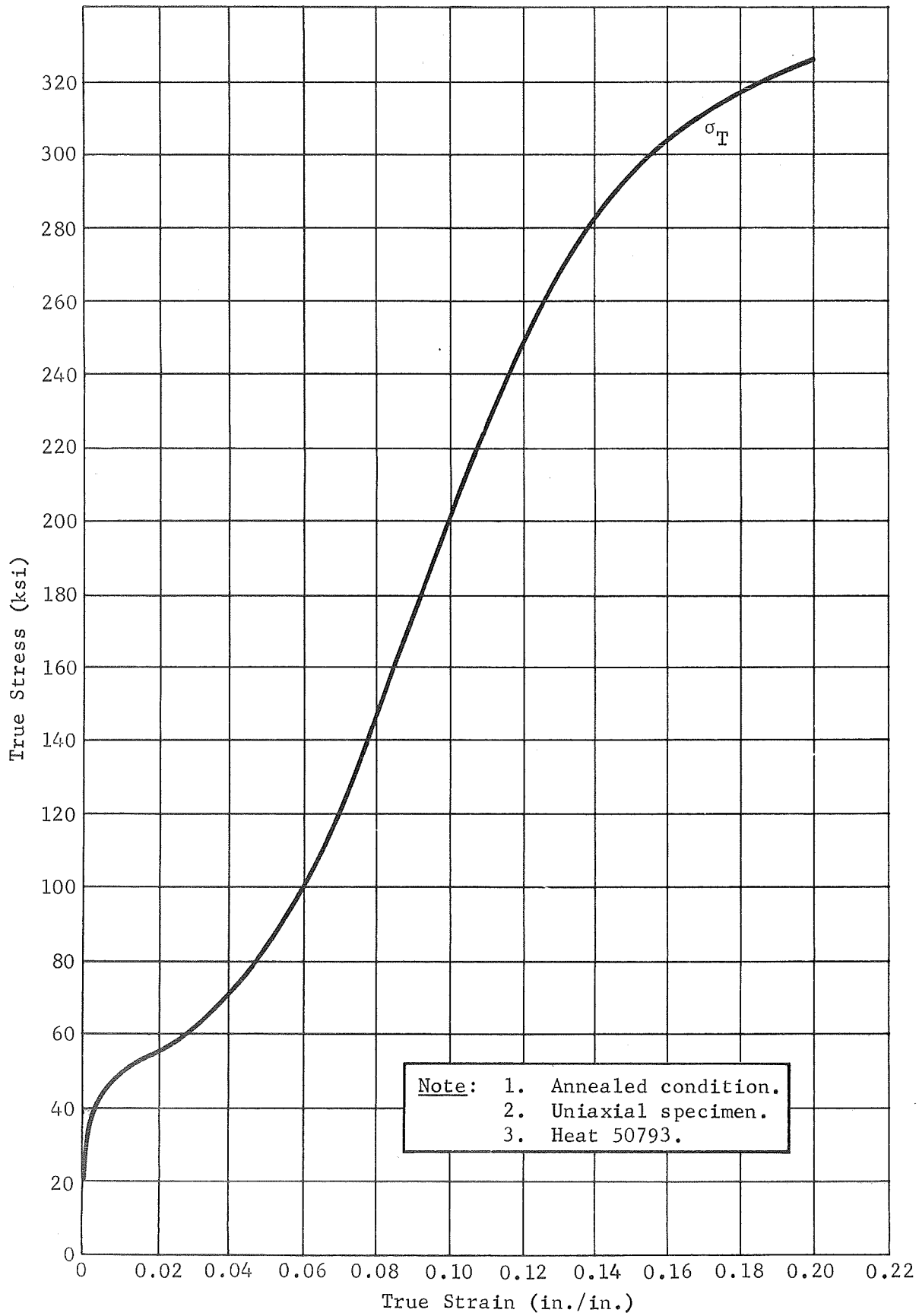
Fig. B-2 True Stress/Strain Curve for Low-Silicon Stainless Steel at -320°F
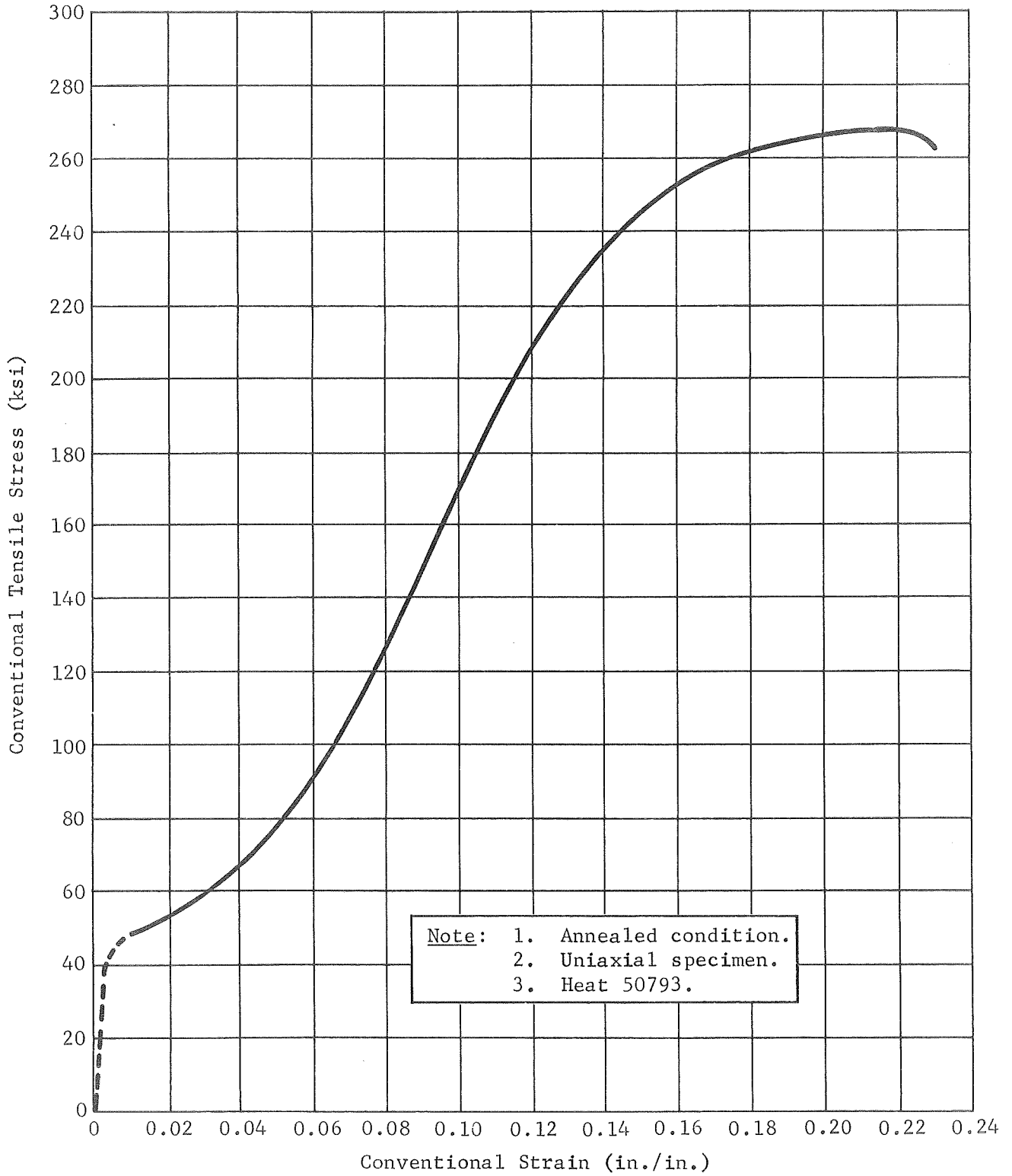
Fig. B-3   Conventional Stress/Strain Curve for Low-Silicon
Stainless Steel at -320°F
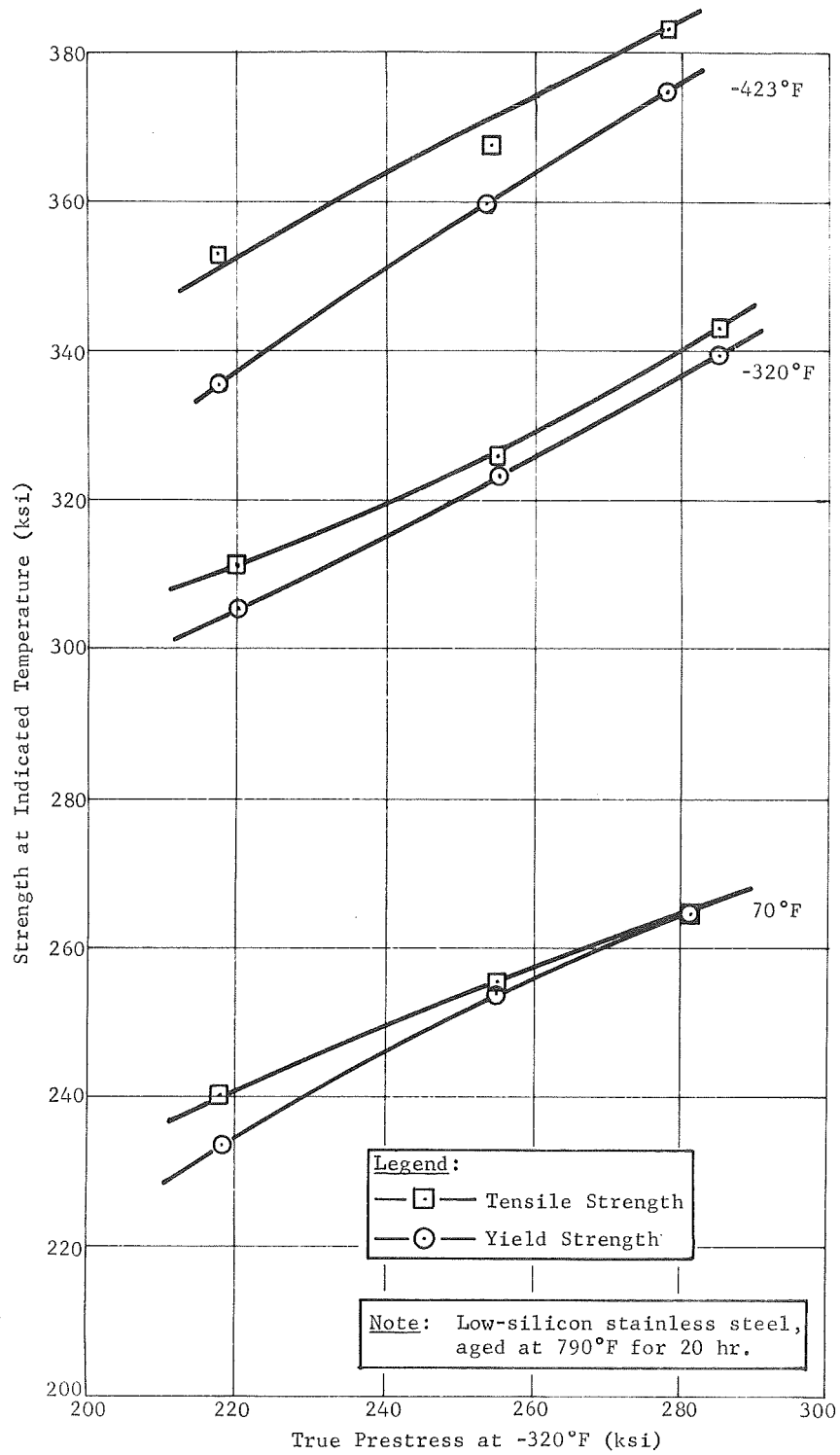
Fig. B-4 Effect of Cryogenic Prestress on Strength of Aged Stainless Steel
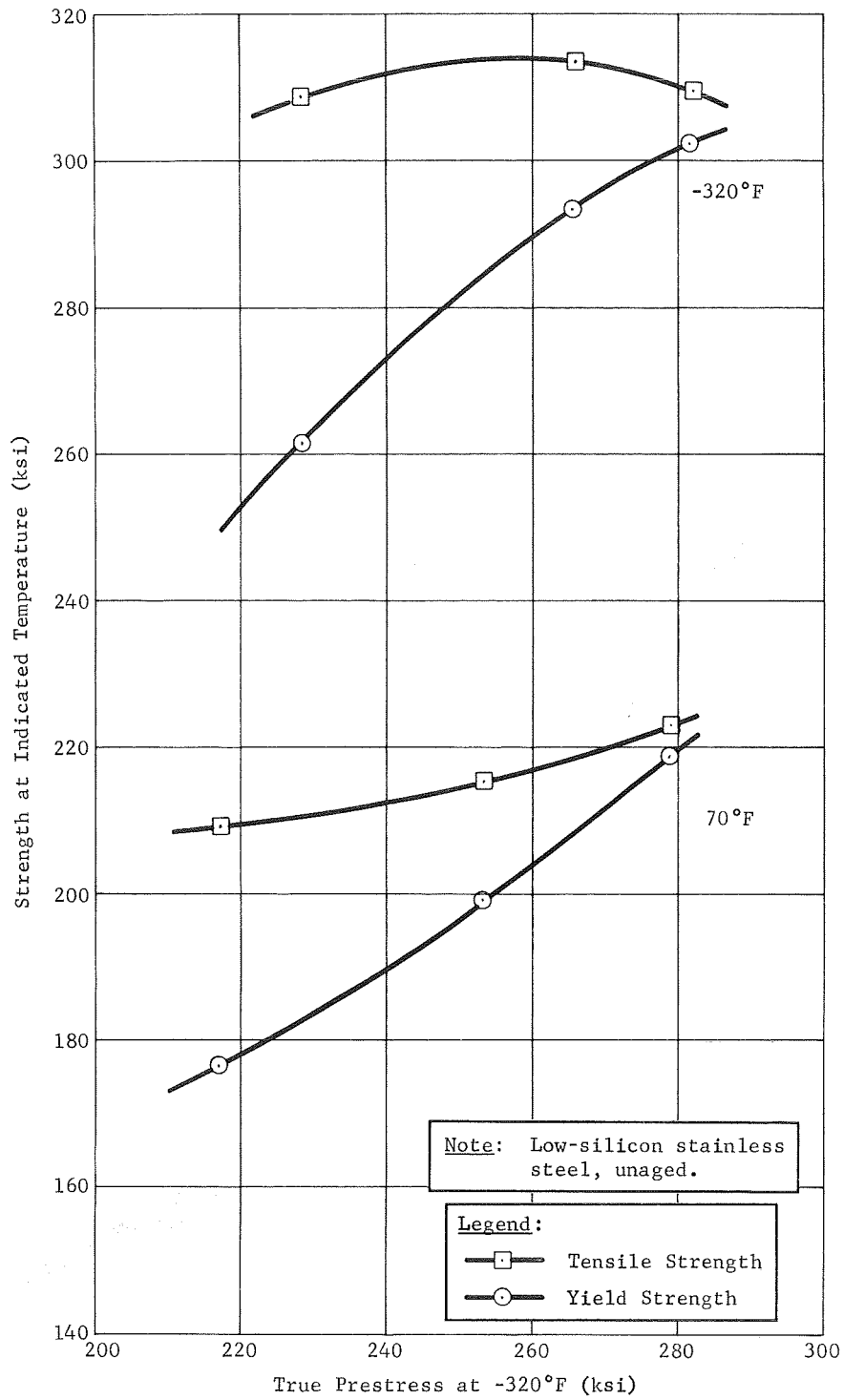
Fig. B-5 Effect of Cryogenic Prestress on Strength of Unaged Stainless Steel
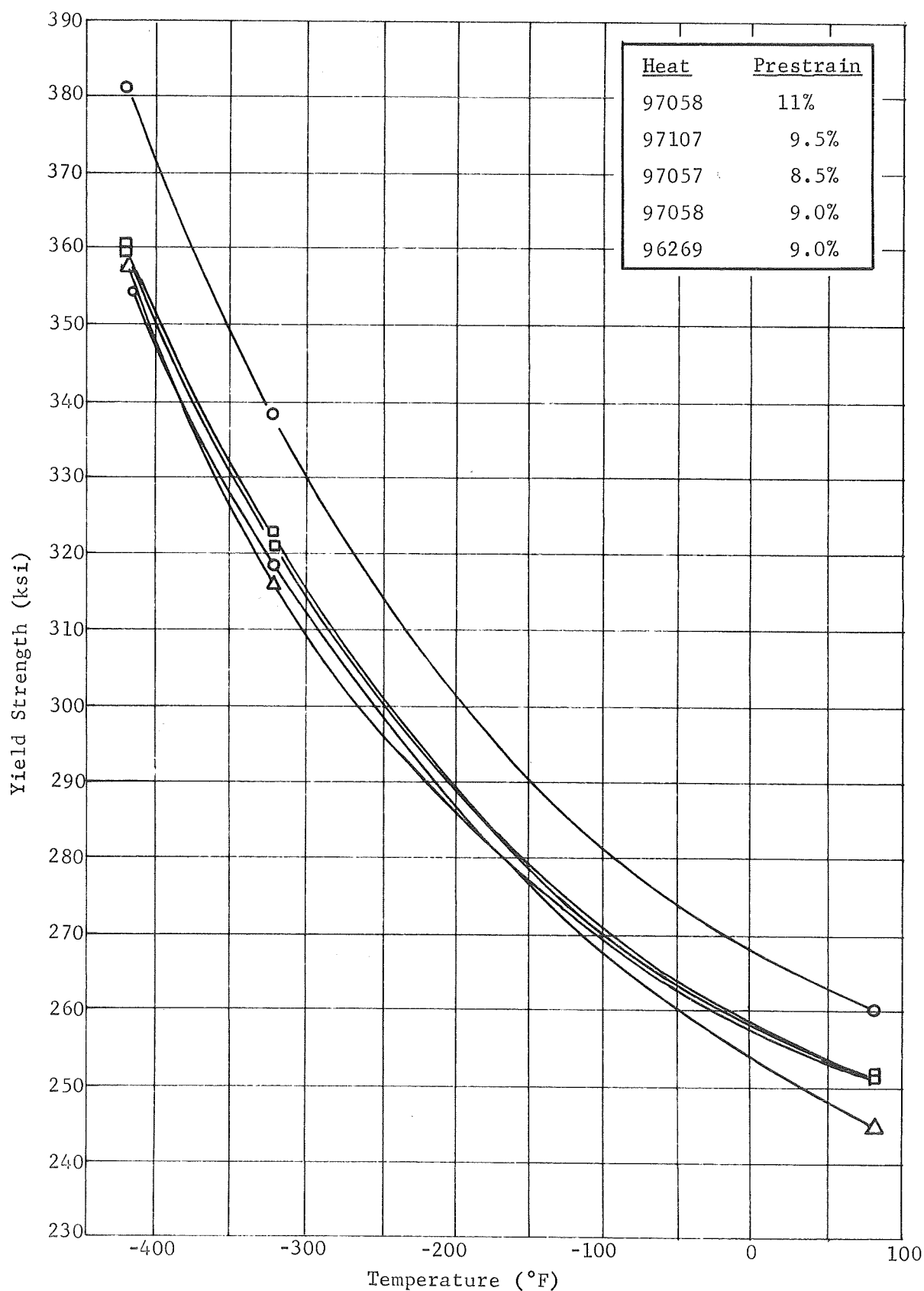
Fig. B-6 Yield Strength of Various Heats of Low-Silicon Stainless Steel
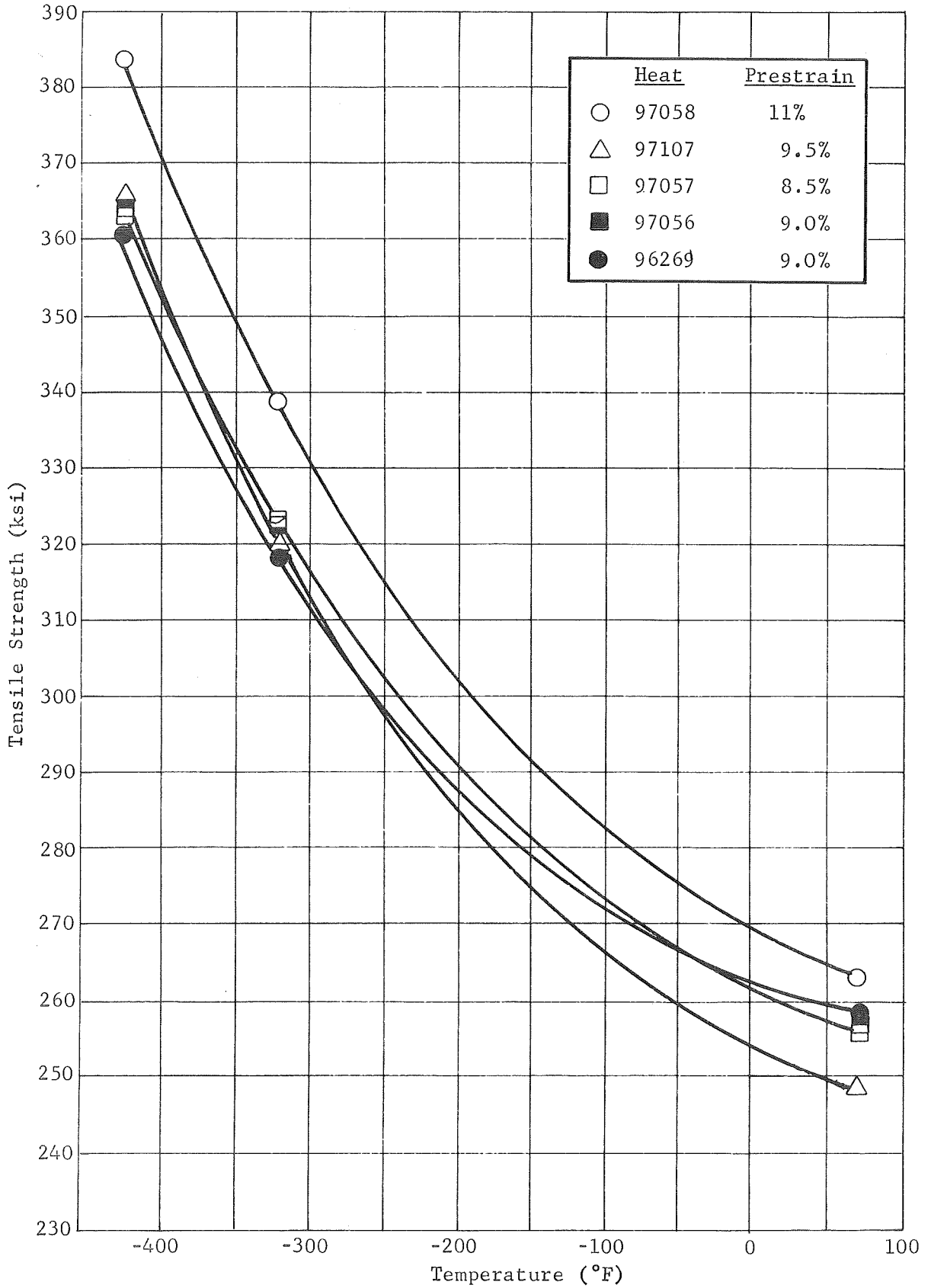
Fig. B-7 Tensile Strength of Various Heats of Low-Silicon Stainless Steel

The testing of four of these heats was performed during the
course of a program for NASA-Marshall Space Flight Center, and
the data are excerpted from Ref. 9. Additional data on the prop-
erties of still another, low-silicon, stainless-steel heat were
obtained from tests on tensile specimens cut from cryoformed
cylinders (Ref. 8). These data are shown in Fig. B-8 and B-9.
Figure B-8 shows the yield strength of the material tested at
room temperature, -320°F, and -423°F. Figure B-9 shows the data
obtained with machined-double-edge notch specimens having a K_T

of 21. Both aged and unaged data are shown.

Notch tests using machined-double-edge notch specimens with
a K_T of 21 as well as a K_T of 10 produced the data presented in
Table B-3. These tests were run at room temperature and -423°F
with aged specimens.

B.   TEST PROCEDURES

As previously explained, the low-silicon material attained
its properties after cryogenic prestraining at -320°F. Specimens
were prestrained in a cryostat at -320°F until they reached the
desired true stress level. Continuous load/strain curves were
plotted automatically using an x-y recorder. Prestraining of
all tensile specimens was performed in a cryostat mounted on a
60,000-lb hydraulic universal testing machine. The cryostat
consisted simply of a double-walled, stainless-steel cylinder
open at the top and mounted on the lower cross-head of the ma-
chine. The -320°F temperature was maintained by filling the
cryostat with liquid nitrogen. All specimens were fabricated,
machined, annealed, and pickled before being prestrained at
-320°F. Thus, smooth tension tests could be carried out on the
prestrained specimens without the need for additional machining.
The specimen's dimensions were remeasured after prestraining.
After prestraining, specimens were either aged at 800°F for 20
hr or left in the unaged condition before testing at the desired
temperature.
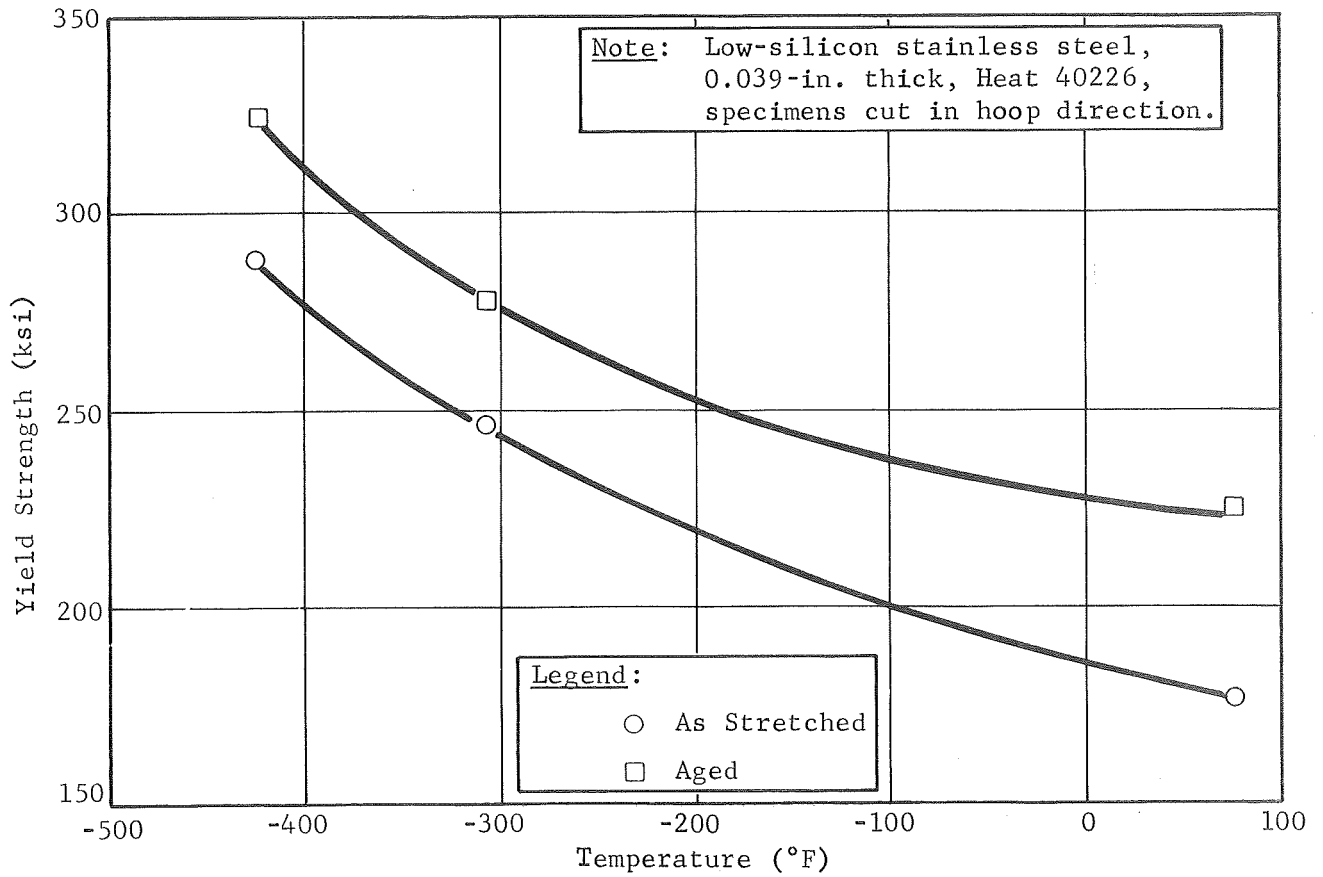
Fig. B-8 Yield Strength of Material Cut from Cryogenically-
Stretch-Formed Cylinders
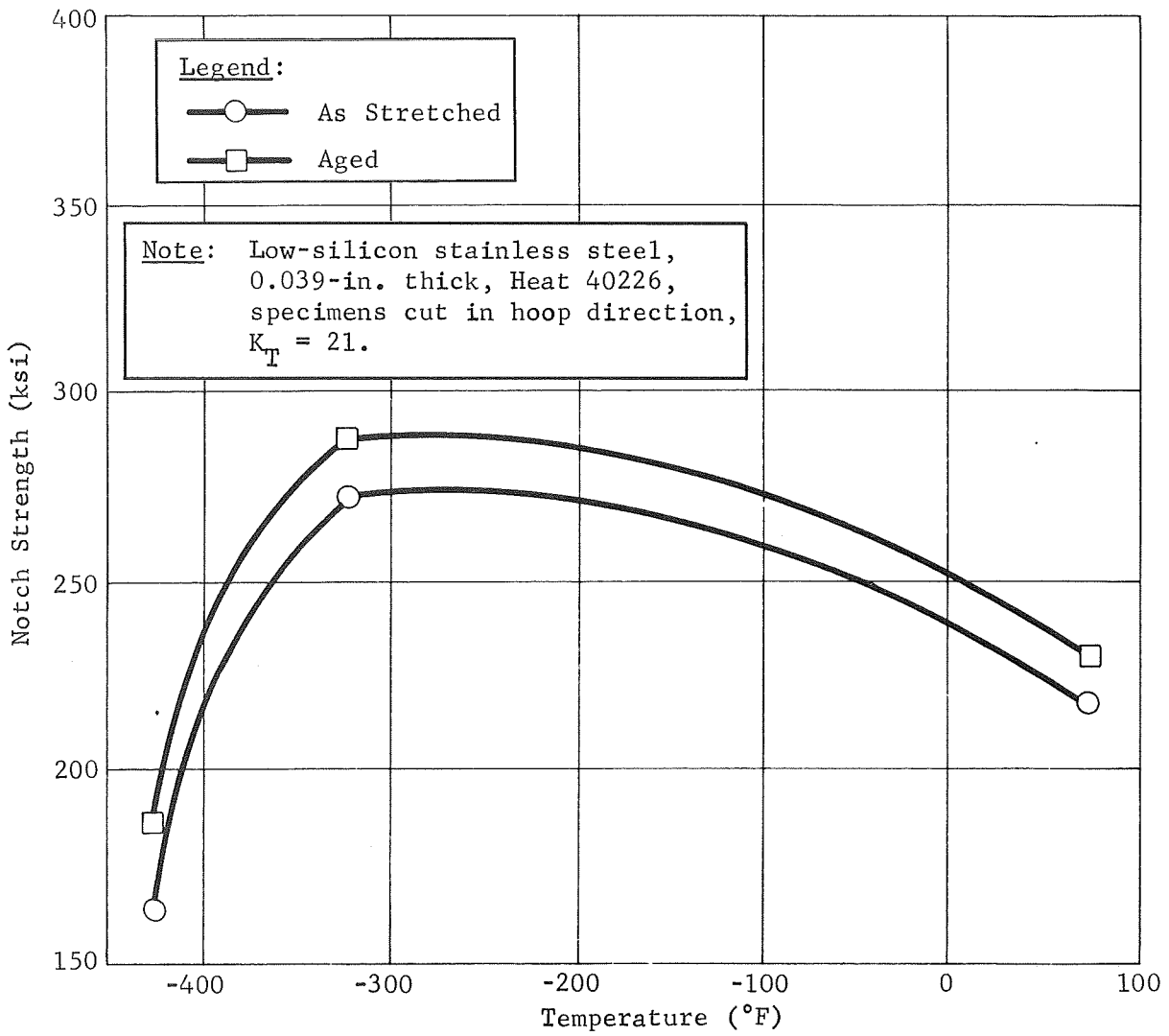
Fig. B-9 Notch Strength of Material Cut from Cryogenically-Stretch-Formed
          Cylinders

Table B-3 Notch Tensile Properties of Low-Silicon Stainless Steel

Heat	Condition	Prestress (ksi)	Test Temperature (°F)	Stress Concentration K_T	Ultimate Strength (ksi)	Yield Strength (ksi)	Notch Strength (ksi)	Notch Strength Ratio	Data Source
	Aged	240	-423	21	362		233	0.64	Wyle Labs
	Aged	240	-423	10	362		283	0.78	Wyle Labs
96269	Aged		70	10	261	259	282	1.08	NASA-MSFC
96269	Aged		-423	10	355	355	260	0.73	NASA-MSFC
97058	Welded	200	70	10	256		297	1.16	NASA-MSFC
97058	Welded	280	-423	10	380		274	0.72	NASA-MSFC
97107	Welded	255	70	10	240		305	1.27	NASA-MSFC
97107	Welded	255	-423	10	366		300	0.82	NASA-MSFC

Notch specimens of two types were tested. These consisted of machined-double-edge notch specimens as well as surface-fatigue-cracked specimens of 0.060-in.-thick sheet with a centrally-located notch. Unfortunately, a valid K_{Ic} value could not be determined for either specimen. Although cracks in the surface-cracked specimens were maintained at a depth of approximately one-half the material thickness, at room temperature and at -320°F, general yielding of the specimen occurred before the onset of rapid crack propagation. Some of the data obtained at -423°F, however, may be valid, inasmuch as the ratio of the gross stress at failure to the yield strength of the material was under 0.8. For truly valid K_{Ic} data, material of heavier cross-section must be tested. This, of course, is the purpose of the present Martin Marietta investigation.

Machined-edge, notch-specimen data are of some interest in that they may be compared with other materials tested with the same specimen configuration. Data for stress concentration factors $\left(K_T\right)$ of 21 and 10 were obtained with machined-edge notch specimens.

All edge-notch specimens were prepared by first prestraining a smooth specimen of appropriate width and then remachining to the gage width required. The notches were then machined in the specimens, and the specimens were aged (if desired) and then tested. The partial-thickness-crack specimen was prepared by prestraining a specimen and then starting a fatigue crack by means of a small punch mark in the center of the specimen. The specimens were fatigue-cracked in bending on a Wiedemann-Baldwin Fatigue Tester. Measurement of the notch was monitored during the fatigue cracking by means of a 30X microscope. Calculations of the nominal K_{Ic} value with this specimen were made, however, on the basis of initial crack dimensions measured after the specimen had been broken.

IV. FABRICATION TECHNIQUES

A. PROCESSING SEQUENCE

The fabrication of pressure vessels by cryogenic stretch-form-
ing requires that a welded preform be built. The preform is then
stretched at -320°F, final-machined, and aged.

The preform components vary with the configuration of the
final vessel. Spherical shells or other surfaces of double curva-
ture may be constructed by hydroforming or deep-drawing, and then
machining to improve thickness tolerances. Cylindrical sections
may be either shear-spun or made by roll-and-weld techniques.
Bosses and ports are machined from forgings or sheet bar and all
details are assembled by welding to produce the preform. No es-
sential differences in fabrication techniques are necessary when
utilizing either Type 301 stainless steel or low-silicon stain-
less steel.

A flow chart, shown in Fig. B-10, lists the detailed process-
ing and inspection steps in the fabrication of a typical spherical
pressure vessel. This chart describes the fabrication of a 22-in.-
diameter sphere made from the low-silicon alloy described in Ref.
9. Some of the more important fabrication steps are discussed in
greater detail below.

B. FORMING

1. Forming Surfaces of Double Curvature

The hydroforming process has been most often selected to pro-
duce details such as hemispherical heads for spheres and cylinders
made by the cryogenic-stretch-forming process. Hydroforming re-
quires relatively-inexpensive initial tooling and is a reliable
means of producing hemispheres from sheet stock. Good uniformity
of thickness results, and parts are generally free from buckles.
The size of such parts is presently limited to diameters of about
22 in. after stretching.

For larger sizes, drawn heads or spinnings may be used. Better results are obtained when sheet or plate are formed into such surfaces than when forgings are made and then machined. Rolled plates or sheets are generally more homogeneous than forgings, and controlling the orientation of the inclusion is more readily accomplished.

Hydroforming of details is generally done in two strikes. During the first strike, a head is drawn to about 95% of its full depth. The head is then cleaned, solution-annealed, and restruck. The second strike is used to shape up the head and achieve closer dimensional control. Materials handling, cleaning, and annealing are performed in accordance with applicable specifications.

2. Starting Material Thickness

Since the thickness of the preform material thins down during stretch-forming, it is necessary to follow certain procedures to ensure that the final thickness of the vessel will be adequate to produce failure at the desired pressure. Tolerances are applied in such a fashion as to minimize the weight of the final article without reducing the burst pressure. As an example, the procedure used with hydroformed hemispheres is discussed below.

The minimum wall thickness of the preform is based on the anticipated thinout resulting from stretch forming. This thinout is calculated from uniaxial and biaxial test data, and is described in Chapter VI of this appendix. Experience has shown that hydroforming or other methods of forming hemispheres generally results in about a 15% total variation in the wall thickness.

The minimum flat sheet stock thickness ordered is, therefore, 15% greater than the minimum as-formed head thickness due to hydroform variations. The specification to which sheet stock is ordered allows a thickness variation which is one-half normal mill tolerances (see Table B-4). These sheet thickness tolerances are, therefore, also allowed for in specifying the starting sheet thickness.

```
┌─────────────────────────────┐         ┌─────────────────────────────┐
│    Receive Sheet Stock      │         │     Receive Boss Stock      │
└─────────────────────────────┘         └─────────────────────────────┘
```

Preform of Hemispherical Head P/N D104347	Preform of Open Boss End of Hemispherical Head P/N D104346	Clevis Boss P/N C104348	Preform Boss P/N E104349
Shear Sheet Stock to Head-Blank Size and Serialize Blanks	Shear Sheet Stock to Head-Blank Size and Serialize Blank	Cut Slugs from Boss Stock, Rough-Machine, and Serialize Slug	Cut Slugs from Boss Stock, Rough-Machine, and Serialize Slug
Inspect	Inspect	Inspect Dimensionally and Ultrasonically	Inspect Dimensionally and Ultrasonically
Hydroform Head at Vendor (First Strike)	Hydroform Head at Vendor (First Strike)	Boss-Machine at Vendor	Boss-Machine at Vendor
Clean, Anneal, and Pickle	Clean, Anneal, and Pickle	Inspect Dimensionally, Dye-Check, and X-Ray	Inspect Dimensionally, Dye-Check, and X-Ray
Inspect	Inspect	Clean and Cold-Pickle	Clean and Cold-Pickle
Hydroform Head at Vendor (Second Strike)	Hydroform Head at Vendor (Second Strike)	Final Acceptance	Final Acceptance
Machine-Off Flange, Machine Entire Outside Surface to Constant Thickness, and Polish Inside Surface	Machine-Off Flange, Machine Entire Outside Surface to Constant Thickness, Polish Inside Surface, and Machine Holes for Bosses		
Inspect Head to B/P, Ultrasonically Inspect, Dye Check	Inspect Head to B/P, Ultrasonically Inspect, Dye Check		
Clean and Cold-Pickle	Clean and Cold-Pickle		
Final Acceptance	Final Acceptance		

Subassemble Hemispherical Head Weldment

P/N E3589-1

Clean all Weld Edges and Fit, Tack Weld, and Weld the Clevis Bosses into the Head

Clean all Weld Edges and Fit, Tack Weld, and Weld the Preform Boss into the Head

Remove all Welding Oxides with a Flap Wheel

Grind Weld Beads on Inside of Head Flush to +0.005 in.

Dye-Check Welds, X-Ray Welds, and Dimensionally Inspect Head Weldment Assembly

Flap Wheel

Grind Weld Beads on
Inside of Head Flush
to +0.005 in.

Dye-Check Welds,
X-Ray Welds, and
Dimensionally
Inspect Head
Weldment Assembly

Clean Assembly

Final Acceptance

Assemble Preform
Vessel Weldment

P/N E3589

Clean Weld Edges and
Fit, Tack Weld, and
Weld Girth

Remove all Welding
Oxides with a Flap
Wheel

Dye-Check and X-Ray
Girth Weld

Clean Preform

Solution-Anneal
Preform Vessel with
Argon Gas Purge on
Inside

Cold-Pickle Preform

Dye-Check Entire
Outside Surface
of Preform

Dimensionally
Inspect Preform

Assemble Helium Bottle
Postform

P/N D3590

Cryogenically-
Stretch Vessel

Dye-Check Entire
Outside Surface of

```
                    Vessel
                      │
        ┌─────────────────────────────┐
        │ Dimensionally Inspect       │
        │ Vessel and Measure          │
        │ Volume                      │
        └─────────────────────────────┘
                      │
        ┌─────────────────────────────┐
        │ Clean Vessel and            │
        │ Passivate Vessel            │
        └─────────────────────────────┘
                      │
        ┌─────────────────────────────┐
        │ Inspect Vessel              │
        └─────────────────────────────┘
                      │
        ┌─────────────────────────────┐
        │ Age Vessel Using            │
        │ Gas Flow on Inside          │
        │ at Vendor                   │
        └─────────────────────────────┘
                      │
        ┌─────────────────────────────┐
        │ Remove Aging Oxides         │
        │ from Vessel by Vacu-        │
        │ Blasting Outside            │
        │ Surface and Grit            │
        │ Scrubbing the Inside        │
        │ Surface                     │
        └─────────────────────────────┘
                      │
        ┌─────────────────────────────┐
        │ Clean Vessel and            │
        │ Passivate Vessel            │
        └─────────────────────────────┘
                      │
        ┌─────────────────────────────┐
        │ Hydrotest Vessel to         │
        │ 3500 psi at a               │
        │ Temperature of              │
        │ 70 ± 10°F                   │
        └─────────────────────────────┘
                      │
        ┌─────────────────────────────┐
        │ Helium-Leak-Test            │
        │ Vessel at 2100 psi          │
        │ Using Mass Spectrometer     │
        │ at Vendor                   │
        └─────────────────────────────┘
                      │
        ┌─────────────────────────────┐
        │ X-Ray all Welds             │
        └─────────────────────────────┘
                      │
        ┌─────────────────────────────┐
        │ Machine Inlet Boss          │
        │ to a 1.440-in.              │
        │ Diameter through Hole       │
        └─────────────────────────────┘
                      │
        ┌─────────────────────────────┐
        │ Inspect Boss                │
        └─────────────────────────────┘
                      │
        ┌─────────────────────────────┐
        │ Clean Vessel and            │
        │ Passivate Vessel            │
        └─────────────────────────────┘
                      │
        ┌─────────────────────────────┐
        │ Final Acceptance and        │
        │ Identification of           │
        │ Vessel                      │
        └─────────────────────────────┘
                      │
        ┌─────────────────────────────┐
        │ Package Vessel              │
        │ for Shipment                │
        └─────────────────────────────┘
```

Fig. B-10 Manufacturing Flow Chart for NASA Helium Bottle

Table B-4 Permissible Variations in Thickness of
Sheet and Plate

Specified Thickness (in.)	Permissible Variations in Thickness, Plus or Minus (in.)
0.016 to 0.026	0.002
0.027 to 0.040	0.002
0.041 to 0.058	0.003
0.059 to 0.072	0.003
0.073 to 0.083	0.004
0.084 to 0.098	0.004
0.099 to 0.114	0.005
0.115 to 0.130	0.005
0.131 to 0.145	0.006
0.146 to 0.176	0.007
0.177 to 0.250	0.010

To reduce the weight of vessels made from such components,
the surface of each hemisphere may be machined to a reasonably
constant thickness. To provide enough material for machining,
the as-formed head thickness is set a minimum of 0.009 in. thicker
than the minimum preform wall thickness. Of course, if machining
is not necessary (i.e., if the small weight penalty is acceptable),
then the machining allowance is omitted. Since machining toler-
ances represent a larger percentage of thin walls than heavy walls,
it is clear that machining yields greater relative weight savings
in heavier-walled vessels. For example, machining to a ±0.007-in.
tolerance on the thickness in a 0.140-in. walled vessel represents
a 4% weight saving over that obtainable by hydroforming alone.
In a 0.030-in.-thick walled vessel, it is obvious that machining
would be useless, since the as-formed total variation of 15% due
to hydroforming represents a tolerance of only about ±0.002 in.
Such a small variation would be difficult to improve by machining.

If all these allowances are made in the starting sheet thick-
ness, experience indicates that design burst pressures, weights,
and volumes will be met in the final product. A discussion of
the assurance of burst pressure capability of stretch-formed pres-
sure vessels is given in Chapter VI of this appendix.

3. Cylinders and Cones

Cylinders and cones are often utilized as components of pres-
sure vessels. These may be made from sheet or plate by rolling
and welding. Experience has indicated that the original sheet

rolling should be done normal to the longitudinal weld. Although
hundreds of pressure vessels have been successfully fabricated in
this way, cylindrical components made by shear-spinning forged
rings have also been successfully incorporated into vessels. Cryo-
genically-stretched, shear-spun cylinders are discussed in Ref.
10. Such vessels were designed for cryogenic service at -320°F.
Their design burst stress at -320°F was 300,000 psi. In setting
thicknesses of starting sheet material for rolled and welded cyl-
inders, no allowances for machining or forming are required and
only the sheet mill tolerances in Table B-4 apply.

C. FORGING AND MACHINING OF BOSSES AND PORTS

Bosses and attachments welded into the shell must be machined
from heavy sections of material. These heavier sections originate
from the same ingot as the sheet material. The material from
which the bosses are fabricated, therefore, has undergone consid-
erably less reduction than the sheet material. For this reason,
some attention must be paid to the orientation of inclusions in
the material. The usual starting material is rolled plate. When
welding bosses to the sheet that forms the vessel shell, the most
favorable condition occurs if the rolling plane of the original
plate lies more or less parallel to the shell surface at which
the weld is being made. Forged bars and pancakes are also used.
These materials are machined in such a fashion that a weld orien-
tation equivalent to that of the plate, previously described, is
maintained when incorporating such details into the structure.

Finished bosses are dimensionally inspected, dye-penetrant-
checked, X-rayed, cleaned, and cold-pickled before final accept-
ance.

D. WELDING

The cryogenic-stretching process requires a weld that will
undergo plastic deformation at -320°F and exhibit a strength equiv-
alent to that of the parent material. Investigations have been
made to determine weld parameters that are reasonably independent
of small changes in parent material composition, and that result
in uniform, reliable welds. Welds produced in a single pass,

rather than multiple passes, have been found advantageous for several reasons. Multiple-pass welding usually causes carbide precipitation immediately adjacent to a weld bead. Instead, when a single-pass weld is made, carbides precipitate some distance from the fusion zone and can be readily dissolved upon subsequent annealing. But when multiple passes are made, the second pass can cause precipitation of carbides close to, and even within, the weld pass below it. The grain boundaries in which these carbides precipitate have been affected by the first pass. Carbides in grain boundaries thus affected have been found very difficult to dissolve. Such grain-boundary carbides reduce the toughness of the material at cryogenic temperatures.

A single-pass weld also eliminates the occurrence of lack of fusion between passes that is frequently experienced in multi-pass welds. Finally, a single-pass weld reduces the amount of filler material introduced into the joint.

An additional factor in welding material is the avoidance of small microcracks that may open during stretching. By removing all restraints during welding, such as backup fixtures, a crack-free weld can be made. Thus, for the process, a single-pass, gas-backed weld is used. The parts to be joined are positioned by means of a series of small tack welds, which are subsequently completely consumed by the weld pass. No chills or restraining fixtures are used. Although the majority of vessels that have been fabricated by this process were made from Type 301 stainless steel, the same techniques can be readily applied to the low-silicon, stainless-steel alloy. In fact, in weld-restraint tests, designed to produce weld cracks in Type 301 stainless steel, the low-silicon alloy demonstrated far less susceptibility to this type of cracking. Experimental data upon which these low-restraint welding techniques are based are described in Ref. 11.

Unless special techniques are used for thicknesses over 0.125 in., a single-pass weld becomes difficult, since the weld bead may drop through if it is not supported. An approach has been developed that produces a horizontal, single-pass weld in thicker material, made with a vertical torch. This is accomplished by means of a closely-controlled, pressurized-gas backup to support the weld. Thicknesses up to 0.375 in. have been welded in this manner, using the tungsten inert gas (TIG) welding process. The filler wire used is Type 308L stainless steel. No special weld preparation or "V" joints are machined into the components before welding. A simple butt joint results in 100% fusion and requires a minimum of weld-wire filler. However, great care is required

in the preweld fitting and alignment of parts. Closely-spaced
tack welds are required to prevent the misalignment of parts dur-
ing welding. All weld surfaces are carefully cleaned to prevent
contamination of the welds.

E. ANNEALING

To eliminate carbides in the weld zone, and to remove any
thermal stresses that may have been created in the vessel during
welding, each vessel is solution-annealed at 1950°F after welding.
Control of the oxidation of the vessel surfaces is therefore re-
quired. Inasmuch as a rapid quench in cold water is required to
maintain carbides in solution with this material, inert gas or
other protective atmospheres are not very feasible for the protec-
tion of exterior vessel surfaces. This is because the vessel has
to be removed from any protective atmosphere anyway for rapid ac-
cess to the quenching tanks. By scrupulously cleaning the vessel
surfaces before it is annealed, it is possible to obtain a uniform
scale that is readily removable by pickling for short times. Ves-
sel interiors, however, are protected from oxidation by means of
an argon purge. Flexible tubes are connected to the vessel's in-
terior in such a way as to permit the flow of argon into and out
of the vessel. The flexible lines allow the vessel to be maneu-
vered into and out of the furnace while the argon flow is main-
tained. After completion of the annealing cycle, the vessel is
removed from the furnace immediately plunged into a water bath,
and covered with a water spray. This rapid quenching prevents
the formation of carbides because the vessel is quickly cooled
through the carbide-precipitation temperature range. The argon
gas purge is maintained throughout the quench cycle at a rate
sufficient to maintain a positive pressure. This prevents buck-
ling of the vessels during quenching. The exterior of the vessel
is cold-pickled to remove annealing oxides. As a final step, each
vessel is dye-penetrant-inspected over its entire surface and
dimensionally inspected.

F.   CRYOGENIC STRETCH FORMING

The stretch-forming facility consists of the stretch pit, a control room and a liquid nitrogen storage and pumping system. The pit is approximately 18 ft deep by 8 ft in diameter and accepts forming tanks of various sizes. These tanks are filled with liquid nitrogen for the stretch-forming operation. The size of the forming tank is dictated by the size of the vessel.

In the case of a vessel which is stretched into a forming die, the preform is first placed in the die and then lowered into the forming tank. The die is used to control the final size of the pressure vessel very accurately. The die is sized to compensate for the elastic rebound that occurs when the pressure is removed. This rebound is approximately 1% of the vessel diameter.

The forming tank is filled with liquid nitrogen to a level at which the preform and die assembly will be covered. The preform is filled with liquid nitrogen. When the preform is full, it is lowered to the bottom of the forming tank. At this time, the forming tank is topped off with liquid nitrogen so that the liquid level is maintained above the vessel. This is done to ensure that boiling off liquid nitrogen in the forming tank will not reduce the liquid level during stretching and cause a failure due to inadequate refrigeration. The preform is then connected to the pressurization source from the control room. A blast mat is placed over the entire pit as a precautionary measure.

The final phase of the operation is the actual pressurization of the preform. Liquid nitrogen is pumped into the refrigerated preform until the predetermined pressure is achieved. When this occurs, a vent valve is opened and the system is rapidly bled down to atmospheric pressure, ending the stretch. The pressurization process is controlled from the control room.

G.   AGING

After a vessel has been stretched, inspected, and cleaned, it may be aged in air at 790°F for 20 hr. In the furnace, the stainless steel oxidizes and becomes covered with a light, golden-brown film. After aging is complete, aging oxides are removed from the outside surface of the vessel by vacu-blasting. In order to remove

any oxides that may have accumulated on the inside of the vessel during aging, the vessel is partially filled with a silicon-carbide grit, set up on a rotating spindle, and slowly rotated. A fixture, used to hold the vessel for this purpose, allows the vessel to be rotated at various angles so that the entire interior surface can be polished with the silicon-carbide grit. After aging oxides are removed, the vessel is thoroughly cleaned with an alkaline detergent solution and then passivated with a nitric acid-sodium dichromate passivating solution.

V. QUALITY CONTROL

A. MATERIAL ACCEPTANCE AND EVALUATION

The material used for applications at cryogenic temperatures is an austenitic stainless steel with very low silicon, manganese, and carbon levels. The Arde specification for this material calls for vacuum-induction melting, followed by consumable-electrode re-melting, using high-purity charging materials. Of special significance are the high standards of material cleanliness included in the specification.

The tests performed to determine conformance to the specification consist of independent check analyses of heat chemistry, metallographic examinations for inclusion distribution and size, and metallographic examinations for grain size and intergranular carbides. In addition, a visual examination of the sheet-surface condition and a dimensional inspection of the mill product are made. Finally, in accordance with the specification, samples from each lot of material are ultrasonically inspected to establish that the material is free from sub-surface gross defects. All these requirements were established at Arde as a result of experience with materials used in cryogenic stretch-forming. In addition to the aforementioned specification requirements, which are imposed on the steel vendor, evaluations are performed on each heat to establish its conformance to the process requirements and minimum-mechanical-property standards. The evaluation consists of weldability tests, tensile specimen tests, and fabrication and testing of small spheres and cylinders to evaluate biaxial stretching characteristics and biaxial mechanical properties. The steps involved in material acceptance are listed in Table B-5.

Material cleanliness has been definitely established as a requirement for the production of reliable welds in preforms. The maximum size of globular oxides is limited to 25 μ. The purpose of this limitation is to eliminate weld porosity, which has been traced to this type of inclusion. The ultrasonic-inspection procedure serves as a further check on the occurrence of non-metallic inclusions in the material. In the past, exogenous inclusions of rather large size were detected by the ultrasonic inspection of sheet. When encountered during welding, this type of inclusion, which is generally highly refractory in nature, can cause high scrap rates during the cryogenic-stretching operation.

Table B-5   Raw Material Acceptance Testing

1. Steel mill submits ladle analysis.

2. Reject or accept heat for consideration.

3. Steel mill provides slab sample for pre-
    liminary cleanliness rating and chemical
    and gas analyses.

4. Steel mill rolls two sample sheets.

5. Arde testing:

    ° Ultrasonic examination - gross defects

    ° Micro and macro examination

    ° Cleanliness rating

    ° Weldability

    ° Uniaxial tensile specimens

    ° Notch sensitivity

    ° Biaxial testing - sample spheres and
       cylinders

Material chemistry has been shown to be the primary factor in establishing the mechanical properties that can be obtained from a given heat of material (see Chapter IV of this appendix). As a result, close tolerances have been established for the constituents of this material.

1. Check Analysis of the Material

A check analysis is made on either a ladle sample from each heat or from a slab of the material. The analysis is performed by an independent laboratory. Wet-chemical analytic methods are used for all elements except hydrogen and oxygen. Oxygen is determined using vacuum-fusion gas analysis of the sample. Nitrogen is determined by the Kjeldahl method. Hydrogen, which is also determined by vacuum-fusion gas analysis, is variable throughout the processing of the ingot and reaches its final level only after conversion of the ingot to slab or sheet bar. Samples for the hydrogen check analysis, therefore, must consist of pieces cut from sheet bar made from each. The specified composition is shown in Table B-6, together with the heat submitted for evaluation to Martin Marietta.

2. Metallographic Examination of the Material

All metallographic examinations are conducted using samples of sheet rolled from the heat. Intergranular carbides are sometimes found to be very lightly scattered throughout all of the sheet samples tested. This is not felt to be serious, inasmuch as the manufacturing process called for a solution-anneal after welding, but before stretch-forming. The specified restriction on intergranular carbides on incoming sheet material was based on findings which showed that embrittlement at cryogenic temperatures occurs if heavy intergranular carbide precipitation is present. Inasmuch as a complete solution-anneal is part of the processing sequence, re-solution of light carbides takes place at the time the parts are annealed.

The cleanliness of the heats are evaluated microscopically in accordance with ASTM E45. The cleanliness rating obtained with Heat 57093 fell within the specification requirement. A comparison of the specification with the ratings obtained for the particular heat submitted to Martin Marietta is shown in Table B-7.

Grain size is also determined from the sheet samples and is rarely larger than the maximum allowed by the specification.

Table B-6 Certification and Check Chemical Analysis of Low-Silicon Stainless Steel

	C (%)	Ma (%)	Si (%)	Cr (%)	Ni (%)	Mo (%)	P and S (%)	N (%)	O(ppm)	H(ppm)
Arde Specification AES 258	0.025 0.045	0.10 †	0.10 †	18.30 18.70	7.10 7.50	0.15 0.35	0.015* †	0.02 0.04	60 †	2† max
Heat 50793 Certi- fication Check	0.030 0.028	0.01 ‡	0.07 0.044	18.16 18.56	7.57 7.24	0.27 0.16	0.015	0.040 0.034	37 11	2 2

*Total.

†Maximum.

‡Trace.

Table B-7 Inclusion Content of Low-Silicon Stainless Steel

Specified Characteristics		Heat 50793
Type	Rating	Rating
A Thin	1	0
A Heavy	0	0
B Thin	1	0
B Heavy	0	0
C Thin	1	0
C Heavy	0	0
D Thin	1	1
D Heavy	1	0

3. Weldability Sample

As an initial check on the weldability of the material, two cylindrical pieces 5.50 in. in diameter are fabricated, and these are welded together using a single-pass girth weld. The cylinders are then cut in half along the longitudinal axis, and the exterior and interior of the weld and the heat-affected zone are dye-checked. The dye-check examination is performed with 30X magnification. A single crack thus detected is cause for rejection of the heat. No cracks were found with Heat 57093. A further check of the weldability occurs subsequently, when the evaluation pressure vessels are fabricated and tested.

4. Material Acceptance Sequence

After acceptance of heat chemistry from a ladle sample or slab, Arde requires submission of two sheets from each heat. Each sheet is 0.060-in. thick and 36 in. wide x 120 in. long. One of these sheets receives 100% ultrasonic inspection. Microsections are prepared and all the metallographic examinations indicated above are performed. The heat chemistry is then checked again using a sample from the sample sheets. The weldability sample is prepared and evaluated. If the sample sheets conform to all specification requirements, uniaxial and biaxial mechanical properties are checked in accordance with the procedures described below. When conformance to mechanical-properties requirements is established, the heat is released by the quality control department for production.

Several of the foregoing inspection procedures are performed, in addition, upon receipt of each lot of finished material from the heat. Metallographic examination, sheet surface and dimensional inspections, and ultrasonic inspection are specified as a requirement for each subsequent shipment of sheet or plate of a given thickness.

Mechanical Properties Evaluation - As described in the previous section, material properties are evaluated from specimens prepared from 0.060-in.-thick sheet samples from each heat.

Two types of unnotched specimens are first fabricated. These consist of an unlocked, smooth tensile specimen and a partial-through-crack type specimen. The notch specimens are used primarily for screening purposes (i.e., a true K_{Ic} value is not measurable with specimens of this thickness, so comparisons are made with previous heats on the basis of a nominal K_{Ic}.

The unnotched specimens are used to establish aged and unaged strength after cryogenic prestraining as a function of the pre-stress at room temperature and at -320°F.

In addition, the -320°F stress/strain curve for the heat is established by testing annealed specimens to failure at -320°F. This stress/strain curve serves as the basis for predicting bi-axial straining of pressure vessels during the stretch-forming process.

On the basis of the uniaxial test data, biaxial design charts are prepared, as discussed in Chapter VI of this appendix. These biaxial design charts, as well as the fabricability of each heat, are checked by building several small pressure vessels. The de-sign charts are then modified to conform to the actual pressure vessel data. The pressure vessels consist of five cylinders and five spheres approximately 6 in. in diameter. The vessels are pressurized to various cryogenic prestresses and the strains are measured to determine conformity with the predicted data from uni-axial specimens. These vessles are then treated by aging, or left in the unaged condition, and tested at room temperature to deter-mine their strength at room temperature. The values thus achieved are compared with tensile specimen data. Gross deviations in strength from tensile specimen data indicate, ordinarily, some de-fect or deficiency in the material.

At least one annealed sphere and one annealed cylinder are cry-ogenically-stretched to burst at -320°F in order to establish the upper limit of the prestress to which such vessels can be subjected during the stretch-forming process. Again, this value is checked against that predicted from uniaxial test data. By establishing this maximum cryogenic prestress, it is possible, during produc-tion, to achieve low scrap rates if stretching pressures are main-tained about 5% below the maximum allowable.

Figure B-11 and Table B-8 show the uniaxial data, and Fig. B-12, the biaxial data, obtained with the subject low-silicon heat, 50793, which has undergone the aforementioned mechanical testing. The data sheets indicate Arde's limits on the allowable mechanical properties. The comparison with actual results may be made on the sheet. A comparison of pressure vessel test results with the pre-dicted biaxial properties is also shown in Fig. B-12.

Note: 1. Vendor = Latrobe.
       2. Material specification = AES 258.
       3. Heat 50793.
       4. Tensile specimens = S/N 184 thru 195.
       5. Notch specimens = S/N 206 thru 215.
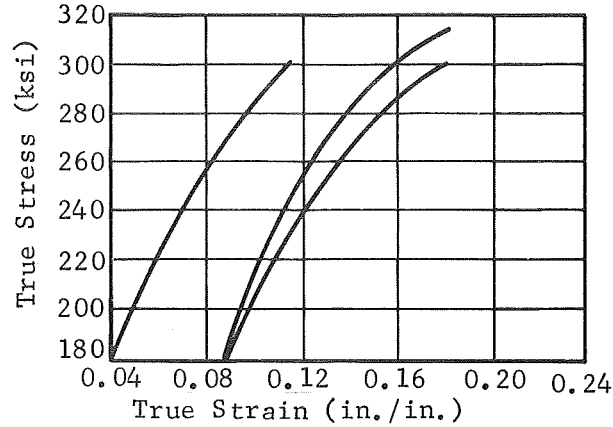
(a) -320°F Stress/Strain Curve - Uniaxial
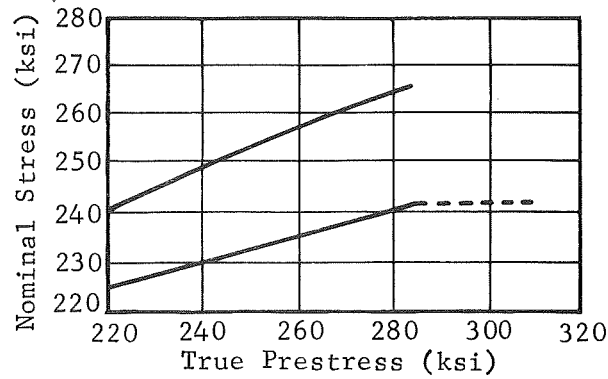
(b) Room Temperature, Aged Nominal
     Ultimate Response - Uniaxial
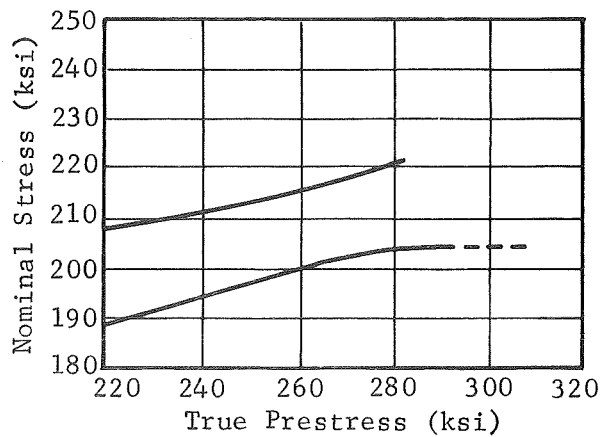
(c) Room Temperature, Unaged Nominal Ultimate
     Response - Uniaxial

Fig. B-11 Arde Low-Silicon Material Evaluation Report
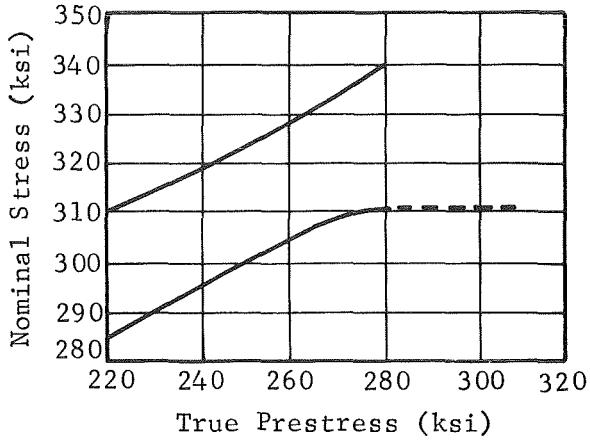
(d)   -320°F Aged Nominal Ultimate
      Response - Uniaxial
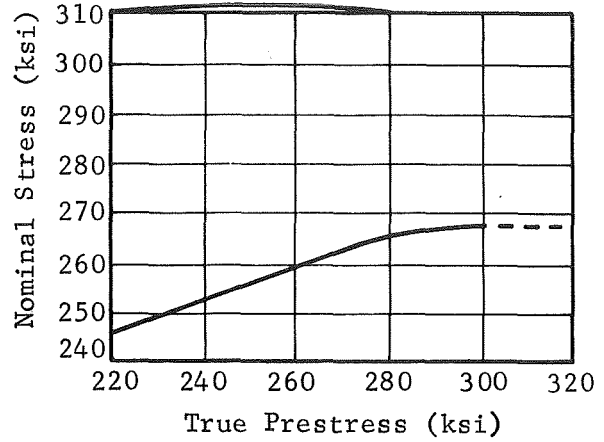
(e)   -320°F Unaged Nominal Ultimate
      Response - Uniaxial
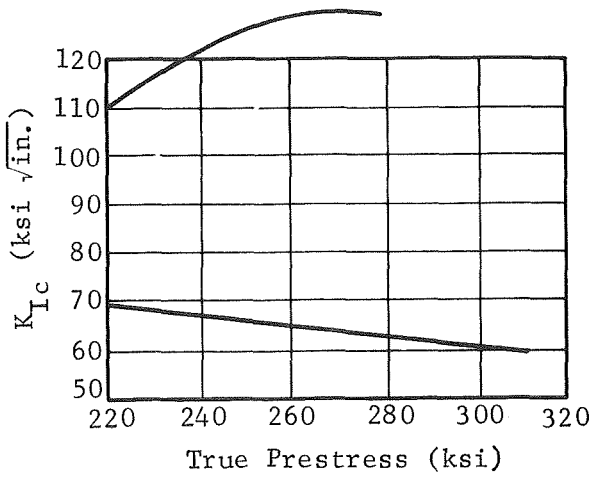
(f)   Aged K_{Ic} at Room Temperature
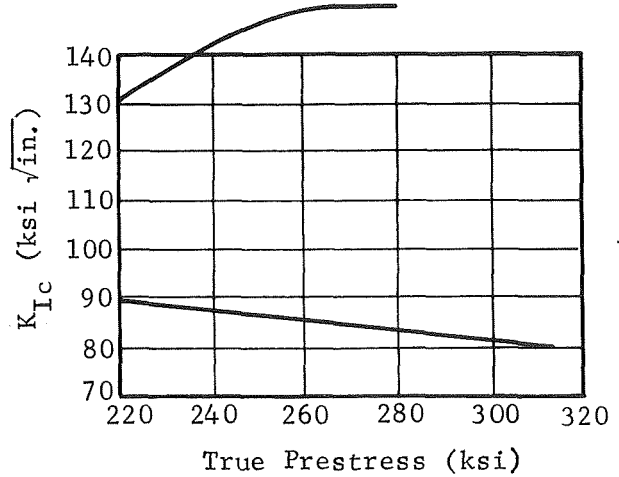
(g)   Aged K_{Ic} at -320°F

Fig. B-11 (Concl)

Table B-8   Results of Arde Low-Silicon Material Evaluation, Heat 50793

Characteristic	Aged Material	Unaged Material
Cylinder Test*		
Serial No.	15	14
Stretched Diameter (in.)	7.962	8.005
Post-Burst Theoretical Thickness	0.0560	0.0556
Stretch Pressure (psi)	4,600	4,700
Burst Pressure (psi)	4,250	3,725
Actual Prestress (psi)	327,000	338,000
Burst Stress (psi)	303,000	268,000
Test Temperature	Ambient	Ambient
Actual Yield Stress (psi)	303,000	≈268,000
Sphere Test*	Aged	Unaged
Serial No.	31	30
Stretched Diameter (in.)	7.432	7.448
Post-Burst Thickness (in.)	0.0514	0.0528
Stretch Pressure (psi)	7,760	7,950
Burst Pressure (psi)	>7,200	>6,250
Actual Prestress (psi)	281,000	280,000
Burst Stress (psi)	>260,000	>220,000
Test Temperature	Ambient	Ambient
Actual Yield Stress (psi)	260,000	220,000
Weldability		
Unrestrained-No. of cracks/in.		
Spec.	0	
Actual	0	

*No fractures.
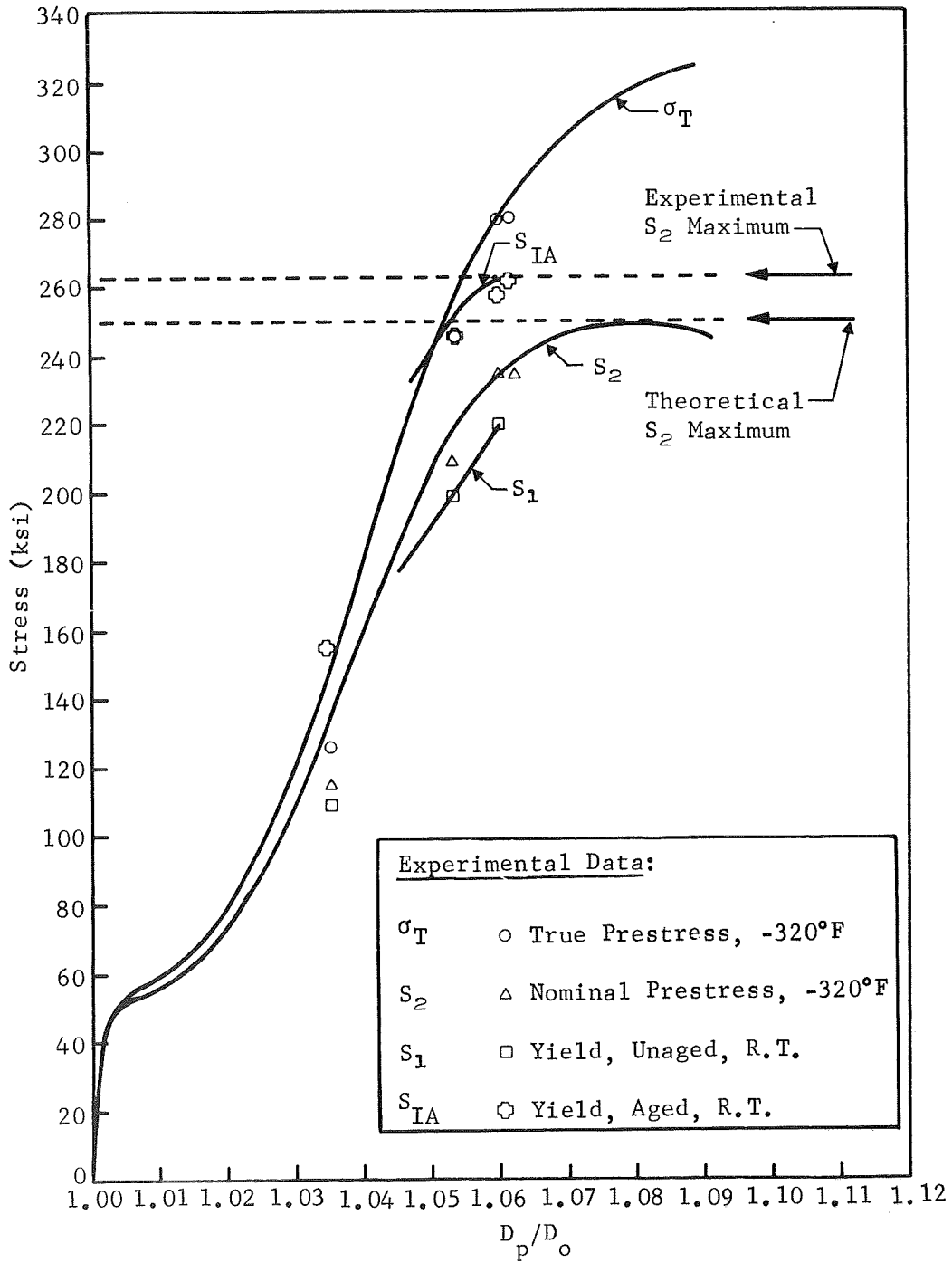
Fig. B-12   Comparison of Sphere Data with Theoretical Design Chart,
            Heat 50793

B.   COMPONENT ACCEPTANCE AND QUALITY CONTROL

1.   Quality Control Items

The relationship of quality assurance to the manufacturing process is shown in Fig. B-10. As can be seen from the flow diagram, assurance of the quality is maintained by inspection and test throughout all the fabrication steps required to produce a given pressure vessel.

As has been noted in the previous chapter, strict adherence to material specifications is a prerequisite for fabrication. The most important items, in addition to verification of material, are:

    1)   Verification of weld quality;

    2)   Verification of vessel strength;

    3)   General assurance of compliance with written processing specifications during fabrication.

2.   Verification of Welds

Welds are verified by means of standard techniques such as radiographic inspection, or dye-penetrant testing. Weld quality standards are defined in an Arde specification and limit the size and distribution of porosity and call for the repair or rejection of any cracks detected by this method. In addition to radiographic inspection of welds, dye-penetrant testing must result in zero dye-check indications in the weld or heat-affected zone in order to pass the weld-quality requirements. Weld X-rays are taken before and after stretch-forming. The preform radiographic inspection is a requirement designed to reduce scrap rates during the cryogenic-stretch-forming operation. The requirement for radiographic inspection after stretching has been established to assure the quality of the final article. It should be noted that the cryogenic-stretch-forming process is, to a great extent, self-inspecting. Weld defects that pass through the cryogenic-stretch-forming process must be so small as to cause little trouble in service. On occasion, undetected weld defects or other defects manifest themselves by the bursting of a vessel during the cryogenic-stretch-forming operation. In addition, consider that tight hair-line cracks of appreciable length are often undetectable by radiographic inspection. These would cause the vessel to burst in stretching or they will open during the stretching operation to the extent that they are detectable, either in the final radiographic inspection or the dye-penetrant inspection.

In summary, then, weld reliability is established by:

1) The material quality;

2) The welding techniques developed for the process;

3) Radiographic and dye-penetrant inspection before and after stretch-forming;

4) The cryogenic-stretch-forming operation itself.

As a final requirement, the entire production vessel is ordinarily proof-tested as a final check on the weld integrity. In addition, helium-leak testing is performed for those applications in which the leak rate is critical.

3. Verification of Vessel Strength

In verifying the strength of a fabricated pressure vessel, it has been demonstrated that the primary requirement for achieving a particular burst pressure is that a cryogenic stretching pressure must be achieved. The basis for this is understood if it is considered that the response to stretching in terms of strength of the material at any temperature is a function of the true cryogenic prestress. For example, if we consider a sphere of radius R and thickness t after stretching to the final size and shape upon pressurization to some pressure P, then σ, the true hoop stress achieved is equal to $\frac{PR}{2t}$. Now consider this same vessel under burst test at some operating temperature. The final dimensions of the pressure vessel after stretching are now the initial dimensions for this burst test, and the nominal stress at burst, S, is equal to $\frac{P_b R}{2t}$, where P_b is the burst pressure. It can thus be seen that the ratio of the two stresses, $\frac{\sigma}{S}$, is $\frac{P}{P_b}$ and that P_b is $\frac{S}{\sigma} P$.

It is true that, when the stretch pressure is achieved, the true stress may vary somewhat over the vessel's surface, depending upon thickness variations in the preform. However, the stretch pressure is based upon the minimum preform thickness and the design burst for this region. Any heavier region, although not strengthened as much, will have a more favorable $\frac{S}{\sigma}$ ratio, and thus, even better load-carrying capabilities. Thus, the burst pressure is controlled by the thinnest region and the stretch pressure. The

thinnest region is determined from dimensional inspection of details and all parts with less than minimum wall rejected. Thus, the burst pressure is strictly dependent on the stretch pressure. This relationship between P and P_b may be seen from Fig. B-13, which shows the burst pressures for a series of spheres that have been stretched to various cryogenic pressures. Note that in the series of actual sphere tests, the deviations from a perfect correlation are very small.

The second assurance that is required in order to verify the vessel strength is the uniformity of the response of the material to the cryogenic stretching. Experience has demonstrated that no large variations have been noted in the ratio of $\frac{P}{P_b}$ within vessels made from a given heat and stretched to approximately the same cryogenic stress. Nevertheless, additional control is available through the fabrication of tensile specimens or even through the fabrication of a simple small sample vessel from each lot of material of a given thickness. It should be emphasized that this control is not presently in use at Arde, since it has not been found necessary. Of course, additional verification of vessel strength is obtained through proof-pressure testing and lot-sample burst testing as required for specific applications.
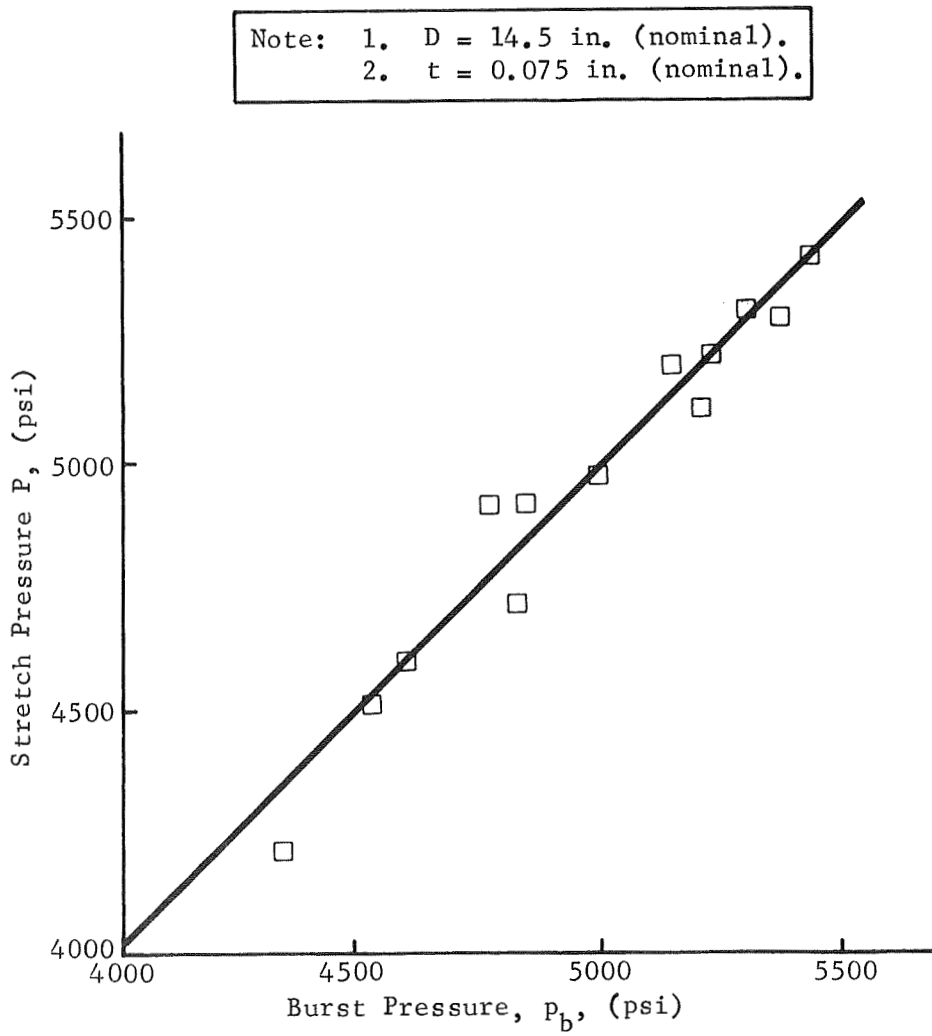
Fig. B-13   Burst Pressure Data for Cryoformed Spheres

VI. PREFORM DESIGN

A. DESIGN PHILOSOPHY

The high strength of cryogenically-formed stainless steel is
obtained through deformation at -320°F. As has previously been
described, the deformation is accomplished by pressurizing a pre-
form fabricated from annealed material. The preform is made smaller
in size than the required final vessel in order to allow for suffi-
cient expansion to achieve the strength required. The design of
the preform, then, must take into consideration the amount of
stretching that will take place, for two reasons:

> 1) After stretching, the vessel must meet the dimensional
>   requirements of the finished product;
>
> 2) After stretching, the vessel must have been coldworked
>   sufficiently to produce the desired strength level.

Obviously, if the preform is too small, then it may burst during
stretching before it is the desired size. If the preform is too
large, then it will reach the desired size readily, but will not
achieve a satisfactory strength level. In addition, the wall thick-
ness must be sized so that the weight and burst pressure of the
finished vessel will be as required, and make full use of the re-
sulting material strength level. In the preform design, therefore,
mill- and manufacturing-thickness tolerances of the material must
also be carefully considered.

A procedure has been established for the design of any preform
whose shape can be described as a surface of revolution. The design
procedure has been programed and computer solutions can be found for
the complex shapes that must be dealt with. The complex shapes can
consist of combinations of cones, cylinders, flat plates, hemi-
spheres, or other surfaces of double curvature. For example, con-
sider a preform that consists of a cylinder, two cones, and two flat
plates. With sufficient deformation, such a preform will become a
sphere. The resulting shape after a series of stretches is shown
in Fig. B-14. The important point in considering such complex pre-
form shapes is that, not only does an increase in size take place
during deformation, but a drastic change in shape takes place as
well.
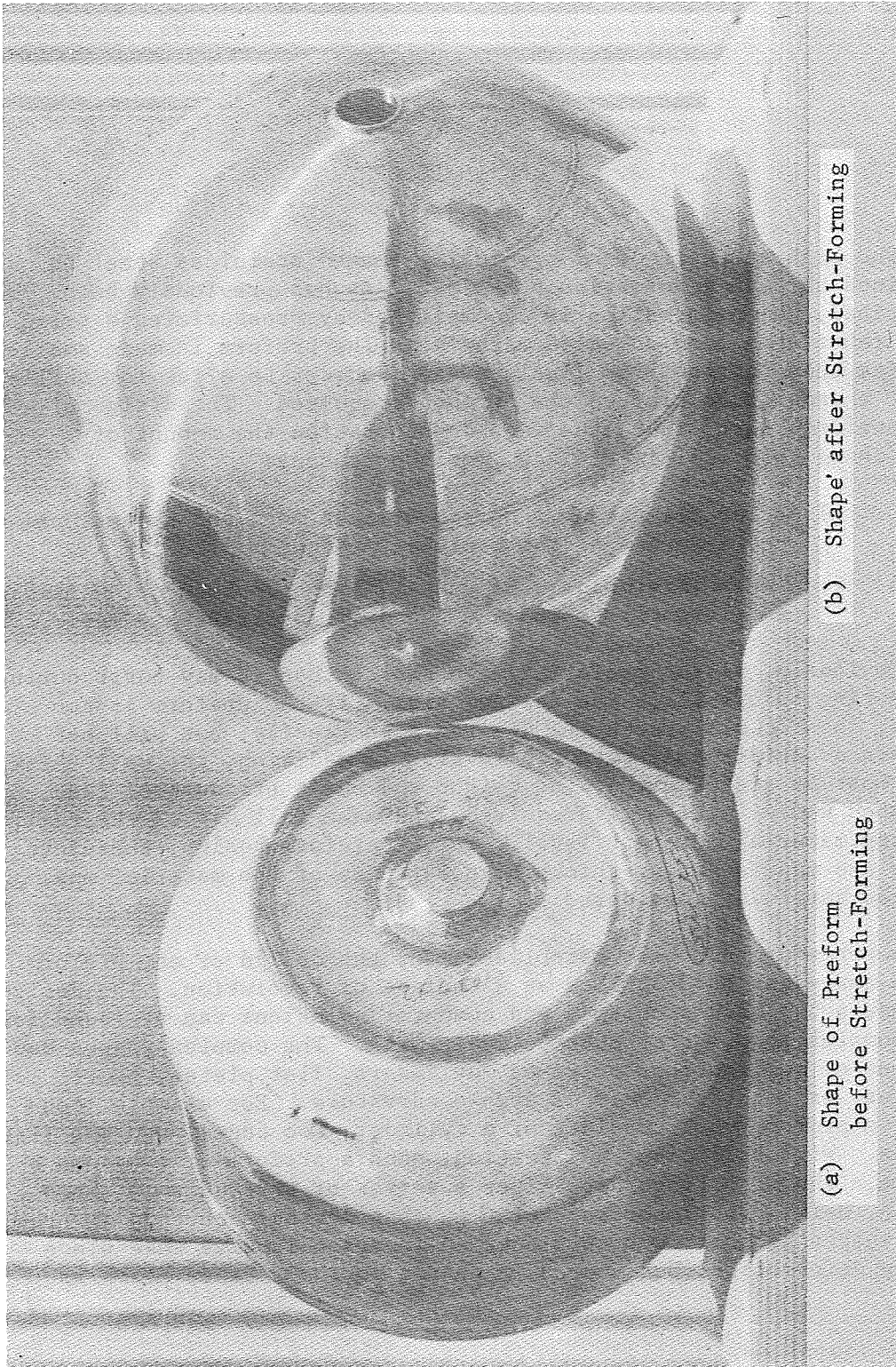
(a)   Shape of Preform
      before Stretch-Forming

(b)   Shape' after Stretch-Forming

Fig. B-14   Hemispherical Stretch-Forming

Simple spheres and long cylinders, on the other hand, undergo more-readily-predictable deformation. This is because there is no shape change, only a change in size and wall thickness. Spheres remain spheres and cylinders remain cylinders during stretch. Therefore, simple design curves are prepared for spheres and cylinders for each heat of material procured.

The procedures used for designing simple shapes such as spheres and cylinders will first be discussed. Then a description of the design procedure used with more complex shapes will be given. Finally, the various shapes that have been formed, and the techniques used in the design of special attachments and other configurational features will be presented in this section. All these techniques are applicable to both commercial, Type 301 stainless steel as well as the low-silicon, stainless-steel alloy.

The design of preforms for cryogenic stretch-forming is based on the behavior of actual subscale pressure vessels and on uniaxial tensile specimen data. From simplified total deformation theory, the following relationships between plastic deformation of spheres and uniaxial specimens may be derived:

$$\epsilon_1 = \frac{1}{2} \bar{\epsilon} \tag{1}$$

and

$$\sigma_1 = \bar{\sigma}, \tag{2}$$

where ϵ_1 is the true hoop strain of a sphere at the true hoop stress (σ_1) and $\bar{\epsilon}$ is the true strain of a uniaxial specimen at a true stress of $\bar{\sigma}$.

An empirical factor based on experience, however, indicates that the plastic strain component from Eq. (1) is more nearly:

$$\epsilon_1 = 0.45 \bar{\epsilon} \tag{3}$$

Using Eq. (2) and (3), a cryogenic biaxial stress/strain curve for spheres may be constructed from a -320°F uniaxial stress/strain curve of the annealed material. Such biaxial curves are prepared during the evaluation of each heat of material and are used to predict the amount of stretching that spheres will undergo when they are pressurized during stretch-forming.

Similarly, for cylinders, by including an empirical strain correction factor

$$\epsilon_{1C} = 0.9 \frac{\sqrt{3}}{2} \bar{\epsilon} \tag{4}$$

where ϵ_{1C} is the true hoop strain of an infinitely long cylinder at a true hoop stress of σ_{1C}, and

$$\sigma_{1C} = \frac{2}{\sqrt{3}} \bar{\sigma} \tag{5}$$

Modifications to these biaxial design curves can then be made on the basis of actual biaxial test data obtained with a series of spheres and cylinders.

An additional design requirement is to predict the strength that results when vessels are stretched a specified amount. It has been shown that the yield strength of cryogenically-stretched spheres is close to the strength of uniaxial specimens that have been cryogenically prestressed to the same true stress levels. The differences between uniaxial and sphere strength diminishes at the highest strength levels.

For cylinders, it has been observed that their strength is $\frac{2}{3}$ the strength of tensile specimens that have been prestressed to a true stress level $\frac{3}{2}$ times the true stress of the cylinder hoop.

Biaxial design charts for Heat 57093 are presented in Fig. B-15 and B-16. The true strains, ϵ_1, has been converted to more familiar engineering strains $[\exp(\epsilon_1) - 1]$ in the chart. Therefore, strains are presented as $\frac{R_p}{R_o}$ (i.e., as 1 + the engineering strain), where R_p is the final radius of the stretched vessel after elastic rebound and R_o is the initial radius of the preform for the vessel.

The design charts show several curves of interest to the designer. The curve labeled σ_T indicates the true hoop stress achieved at -320°F during the cryogenic-stretching process, and is derived from the uniaxial data using Eq. (2) and (3) (for spheres), or Eq. (4) and (5) (for cylinders). The curves include corrections for elastic strain. The curve labeled S_2 is more useful for the designer, since it predicts the nominal cryogenic-stretching stress required to stretch a preform a given amount.
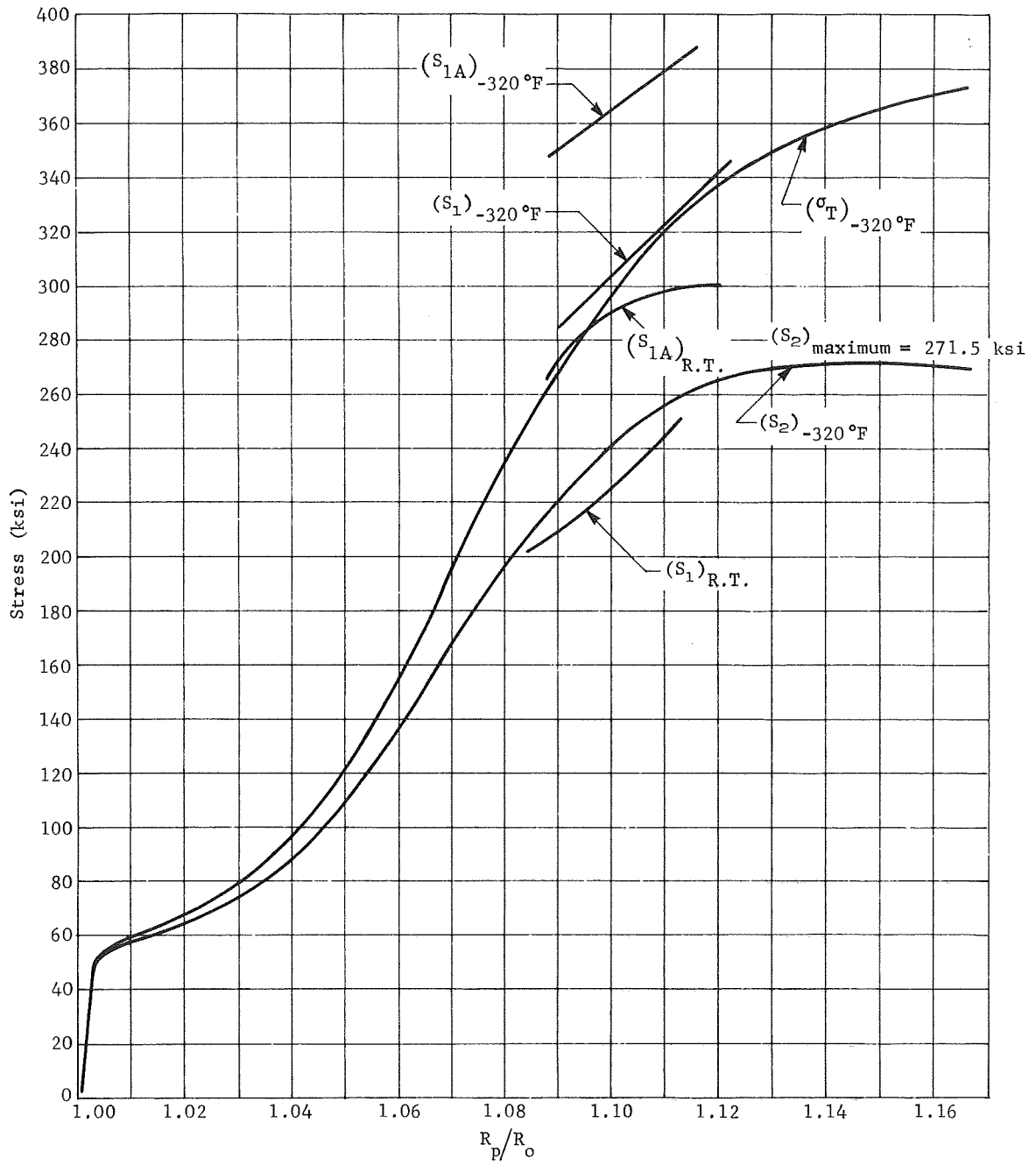
Fig. B-15 Cylinder Design Chart from Tensile Coupon Data (Heat 50793)
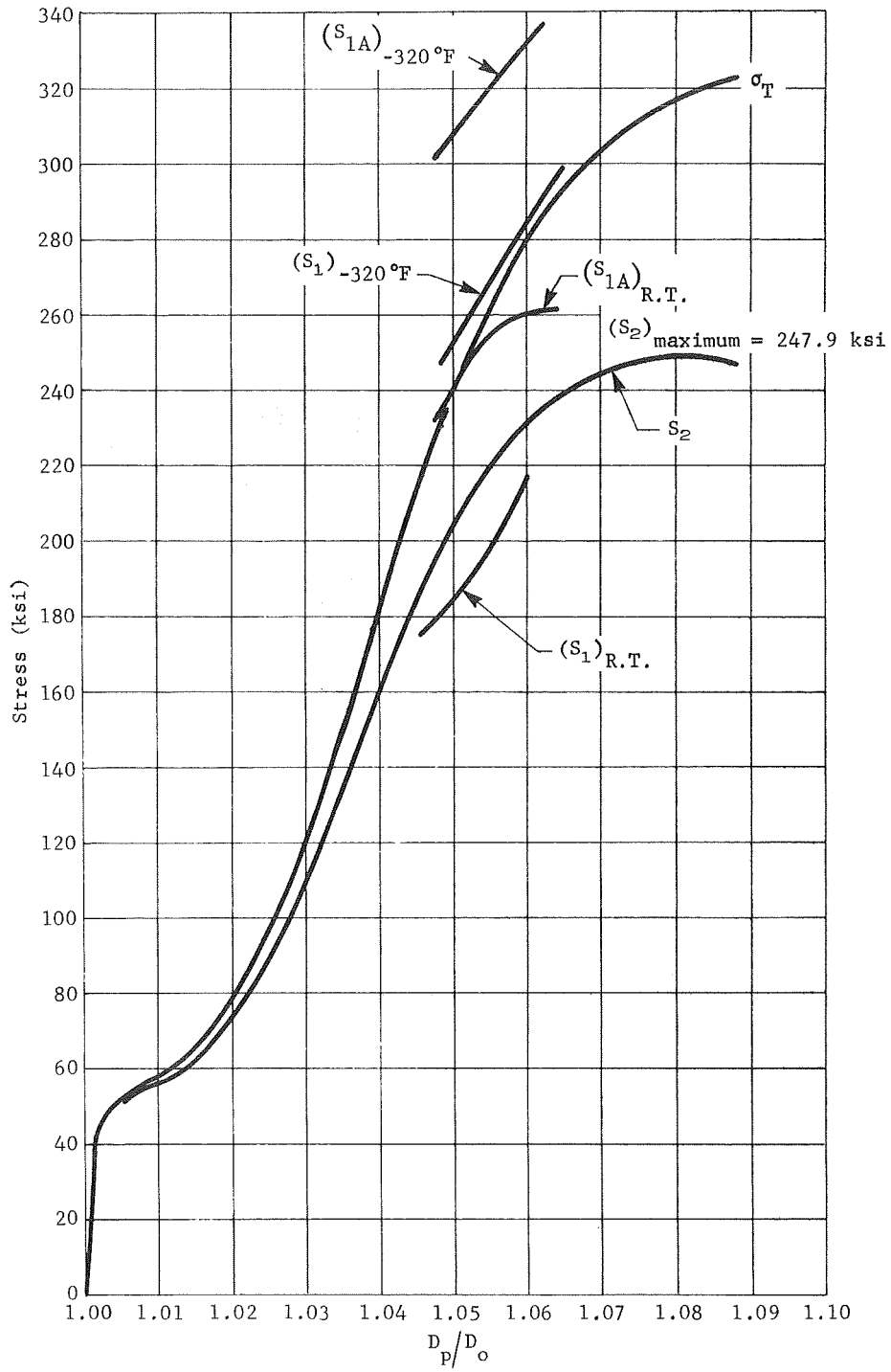
Fig. B-16 Sphere Design Chart from Tensile Coupon Data (Heat 50793)

Note that the S_2 curve exhibits a theoretical maximum. This maximum
represents the limiting nominal stress and strain of vessels made
from this material during the cryogenic-stretching process. The
maximum nominal stretching stress $(S_2)_{maximum}$ is verified experi-
mentally with actual pressure vessels bursting annealed vessels at
-320°F. The maximum strain allowable is estimated from uniaxial
data. Exceeding the stress or strain at the maximum will cause a
vessel to burst during the stretch. The S_{1A} curves show the burst
strengths at different operating temperatures for vessels that have
been stretched to a diameter ratio of $\frac{D_p}{D_o}$ and have then been aged.

B.   SHELL DESIGN

A design yield strength that appears reliable from the uniaxial
and biaxial data available at the appropriate operating temperature
is selected. For example, if a cylinder is being designed, a design
yield stress of 294 ksi at room temperature (see Fig. B-15) is within
the capability of the material.

From the S_{1A} curve in Fig. B-15, a room temperature strength of
294 ksi is seen to correspond to an R_p/R_o value of 1.105 (i.e., 10.5%
strain). At this strain, the nominal cryogenic-forming stress re-
quired (obtained from the curve marked S_2) is 250 ksi. Before pro-
ceeding, the design cryogenic forming stress of 250 ksi must be com-
pared with the maximum forming stress for a cylinder [$(S_2)_{maximum}$ =
271 ksi] obtainable with this heat of material. Since a margin of
about 7.7% exists, this indicates that the required stretching
stress may be achieved with reasonably low scrap rates. A margin
as low as 5% may be used with good success, but 10% is the margin
most usually used.

From the design chart then, the nominal cryogenic stretch form-
ing stress of 250 ksi, and a strain of 10.5% have been determined.
In addition, the desired strength at room temperature, 294 ksi, has
been shown to be achievable under these stretch conditions.

The minimum final wall thickness of the vessel is next deter-
mined from the design burst stress (burst is assumed to occur at
yield as a slight design safety factor) at the operating tempera-
ture as follows:

$$t_f = \frac{P_B \left(D_p \right)}{2 \left(S_{1A} \right)} , \qquad (6)$$

where P_B is the design burst pressure, D_p is the design maximum
outside radius, and S_{1A} is the design stress (294,000 psi) at burst.
The final minimum wall thickness can then be obtained from Eq. (6).

At this point, the dimension of the preform may be determined.
The maximum outer diameter of the preform is determined from the
strain obtained from the design chart and the desired final outer
diameter.

$$D_o = D_p \left(\frac{D_p}{D_o} \right). \qquad (7)$$

In order to determine the wall thickness of the preform it is
necessary to know the relationship between the wall thickness of
the preform and the final wall thickness of the vessel for a known
stretch percentage. This relationship may be shown to be:

$$t_o = t_f \left(\frac{D_p}{D_o} \right), \qquad (8)$$

where t_o is the minimum thickness of the preform.

The preform design of the cylindrical shell is now accomplished
except for manufacturing tolerances.

The design of spheres proceeds along similar lines except that
Eq. (6) becomes:

$$t_f = \frac{P_B \left(D_p \right)}{4 \left(S_{1A} \right)} \qquad (9)$$

and Eq. (8) becomes

$$t_o = t_f \left(\frac{D_p}{D_o} \right)^2. \qquad (10)$$

For greater uniformity of stretching and reduced weight, sphere-preform components may be machined all over, rather than used with as-hydroformed dimensions. Arde's experience with hydroformed and deep-drawn hemispheres has shown that the total variation in thickness can be as much as 15%. On the other hand, by machining the hemispherical components that constitute the preform, a total variation of 0.005 in. may be obtained. Based on these tolerances, the preform thickness may be specified as t_o + tolerances.

A final consideration is the anticipated minimum contained volume of the vessel after stretching the preform. If the vessel has a maximum-diameter restriction due to envelope requirements, for a vessel stretched without a die, the minimum volume guarantee would have to be based on a diameter about 0.5T less than the maximum allowable diameter. This represents the maximum tolerance between the predicted and actual strains achieved when stretching a new design. The repeatability from vessel to vessel, however, is within 0.25% of the diameter. For closer control of final size, vessels can be stretched in a forming die to reduce the diametric tolerance.

C.   DESIGN OF COMPLEX PREFORMS

The design of a preform that can be described as a general surface of revolution has been treated in Ref. 12. The design procedure is conducted by initiating the problem at an apex of the preform on the centerline of the surface of revolution. In such a case, the two principal strains (meridianal and hoop) are equal. A value is assumed for one of the strains. From these conditions, the strains and the stresses may now be determined at a position that is an arbitrary meridianal increment of length along the preform surface away from the apex. The conditions at the end of this arbitrary incremental distance now serve to establish these quantities at a location a small distance further away from the apex. This procedure is continued to subsequent stations around the preform. The resulting stretched shape, defined on the basis of the strain assumed by the apex, is then compared with certain required boundary conditions that depend on the preform being considered. For example, the boundary conditions imposed on a preform containing a semi-infinite cylindrical portion are that the slope of the preform surface must be in the meridianal direction parallel to the centerline of the surface of revolution, and that the final diameter at stations near the middle of the cylindrical section must not exceed that of an infinitely-long cylinder. If the stretched shape

does not conform to these boundary conditions, the entire calcula-
tion is repeated using a new assumed strain at the apex. Repeated
trials are made with new apex strains until the boundary conditions
are satisfied within specified tolerances. The shape that results
when the assumed initial strain results in conformance to the
boundary conditions is the final predicted stretch shape. This
procedure has been programed for obtaining computer solutions, as
it is obvious that the accuracy of the results depends on using a
large number of incremental steps along the surface of the preform.
An example of a shape stretched on the basis of such a design pro-
cedure is shown in Fig. B-14.

D. CONFIGURATIONAL FEATURES

A wide variety of shapes can be incorporated into cryogenically-
stretch-formed vessels by proper design. Several reports describing
the types of shapes and attachments that have been fabricated by the
stretch-forming process have been published. Development programs
performed to demonstrate the fabrication of a variety of configura-
tional features are described in Ref. 12. Elliptical heads, skirts,
and heavy ring sections were formed in vessels utilizing the cryo-
genic-stretch-forming process. By one technique, the heavy rings
were attached to the preform by welding separately-stretched rings
to cryogenically-stretched vessels. A joint between the rings and
the rest of the vessels was then strengthened by a cryogenic re-
stretch.

Reference 13 describes how a twice-thickness ring section was
incorporated as part of the preform in the cylindrical portion of
the vessel and stretched integrally with the entire preform by
pressurizing in a cylindrical die. In such a case, the thin-walled
sections first move out to the die and are then supported by the
die wall. Sufficient high pressure is then applied to move the
heavy-walled region out to the desired diameter.

A wide variety of shapes may be fabricated by means of the cry-
ogenic-stretch-forming process. Vessels with wall thicknesses rang-
ing from 0.020 to 0.375 in. have been fabricated and cylindrical
vessels with diameters up to 40 in. have been successfully stretch-
formed. The only theoretical limit to vessel size is the size of
the stretch facility. As may be seen from the examples above, com-
plex shapes are fabricated by two basic methods.

In the first method, a preform containing all the desired con-
figurational features is stretched to the required size and shape.
The vessels described in Ref. 11 utilized this technique in stretch-
ing the twice-thickness ring. Most ports or bosses in spheres and
in the heads of cylindrical vessels can usually be stretched in
this manner.

In the second method, a preform incorporating some of the feat-
ures is first stretched; then additional features are welded to the
stretched vessels. The subscale Sparrow motor case vessels in
Fig. B-17 utilized this technique to a great extent. Features of
a cross-section much heavier than the basic membrane thickness are
generally required to be attached in this fashion. After welding,
the locally-annealed regions of the stretched vessel are strength-
ened by a cryogenic restretch. The local deformation that results
from the second stretch does not change the vessel shape, but raises
the load-carrying capability of the restretch area to within about
5% of the rest of the vessel.

Integrally-stretched preforms are preferable to those that re-
quire post-stretch welding and restretching. Although the restretch
procedure does provide sufficient strength, it should be recognized
that intergranular carbides are not removed by this procedure. In
applications requiring exposure to corrosive environments, the ef-
fect of the intergranular carbides should be evaluated before ap-
plication of such designs is considered. The integrally-stretched
preform, on the other hand, is fully annealed and quenched before
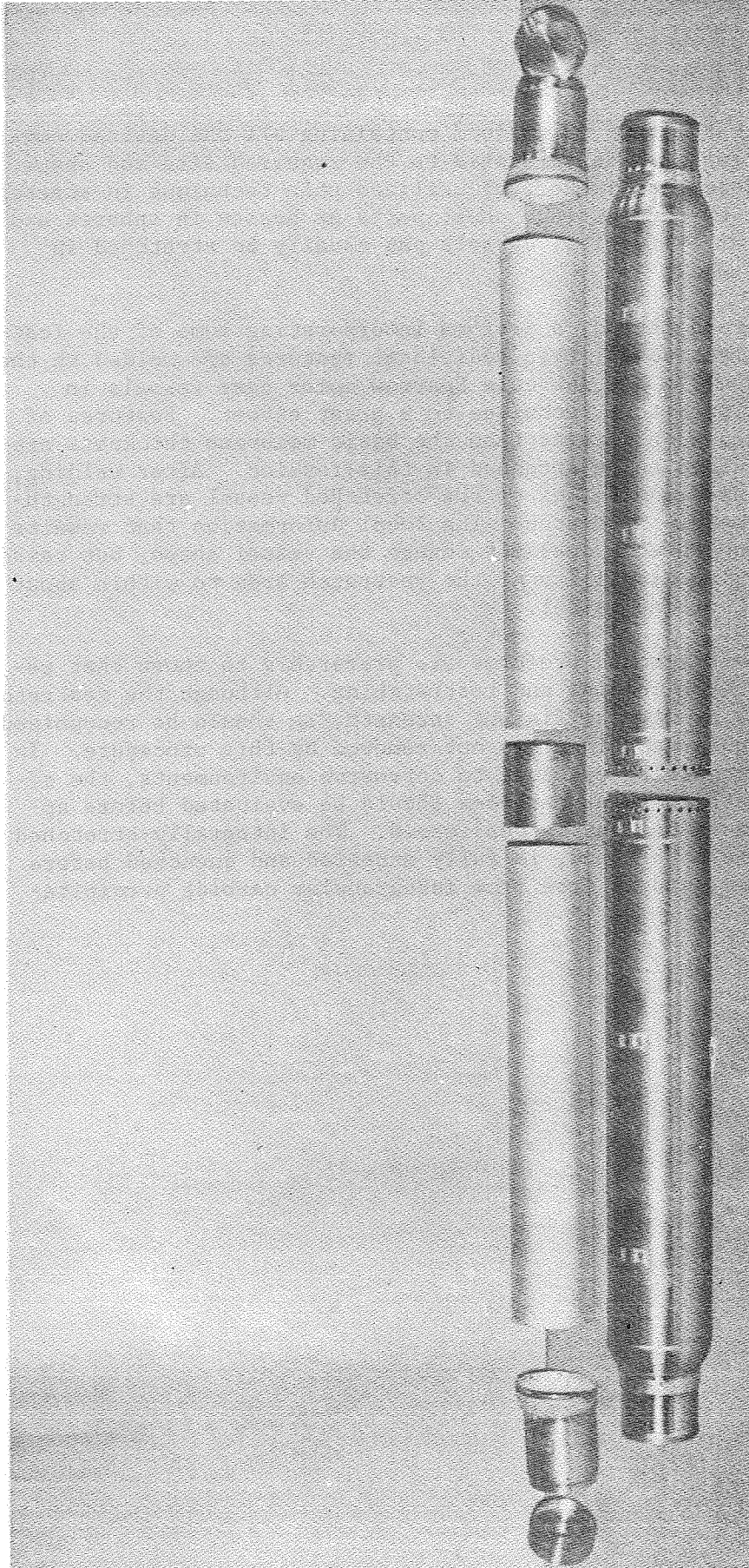being stretched, and is free from integranular carbide precipita-
tion.

Fig. B-17 Two Finished Sparrow Missile Motor Cases and the Components from Which They Were Fabricated

VII. REFERENCES

1. F. R. Schwartzberg, S. H. Osgood, R. D. Keys, and T. F. Kiefer: Cryogenic Materials Data Handbook. ML-TDR-64-280. Martin Marietta Corporation, Denver, Colorado, August 1964.

2. V. N. Krivobok and A. M. Talbot: "Effect of Temperature on the Mechanical Properties, Characteristics, and Processing of Austenitic Stainless Steels." Proc. Am. Soc. Testing Materials, Vol 50, 1950, P 895.

3. T. W. Orange: Tensile Coupon Tests of Cryoformed AISI 301 Stainless Steel Pressure Vessels at Cryogenic Temperatures. NASA TN D2202. Lewis Research Center, Cleveland, Ohio, October 1964.

4. R. H. Alper: "Cryogenically-Stretch-Formed Type 301 Stainless Steel for Cryogenic Service." Materials Research and Standards Vol 4, No. 10, October 1964, p 525.

5. S. Florien and J. R. Mihailisin: "High-Strength Stainless Steel by Deformation at Low Temperatures." Advances in the Technology of Stainless Steels and Related Alloys, STP No. 369. Am. Soc. Testing Materials, 1965, pp 17-25.

6. J. D. Morrison, M. A. Campbell, and J. P. Kattus: Development of High Strength and Fracture Toughness in Steels Through Strain-Induced Transformations. WAL TR-323. 4/2-3: DDC No. AD-421738. Southern Research Institute, September 1963.

7. R. H. Alper: Final Report, Development of High-Strength Alloys by Cryogenic Stretch-Forming. BuWeps Contract No. NOw 63-0387c. Arde-Portland, Inc, September 1964.

8. T. W. Orange: Evaluation of Special 301-Type Stainless Steel for Improved Low-Temperature Notch Toughness of Cryoformed Pressure Vessels. NASA TN D3445. Lewis Research Center, Cleveland, Ohio, May 1966.

9. Data Obtained by Arde, Inc under NASA Contract No. NAS 8-20713. Final Report to be Published.

10. R. G. McDonough: Final Report, Research and Development on Cryogenically-Stretch-Formed Helium Bottles for the Saturn V, S-IC Vehicle. Arde-Portland, Inc. December 1966.

11. R. H. Alper: Final Report, Cryogenic Stretch-Forming of Rocket Motor Cases. BuWeps Contract No. NOw 60-0263c. Arde-Portland, Inc, May 1961.

12. R. G. McDonough and R. H. Alper: Final Report, Cryogenic
     Forming of Flight-Weight Experimental Solid Propellant Rocket
     Cases. U. S. Army Missile Command Contract No. DA 30-069-
     ORD-3501. July 1965.

13. J. J. Cioffi: Final Report, Development of Production Tech-
     niques for the Manufacture of the Sparrow Rocket Motor Case
     by the Ardeform Process. BuWeps Contract No. NOw 62-0730c.
     Arde-Portland, Inc, September 1963.

APPENDIX C

DYNAMIC MODULUS AND THERMAL
EXPANSION PROPERTIES OF 2021-T81 AND
X7007-T6 ALUMINUM ALLOYS

Performed by

Dr. David Eash
Los Alamos Scientific Laboratories

CONTENTS

SUMMARY AND INTRODUCTION

The work described in this appendix was performed by Dr. David Eash of Los Alamos Scientific Laboratories in an attempt to compare dynamic modulus data with those obtained using strain-gage techniques. Martin Marietta supplied Dr. Eash with 1/4-in.-diameter x 4-in.-long rods of the two aluminum alloys in each grain direction for his work.

In addition to performing dynamic Yong's modulus and shear modulus testing, he also determined the thermal expansion charac-teristics of each composition. Modulus data are given in Fig. C-1 thru C-4 and expansion data in Fig. C-5 and C-6.

The apparatus used for this work is described in *Advances in Cryogenic Engineering*.[*]

---

[*]P. E. Armstrong and D. T. Eash: "Simultaneous Measure-ment of Young's and the Shear Modulus at Low Temperatures." *Advances in Cryogenic Engineering*, Vol 14, Plenum Press, 1969.

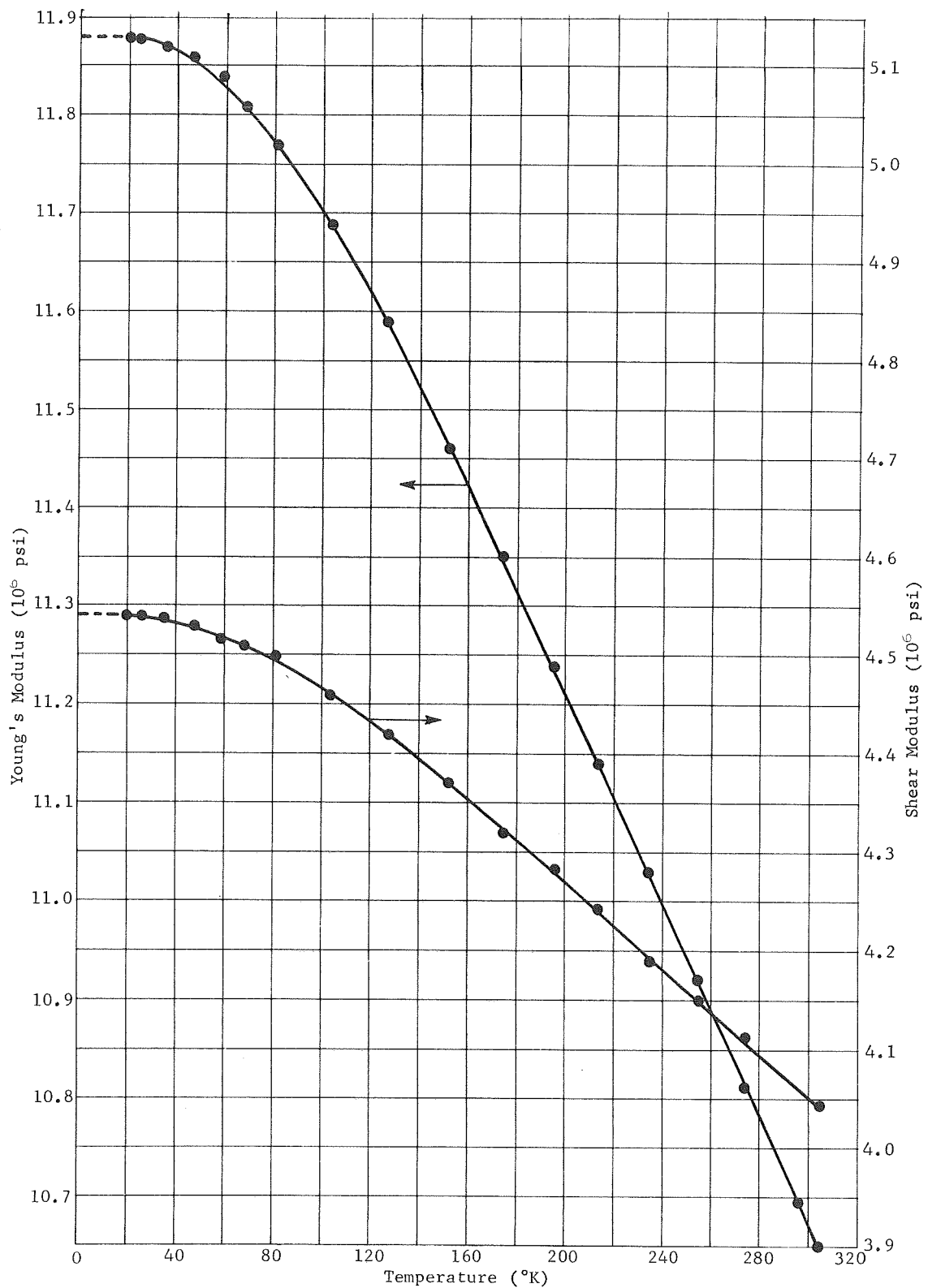Fig. C-1 Dynamic Moduli of 2021-T81 Aluminum Alloy, Longitudinal Direction
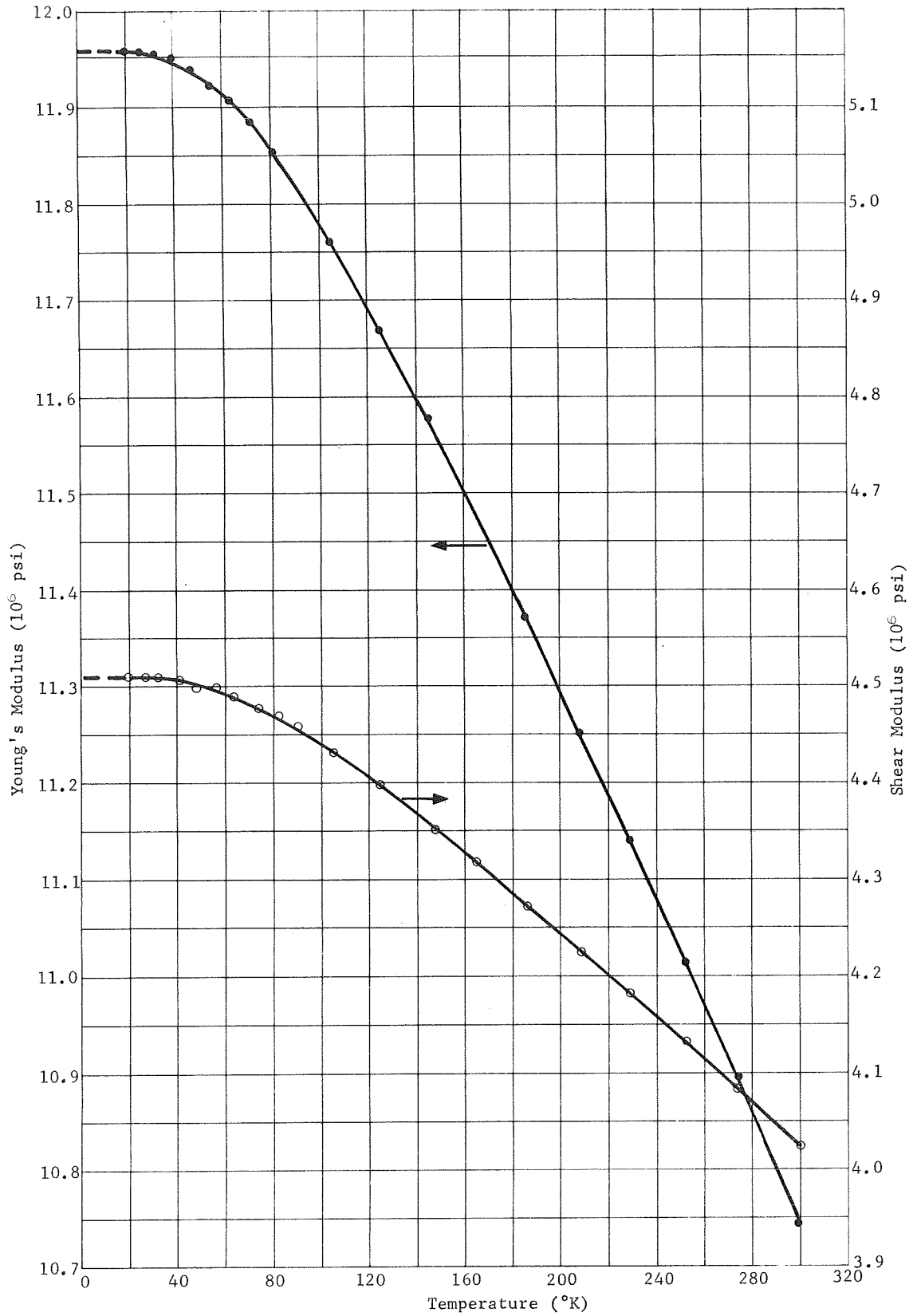
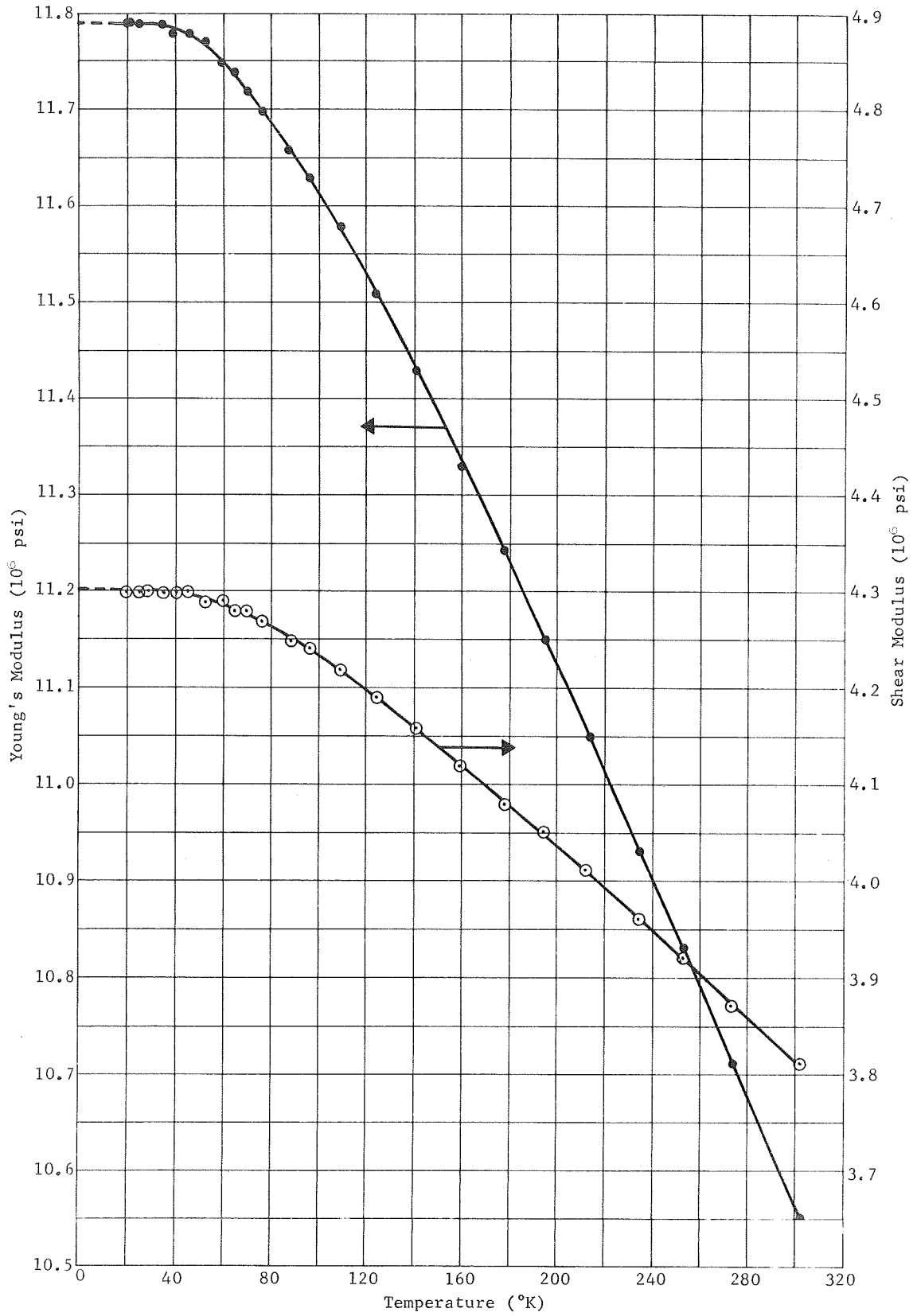Fig. C-2 Dynamic Moduli of 2021-T81 Aluminum Alloy, Transverse Direction

Fig. C-3 Dynamic Moduli of X7007-T6 Aluminum Alloy, Longitudinal Direction
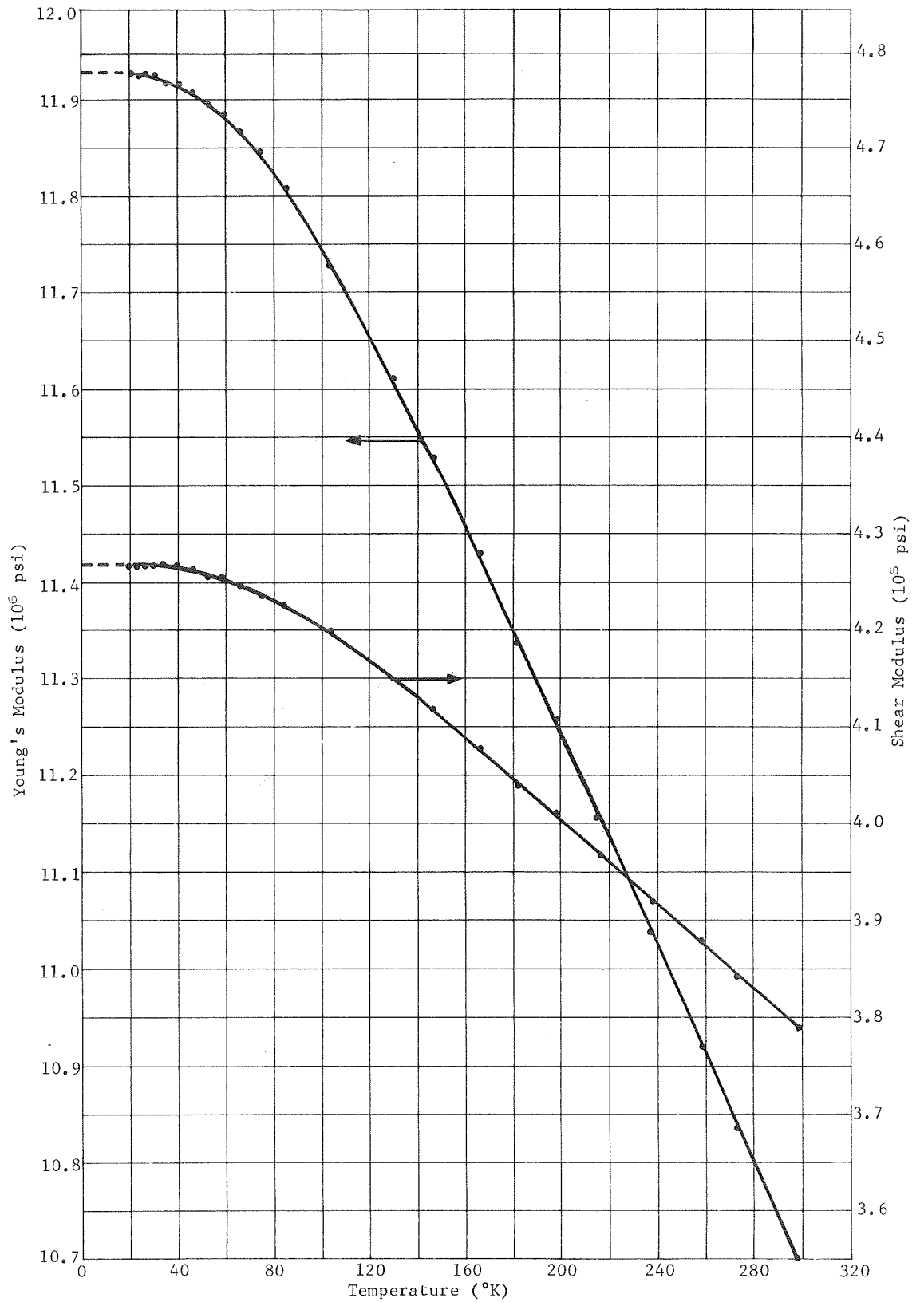
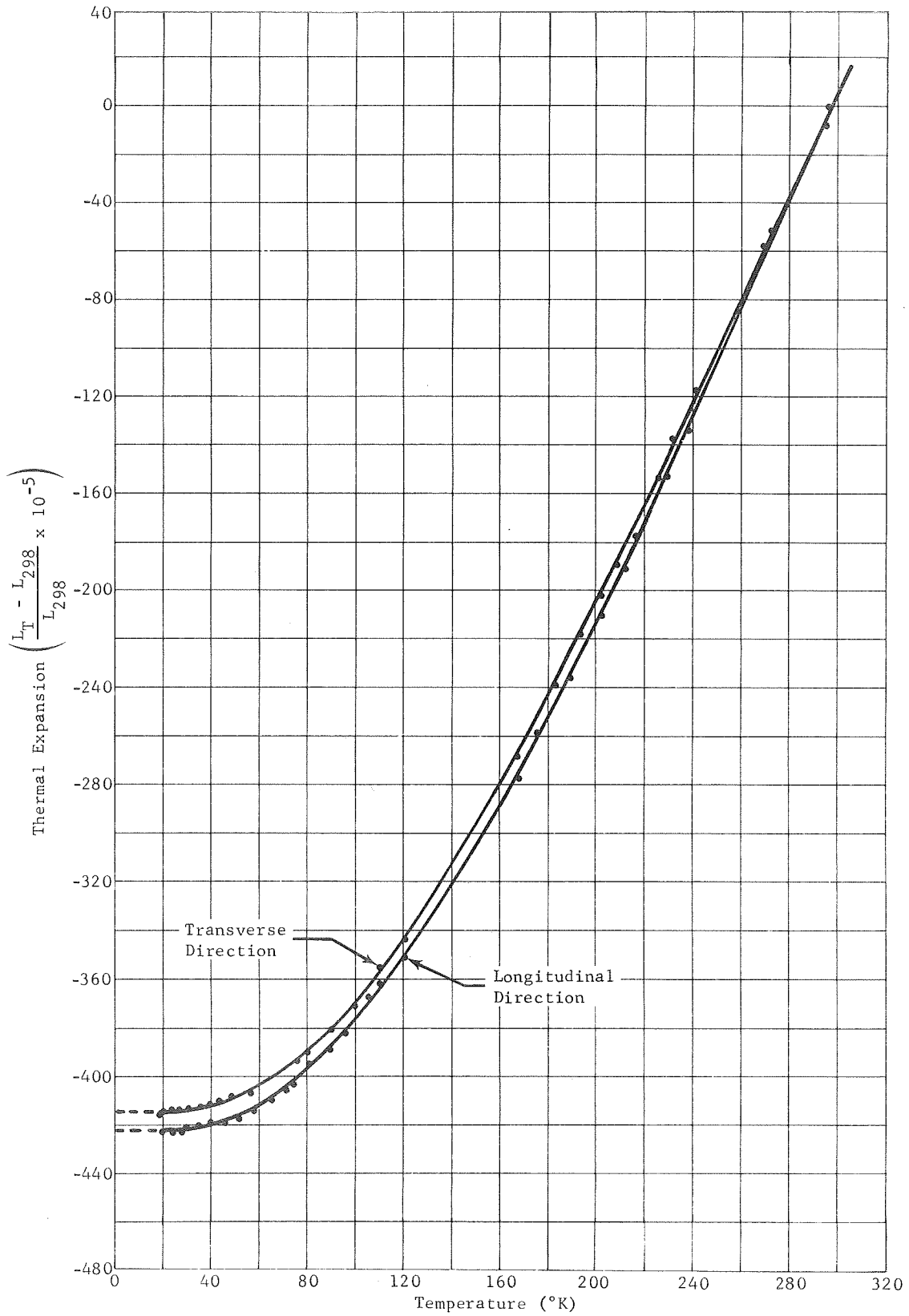Fig. C-4 Dynamic Moduli of X7007-T6 Aluminum Alloy, Transverse Direction

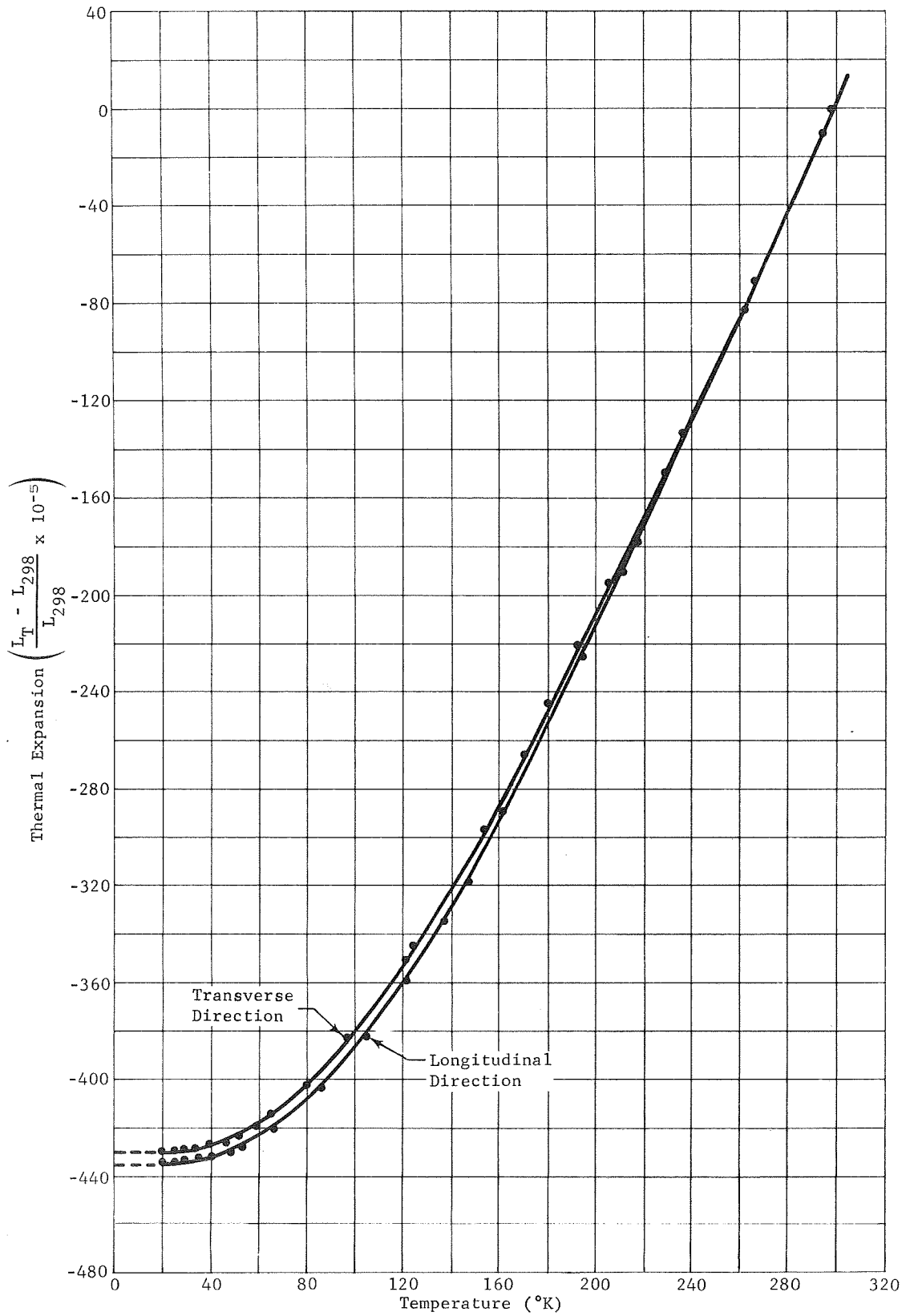Figure C-5 Thermal Expansion of 2021-T81 Aluminum Alloy

Fig. C-6   Thermal Expansion of X7007-T6 Aluminum Alloy

APPENDIX D

DISTRIBUTION

INTERIM REPORT NASA CR-72617

Contract NAS3-11203

"Cryogenic Alloy Screening"

Note: Copies of this report have been sent directly to the "Recipient" and
       "Designee" according to the quantities specified in columns R and D.
       When no copies are specified in column D, a copy of the letter of
       transmittal only has been sent to the person named as designee.

Report
Copies

R   D   Recipient   Designee

        National Aeronautics & Space Administration
        Lewis Research Center
        21000 Brookpark Road
        Cleveland, Ohio 44135
1   Attn: Contracting Officer, MS 500-313   .
5   Liquid Rocket Technology Branch, MS 500-209
1   Technical Report Control Office, MS 5-5
1   Technology Utilization Office, MS 3-16
2   AFSC Liaison Office, MS 4-1
2   Library
1   Office of Reliability & Quality Assurance,
                 MS 500-111
1   D. L. Nored, Chief, LRTB, MS 500-209
3   J. R. Faddoul, Project Manager, MS 500-209
1   W. F. Brown, MS 105-1
1   R. H. Kemp, MS 49-1
1   J. E. Sprawley, MS 105-1
1   J. G. Kennard, MS 3-14
1   G. T. Smith, MS 500-209

2   Chief, Liquid Propulsion Technology, RPL
        Office of Advanced Research & Technology
        NASA Headquarters
        Washington, D.C. 20546

Report
Copies

R   D   Recipient   Designee

1   Director, Launch Vehicles & Propulsion, SV
           Office of Space Science & Applications
           NASA Headquarters
           Washington, D.C. 20546

1   Chief, Space Vehicles Structures
           Office of Advanced Research & Technology
           NASA Headquarters
           Washington, D.C. 20546

1   Director, Advanced Manned Missions, MT
           Office of Manned Space Flight
           NASA Headquarters
           Washington, D.C. 20546

6   NASA Scientific & Technical Information Facility
           P.O. Box 33
           College Park, Maryland 20740

1   Director, Technology Utilization Division
           Office of Technology Utilization
           NASA Headquarters
           Washington, D.C. 20546

1   National Aeronautics & Space Administration
           Ames Research Center
           Moffett Field, California 94035
           Attn: Library

1   National Aeronautics & Space Administration
           Flight Research Center
           P.O. Box 273
           Edwards, California 93523
           Attn: Library

1   National Aeronautics & Space Administration
           Goddard Space Flight Center
           Greenbelt, Maryland 20771
           Attn: Library

Report
Copies

R	D	Recipient	Designee
1		National Aeronautics & Space Administration John F. Kennedy Space Center Cocoa Beach, Florida 32931 Attn: Library	
1		National Aeronautics & Space Administration Langley Research Center Langley Station Hampton, Virginia 23365 Attn: Library	
1		National Aeronautics & Space Administration Manned Spacecraft Center Houston, Texas 77001 Attn: Library	
1		National Aeronautics & Space Administration George C. Marshall Space Flight Center Huntsville, Alabama 35812 Attn: Library	
1	1	Jet Propulsion Laboratory 4800 Oak Grove Drive Pasadena, California 91103 Attn: Library	R. Boundy
1		Defense Documentation Center Cameron Station Building 5 5010 Duke Street Alexandria, Virginia 22314 Attn: TISIA	
1		Office of the Director of Defense Research & Engineering Washington, D.C. 20301 Attn: Office of Asst. Dir. (Chem. Technology)	
1		RTD (RTNP) Bolling Air Force Base Washington, D.C. 20332	

Report
Copies

R	D	Recipient	Designee
1		Arnold Engineering Development Center Air Force Systems Command Tullahoma, Tennessee 37389 Attn: Library	
1		Advanced Research Projects Agency Washington, D.C. 20525 Attn: Library	
1		Air Force Missile Test Center Patrick Air Force Base, Florida Attn: Library	
1		Air Force FTC (FTAT-2) Edwards Air Force Base, California 93523 Attn: Library	
1		Air Force Office of Scientific Research Washington, D.C. 20333 Attn: Library	SREP, Dr. J. F. Masi
1		Space & Missile Systems Organization Air Force Unit Post Office Los Angeles, California 90045	
1		U.S. Army Missile Command Redstone Scientific Information Center Redstone Arsenal, Alabama 35808 Attn: Document Section	
1		Bureau of Naval Weapons Department of the Navy Washington, D.C. Attn: Library	
1	1	Director (Code 6180) U.S. Naval Research Laboratory Washington, D.C. 20390 Attn: Library	J. M. Krafft

Report
Copies

R   D   Recipient   Designee

1   Picatinny Arsenal
           Dover, New Jersey 07801
           Attn: Library

1   Aerojet-General Corporation
           P.O. Box 296
           Azusa, California 91703
           Attn: Library

1   Aerojet-General Corporation
           Ordnance Division/Chino Facility
           601 S. Placentia
           Fullerton, California 92631
           Attn: Library

1   1   Aerojet-General Corporation   C. E. Hartbower
           P.O. Box 15847
           Sacramento, California 95803
           Attn: Technical Library 2484-2015A

1   Aeronutronic Division of Philco Ford Corp.
           Ford Road
           Newport Beach, California 92662
           Attn: Technical Information Department

1   Aerospace Corporation
           2400 E. El Segundo Blvd.
           Los Angeles, California 90045
           Attn: Library-Documents

1   Battelle Memorial Institute
           505 King Avenue
           Columbus, Ohio 43201
           Attn: Report Library, Room 6A

1   Beech Aircraft Corporation
           Boulder Facility
           Box 631
           Boulder, Colorado
           Attn: Library

Report
Copies

R	D	Recipient	Designee
1		Bell Aerosystems, Inc. Box 1 Buffalo, New York 14205 Attn: Library	T. Reinhardt
1	1	Boeing Company Space Division P.O. Box 868 Seattle, Washington 98124 Attn: Library	C. F. Tiffany
1		Boeing Company 1625 K Street NW Washington, D.C. 20006	
1		Chemical Propulsion Information Agency Applied Physics Laboratory 8621 Georgia Avenue Silver Spring, Maryland 20910	Tom Reedy
1		Chrysler Corporation Space Division New Orleans, Louisiana Attn: Librarian	
1	1	Syracuse University Research Institute Department of Metallurgy Syracuse, New York	Volker Weiss
1		Curtiss-Wright Corporation Wright Aeronautical Division Attn: Library	
1	1 1	General Dynamics/Convair P.O. Box 1128 San Diego, California 92112 Attn: Library	W. Witzel J. Christian
1		Missiles and Space Systems Center General Electric Company Valley Forge Space Technology Center P.O. Box 855 Philadelphia, Pa. 190101 Attn: Library	

Report
Copies

R	D	Recipient	Designee
1		Grumman Aircraft Engineering Corporation Bethpage, Long Island, New York Attn: Library	
1		Hercules Powder Company Allegheny Ballistics Laboratory P.O. Box 210 Cumberland, Maryland 21501 Attn: Library	
1		IIT Research Institute Technology Center Chicago, Illinois 60616 Attn: Library	C. K. Hersh K. E. Hofer
1		Ling-Temco-Vought Corporation P.O. Box 5907 Dallas, Texas 75222 Attn: Library	
1		Lockheed Missiles and Space Company P.O. Box 504 Sunnyvale, California 94087 Attn: Library	
1		Lockheed-California Company 10445 Glen Oaks Blvd. Pacoima, California Attn: Library	
1		Marquardt Corporation 16555 Saticoy Street Box 2013 - South Annex Van Nuys, California 91409	
1		Martin-Marietta Corporation (Baltimore Division) Baltimore, Maryland 21203 Attn: Library	John Calathes
1	1 1	Denver Division Martin-Marietta Corporation P.O. Box 179 Denver, Colorado 80201 Attn: Library	R. D. Keys F. R. Schwartzberg

Report
Copies

R	D	Recipient	Designee
1	1	Western Division	R. Rawe
	1	McDonnell Douglas Aircraft Company, Inc. 3000 Ocean Park Blvd. Santa Monica, California 90406 Attn: Library	B. V. Whiteson
1		McDonnell Douglas Aircraft Corporation P.O. Box 516 Lambert Field, Missouri 63166 Attn: Library	
1		Space & Information Systems Division North American Rockwell 12214 Lakewood Blvd. Downey, California Attn: Library	
1		Purdue University Lafayette, Indiana 47907 Attn: Library (Technical)	
1		Stanford Research Institute 333 Ravenswood Avenue Menlo Park, California 94025 Attn: Library	
1		TRW Systems Inc. 1 Space Park Redondo Beach, California 90278 Attn: STL Tech. Lib. Doc. Acquisitions	
1		TRW Incorporated 23555 Euclid Avenue Cleveland, Ohio 44117	E. A. Steigerwald
1		United Aircraft Corporation United Technology Center P.O. Box 358 Sunnyvale, California 94038 Attn: Library	

Report
Copies

R	D	Recipient	Designee
1		Wright-Patterson Air Force Base, Ohio 45433 Attention: AFML (MAAE)	
1		Wright-Patterson Air Force Base, Ohio 45433 Attention: AFML (MAAM)	
1		Department of the Army U.S. Army Material Command Washington, D.C. 20315 Attention: AMCRD-RC	
1		Commander U.S. Naval Ordnance Laboratory White Oak Silver Spring, Maryland 20910 Attention: Library	
1		Commanding Officer U.S. Naval Weapons Laboratory Dehlgren, Virginia 22448 Attention: Technical Library	
1	1	Colorado State University Fort Collins, Colorado 80521 Attention: Library	F. W. Smith
1	1	Brown University Providence, R. I. 02912 Attention: Library	J. R. Rice
1		California Institute of Technology 1201 E. California Blvd Pasadena, California Attention: Security Officer	
1		General Electric Company Apollo Support Department P.O. Box 2500 Daytona Beach, Florida 32015 Attention: Library	C. Day

Report
Copies

R	D	Recipient	Designee
1	1	Carnegie Institute of Technology Department of Civil Engineering Pittsburgh, Pennsylvania Attention: Library	R. B. Anderson
1	1	Frankford Arsenal Philadelphia, Pennsylvania 19137 Attention: 1320, Library	Carl Carman
1	1	Cornell University Department of Materials Science & Engineering Ithaca, New York 14850 Attention: Library	H. H. Johnson
1		Sandia Corporation P.O. Box 969 Livermore, California 94550 Attention: Technical Library	H. Lucas
1		Sandia Corporation Sandia Base Albuquerque, New Mexico Attention: Library	H. E. Montgomery B. R. Allen W. Herrmann
1		Brunswick Corporation Defense Products Division P.O. Box 4594 43000 Industrial Avenue Lincoln, Nebraska Attention: Library	J. Carter
1		General Dynamics P.O. Box 748 Fort Worth, Texas 76101 Attention: Library	D. E. Westerheide
1	1	Institution of Aerospace Studies University of Toronto Toronto 5, Ontario Attention: Library	Dr. I. I. Class